UNIVERSITY OF SOUTHAMPTON

FACULTY OF ENGINEERING, SCIENCE AND MATHEMATICS

School of Chemistry

Synthesis and Complexes of New Selenoether Macrocycles

by

Joanna Margaret Manning

Thesis for the degree of Doctor of Philosophy

March 2010

UNIVERSITY OF SOUTHAMPTON

ABSTRACT

FACULTY OF ENGINEERING, SCIENCE AND MATHEMATICS
SCHOOL OF CHEMISTRY

Doctor of Philosophy

Synthesis and Complexes of New Selenoether Macrocycles
by Joanna Margaret Manning

The first known examples of alkyl Pt(II) complexes with macrocyclic selenoethers [$PtMe_2L$] (L = [8]aneSe_2 and [16]aneSe_4) have been synthesised and characterised as part of a series of dimethyl Pt(II) complexes with selenoether ligands (L = $MeSe(CH_2)_nSeMe$, n = 2, 3; *o*-$C_6H_4(CH_2SeMe)_2$). A new series of [$PtMe_3I(\kappa^2$-L-L)] complexes has been synthesised and characterised, which includes the first examples of this type with macrocyclic selenoethers (L-L = *o*-$C_6H_4(CH_2EMe)_2$, E = Se, Te; $MeC(CH_2SeMe)_3$; [8]aneSe_2 and [16]aneSe_4). The first bridging ditelluroether trimethyliodo Pt(IV) complex, [$(PtMe_3I)_2(MeTeCH_2TeMe)$] has also been characterised. [$PtMe_3(\kappa^3$-[16]ane$Se_4)$]PF_6 was isolated and characterised, which is the first cationic trialkylplatinum(IV) complex with a macrocyclic selenoether ligand, and an unusual example of κ^3-[16]aneSe_4 coordination.

Five novel macrocycles containing a mixed O/Se donor set of the type O_xSe_{2x}, two small ring Se_3 macrocycles and two Se_2N macrocycles have been synthesised. Two methods of production have been investigated from the same precursors, a $NaBH_4$ reduction and a low temperature $Na/NH_{3\ (l)}$ reduction, demonstrating that reaction conditions are very important for determining preferred ring size and yields. The Se_3 and Se_2N macrocycles have been synthesised in multigram quantities, and crystal structures of two of these macrocycles have been obtained.

The first examples of complexes with tridentate homoleptic selenoether macrocycles and tridentate Se_2N macrocycles have been prepared and characterised. Platinum(II) dichloride complexes were prepared for L^6-L^9, but proved to be extremely poorly soluble. No evidence of platinum(II) complexation with methyl co-ligands was observed. Reaction of [$PtMe_3I$] with L^6-L^{10} resulted in the production of *fac*-coordinated, cationic Pt(IV) complexes of the type [$PtMe_3L$]I. This geometry is confirmed by two crystal structures, of [$PtMe_3(L^6)$]I and [$PtMe_3(L^9)$]I. Cr(III) complexes of the type [$CrCl_3L$] have been produced and characterised for L^1, $L^{6\text{-}10}$, and are generally hydrolytically sensitive, insoluble solids.

Table of Contents

Table of Tables

Table of Figures

Declaration of Authorship

I, Joanna Margaret Manning

declare that the thesis entitled

Synthesis and Complexes of New Selenoether Macrocycles

and the work presented in the thesis are both my own, and have been generated by me as the result of my own original research. I confirm that:

- this work was done wholly or mainly while in candidature for a research degree at this University;
- where any part of this thesis has previously been submitted for a degree or any other qualification at this University or any other institution, this has been clearly stated;
- where I have consulted the published work of others, this is always clearly attributed;
- where I have quoted from the work of others, the source is always given. With the exception of such quotations, this thesis is entirely my own work;
- I have acknowledged all main sources of help;
- where the thesis is based on work done by myself jointly with others, I have made clear exactly what was done by others and what I have contributed myself;
- parts of this work have been published as:
- Levason, W.; Manning, J. M.; Pawelzyk, P.; Reid, G. *Eur. J. Inorg. Chem.* **2006**, 4380 – 4390.
- Levason, W.; Manning, J. M.; Nirwan, M.; Ratnani, R.; Reid, G.; Smith, H.; Webster, M. *Dalton Trans.* **2008**, 3486 – 3492.
- Levason, W.; Manning, J. M.; Reid, G.; Tuggey, M.; Webster, M. *Dalton Trans.* **2009**, 4569 – 4577.
- Evans, J.; Levason, W.; Manning, J. M.; Reid, G.; Tsoureas, N.; Webster, M. *Dalton Trans.* **2007**, 1986 – 1988.

Signed: ……..

Date:…….

Dedication

I would like to thank a number of people who have given invaluable assistance over the course of my PhD. First and foremost my supervisor, Gill Reid, for all the help, guidance and patience she has shown me and for letting me go to a conference in Cancun. Also, thanks go to Bill Levason for running so many multinuclear NMR spectra for me, Marek Jura, Stuart Reid and Nikos Tsoureas for help running crystal data collections, and Mike Webster for help with some of the difficult structure determinations.

Special thanks go to Hayley Smith and Matthew Tuggey, for being every PhD student's dream: intelligent, capable project students. Thanks guys, you worked brilliantly for me.

Some blame must go to Mike Brown, for talking me into doing a PhD and thanks too, for being a shoulder to cry on when reactions went horribly wrong. I'd also like to thank all those in the Reid/Levason group over the years, for some great times in the lab, and some wonderful weekend excursions and parties.

I am indebted forever to my flatmate, Gemma Davis, for keeping me sane, during some rough times.

This work is dedicated to my parents, and family, but most of all to my grandmother. I wish you could read this, Gran. I know you'd be proud.

List of Abbreviations

Bu	butyl
Me	methyl
Et	ethyl
Ph	phenyl
cod	cyclooctadiene
dmf	dimethylformamide
dmso	dimethylsulfoxide
nbd	norbornadiene
picrate	2,4,6-trinitrophenolate
thf	tetrahydrofuran
12-crown-4	1,4,7,10-tetraoxacyclododecane
15-crown-5	1,4,7,10,13-pentaoxacyclopentadecane
18-crown-6	1,4,7,10,13,16-hexaoxacyclooctadecane
[9]aneS_2O	1-oxa-4,7-dithiacyclononane
[15]aneS_2O_3	1,4,7-trioxa-10,13-dithiacyclopentadecane
[18]aneS_3O_3	1,4,7-trioxa-10,13,16-trithiacyclooctadecane
[9]aneS_3	1,4,7-trithiacyclononane
[10]aneS_3	1,4,7-trithiacyclodecane
[12]aneS_4	1,4,7,10-tetrathiacyclododecane
[14]aneS_4	1,4,8,11-tetrathiacyclotetradecane
[15]aneS_5	1,4,7,10,13-pentathiacyclopentadecane
[18]aneS_6	1,4,7,10,13,16-hexathiacyclooctadecane
[9]aneO_2Se	1,4-dioxa-7-selenacyclononane
[12]aneO_2Se_2	1,7-dioxa-4,10-diselenacyclododecane
[15]aneO_3Se_2	1,4,10-trioxa-7,13-diselenacyclopentadecane
[18]aneO_4Se_2	1,4,10,13-tetraoxa-7,16-dieselenacyclooctadecane
dibenzo[18]aneO_2Se_4	5,6,14,15-dibenzo-1,10-dioxa-4,7,13,16-tetraselenacyclooctadecane
dibenzo[24]aneO_4Se_4	8,9,20,21-dibenzo-1,4,13,16-tetraoxa-7,10,19,22-tetraselenacyclotetracosane
dibenzo[30]aneO_6Se_4	11,12,26,27-dibenzo-1,4,7,16,19,22-hexaoxa-10,13,25,28-tetraselenacyclotriacontane
[16]aneS_2Se_2	1,5-dithia-9,13-diselenacyclohexadecane
sebc	3*H*-1,4,5,7-tetrahydro-2,6-benzodiselenonine
[8]aneSe_2	1,5-diselenacyclooctane
[8]aneSe_2(OH)	1,5-diselenacyclooctane-3-ol
Me_4[8]aneSe_2	3,3,7,7-tetramethyl-1,5-diselenacyclooctane
[12]aneSe_3	1,5,9-triselenadodecane
Me_6[12]aneSe_3	3,3,7,7,11,11-hexamethyl-1,5,9-triselenadodecane
[12]aneSe_4	1,3,7,9-tetraselenacyclododecane
[14]aneSe_4	1,4,8,11-tetraselenacyclotetradecane
dibenzo[14]aneSe_4	6,7,13,14-dibenzo-1,5,8,12-tetraselenacyclotetradecane
[16]aneSe_4	1,5,9,13-tetraselenacyclohexadecane
[16]aneSe_4(OH)	1,5,9,13-tetraselenacyclohexadecane-3-ol
[16]ane$Se_4(OH)_2$	1,5,9,13-tetraselenacyclohexadecane-3,11-diol
Me_8[16]aneSe_4	3,3,7,7,11,11,15,15-octamethyl-1,5,9,13-tetraselenacyclohexadecane
[18]aneSe_6	1,3,7,9,13,15-hexaselenacyclooctadecane
[20]aneSe_5	1,5,9,13,17-pentaselenacyclocosane
[24]aneSe_6	1,5,9,13,17,21-hexaselenacyclotetracosane

[9]aneO_2Te	1,4-dioxa-7-telluracyclononane
[18]aneO_4Te_2	1,4,10,13-tetraoxa-7,16-ditelluracyclooctadecane
[9]aneS_2Te	1,4-dithia-7-telluracyclononane
[11]aneS_2Te	1,4-dithia-8-telluracycloundecane
[12]aneS_2Te	1,5-dithia-9-telluracyclododecane
[14]aneS_3Te	1,4,7-trithia-11-telluracyclotetradecane
[8]aneTe_2	1,5-ditelluracyclooctane
[12]aneTe_3	1,5,9-tritelluracyclododecane
Cl_6[12]aneTe_3	3,3,7,7,11,11-hexachloro-1,5,9-tritelluracyclododecane

NMR	Nuclear Magnetic Resonance
d	doublet
FT	Fourier Transform
Hz	Hertz
J	coupling constant
ppm	parts per million
q	quartet
RT	Room temperature
s	singlet
t	triplet
VT	Variable temperature

MS	Mass Spectrometry
APCI	Atmospheric pressure chemical ionisation
ES	Electrospray
EI	Electron impact
GC	Gas chromatography

IR	Infrared
br	broad
m	medium
s	strong
sh	shoulder
w	weak

UV-vis	Ultraviolet-visible
B	Racah parameter
β	nephelauxetic ratio
CT	charge transfer
Dq	ligand field splitting parameter

μ_B	Bohr magneton
S	total spin quantum number

Chapter 1: Introduction

1.1 – General Introduction

Selenium was discovered in 1817 by Jöns Jacob Berzelius, after he investigated the red-brown sediment deposited in chambers used in the production of sulfuric acid. Elemental selenium has two forms; one is a silvery metal which has the curious property of conducting electricity better (by a factor of 10^4) when light shines on it, and the other is a red powder which can be converted to the metallic form by heating.[1] Sulfur has been used since ancient times, but was only postulated to be an element in 1777 by Antoine Lavoisier, and subsequently proved by Joseph Gay-Lussac and Louis-Jacques Thénard in 1809.[1] Tellurium was discovered in 1793 by Franz Joseph Müller von Reichenstein, and is usually obtained as a grey powder by the electrolytic reduction of sodium telluride solution.[1] Sulfur, selenium and tellurium are members of Group 16 of the Periodic Table, a group also known as the chalcogens. Table 1.1 gives some physical constants of the chalcogen elements.

Table 1.1: Comparison of physical constants of Group 16 elements.

Constant	**Oxygen**	**Sulfur**	**Selenium**	**Tellurium**
Electronegativity (Pauling)	3.5	2.5	2.4	2.1
Ionization potential (eV)	13.61	10.36	9.75	9.01
Covalent radius (Å)	0.66	1.04	1.17	1.37
Bond energy: E–C (kcal/mol) in Et_2E	86.5	69.7	59.9	56.0
Bond length E–C (Å) in Et_2E	1.42	1.82	1.96	2.12
Bond energy: E–H (kcal/mol) in H_2E	119	91	73	64
Bond length E–H (Å) in H_2E	0.96	1.35	1.46	1.69

The chemistry of neutral group 16 ligands, ER_2 (E = S, Se, Te), was developed rather later than that of group 15 ligands, and the heavier elements (especially Te) are still relatively little studied. They were generally thought of as malodorous and poor σ-donors. However, development of FT NMR has increased interest over the last two decades or so, as both selenium and tellurium have $I = ½$ nuclei (see Table 1.2) making them highly useful analytical tools.[2] The quadrupolar nature of ^{33}S, together with its low abundance and receptivity mean it is not useful as a probe in organosulfur chemistry. In the last 30 years interest in group 16 ligands has greatly increased, although selenoethers and telluroethers remain less studied compared to the sulfur analogues. There have been a number of reviews summarising the current knowledge of the area, notably Blake and Schröder (*Advances in Inorg. Chem.*, **1990**),[3] Cooper and Rawle (*Structure and Bonding*, **1990**),[4] Hope and Levason (*Coord. Chem. Rev.*, **1993**),[5] Levason, Orchard and Reid (*Coord. Chem. Rev.*,

2002),[6] Levason and Reid (*Comprehensive Coordination Chemistry II*, **2003**)[2] and Panda (*Coord. Chem. Rev.*, **2009**).[7,8]

Table 1.2: Comparison of NMR active isotopes of chalcogens. a – Relative to ^{13}C.

	Spin	**Abundance**	**Receptivity[a]**
Sulfur-33	$^3/_2$	0.76%	0.097
Selenium-77	½	7.58%	2.98
Tellurium-125	½	6.99%	12.5

Indeed, there are vast number of acyclic, cyclic and macrocyclic thioether ligands in the literature, with many different methods available for their production. For example, dithioethers can be produced from reaction of the relevant dithiol with sodium ethoxide, followed by addition of MeI (e.g. $MeS(CH_2)_nSMe$, n = 2, 3).[9] In contrast, reaction of thiophenol with sodium followed by addition of dihaloalkane can be used to produce $PhS(CH_2)_nSPh$ (n = 2, 3).[9] A phenylene backbone can be introduced by reaction of NaSMe (often produced from Na and Me_2S_2 in liquid ammonia) with *o*-$C_6H_4Cl_2$ to produce the monosubstituted species *o*-$C_6H_4Cl(SMe)$. This can then be reacted with BuLi and Me_2S_2 to form *o*-$C_6H_4(SMe)_2$.[10] The xylyl-based ligand *o*-$C_6H_4(CH_2SMe)_2$ can be produced by direct reaction of *o*-$C_6H_4(CH_2Br)_2$ with NaSMe. It has been shown that variation in both terminal substituent and backbone plays a significant role in governing the ligand properties in these dithioethers.[11]

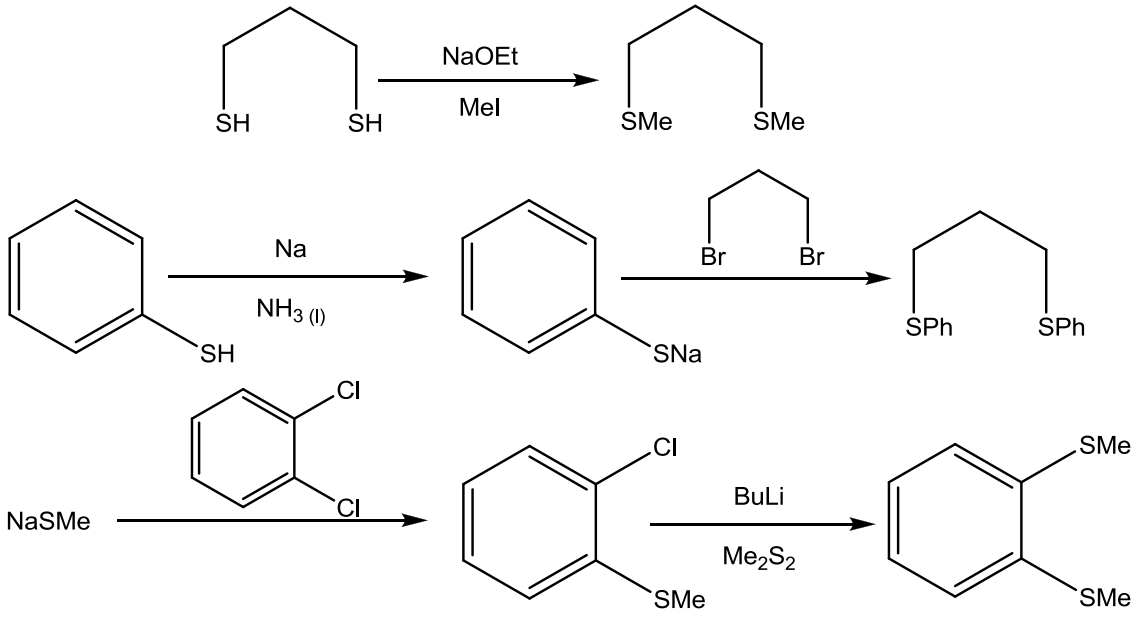

Figure 1.1: Schemes for production of a selection of di-thioether ligands.

For selenium, however, precursors analogous to those used in thioether ligand preparations are often not readily available, for example, RSeH and H_2Se are unstable, toxic and extremely malodorous and thus are not useful synthons. Alternative routes are required. Diselenoalkanes, $MeSe(CH_2)_nSeMe$, of varying lengths (n = 1, 2, 3, 6, 12) can be produced by either reaction of $MeSe^-Li^+$ (obtained by reaction of elemental Se with MeLi in thf at 77 K)[12] or $MeSe^-Na^+$ (generated from Me_2Se_2 and Na in liquid ammonia) with dihaloalkanes.[13] Reaction using the sodium salt takes two days, and while the lithium salt requires cooling to 77 K to form, the reaction with the α, ω-dihaloalkane only takes a few hours, making this the preferred route. *cis*-MeSeCH=CHSeMe can be produced from the lithium salt and *cis*-1,2-dichloroethene, but requires the reaction to be conducted in ethanol not thf and needs a molar equivalent of NaOEt.[12] Reaction of PhLi with selenium gives only moderate yields of PhSeLi; better yields are obtained by cleaving Ph_2Se_2 with Rongalite ($HOCH_2SO_2Na.2H_2O$) in ethanol or with $LiAlH_4$ in thf.[12] This can then be reacted with dihalides in the same way as the methylselenolate salt.

There are two main ways to incorporate aromatic units into the backbone of diselenoethers. RSe^- ions are not nucleophilic enough to react directly with *o*-dichloro-(or dibromo-)benzene. Instead, *o*-$C_6H_4(SeMe)_2$ can be produced by addition of Me_2Se_2 to benzyne in *o*-$C_6H_4Cl_2$ solution[12] or by cleaving polymeric $(–o\text{-}SeC_6H_4Se–)_n$ with Rongalite followed by methylation.[14] The polymer is produced by reaction of *o*-$C_6H_4Br_2$ and Na_2Se_2 in hot dmf.[14] RSe^- can react with *o*-$C_6H_4(CH_2Br)_2$, however, to produce *o*-$C_6H_4(CH_2SeMe)_2$.

It is also possible to make three and four selenium containing chains, for example $MeSe(CH_2)_3Se(CH_2)_3SeMe$[12] and $MeSe(CH_2)_2Se(CH_2)_3Se(CH_2)_2SeMe$.[2] Tripods from a central selenium atom are not possible in the way phosphorus tripods are, but can be produced using carbon as the pivot (e.g. $MeC(CH_2SeMe)_3$).[12] This can be achieved by reaction of MeSeLi and $MeC(CH_2Br)_3$ in 6:1 molar ratio in thf.[12] The two-fold excess of $MeSe^-$ is required to promote complete replacement of bromide. It is also possible to produce tetradentate ligands with four selenium containing groups from a central carbon, e.g. $C(CH_2SeMe)_4$.[12,15] Figure 1.2 shows the synthetic routes for the ligands used in Chapter 2.

The xylyl based ligand *o*-$C_6H_4(CH_2SeMe)_2$ has been shown to form a number of stable complexes, despite the 7-membered chelate ring formed.[16] As with thioethers, variation in terminal substituent allows ligating properties to be altered with the addition of groups which have greater or lesser electron withdrawing properties.

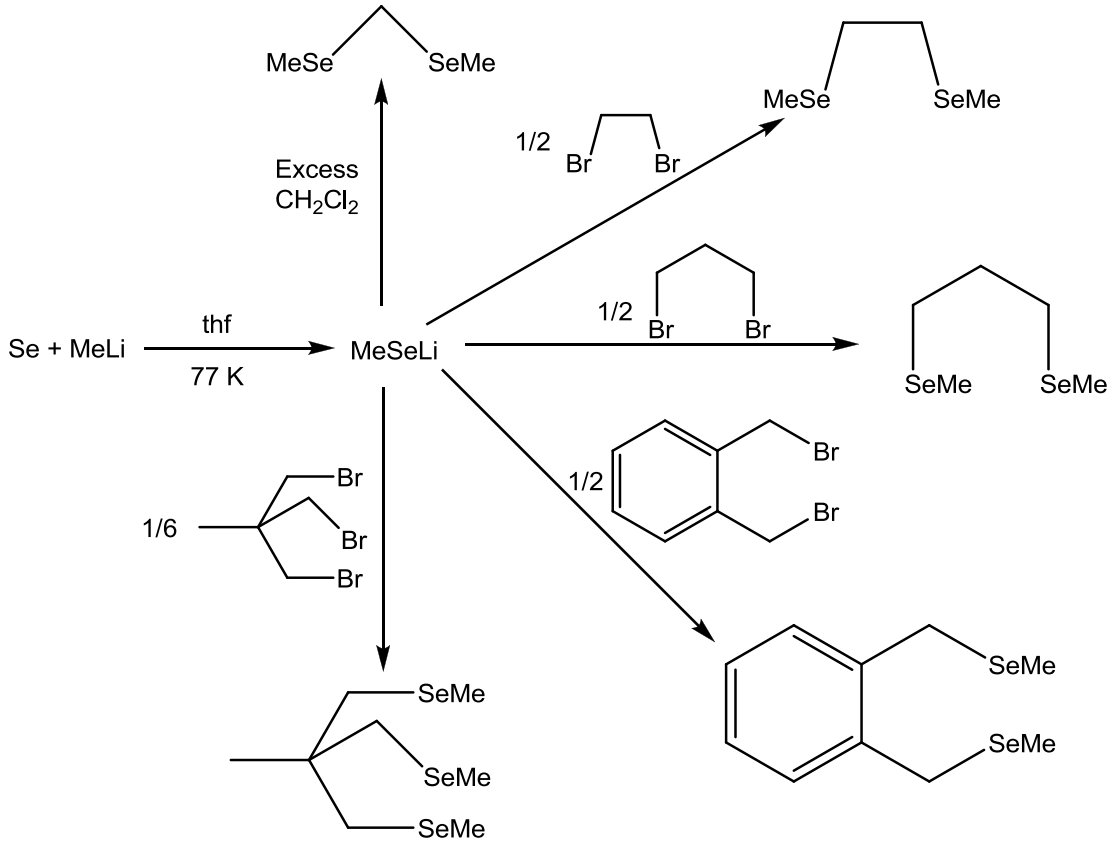

Figure 1.2: Syntheses of selenoethers used in Chapter 2.

The chemistry of telluroethers is less well known than that of selenoethers, due to the increased sensitivity of tellurium ligands. They are malodorous and generally air-sensitive. There are also fewer known Te ligands, due to the unavailability of many of the corresponding precursors that are used in sulphur/selenium chemistry. In particular, the instability of Te-H bonds makes tellurols (RTeH) useless as synthons,[17] and weak Te-C bonds mean elimination may be favoured over substitution.[18] The weakness of Te-H and Te-C bonds is primarily due to the mismatch in orbital size between the diffuse 5s/5p orbitals on Te and the much smaller 1s and 2s/2p orbitals on H and C respectively. RLi (R = Me, Ph) will react with powdered tellurium in thf at 77 K to produce high yields of RTeLi.[18] This contrasts with selenium, which gives only moderate yields of PhSeLi. Chains of the form $RTe(CH_2)_nTeR$ (R = Me, Ph; n = 1, 3, 6 or 10) can be formed from reaction of RTeLi with dihaloalkane at 77 K. The reactions again contrast with the selenoether syntheses, as the dihalides must be added to frozen solutions of RTeLi,[18] but can be added at room temperature to RSeLi.[12] Attempts to produce $RTe(CH_2)_2TeR$ or RTeCH=CHTeR result in elimination of ethene and ethyne respectively due to the stability of Te-Te bonds and the fragility of Te-C bonds, and formation of ditellurides.[18] The only C_2 backbone available at present is *o*-$C_6H_4(TeMe)_2$, made by reaction of *o*-dibromobenzene and MeTeLi.[10] This can be contrasted with $MeSe^-$ and MeS^- used in the same conditions, which do not react. Thus it is clear that RTe^- is more nucleophilic than RSe^-, which is in turn more nucleophilic than RS^-. Attempts to make $RTe(CH_2)_nTeR$ (n = 4, 5) result in

the formation of heterocycles as the major product.[18] A C_4 backbone can be incorporated by reacting α,α'-dibromo-*o*-xylene with frozen MeTeLi, producing *o*-$C_6H_4(CH_2TeMe)_2$ in good yield.[19]

There are very few multidentate acyclic telluroethers known – the linear tritelluroether $Te(CH_2CH_2CH_2TeR)_2$ is made by reaction of $RTe(CH_2)_3Cl$ and Na_2Te in liquid ammonia,[17] and the tri- and tetradentate ligands $CH_3(CH_2TeR)_3$ and $C(CH_2TePh)_4$ can be produced from RTeLi and the appropriate bromoalkane.[18] Reaction temperature must be kept low for these reactions, to reduce the competing Te-C scission elimination reactions. $C(CH_2TeMe)_4$ cannot be produced in this way, as reaction of MeTeLi and $C(CH_2Br)_4$ results in elimination of two Te-Me units to form MeTeTeMe, and production of a cyclopropane derivative, $\overline{CH_2CH_2C}(CH_2TeMe)_2$.[15,18] Figure 1.3 shows the synthetic routes for the ligands used in Chapter 2.

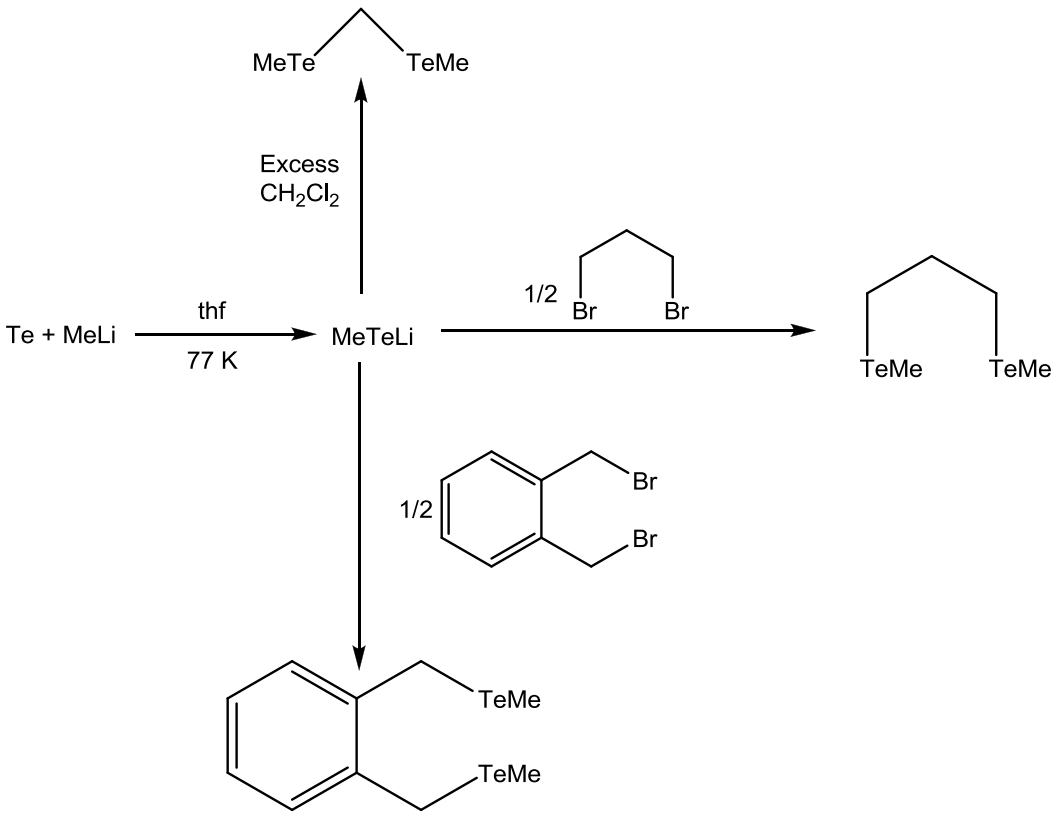

Figure 1.3: Syntheses of telluroethers used in Chapter 2.

1.2 – Preparation Methods for Macrocycles

In the context of this thesis, macrocycles can be defined as cyclic organic molecules with nine or more atoms, at least three of which are donor heteroatoms. The dominant factor controlling the synthesis of macrocycles is entropic.[20] Generally, the final reaction step is the cyclisation, where two ends of a chain come together to create the ring forming bond (Figure 1.4). However, unless

highly preorganised or rigid systems are involved, the probability of the two ends being in close enough proximity to react is very low, and polymerisation is much more likely.

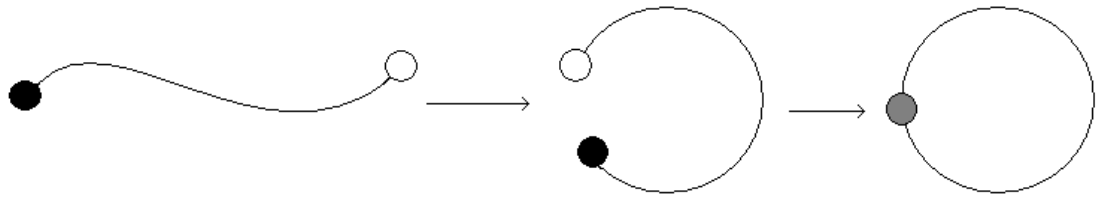

Figure 1.4: A schematic view of the cyclisation step involved in macrocycle synthesis. The filled and open circles represent mutually reactive functional groups. The first step involves the adoption of a conformation in which the two reactive groups are close to one another and in the correct orientation for reaction. Finally, the new bond is formed and the macrocycle is formed.[20]

One widely used method to overcome this is to use high dilution conditions. To achieve this, the acyclic precursors may be added simultaneously dropwise to large quantities of solvent, or one precursor may be added dropwise to a dilute solution of another precursor to promote the statistical probability of cyclisation over polymerisation.[21] For example, the production of [14]aneS_4, shown in Figure 1.5, has been shown to increase from 7.5 % yield[22] to 55 % yield purely by increasing the dilution of the reactants.[23] > 90 % yield has been achieved in production of a range of cyclic selenophanes by a high dilution method (0.005 mol reactant added dropwise into 1000 cm^3 solvent).[24] Drawbacks to this tactic include the cost of large volumes of solvents, which must often be anhydrous, the environmental cost of disposing of the solvent after the reaction and inherent difficulties in handling these quantities in the laboratory, both in terms of glassware and in achieving precision of simultaneous slow addition.

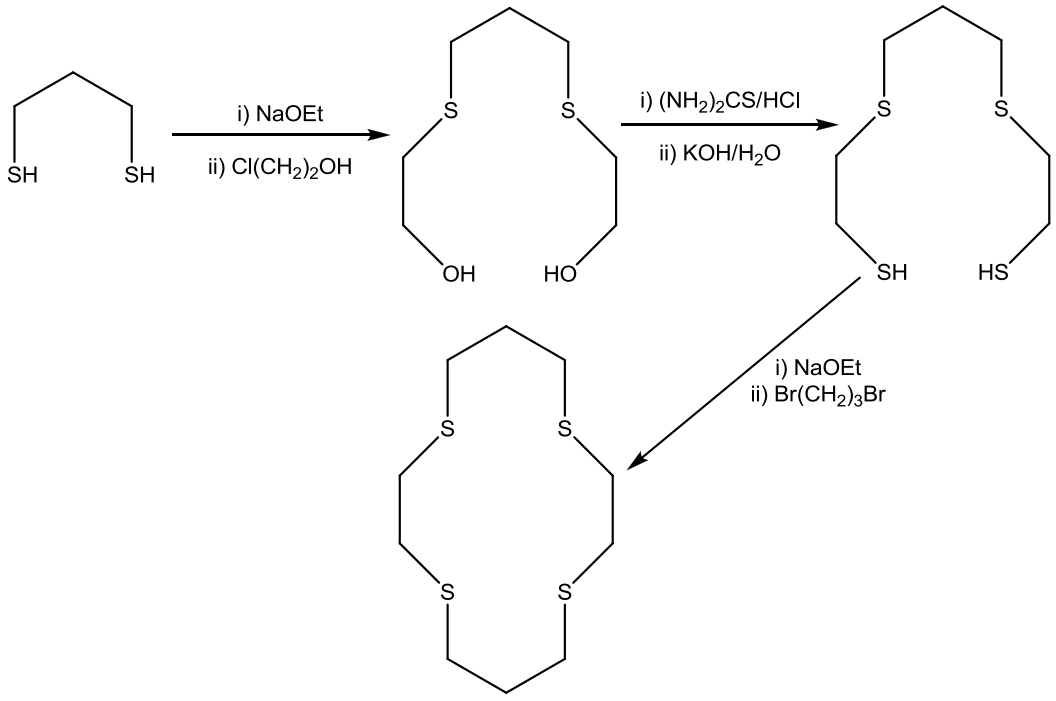

Figure 1.5: Synthesis of [14]aneS_4.[21]

In an alternative, transition metals, such as for example copper, cobalt or manganese, but most commonly nickel, can be used to bind the precursors so they are held in proximity to each other before reacting (template synthesis).[20,25] The produced macrocycle must often be demetallated to release it before it can be used. Demetallation of the formed macrocycle can present problems as the macrocycle will often bind more strongly to the metal centre than the acyclic precursors (see Section 1.5 for a discussion of the Macrocyclic Effect). However, addition of excess acid to a coordinated amine containing macrocycle, or addition of a strongly competing ligand, such as CN^- for example, can displace the macrocycle and allow it to be isolated.[25] Use of metal ions is less important for thioethers,[21] owing to the weaker binding of sulfur compared to oxygen or nitrogen, but [9]aneS_3 has been produced in 60 % yield by a template reaction (Figure 1.6).[26]

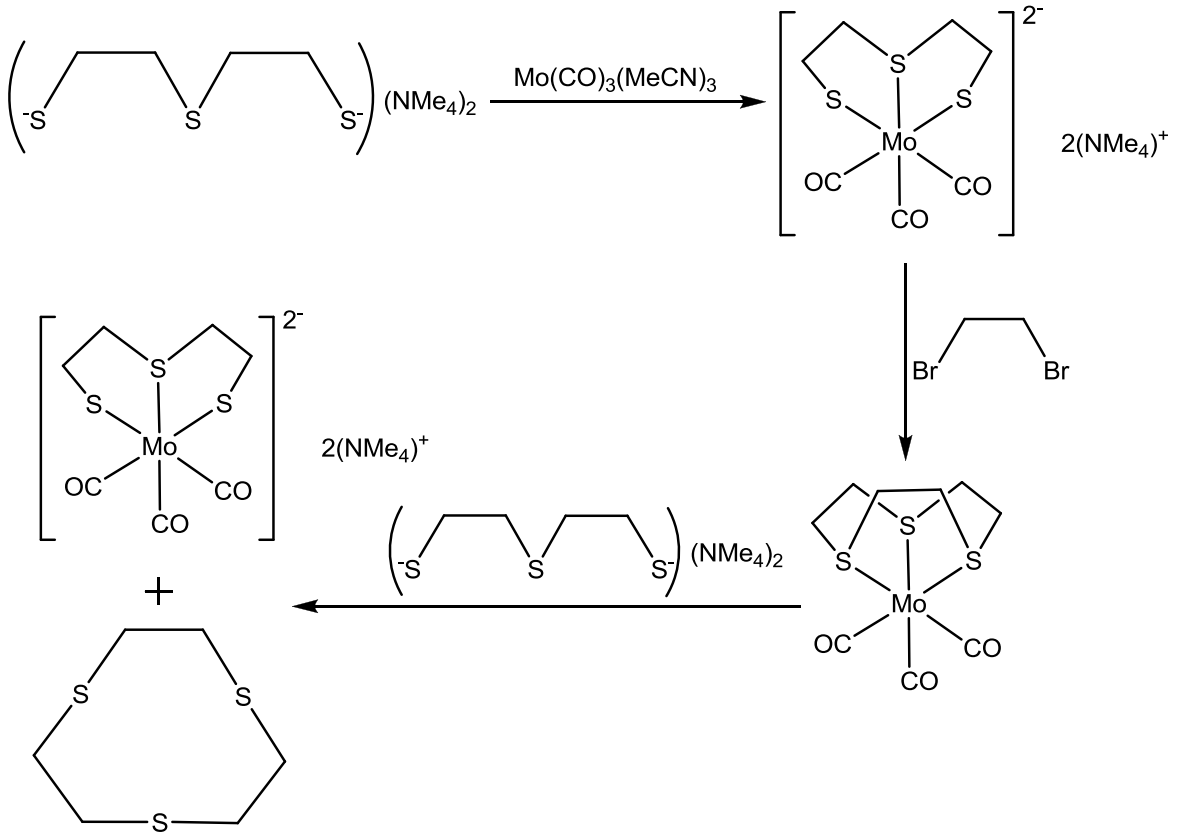

Figure 1.6: Template synthesis of [9]aneS_3.[26]

One advantage of using metal ions, is that different metals can promote different ring sizes in the same reaction conditions. The diameter of the metal ion affects the macrocycle produced, but not always in predictable ways.[25] For example, the oligomerisation of oxirane by BF_3 produces different ratios of crown ethers (Figure 1.7), with the larger metals producing the larger rings.[20] High dilution reactions often can not be modified in similar ways to promote different ring sizes. However, if a macrocycle has a flexible backbone, it can accommodate a larger metal ion than expected, and in some cases a much larger macrocycle is produced than expected, as with the condensation of 2,6-diacetylpyridine with $H_2NCH_2CHOCH_2NH_2$ in the presence of manganese (II),

which produces a tetramanganese complex of the [4+4] macrocycle, rather than the expected [2+2] macrocycle.[20]

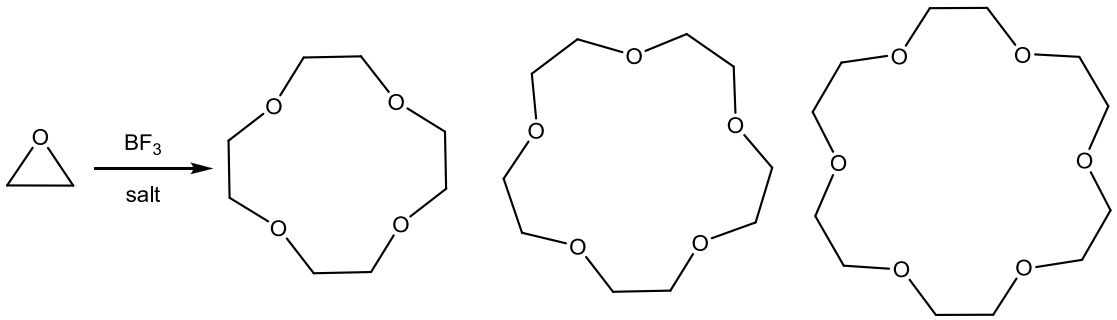

Salt	%	%	%
none	15	5	4
$LiBF_4$	30	70	-
$NaBF_4$	25	50	25
KBF_4	-	50	50
$RbBF_4$	-	-	100
$CsBF_4$	-	-	100

Figure 1.7: Production of crown ethers as promoted by Group 1 metal ions.[20]

An in-depth literature review of seleno- and telluroether macrocycles is presented in Chapters 3 (mixed chalcogen donor macrocycles) and 4 (homoleptic and mixed donor N/Se, N/Te macrocycles). Figure 1.8 (below) shows the new selenoether macrocycles produced in this work.

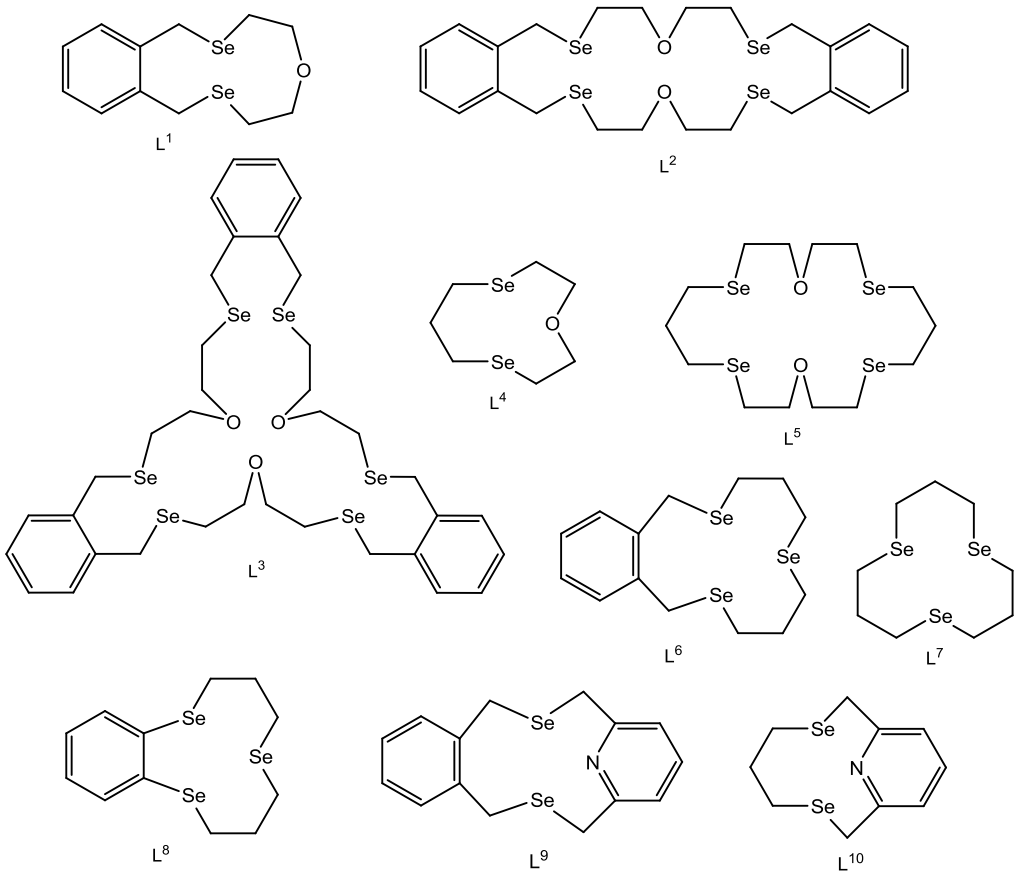

Figure 1.8: New selenium-rich macrocycles prepared in this work. See Chapter 3 for L^{1-5} and Chapter 4 for L^{6-10}.

1.3 – Metal-Chalcogenoether Bonding

Group 16 elements have the ground state electronic configuration $ns^2\ np^4\ nd^0$. Murray and Hartley describe the nature of the orbitals in an in-depth review of chalcogenoether ligand metal complexes.[11] They suggest that the *s* and *p* orbitals vary from fully hybridised on oxygen to virtually unhybridised on tellurium, with sulfur and selenium between these two extremes. It is easiest to consider the chalcogenoethers as neutral R_2E compounds with two lone pairs. As they only have two substituents, steric effects are greatly reduced compared to Group 15 ligands, however, the interdonor backbone and resulting chelate ring size will still affect the coordination of polydentates and macrocycles in the usual way. The electronic effects of the R groups are generally less important for chalcogenoethers than for phosphines or arsines.

While one lone pair is used in forming a σ-bond to a metal acceptor, there are several possibilities for the second lone pair. It may remain non-bonding and cause stereoelectronic repulsion with electron-rich metal centres, weakening the overall bond. It may form a σ-bond to a second metal centre, resulting in a R_2E bridged complex. This behaviour has been observed for all three chalcogens (S, Se, Te), in the polymeric chain $[Ag(MeS\{CH_2\}_3SMe)]^+$ and in $[(\{\eta^5\text{-}MeC_5H_4\}Mn\{CO\}_2)_2(\mu\text{-}Me_2Se)]$, for example.[2] In principle, it is also possible that the second lone pair could behave as a π-donor to a suitable metal *d*-orbital, particularly to electron poor metals, however there is little good evidence that this occurs.[6]

The chalcogen could also behave as a π-acceptor, using either the lowest empty *d*-orbital (like the Chatt model for phosphines[27]) or more likely the E-Cσ^* orbitals (like the Orpen-Connelly phosphine model[28]). It is difficult to observe π back donation directly, as this requires comparing the E-C bond distances in crystal structures of redox pairs, but comparing the observed bond length to the sum of the covalent radii of the elements can provide an indication of π back donation. However, so far such observations in chalcogenoether complexes have been of little statistical significance. The consensus is that chalcogenoethers are weak σ-donors with little or no π component to the bonding,[3,4,11] although it has been suggested that π-acceptor behaviour may be significant in some macrocyclic thioether complexes.[29]

Studies on Fe(0)[30] and Mn(I)[31,32] systems with Group 16 ligands have shown that the stability and inertness of the M-L bond increases Te >> Se > S > O. This was attributed to the decreasing electronegativity of the donors down the group causing increased σ-donation. For higher oxidation states, for example Rh(III) systems[33] the strongest donation appears to be Se > Te. This is most likely due to the spatial extension of the *d*-orbitals on the metal. Low valent metals will have better overlap with the large Te *s*-orbital than the contracted orbitals on harder, higher oxidation state metals.

1.4 – Pyramidal Inversion

As discussed above, π- bonding between chalcogenoethers and metal centres (which would place the two R groups planar with the metal-E bond) is rare. When σ-bonded to a metal centre through one lone pair, R_2E adopts a distorted tetrahedral geometry. This means that chalcogenoethers have the potential for pyramidal inversion to occur. Inversion involves neither bond cleavage nor requires the presence of an additional reagent; it is a subtle molecular rearrangement. Figure 1.9 shows one possible inversion mechanism, *via* a planar transition state, but alternative inversion mechanisms have also been shown to exist.[34]

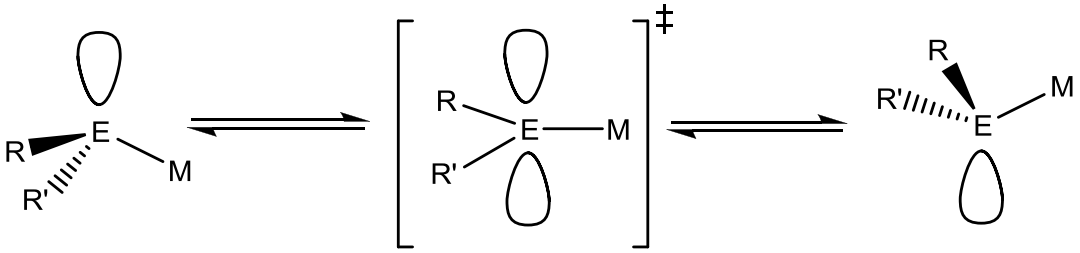

Figure 1.9: Possible inversion mechanism involving a planar intermediate.

The equivalent configurations produced by inversion are referred to as invertomers. If the configurations are mirror images of each other, and thus not super-imposable on one another, they are called enantiomers. Diastereoisomers are non-superimposable invertomers which are not related by reflection. Only non-superimposable invertomers can be distinguished from each other, and to observe individual invertomers in a system undergoing fast pyramidal inversion, the system must be cooled to reduce the energy available and hence slow the inversion relative to the appropriate NMR timescale. Once this is below the activation energy for inversion, the separate invertomers can be distinguished by VT NMR. A number of factors influence the inversion activation energy. The energy required increases down the group, so Te > Se > S. The coalescence temperatures for *trans*-$[PtI_2(EEt_2)_2]$ (E = S, Se, Te)[35,36] illustrate this effect. The presence of a coordinated metal has two major effects. Firstly, the electropositive nature of the metal decreases the *s* character of the non-bonding lone pair. This allows easier access to the transition state, shown in Figure 1.9, in which the inverting lone pair adopts a purely *p* character orbital. Secondly, (*p*-*d*)π coordination may occur between the non-bonding lone pair and the metal centre, which again stabilises the planar transition state. A study of platinum and palladium complexes by Abel et al. also investigated various other factors which lower the inversion barrier.[37] These include the presence of unsaturated substituents,[6] the release of ring strain in chelating ligands in the planar transition state ($-(CH_2)_2- > -o-C_6H_4 > -(CH_2)_3-$)[34] and less electronegative substituents *trans* to the chalcogen.[9,38]

In chelating bidentate acyclic chalcogenoethers there are usually three possible invertomers, shown in Figure 1.10. The *DL* invertomers (enantiomers) are NMR indistinguishable. If there are different ligands above and below the M-E_2 plane, however, the *meso* form splits into two separate forms (one with the substituents above, and one with the substituents below the metal-chalcogen plane) which are not degenerate. The nature of the backbone between chalcogens can also influence the number of invertomers in these situations, as a backbone which sits out of the M-E_2 plane will be spatially closer to one or other of any axial ligands present, resulting in different invertomers.

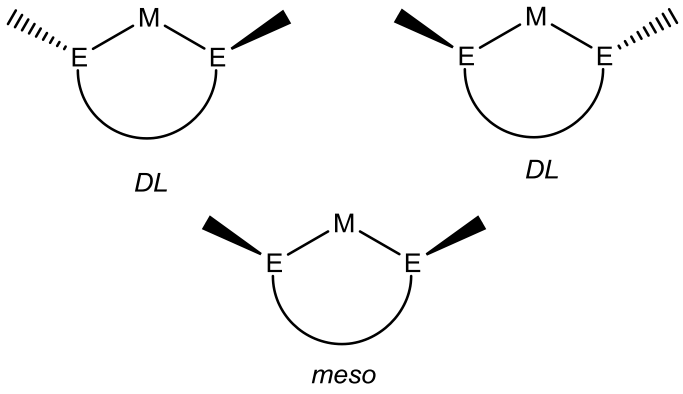

Figure 1.10: Diastereoisomers of a coordinated dichalcogenoether.

1.5 – Chelate and Macrocyclic Effects

Complexes with multidentate ligands are more stable than those containing the same number of equivalent monodentate ligands.[20] This is known as the Chelate Effect, and the size of chelate stabilisation usually increases with the number of chelate rings formed during ligand coordination. The effect is also dependant on the size of the chelate rings, with 5- (most stable) and 6-membered chelate rings offering greatest stabilisation.

The thermodynamic advantage of multidentate ligand (L_n, n = denticity) coordination over that of the equivalent number (n) of monodentate ligands (L) can be seen by observing the equilibrium between the two systems:

$$M(L)_n + L_n \leftrightarrows M(L_n) + n(L)$$

The equilibrium constant (K) associated with this scheme is related to the standard free energy, and therefore the enthalpy and entropy of the reaction by the equations:

$$\Delta G^{\circ} = -RT\,(\ln K)$$

$$\Delta G^{\circ} = \Delta H^{\circ} - T\,\Delta S^{\circ}$$

The direction of the equilibrium is thus dependant on the enthalpic and entropic contributions of the two systems. For ligands involving the same donor atoms, the strength of individual metal-

donor interactions remain relatively independent of ligand denticity and hence the enthalpy terms of each system are comparable. However, considering the entropy of the two systems, it is evident that multidentate ligand coordination leads to more free species and hence greater entropy. The net result is a more negative free energy and therefore greater stabilisation for the multidentate complex.

It is to be expected that a macrocycle of denticity *n*, coordinating to a metal ion will be more stable than the corresponding *n*-dentate open chain ligand, as more chelate rings will be formed. However, greater stabilisation is observed than would be expected for the cumulative chelate stabilisation.[25] This is known as the Macrocyclic Effect.[39] The basis of the thermodynamic stabilisation can be recognised by observing the equilibrium between macrocyclic coordination and that for an analogous open chain ligand of equal denticity:

$$M(L_{chain}) + L_{macrocycle} \leftrightarrows M(L_{macrocycle}) + L_{chain}$$

The entropic contribution is no longer as obvious, as both complexes result in the same number of free species present. The entropic term now comes from the degrees of freedom possible. Open chain ligands potentially possess more rotational and vibrational degrees of freedom when uncoordinated, while the ring structure of macrocycles results in less entropic loss on coordination (as they are inherently more rigid). This increase in entropy has been observed for aza-macrocyclic ligands on coordination with Ni(II),[40] along with a significant enthalpic effect.

The degree of preorganisation present in ligands can also influence the enthalpic contribution, which is mainly governed by solvation effects. Macrocyclic coordination shows maximum stability when there is a very good match between the macrocycle ring size and the size of the metal centre.[20] Similarly, certain ring sizes lead to "free" conformations where the donor atoms are *exo* to the ring (e.g. [14]aneS_4) and therefore require reorganisation prior to coordination. This increases the activation energy to coordination and hence reduces the net enthalpic stabilisation. Solvation effects can also influence the effectiveness of macrocyclic coordination, however, these are only significant for hard donor macrocycles (e.g. O or N), and less important for the soft donor ligands (e.g. S or Se).[25]

1.6 – Uses of Macrocycles

Many important natural compounds involve macrocycles, such as valinomycin, chlorophyll and the heme group in haemoglobin (Figure 1.11), and there are several metal-complexing proteins, whose properties can be studied using macrocyclic ligands which can mimic the coordination set and arrangement on a smaller scale, thus allowing greater analysis than may be possible on the natural system.[20,25]

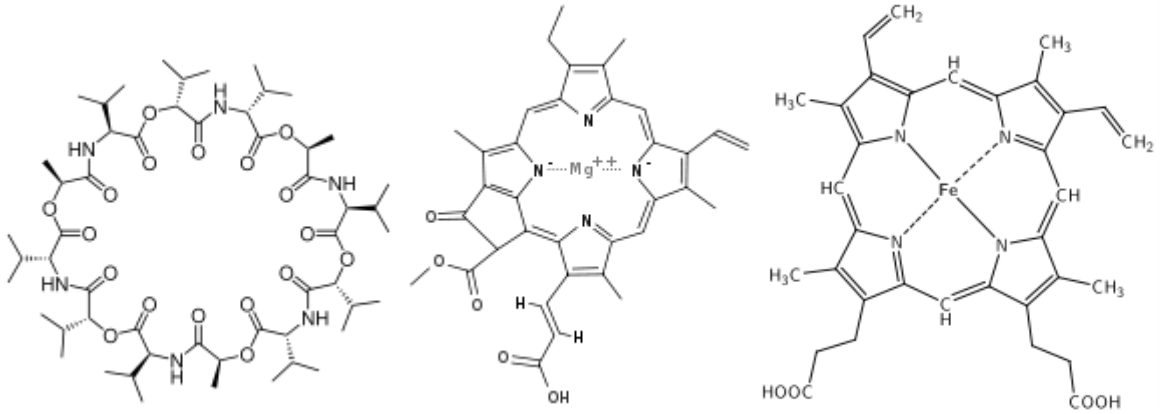

Figure 1.11: Three naturally occurring macrocycles. From left to right: valinomycin, chlorophyll *c1* and a heme group.

Valinomycin shows a strong selectivity towards K^+ ions, and is part of the ion transport system in cells. This possibility of making macrocycles which are highly selective towards different ions (as mentioned briefly in Section 1.2) has also lead to applications in metal extraction from ores, offering more environmentally friendly methods than traditional pyrometallurgy. The strong binding caused by the Macrocyclic Effect (see Section 1.5) allows macrocycles to function well in chelation therapy, to remove harmful metal ions from the human body, or as imaging agents, for instance gadolinium complexes are used in Magnetic Resonance Imaging. The free Gd ion is highly toxic, and must be part of a strongly bound complex to prevent dissociation occurring. The Macrocyclic Effect can also allow the stabilisation of "unusual" oxidation states. For example, $[Pt([9]aneS_3)_2]^{2+}$ has been shown to undergo a reversible electrochemical oxidation to a stable Pt(III) species, but $[Pt([14]aneS_4)]^{2+}$ and $[Pt([18]aneS_6)]^{2+}$ show no similar oxidative activity.[41] The small ring macrocycle $[9]aneS_3$ has been shown to stabilise a range of metals in unusual oxidations states, including Pd(III) obtained from chemical oxidation or electrolysis of $[Pd([9]aneS_3)_2]^{2+}$,[42] Rh(II) obtained from the electrochemical reduction of $[Rh([9]aneS_3)_2]^{3+}$,[43] and Au(II) obtained by reaction of $[9]aneS_3$ with $HAuCl_4$ in HBF_4.[44]

1.7 – Multinuclear NMR (^{77}Se, ^{125}Te, ^{195}Pt)

There is only one NMR active isotope for selenium, ^{77}Se, but there are two NMR active isotopes of tellurium, ^{123}Te and ^{125}Te, both of which are I = ½. However, ^{123}Te is only 0.89% abundant and has low receptivity (0.89 relative to ^{13}C), making ^{125}Te the only practical tellurium nucleus for NMR spectroscopy. Although ^{125}Te has a negative magnetogyric ratio (-8.498 x 10^7 rad T^{-1} s^{-1})[45] proton-tellurium distances are usually so great that the Nuclear Overhauser Effect is normally negligible, and standard spin-½ methods may be used for both ^{77}Se and ^{125}Te nuclei in the majority of cases.

An important feature of ^{77}Se and ^{125}Te NMR spectroscopy is that tellurium and selenium shielding run closely parallel in equivalent compounds, and thus a plot of δ^{125}Te against δ^{77}Se is linear with a gradient of *ca*. 1.8.[46] To some extent, the great sensitivity of δ^{125}Te to electronic changes may be attributed to the larger radial expansion term for tellurium in the paramagnetic nuclear shielding equation given below (where the Q terms denote the imbalance of charge in the valance shell, and ΔE is an effective excitation energy):

$$\sigma_p = -[(\langle r_{5p}^{-3} \rangle)/\Delta E]*\Sigma Q$$

A similar expression exists for Se involving the mean inverse cube of the radius of the 4p orbitals. However, the ratio $\langle r_{5p}^{-3} \rangle$(Te)/ $\langle r_{4p}^{-3} \rangle$(Se) = *ca*. 1.25, which would imply that a still unexplained factor must come from the difference in the ΔE terms.

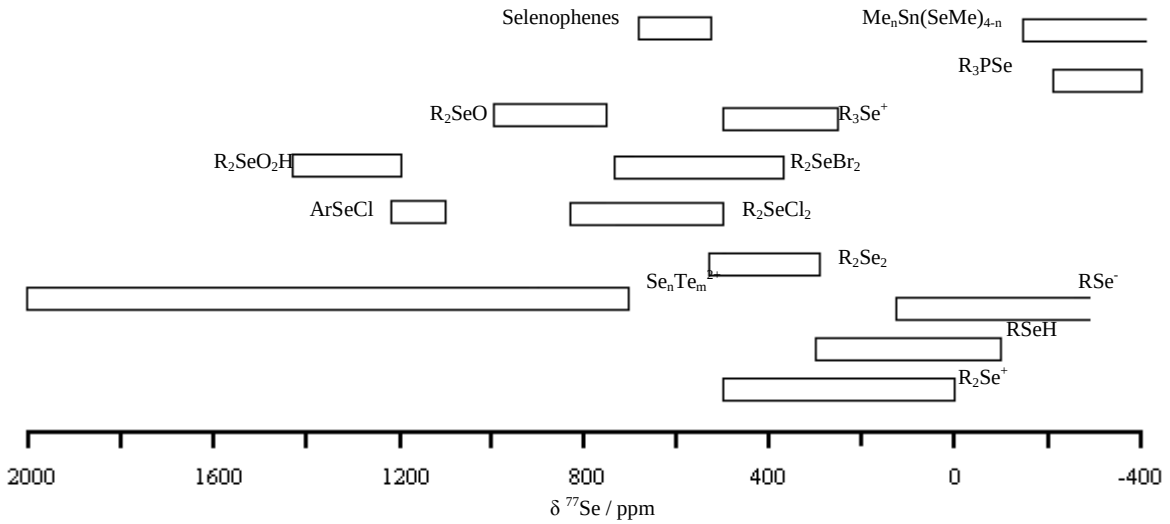

Figure 1.12: Approximate chemical shift ranges for δ^{77}Se.[47]

Several reference compounds have been used in ^{77}Se and ^{125}Te NMR spectroscopy, but it is now generally accepted that Me_2Se and Me_2Te are the most suitable reference materials. It has, however, been found that the chemical shifts of Me_2Se and Me_2Te are relatively sensitive to solvent and concentration and thus all chemical shifts are reported relative to neat samples. In fact, variations of about 10 ppm for ^{77}Se and 20 ppm for ^{125}Te can occur with solvent and temperature for any resonance.[47] ^{77}Se has a shift range of ~3000 ppm (e.g. $Li(SeSiH_3)$ δ = -736 ppm; $Bu_2C{=}Se$ δ = 2131 ppm), while ^{125}Te has a larger range of ~ 4000 ppm (e.g. $Te(SnMe_3)_2$ δ = -1214 ppm; TeI_2 δ = 3219 ppm).

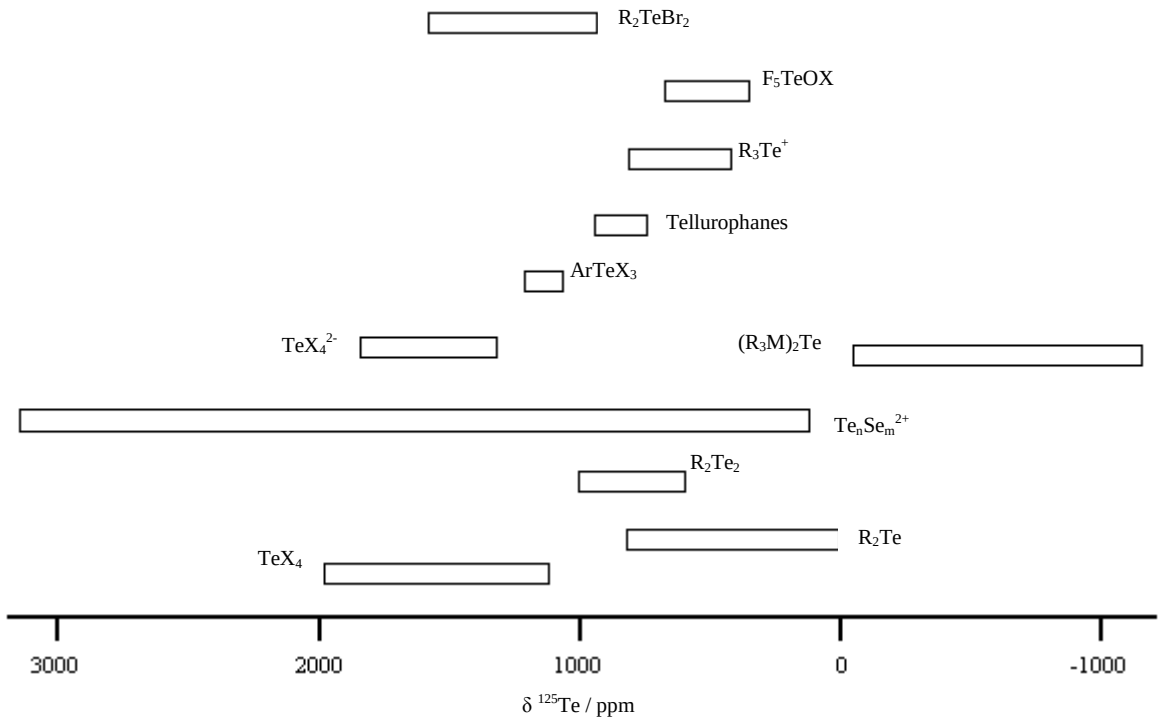

Figure 1.13: Approximate chemical shift ranges for δ^{125}Te.[47]

Platinum has only one NMR active nucleus, ^{195}Pt, which has I = ½, D_c = 19.9 and is 33.8% abundant. It also has rapid relaxation times in fairly asymmetric environments, allowing for fast pulsing rates and thus relatively short acquisition times. The most widely used reference now is aqueous 1 mol dm^{-3} $[PtCl_6]^{2-}$ in D_2O, although older papers may quote shifts relative to Ξ Pt, (reference frequency = 21.4 MHz, δ $[PtCl_6]^{2-}$ = δ (Ξ Pt) – 4533). The chemical shift range for ^{195}Pt is ~12,000 ppm for example, δ ^{195}Pt $[PtF_6]^{2-}$ = 7326, and δ ^{195}Pt $[PtI_6]^{2-}$ = -5120 ppm.[48] This large range of shifts makes it impractical to cover the whole range in a single frequency width; it is vital to make an approximation of the shift beforehand to enable the range window to be set to the correct range. Chemical shifts and coupling constants are very sensitive to both the oxidation state and ligand set around Pt ($PtCl_6^{2-}$ = 0 ppm, $PtCl_4^{2-}$ = -1614 ppm).[49] The geometry of the complex also plays an important role, as *cis* and *trans* isomers can have significantly different chemical shifts ($[PtCl_2(CO)(PEt_3)]$ *cis* = -4207, *trans* = -3840 ppm).[49]

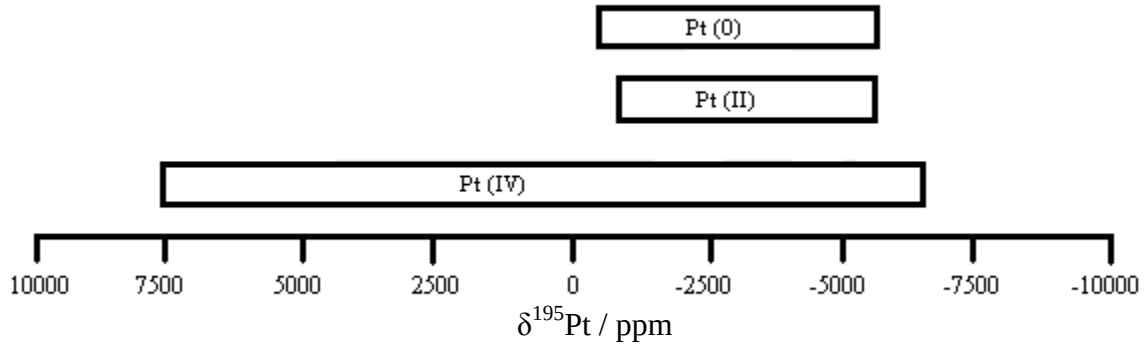

Figure 1.14: Approximate range of δ^{195}Pt (relative to $[PtCl_6]^{2-}$) for different oxidation states.[48]

1.8 – Aims of this Thesis

This work aims to increase the knowledge of chalcogenoether systems, with the emphasis on macrocyclic selenoethers. To this end, Chapters 2 and 6 examine new acyclic complexes with Pt(II) and Pt(IV) (Chapter 2) and with Co(II) (Chapter 6), investigating especially the possibility of stable 7-membered chelate rings using xylyl backbones. Chapter 2 also investigates the properties of some known selenoether macrocycles in new dimethyl Pt(II) and Pt(IV) complexes. Chapter 3 details the production of new mixed donor macrocycles of the type O_xSe_{2x} with a variety of backbones and explores complexation chemistry of these new macrocycles with some selected transition metals.

Chapter 4 investigates high yielding, multi-gram production of new Se_2N and Se_3 macrocycles. Chapters 5 and 6 deal with coordination chemistry of these new macrocycles, investigating Pt(IV) in Chapter 5, as there are a large number of known acyclic Pt(IV) selenoether complexes for comparison, and Cr(III) and V(III) in Chapter 6 as it is hoped that the macrocyclic effect will improve stability of the soft selenoethers towards the hard metals. The presence of the hard O and pyridyl N donors may also increase stability.

1.9 – References

1. Emsley, J. *Nature's Building Blocks*, Oxford University Press, 2001.
2. Levason, W.; Reid, G. In: *Comprehensive Co-ordination Chemistry II*, Vol. 1, Elsevier Ltd., 2003, 391 – 398.
3. Blake, A. J.; Schröder, M. In: *Advances in Inorganic Chemistry,* Academic Press, Inc., San Diego, 1990, 1 – 80.
4. Cooper, S. R.; Rawle, S. C. *Struct. Bonding* (Berlin) **1990**, *72*, 1 – 72.
5. Hope, E. G.; Levason, W. *Coord. Chem. Rev.* **1993**, *122*, 109 – 170.
6. Levason, W.; Orchard, S. D.; Reid, G. *Coord. Chem. Rev.* **2002**, *225*, 159 – 199.
7. Panda, A. *Coord. Chem. Rev.* **2009**, *253*, 1056 – 1098.
8. Panda, A. *Coord. Chem. Rev.* **2009**, *253*, 1947 – 1965.
9. Hartley, F. R.; Levason, W.; McAuliffe, C. A.; Murray, S. G.; Soutter, H. E. *Inorg. Chim. Acta* **1979**, *35*, 265 – 277.
10. Kemmitt, T.; Levason, W. *Organometallics* **1989**, *8*, 1303 – 1308.
11. Murray, S. G.; Hartley, F. R. *Chem. Rev.* **1981**, *81*, 365 – 414.
12. Gulliver, D. J.; Hope, E. G.; Levason, W.; Murray, S. G.; Potter, D. M.; Marshall, G. L. *J. Chem. Soc., Perkin Trans. II* **1984**, 429 – 434.
13. Aysnley, E. E.; Greenwood, N. N.; Leach, J. B. *Chem. Ind.* **1966**, 379 – 380.
14. Hope, E. W.; Kemmitt, T.; Levason, W. *J. Chem. Soc., Perkins Trans. II* **1987**, 478 – 490.
15. Levason, W.; Ollivere, L. P.; Reid, G.; Tsoureas, N.; Webster, M. *J. Organomet. Chem.* **2009**, *694*, 2299 – 2308.
16. Levason, W.; Nirwan, M.; Ratnani, R.; Reid, G.; Tsoureas, N.; Webster, M. *Dalton Trans.* **2007**, 439 – 448.
17. Barton, A. J.; Levason, W.; Reid, G.; Ward, A. J. *Organometallics* **2001**, *20*, 3644 – 3649.
18. Hope, E. G.; Kemmitt, T.; Levason, W. *Organometallics* **1988**, *7*, 78 – 83.
19. Levason, W.; Patel, B.; Reid, G.; Ward, A. J. *J. Organomet. Chem.* **2001**, *619*, 218 – 225.
20. Constable, E. C. *Coordination Chemistry of Macrocyclic Compounds*, Oxford University Press, 1999.
21. Ochrymowycz, L. A.; Mak, C-P.; Michna, J. D. *J. Org. Chem.* **1974**, *39*, 2079 – 2084.
22. Rosen, W.; Busch, D. H. *J. Am. Chem. Soc.* **1969**, 4694 – 4697.
23. Travis, K.; Busch, D. H. *Inorg. Chem.* **1974**, *11*, 2591 – 2598.
24. Hojjatie, M.; Muralidharan, S.; Freiser, H. *Tetrahedron* **1989**, *45*, 1611 – 1622.

25. Lindoy, L. F. *The Chemistry of Macrocyclic Ligand Complexes*, Cambridge University Press, 1989.

26. Sellmann, D.; Zapf, L. *J. Organomet. Chem.* **1985**, *289*, 57 – 69.

27. Chatt, J. *Nature* **1950**, *165*, 637.

28. Orpen, A. G.; Connelly, N. G.; *J. Chem. Soc., Chem. Commun.* **1985**, 1310 – 1311.

29. Mullen, G. E. D.; Fassler, T. F.; Went, M. J.; Howland, K.; Stein, B.; Blower, P. J. *J. Chem. Soc., Dalton Trans.* **1999**, 3759 – 3766 and references therein.

30. Schumann, H.; Arif, A. M.; Rheingold, A. L.; Janiak, C.; Hoffmann, R.; Kuhn, N. *Inorg. Chem.* **1991**, *30*, 1618 – 1625.

31. Levason, W.; Orchard, S. D.; Reid, G. *Organometallics* **1999**, *18*, 1275 – 1280.

32. Levason, W.; Orchard, S. D.; Reid, G. *J. Chem. Soc., Dalton Trans.* **1999**, 823 – 824.

33. Levason, W.; Orchard, S. D.; Reid, G.; Street, J. M. *J. Chem. Soc., Dalton Trans.* **2000**, 2537 – 2543.

34. Abel, E. W.; Bhargava, S. K.; Orrell, K. G. *Prog. Inorg. Chem.* **1984**, *32*, 1 – 118.

35. Cross, R. J.; Green, T. H.; Keat, R. *J. Chem. Soc., Chem. Commun.* **1974**, 207 – 208.

36. Cross, R. J.; Green, T. H.; Keat, R. *J. Chem. Soc., Dalton Trans.* **1976**, 1150 – 1152.

37. Abel, E. W.; Bhargavam S. K.; Kite, K.; Orrell, K. G.; Šik, V.; Williams, B. L. *Polyhedron* **1982**, *1*, 289 – 298.

38. Cooke, J.; Green, M.; Stone, F. G. A. *J. Chem. Soc. (A)* **1968**, 170 – 173.

39. Cabbiness, D. K.; Margerum, D. W. *J. Am. Chem. Soc.* **1969**, *91*, 6540 – 6541.

40. Micheloni, M.; Paoletti, P.; Sabatini, A. *J. Chem. Soc., Dalton Trans.* **1983,** 1189 – 1192.

41. Blake, A. J.; Gould, R. O.; Holder, A. J.; Hyde, T. I.; Lavery, A. J.; Odulate, M. O.; Schröder, M. *J. Chem. Soc., Chem. Commun.* **1987**, 118 – 120.

42. Blake, A. J.; Holder, A. J.; Hyde, T. I.; Roberts, Y. V.; Lavery, A. J.; Schröder, M. *J. Organomet. Chem.* **1987**, *323*, 261 – 270.

43. Blake, A. J.; Gould, R. O.; Holder, A. J.; Hyde, T. I.; Schröder, M. *J. Chem. Soc., Dalton Trans.* **1988**, 1861 – 1865.

44. Shaw, J. L.; Wolowska, J.; Collison, D.; Howard, J. A. K.; McInnes, E.; McMaster, J.; Blake, A. J.; Wilson, C.; Schröder, M. *J. Am. Chem. Soc.* **2006**, *128*, 13827 – 13839.

45. Fuller, G. H. *J. Phys. Chem. Ref. Data 5*, **1976**, 835 – 1092.

46. Luthra, N. P.; Odom, J. D. In: *The Chemistry of Organic Selenium and Tellurium Compounds*, Wiley, New York, 1986, 189 – 241.

47. McFarlane, H. C. E.; McFarlane, W. In: *Multinuclear NMR*, Plenum, 1987, 417 – 435.

48. Still, B. M.; Kumar, P. G. A.; Aldrich-Wright, J. R.; Price, W. S. *Chem. Soc. Rev.* **2007**, *36*, 665 – 686.

49. Pregosin, P. S. *Coord. Chem. Rev.* **1982**, *44*, 247 – 291.

Chapter 2: Alkyl Platinum (II) and (IV) Complexes with Acyclic Seleno- and Telluroethers and Macrocyclic Selenoethers[1]

2.1 – Introduction

There are many known Pt(II) complexes with seleno- and telluroethers, but these are mostly dihalide complexes, with some examples of homoleptic chalcogenoether co-ordination. $[PtCl_2L_2]$ (L = $RSeCH_2SeR$, R = Me, Ph) can be made by reaction of $K_2[PtCl_4]$ or $[PtCl_2(MeCN)_2]$ with L in a 1:2 ratio. The 1:1 complexes $[(PtLCl_2)_n]$ form as a by-product, but can be easily separated due to their insolubility in common solvents.[2] The 2:1 complexes both have vibrational spectra consistent with a *cis* geometry in the solid state, but in solution $[PtCl_2(PhSeCH_2SePh)_2]$ shows a mixture of *cis/trans* isomers (Figure 2.1), while $[PtCl_2(MeSeCH_2SeMe)_2]$ shows only the *trans* isomer.[2]

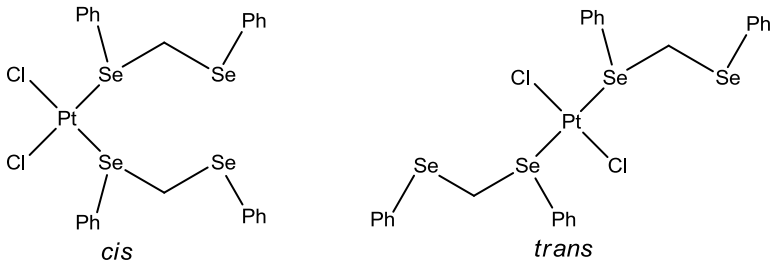

Figure 2.1: Structural diagrams of $[PtCl_2(PhSeCH_2SePh)_2]$ showing *cis* and *trans* isomers.

Complexes of the type $[PtX_2(L\text{-}L)]$ (X = Cl, Br, I) have been produced for a range of bidentate selenoether ligands by reaction of $[PtX_2(MeCN)_2]$ or $[PtX_4]^{2+}$ with the appropriate chalcogenoether (L-L = $RSe(CH_2)_2SeR$ (R = Me, Ph), MeSeCH=CHSeMe, $MeSe(CH_2)_3SeMe$, *o*-$C_6H_4(SeMe)_2$).[3] These complexes all have *cis* planar structures with the selenoether coordinating in a bidentate manner, are all very slightly soluble in chlorocarbons, and are more (though still poorly) soluble in dmso.[3] Reaction of the cyclic selenoether [8]aneSe_2 with $[PtCl_2(MeCN)_2]$ in refluxing MeCN produces $[PtCl_2([8]aneSe_2)]$ as a poorly soluble white solid.[4] Addition of two equivalents of $TlPF_6$ to $[PtCl_2(MeCN)_2]$ and two equivalents of $MeSe(CH_2)_3SeMe$,[5] *o*-$C_6H_4(CH_2SeMe)_2$[6] or [8]aneSe_2[4] generates the homoleptic complexes $[Pt(L\text{-}L)_2](PF_6)_2$. Reaction of $K_2[PtCl_4]$ in water with $MeC(CH_2SeMe)_3$ in EtOH yields $[PtCl_2(MeC\{CH_2SeMe\}_3)]$ as a yellow solid, while a similar reaction with $Se(CH_2CH_2CH_2SeMe)_2$ gives only an intractable oil. Addition of $NaPF_6$, however, allows the isolation of $[PtCl(Se\{CH_2CH_2CH_2SeMe\}_2)]PF_6$ as a yellow crystalline solid. Both these complexes are poorly soluble.[7] The steric constraints of $MeC(CH_2SeMe)_3$ prevent tridentate coordination to a square planar metal, however use of two equivalents of $TlPF_6$ and $MeC(CH_2SeMe)_3$ allows the production of $[Pt(MeC\{CH_2SeMe\}_3)_2](PF_6)_2$ as a stable, pale yellow solid. The crystal structure of $[Pt(MeC\{CH_2SeMe\}_3)_2](PF_6)_2$ (Figure 2.2) shows the bidentate

coordination of two selenoether tripods in a square planar geometry, with the uncoordinated arms pointing away from the platinum centre.[8]

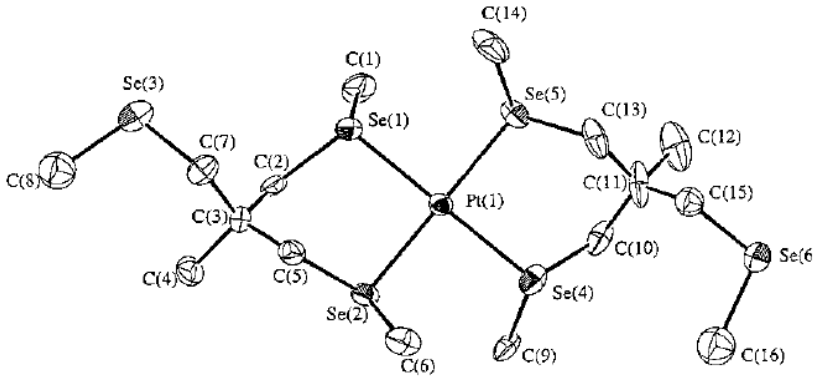

Figure 2.2: Crystal structure of $[Pt(MeC\{CH_2SeMe\}_3)_2]^{2+}$. Ellipsoids shown at 40 % probability, H atoms omitted for clarity.[8]

There is one example of a tetradentate macrocyclic selenoether in homoleptic coordination on Pt(II). Reaction of one equivalent of [16]aneSe_4 with $[PtCl_2(MeCN)_2]$ and two equivalents of $TlPF_6$ affords $[Pt([16]aneSe_4)](PF_6)_2$ as colourless crystals. The crystal structure of this complex shows the macrocycle to adopt an *up, up, down, down* configuration.[5]

A series of monodentate telluroether ligands have been reacted with $[PtX_2(MeCN)_2]$ (X = Cl, Br, I) to produce $[PtX_2L_2]$ (L = $TeMe_2$, $TePh_2$, TePhMe).[9] $^{125}Te\{^1H\}$ and $^{195}Pt\{^1H\}$ NMR spectroscopic studies of these complexes have shown them to be a mixture of *cis* and *trans* isomers in solution for the dichloro and dibromo complexes, but the diiodo complexes were purely the *cis* isomer in solution.[9] Attempts to produce $[PtCl_2L]$, where L is either of the C_1 linked ditelluroethers $MeTeCH_2TeMe$ or $PhTeCH_2TePh$, from $[PtCl_2(MeCN)_2]$ result in the formation of insoluble $[(PtLCl_2)_n]$, even with a large excess of ligand present.[2] Reaction of $[PtX_2(MeCN)_2]$ (X = Cl, Br) with one equivalent of ditelluroether in CH_2Cl_2 produces $[PtX_2L]$ in good yield (L = $RTe(CH_2)_3TeR$, R = Me, Ph;[9] *o*-$C_6H_4(TeMe)_2$).[9] The analogous diiodo complexes were made by reaction of $[Na_2PtCl_4]$ with NaI in EtOH, followed by addition of ditelluroether to yield $[PtI_2L]$.[9,10] Even with addition of a large excess of ligand, only the 1:1 complexes were formed. In the case of the xylyl backbone ditelluroether *o*-$C_6H_4(CH_2TeMe)_2$, only the dichloride Pt(II) complex has been reported.[11] All these Pt(II) complexes with ditelluroethers are poorly soluble in chlorocarbons, and though they are more soluble in dmso, decomposition occurs in dmso solutions over time.[10]

As with the analogous triselenoether, reaction of the tritelluroethers $Te(CH_2CH_2CH_2TeR)_2$ (R = Me, Ph) with $[PtCl_2(MeCN)_2]$ gives no identifiable products, but use of one molar equivalent of $TlPF_6$ to abstract chloride allows production of $[PtCl(Te\{CH_2CH_2CH_2TeR\}_2)]PF_6$ in which the

telluroether binds to planar Pt(II) through all three donor atoms.[12] Reaction of $[PtCl_2(MeCN)_2]$ with two equivalents of the tridentate telluroethers $MeC(CH_2TeR)_3$ (R = Me, Ph) and $TlPF_6$ affords the homoleptic complexes $[Pt(MeC\{CH_2TeR\}_3)_2](PF_6)_2$ in moderate yield, wherein the tripodal telluroether binds in a bidentate fashion. $[Pt(MeC\{CH_2TeMe\}_3)_2](PF_6)_2$ is unstable in solution, decomposing over a few hours.[8] Using two equivalents of $TlPF_6$ and ditelluroether with $[PtCl_2(MeCN)_2]$ produces complexes of the type $[Pt(L\text{-}L)_2](PF_6)_2$ (L-L = *o*-$C_6H_4(TeMe)_2$,[13] $RTe(CH_2)_3TeR$ (R = Me, Ph),[13] *o*-$C_6H_4(CH_2TeMe)_2$).[11] These homoleptic complexes are more soluble than the analogous dichloride complexes.[11]

Whilst a range of late TM halide and homoleptic seleno-/ telluroether complexes have been reported, examples involving organometallic fragments are rare. The only reported examples are of Pt(II) complexes with mixed halide/methyl co-ligands are $[PtXMe(MeSe\{CH_2\}_2SeMe)]$ (X = Cl, Br, I).[14] These were produced by refluxing [PtXMe(cod)] with excess $MeSe(CH_2)_2SeMe$ in chloroform. After recrystallisation, the complexes were isolated as orange solids. These were produced as part of an NMR spectroscopic investigation in to pyramidal inversion at chalcogen donors, and showed that selenoether complexes have a higher inversion energy than the corresponding thioether complexes.[14]

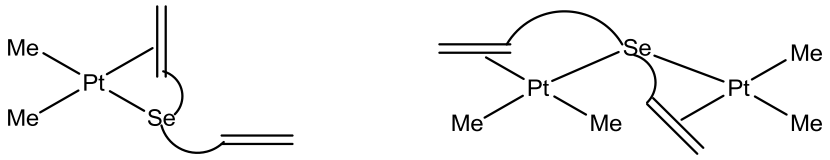

Figure 2.3: Simplified structures of $[PtMe_2\{Se(CH_2CH_2CH{=}CH_2)_2\}]$ (left) and $[Pt_2Me_4\{\mu\text{-}Se(CH_2CH_2CH{=}CH_2)_2\}]$ (right).

There are only two known dimethylplatinum(II)-selenoether complexes, $[PtMe_2\{Se(CH_2CH_2CH{=}CH_2)_2\}]$ and $[Pt_2Me_4\{\mu\text{-}Se(CH_2CH_2CH{=}CH_2)_2\}]$. They are produced by reaction of 0.5 or 1 molar equivalents of $Se(CH_2CH_2CH{=}CH_2)_2$ with $[PtMe_2(SMe_2)_2]$ generated *in situ* from $[PtCl_2(SMe_2)_2]$ and MeLi.[15] The ligand co-ordinates through both the selenium and through either one (monomer) or both (dimer) of the alkene moieties (Figure 2.3). A crystal structure has been reported for the dimer, showing the two square planar Pt moieties to be folded in towards each other at the bridging Se.[15] With the analogous telluroether, $Te(CH_2CH_2CH{=}CH_2)_2$, dichloro and dibromoplatinum(II) complexes have been reported from reaction with $[PtX_2(SMe_2)_2]$ in non-aqueous solvents at low temperature.[16] These complexes are poorly soluble and unstable in solution and no alkylplatinum(II) telluroether complexes are known.

Abel and Orrell collected a large amount of data on Pd/Pt(II) halides with chalcogens whilst investigating pyramidal inversion rates.[14] Abel et al. investigated Pt(IV) complexes with a range of

bidentate thio- and selenoethers in the 1980's. With selenoether ligands, a series of Pt(IV) trimethyl halide complexes was produced, featuring both mononuclear ([$PtMe_3X(L\text{-}L)$], X = Cl, Br, I; L-L = $MeSe(CH_2)_nSeMe$, n = 2, 3,[17,18] MeSeCH=CHSeMe[19]) and dinuclear Pt coordination ([$(PtMe_3X)_2(MeSe\{CH_2\}_nSeMe)$], X = Cl, Br, I, n= 0; X = Cl, Br, n = 1).[20] The complexes were made by dissolving [$(PtXMe_3)_4$] in chloroform, adding excess ligand and stirring at room temperature for 1-2 hours. The reaction mixture is then concentrated and light petroleum added to precipitate the products. The complexes are white or yellow crystalline solids after recrystallisation, and are stable both in air, and in solution. Excess ligand does not affect the stoichiometry of the complexes formed, with $MeSe(CH_2)_nSeMe$ (n = 2, 3) only giving 1:1 L:Pt complexes, never 2:1 L:Pt, while the dinuclear complexes likewise never show evidence of mononuclear species.[20]

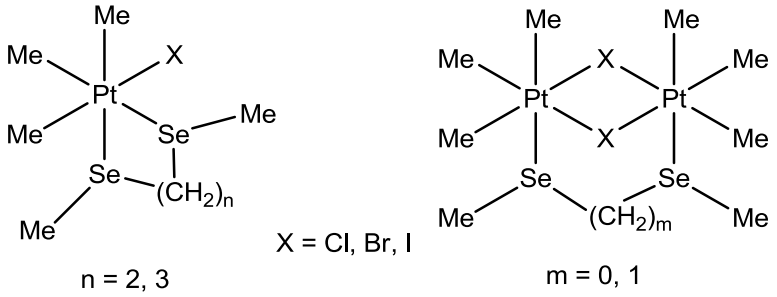

Figure 2.4: Mononuclear and dinuclear Pt(IV) species produced by Abel et al.[17,18,20]

While the principle aim of these works was the use of VT ^1H NMR data to calculate invertomer populations and pyramidal inversion barriers in the mononuclear species, ^{13}C, ^{77}Se and ^{195}Pt NMR data have also been reported for many of these complexes.[18] VT ^1H NMR spectroscopic studies found that the inversion rates in these Pt(IV) complexes are extremely fast compared to those found in selenoxides, and that the activation energy for inversion at Se is 9 – 12 kJ mol^{-1} higher than in analogous S complexes. The nature of the halide ligand was found to have little to no effect on barrier energies.[17] Introduction of an olefinic backbone decreases the activation energy by 9 – 15 kJ mol^{-1}.[19]

Crystal structures have been reported for [$PtMe_3X(MeSeCH=CHSeMe)$] (X = Cl, I) and illustrate the effect of the halide on the stereochemistry of the ligand. Where X = Cl, the crystal structure shows the methyl groups on the selenoether oriented towards the same side of the Me_2-Pt-Se_2 as the halide, but when X = I (Figure 2.5) they are on the opposite side. This is due to the larger halide preferring the less sterically crowded conformation.[19]

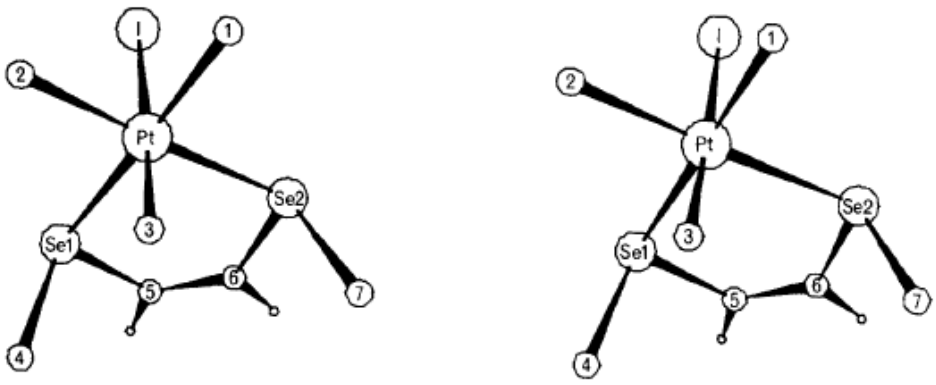

Figure 2.5: Stereoview of X-ray crystal structure of $[PtMe_3I(MeSeCH=CHSeMe)]$.[19]

A cationic trimethyl Pt(IV) complex has been reported, with the facultative tridentate ligand $Se(CH_2CH_2SeMe)_2$. This was made by reaction of $[(PtMe_3)_2SO_4]\cdot 4H_2O$ and $Se(CH_2CH_2SeMe)_2$ in acetone, followed by addition of $NaBF_4$ producing $[PtMe_3(Se\{CH_2CH_2SeMe\}_2)]BF_4$ as a white solid. NMR spectroscopy revealed the selenoether to be coordinated in a *fac* geometry.[21] The only reported Pt(IV) complexes with a selenoether macrocycle are $[PtX_2([16]aneSe_4)](PF_6)_2$ (X = Cl, Br), which are produced by oxidative addition of X_2 to the Pt(II) complex $[Pt([16]aneSe_4)](PF_6)_2$ in CCl_4/MeCN.[22]

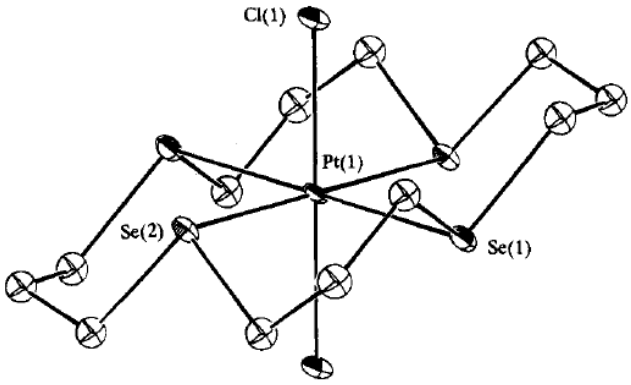

Figure 2.6: Crystal structure of $[PtCl_2([16]aneSe_4)]^{2+}$ showing *up,up,down,down* configuration. H atoms omitted for clarity.[22]

The only previously reported Pt(IV) complexes with ditelluroether ligands are $[PtMe_3I(o\text{-}C_6H_4\{TeMe\}_2)]$ and $[PtMe_3I(RTe\{CH_2\}_3TeR)]$ (R = Me, Ph) made by reaction of the telluroether and $[PtMe_3I]$ in $CHCl_3$.[23] They have been analysed by VT multinuclear NMR with the focus of the work on pyramidal inversion barrier calculations. By changing the inverting atom from Se to Te, the pyramidal energy barrier increases by ~12 kJ mol^{-1}.[23]

2.2 – Aims of this Chapter

The purpose of this chapter is to investigate a new series of dimethylPt(II) complexes with acyclic diselenoether and ditelluroether ligands and with selenoether macrocycles, and a new series of

Pt(IV) species with seleno- and telluroether ligands. The possibility of redox behaviour in these complexes will also be investigated.

2.3 – Ligand Syntheses

The ligands used in this chapter were all made by literature methods. MeELi (E = Se, Te) is made by addition of MeLi to the elemental chalcogen in thf at 77 K. Allowing this to warm to room temperature and stirring for one hour produces a clear solution of MeELi. The saturated ligands $MeSe(CH_2)_nSeMe$ (n = 1, 2, 3) are made by the addition of 0.5 molar equivalent of the appropriate α,ω-dihaloalkane.[24] The xylyl ligands *o*-$C_6H_4(CH_2EMe)_2$ are made in good yield from MeELi and 0.5 molar equivalent *o*-$C_6H_4(CH_2Br)_2$. The diselenoether is produced by addition of *o*-$C_6H_4(CH_2Br)_2$ at room temperature,[6] while production of the ditelluroether requires the MeTeLi being refrozen to 77 K before addition of *o*-$C_6H_4(CH_2Br)_2$.[11] $MeTe(CH_2)_3TeMe$ is made similarly from reaction of refrozen MeTeLi and 0.5 molar equivalents $Br(CH_2)_3Br$.[25] The ditelluromethane, $MeTeCH_2TeMe$, was produced by reaction of refrozen MeTeLi and excess CH_2Cl_2.[25] The tripodal ligand $MeC(CH_2SeMe)_3$ was produced from reaction of 6 molar equivalents MeSeLi with $MeC(CH_2Br)_3$.[24] [8]aneSe_2 and [16]aneSe_4 were produced by reaction of $NCSe(CH_2)_3SeCN$ with Na in $NH_{3\,(l)}$ at -45°C, followed by addition of $Br(CH_2)_3Br$. After hydrolysis and extraction with CH_2Cl_2, pure samples of the macrocycles were obtained by distillation ([8]aneSe_2) and subsequent column chromatography ([16]aneSe_4, eluent 19:1 hexane:ethyl acetate).[26]

Table 2.1: ^{77}Se and ^{125}Te NMR spectroscopic shifts for ligands used in this chapter. Data from samples in $CH_2Cl_2/CDCl_3$.

Ligand	δ ^{77}Se / ppm	δ ^{125}Te / ppm
$MeSeCH_2SeMe$	117	-
$MeSe(CH_2)_2SeMe$	121	-
$MeSe(CH_2)_3SeMe$	74	-
o-$C_6H_4(CH_2SeMe)_2$	149	-
$MeC(CH_2SeMe)_3$	23	-
[8]aneSe_2	134	-
[16]aneSe_4	158	-
$MeTeCH_2TeMe$	-	212
$MeTe(CH_2)_3TeMe$	-	104
o-$C_6H_4(CH_2TeMe)_2$	-	264

2.4 – Novel Dimethyl Platinum(II) Complexes

$[PtMe_2([9]aneS_3)]$ is produced from reaction of [9]aneS_3 with $[PtMe_2(cod)]$ in refluxing acetonitrile.[27] $[PtMe_2(Ph_2Sb(CH_2)_3SbPh_2)]$ is produced similarly from $[PtMe_2(cod)]$ in toluene.[28]

However, initial attempts to produce dimethylPt(II) selenoether complexes by refluxing a bidentate selenoether such as $MeSe(CH_2)_3SeMe$ with $[PtMe_2(cod)]$ in $CHCl_3$ showed substitution of cod by selenoethers to be difficult and yield incomplete substitution, so a more labile ligand such as Me_2S was required. The initial Pt(II) species $[PtCl_2(SMe_2)_2]$ was produced from reaction of K_2PtCl_4 and dimethyl sulfide in distilled water. The mixture of pink and yellow precipitates was heated for ca. 30 minutes until all the precipitate was yellow.[29] Successful production of this precursor was confirmed by ^1H NMR spectroscopy. This compound was then reacted with two molar equivalents of MeLi in diethyl ether at low temperature. Water was added to quench the reaction, and one molar equivalent of $MeSe(CH_2)_2SeMe$ were then added at room temperature and the two-phase reaction stirred for 2.5 hours. The precipitate was filtered off and washed with Et_2O, then redissolved in CH_2Cl_2, filtered and the solvent was removed *in vacuo*. The yellow solid thus obtained was analysed by ES^+ MS, ^1H, $^{13}C\{^1H\}$, $^{77}Se\{^1H\}$ and ^{195}Pt NMR spectroscopy and microanalysis. ^1H NMR spectroscopy showed two Pt-Me environments, with $^2J_{Pt\text{-}H}$ coupling indicative of Me *trans* Se (~84 Hz). The $^3J_{PtH}$ coupling observed on the Se-Me groups (~21 Hz) was also consistent with the ligand chelating in a *cis* fashion. ^{77}Se NMR spectroscopy showed two selenium environments, both with $^1J_{Pt\text{-}Se}$ coupling, and the ^{195}Pt NMR spectrum also showed two platinum environments. The observance of two resonances in each spectrum can be explained by the presence of two invertomers, *meso* and *DL*, as predicted from pyramidal inversion arguments (see Chapter 1). $MeSe(CH_2)_3SeMe$ was similarly reacted with $[PtCl_2(SMe_2)_2]$. The resulting yellow solid was analysed by ES^+ MS, ^1H, $^{13}C\{^1H\}$, $^{77}Se\{^1H\}$ and ^{195}Pt NMR spectroscopy and microanalysis which confirmed the formulation as planar $[PtMe_2(MeSe\{CH_2\}_3SeMe)]$ with the selenoether chelating in a bidentate fashion. Figure 2.7 shows the ^{77}Se NMR spectrum, showing two selenium environments at δ = 102 and 114 ppm (free ligand δ = 74 ppm). $^1J_{Pt\text{-}Se}$ couplings of 429 and 427 Hz respectively are also observed.

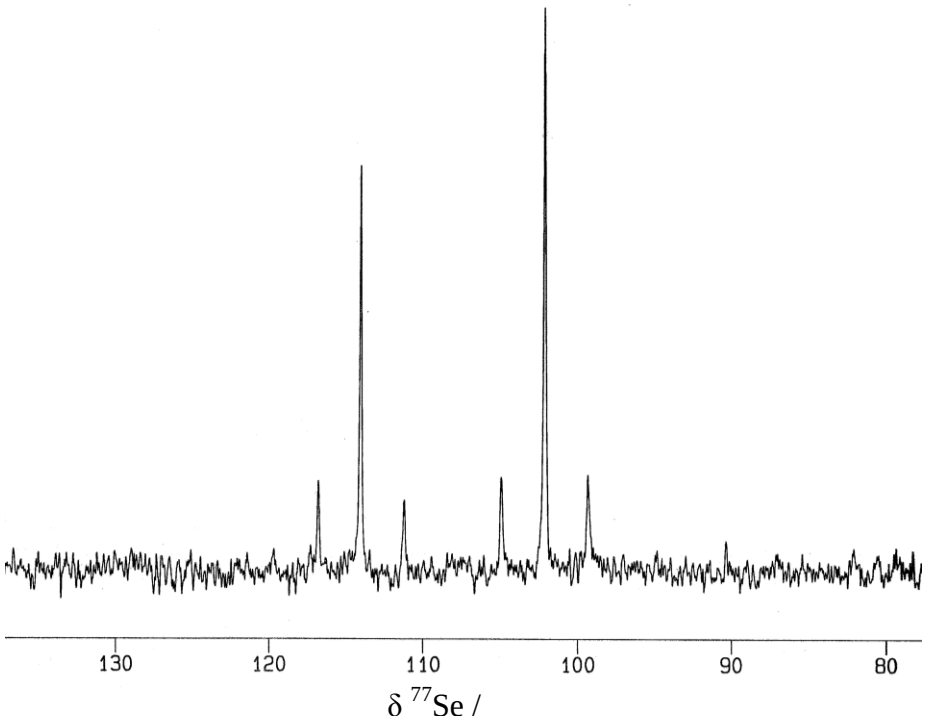

Figure 2.7: $^{77}Se\{^{1}H\}$ NMR spectrum of [$PtMe_2$(MeSe{CH_2}$_3$SeMe)] recorded in CH_2Cl_2/$CDCl_3$ at 243 K.

Recent work in this group has established that despite the seven-membered ring chelate, incorporation of the *o*-xylyl linkage in a range of ligand types (diphosphane, distibane, ditelluroether) leads to an increased tendency towards *cis*-chelation compared to aliphatic C_4-linked analogues. These have been shown to be very effective ligands for a range of transition metal ions, for example complexes of *o*-$C_6H_4(CH_2TeMe)_2$ are known with Mn, Mo, W, Pt, Pd, Rh, Ru, Os, Cu, and Ag.[6,11] The distibine *o*-$C_6H_4(CH_2SbMe_2)_2$ has also been shown to form stable alkyl Pt complexes, with a crystal structure of [$PtMe_3I$(*o*-C_6H_4{CH_2SbMe_2}$_2$)] having been reported.[28]

[$PtMe_2$(*o*-C_6H_4{CH_2SeMe}$_2$)] was produced in good yield from the reaction of [$PtCl_2(SMe_2)_2$], MeLi and one molar equivalent of *o*-$C_6H_4(CH_2SeMe)_2$ as detailed above. The resulting cream solid turned out to be unstable in solution in chlorinated solvents, decomposing after a few hours, and poorly soluble in non-chlorinated solvents. All of the dimethylPt(II) selenoether complexes showed this instability – the solids deteriorate with significant darkening of the powders over a period of days to weeks even when stored under N_2 in a dry glove box. Substantial sample degradation was clearly evident from the NMR spectra recorded after standing in solution for a few hours. Data quoted were therefore recorded from freshly prepared samples. The related halide complexes [PtX_2(L-L)] (X = Cl, Br, I; L-L = $MeSe(CH_2)_2SeMe$, $MeSe(CH_2)_3SeMe$, *o*-$C_6H_4(SeMe)_2$) are all very poorly soluble in chlorocarbon solvents and acetonitrile. Data for these

complexes was obtained from solutions in dmso.[3] The low solubility and stability of these dimethylPt(II) complexes also hindered attempts to obtain crystal structures, as dilute solutions left to crystallise tended to decompose before crystals appeared.

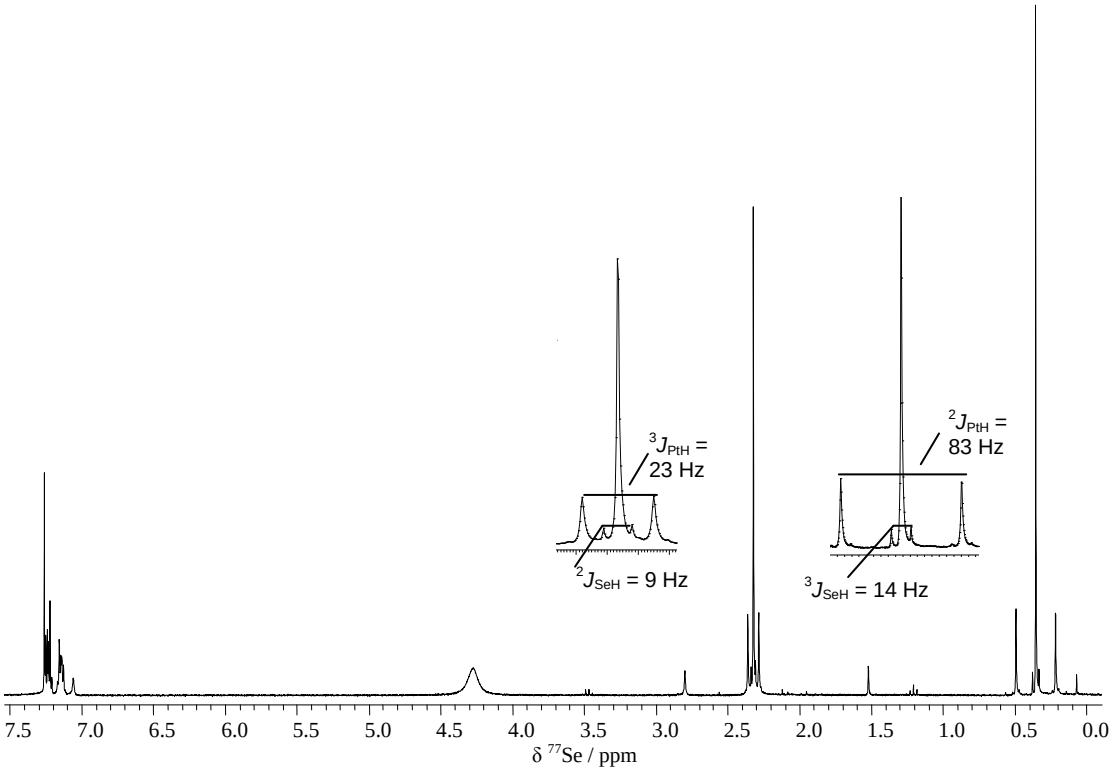

Figure 2.8: ^{1}H NMR spectrum of [$PtMe_2$(*o*-C_6H_4{CH_2SeMe}$_2$)] recorded in $CDCl_3$ at 298 K showing fast pyramidal inversion.

Figure 2.8 shows the room temperature ^{1}H NMR spectrum of [$PtMe_2$(*o*-C_6H_4{CH_2SeMe}$_2$)]. The Pt-H coupling on methyl groups on both Pt and Se is clearly visible. These coupling constants help confirm the stereochemistry of the complex, as the values are in the range expected for PtMe *trans* to Se. The resonance associated with the CH_2 protons is observed as a broad peak, indicating rapid pyramidal inversion is occurring. Low temperature ^{1}H NMR spectroscopy (213 K) resolved this, with a *meso* and *DL* forms of this complex clearly visible. The *meso* form has one δ^{77}Se resonance with ^{195}Pt satellites (δ = 160.6) and one δ^{195}Pt resonance (δ = –4308), while the *DL* form results in two δ^{77}Se resonances of equal intensity, each with ^{195}Pt satellites (δ = 169.1, 155.9) and one δ^{195}Pt resonance (δ = –4316).

Figure 2.9 shows the different invertomers possible for this complex. The d^8 Pt(II) ion characteristically prefers a square planar geometry, so the Me_2-Pt-Se_2 core can be considered to be flat. The two *DL* forms are degenerate, and cannot be distinguished by NMR spectroscopy. The two *meso* forms expected are no longer degenerate, as *meso* 1 has the Se-Me groups on the same side of the Me-Pt-Se plane as the xylyl backbone, while *meso* 2 has them on opposite sides. The

meso form observed in the NMR spectra is most likely *meso* 2, as this would be less sterically crowded.

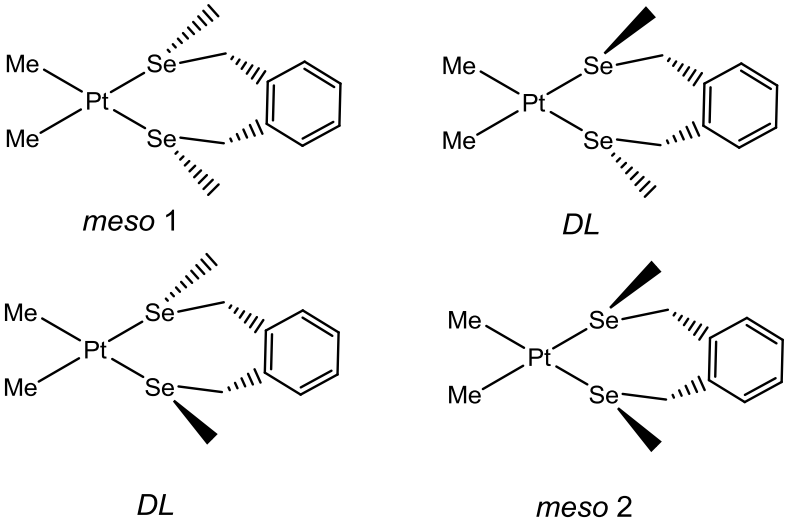

Figure 2.9: Invertomers (stereoisomers) generated by the xylyl backbone sitting out of the Me_2-Pt-Se_2 plane. The two *DL* enantiomers are superimposable and thus indistinguishable by NMR spectroscopy.

Reaction of $[PtMe_2(SMe_2)_2]$ and the diselenomethane, $MeSeCH_2SeMe$, under the same conditions used previously, was investigated, in the hope that this would generate the selenoether bridged dinuclear species $[Me_2Pt(\mu\text{-}MeSeCH_2SeMe)_2PtMe_2]$. The reaction was attempted several times, both by generating the $[PtMe_2(SMe_2)_2]$ *in situ* from $[PtCl_2(SMe_2)_2]$ and using pre-made $[PtMe_2(SMe_2)_2]$ (see telluroether reactions below). The reaction was also attempted at low temperatures, using an ice bath. Each time the only product was a species that was very poorly soluble in chlorocarbons and which showed many overlapping peaks in ^1H NMR spectra, none of which could be firmly identified as either starting material. The only peak obtained in $^{77}Se\{^1H\}$ NMR spectra of any of these attempts corresponded to free ligand.

Reaction of one molar equivalent of [8]aneSe_2 in diethyl ether with $[PtMe_2(SMe_2)_2]$ generated *in situ* from $[PtCl_2(SMe_2)_2]$ as above yielded $[PtMe_2$[8]ane$Se_2]$ as a beige solid. This is the first known complex of Pt(II) with a cyclic selenoether with alkyl co-ligands. This solid was only sparingly soluble in chlorocarbons and dmf, but was soluble enough to allow ^1H, ^{13}C, ^{77}Se and ^{195}Pt NMR data to be collected. The cyclic structure of [8]aneSe_2 means that the two C_3 backbones must be either side of the Me_2PtSe_2 plane, and thus the complex is symmetrical. This eliminates the possibility of stereoisomers, and the $^{77}Se\{^1H\}$ NMR spectrum shows a single peak at 140.8 ppm (Figure 2.10). This is only a very small shift from uncoordinated [8]aneSe_2 (δ = 138 ppm), and might simply be due to solvent effects, but the singlet exhibits clear coupling ($^1J_{PtSe}$ = 323 Hz), confirming the production of $[PtMe_2$([8]ane$Se_2)]$. This is significantly lower than the corresponding dichloro species $[PtCl_2$([8]ane$Se_2)]$, which has $^1J_{PtSe}$ = 680 Hz ($\delta^{77}Se$ = 194 ppm),

and is consistent with replacement of the chloro ligands with strong σ-donor Me groups which have a much greater *trans* influence and hence substantially reduce the Pt–Se coupling constants.[4] The ^{195}Pt NMR shift for [$PtMe_2$([8]aneSe_2)], –4325 ppm, also reflects the incorporation of the much stronger σ-donating Me ligands (δ^{195}Pt [$PtCl_2$([8]aneSe_2)] = –3825 ppm).

Reaction of [16]aneSe_4 with either one or two molar equivalents of [$PtMe_2(SMe_2)_2$] generated *in situ* from [$PtCl_2(SMe_2)_2$] as above yielded only the 1:1 species [$PtMe_2$[16]aneSe_4)]. The yellow solid was insoluble in chlorocarbons and alcohols, and only very poorly soluble in dmso. This poor solubility of the 1:1 complex causes it to precipitate immediately from the reaction solution and probably prevents further complexation of second $PtMe_2$ unit, despite having an excess present.
Due to the poor solubility, [$PtMe_2$[16]aneSe_4)] was characterised by ES^+ mass spectrometry, microanalysis and ^{1}H NMR spectroscopy. No further NMR data could be obtained. The ^{1}H NMR spectrum was obtained in deuterated dmso, and showed only two resonances associated with coordinated selenoether, which would be more consistent with a 2:1 complex than the 1:1 complex, but integration against the singlet occurring at 0.48 ppm agreed with the 1:1 formulation confirmed by microanalysis. The singlet at 0.48 ppm had clear Pt–H couplings of 81 Hz which is consistent with the dimethylPt(II) complexes described above.

Table 2.2 shows the ^{77}Se and ^{195}Pt NMR data for the four new dimethylPt(II) seleneoether complexes that this data could be obtained for, and also for the corresponding halide complexes.[3,4] It also shows the difference, Δ(δ^{77}Se), in the ^{77}Se shift for the ligands upon chelation. This has been calculated by subtracting the shift of uncoordinated, or "free" ligand from that of the complex. An unweighted average shift has been used for complexes with two or more invertomers. It is noticeable that chelation to a Pt(II) centre leads to a positive shift in δ(^{77}Se) in all cases. There is a clear trend in the ^{77}Se NMR data for the dimethyl Pt(II) complexes. As the length of the backbone between selenium atoms increases, Δ(δ^{77}Se) decreases. [$PtMe_2$(MeSe{CH_2}$_2$SeMe)] has Δ = 128.0 ppm, while [$PtMe_2$(MeSe{CH_2}$_3$SeMe)] and [$PtMe_2$(*o*-C_6H_4{CH_2SeMe}$_2$)] drop to 34.0 and 12.6 ppm respectively. The cyclic selenoether [8]aneSe_2 shows the smallest change in ^{77}Se NMR shift, possibly due to the macrocyclic effect, as the ^{77}Se NMR shift for [$PtMe_2$([8]aneSe_2)] is ~30-40 ppm higher than that of [$PtMe_2$(MeSe{CH_2}$_3$SeMe)] which has a very similar structure. Comparing these new dimethylPt(II) complexes with previously reported dihalide complexes [PtX_2(L-L)] (X = Cl, Br, I; L-L = MeSe$(CH_2)_n$SeMe, n = 2, 3)[3] reveals that the *trans* substituent has a clear effect on Δ(^{77}Se) upon chelation. The electronegative halide ligands cause much larger shifts than the strongly σ-donating methyl ligands which have a greater *trans* influence.

Table 2.2: Selected NMR data for Pt(II) complexes with selenoethers. a = $^{1}J_{(Pt\text{-}Se)}$/Hz in parentheses. b $\Delta = \delta(\text{complex}) - \delta(\text{"free" ligand in relevant solvent})$; the unweighted average of the chemical shifts of the different invertomers was used for complex. c = Spectra recorded in $(CD_3)_2SO$ at 298 K. d = Spectra recorded in $CH_2Cl_2/CDCl_3$ at 243 K. e = Spectra recorded in $CH_2Cl_2/CDCl_3$ at 193 K. f = Spectra recorded in D_6-dmf at 298 K.

Complex	δ^{77}Se /ppm[a]	$\Delta(\delta^{77}Se)$[b]	δ^{195}Pt /ppm	Reference
$[PtCl_2(MeSe\{CH_2\}_2SeMe)]$[c]	349.5 (515) 351.4 (503)	230.0	-3426 -3405	3
$[PtBr_2(MeSe\{CH_2\}_2SeMe)]$[c]	364.6 (403) 369.4 (381)	252.6	-3832 -3812	3
$[PtI_2(MeSe\{CH_2\}_2SeMe)]$[c]	384.4 (207) 395.1 (177)	275.0	-5185 -5165	3
$[PtMe_2(MeSe\{CH_2\}_2SeMe)]$[d]	247.9 (457) 250.1 (438)	128.0	-4383 -4395	This work
$[PtCl_2(MeSe\{CH_2\}_3SeMe)]$[c]	178.2 (500) 163.2 (518)	104.4	-3257 -3204	3
$[PtBr_2(MeSe\}CH_2\}_3SeMe)]$[c]	171.5 (434) 162.9 (396)	100.9	-3659 -3616	3
$[PtI_2(MeSe\{CH_2\}_3SeMe)]$[c]	164.7 (196) 153.7 (236)	92.9	-4960 -4991	3
$[PtMe_2(MeSe\{CH_2\}_3SeMe)]$[d]	114.0 (427) 102.1 (429)	34.0	-4247 -4309	This work
$[PtMe_2(o\text{-}C_6H_4\{CH_2SeMe\}_2)]$[e]	169.1 (526) 160.6 (492) 155.9 (438)	12.6	-4308 -4316	This work
$[PtCl_2([8]aneSe_2)]$[f]	194 (680)	56	-3825	4
$[PtMe_2([8]aneSe_2)]$[f]	140.8 (323)	1.2	-4318	This work

The ^{195}Pt NMR data do not show a similar, clearly defined trend, as $[PtMe_2(MeSe\{CH_2\}_2SeMe)]$ shows the most negative $\delta(^{195}Pt)$ at ~ –4390, while the other three dimethylPt(II) complexes shows more similar shifts (~ –4312), except for one invertomer of $[PtMe_2(MeSe\{CH_2\}_3SeMe)]$ (~ –4247). There is also a smaller difference between $\delta(^{195}Pt)$ values for the two $[Me_2Pt(MeSe\{CH_2\}_nSeMe)]$ complexes than there is between the corresponding dihalide complexes.[3] Where there is comparable data, it can be seen that the ^{195}Pt NMR shifts for the dimethyl complexes fall in between the dibromo and diiodo complexes, and the Pt-Se couplings fall between those for the dichloro and dibromo complexes.

Similar reactions were also attempted with the ditelluroethers $MeTe(CH_2)_3TeMe$ and *o*-$C_6H_4(CH_2TeMe)_2$ and $[PtMe_2(SMe_2)_2]$, generated *in situ* from $[PtCl_2(SMe_2)_2]$, in diethyl ether. It was hoped that this would produce the first examples of dimethylplatinum(II) species with telluroethers. The complexes $[PtX_2(L\text{-}L)]$ (L-L = $MeTe(CH_2)_3TeMe$,[10] *o*-$C_6H_4(TeMe)_2$,[9] *o*-$C_6H_4(CH_2TeMe)_2$[11]) have been described previously as poorly soluble solids. The reactions with $[PtMe_2(SMe_2)_2]$ failed to give the desired products, giving only dark brown, poorly soluble materials. This may be due to the greater sensitivity of telluroethers to reaction conditions, especially towards dealkylation and redox chemistry compared to the corresponding selenoethers. Production of $[PtX_2(Te\{CH_2CH_2CH{=}CH_2\}_2)]$ (X = Cl, Br) complexes failed in aqueous and non-aqueous media at room temperature, and had to be performed in non-aqueous solvents at low temperature – contrasting with production of corresponding thio/selenoether complexes.[16] This would indicate that generating $[PtMe_2(SMe_2)_2]$ *in situ* may have inhibited reaction with the telluroethers, as water is added to hydrolyse any unreacted MeLi before the ligand is added.

$[PtMe_2(SMe_2)_2]$ was produced from reaction of $[PtCl_2(SMe_2)_2]$ and MeLi in diethyl ether at low temperature, and isolated as a mixture of the monomer and the dimer, $[(PtMe_2)_2(\mu^2\text{-}SMe_2)_2]$.[29] The integration of the ^{1}H NMR spectrum obtained allowed the proportions of monomer and dimer present to be determined, and the monomer/dimer mixture was used in subsequent reactions, using the correct molar ratio. Reactions were attempted with *o*-$C_6H_4(CH_2TeMe)_2$ and $MeTe(CH_2)_3TeMe$ at room temperature in anhydrous diethyl ether, but these produced no identifiable products. Repeating the reactions at low temperature yielded orange/brown materials. The ES^+ MS from these materials show common features consistent with diplatinum compounds involving TeMe fragments. The various isotopes of platinum and tellurium combine to produce highly characteristic patterns of peaks in MS spectra. Both materials show clusters around *m/z* = 943 and 667. The ^{1}H NMR spectrum of the material formed with $MeTe(CH_2)_3TeMe$ shows clear evidence for Pt-Me units at δ = 0.71 and 0.59 ppm ($^2J_{Pt\text{-}H}$ = 82 Hz), but no Te-Me groups could be observed. In the ^{1}H NMR spectrum of the material obtained from the reaction with *o*-$C_6H_4(CH_2TeMe)_2$ no Pt-Me groups could be clearly identified. Both materials showed several peaks in ^{125}Te NMR spectra, but PtTe coupling could not be clearly identified. These results strongly indicate that significant Te-C bond fission occurs in these reactions, probably due to the fragility of Te-C bonds (see Chapter 1).[30,31]

2.5 – Novel Trialkyl Platinum(IV) Complexes

$K_2[PtCl_6]$ was produced in good yield by dissolving $H_2[PtCl_6]$ in water, adding two molar equivalents of KOH and stirring overnight. The yellow precipitate was filtered off and dried thoroughly *in vacuo*. $[PtMe_3I]$ was produced from reaction of Mg and MeI to form the Grignard,

which was added to $K_2[PtCl_6]$ at low temperature.[32] Workup yielded $[PtMe_3I]$ as a yellow-brown solid. $[PtMe_3I]$ actually exists as the tetrameric $[PtMe_3I]_4$, so the ^1H NMR spectrum shows a single methyl resonance with platinum coupling ($^2J_{PtH}$ = 78.2 Hz) at 1.85 ppm in C_6D_6.

$[PtMe_3I]$ was reacted with one molar equivalent of *o*-$C_6H_4(CH_2SeMe)_2$ in refluxing chloroform for 20 hours. This produced $[PtMe_3I(o\text{-}C_6H_4\{CH_2SeMe\}_2)]$ as a yellow solid in good yield, which was analysed by ES^+ MS, ^1H, $^{13}C\{^1H\}$, $^{77}Se\{^1H\}$ and ^{195}Pt NMR and microanalysis. The complex was more stable in solution than the corresponding dimethylPt(II) complex. ES^+ MS (Figure 2.10) clearly shows a cluster of peaks with the expected isotope pattern at *m/z* = 533, (calculated mass for $[^{195}PtMe_3(o\text{-}C_6H_4\{CH_2{}^{80}SeMe\}_2)]^+$ is 534). The ^1H NMR spectrum was broad at room temperature and difficult to interpret; cooling to 223 K allowed observation of Pt-H coupling and assignment of the peaks.

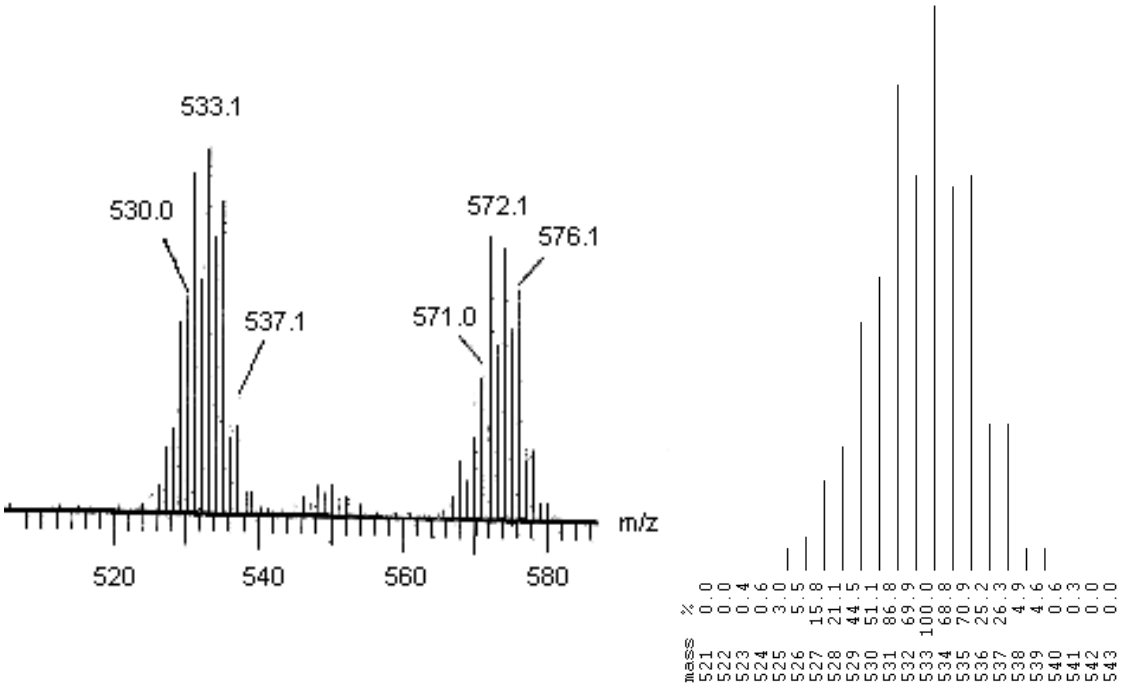

Figure 2.10: Left: ES^+ MS of $[PtMe_3I\{o\text{-}C_6H_4(CH_2SeMe)_2\}]$ in MeCN showing peak clusters corresponding to $[PtMe_3\{o\text{-}C_6H_4(CH_2SeMe)_2\}]^+$ and $[PtMe_3\{o\text{-}C_6H_4(CH_2SeMe)_2\}]^+\cdot MeCN$. Right: simulated isotope pattern for $[PtMe_3\{o\text{-}C_6H_4(CH_2SeMe)_2\}]^+$.

The ^{77}Se NMR spectrum (233 K) shows four selenium environments, all with $^1J_{PtSe}$ coupling between 280 and 312 Hz (δ = 95.5, 97.8, 98.7, 114.0 ppm; free ligand = 149.3 ppm). This coupling is similar in magnitude to that observed on $[PtMe_3I(MeSe\{CH_2\}_nSeMe)]$ (n = 2, 3).[17] The peak at δ = 95.5 ppm is of much lower intensity than the other three, indicating that this is a minor isomer. This is most likely to be the *meso* 2 form, shown in Figure 2.11, as the steric clash between the selenium-methyl groups and the bulky iodide would probably be worse than that between the selenium-methyl groups and the xylyl backbone in *meso* 1, making this less favourable. The ^{195}Pt

NMR spectrum showed only two peaks, the minor isomer not being observed. Despite the large, 7 membered chelate ring, this complex is stable in solution, and soluble in chlorocarbons.

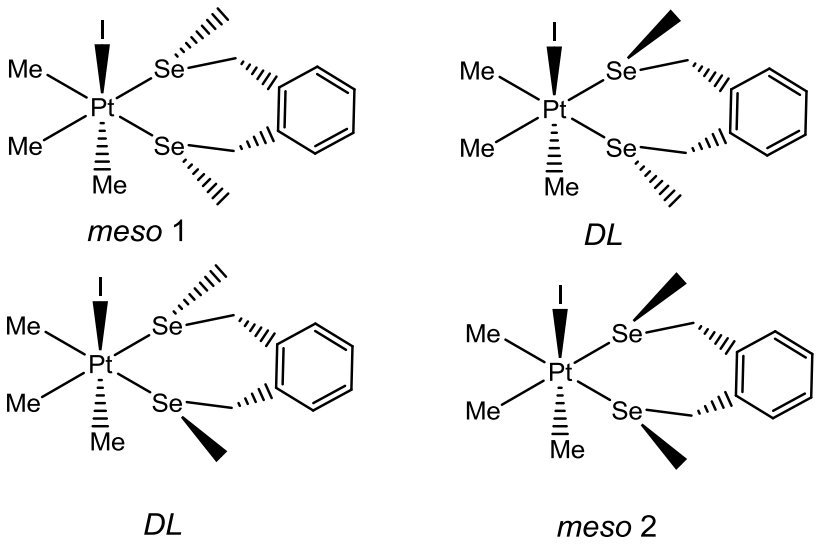

Figure 2.11: Possible invertomers of [$PtMe_3I(o\text{-}C_6H_4\{CH_2SeMe\}_2)$] assuming xylyl backbone remains away from iodide to reduce steric hindrance. *DL* enantiomers are superimposable and thus not individually distinguishable by NMR spectroscopy.

Crystals were obtained from slow evaporation of a solution of [$PtMe_3I(o\text{-}C_6H_4\{CH_2SeMe\}_2)$] in CH_2Cl_2/hexane. An X-ray structure analysis confirms a distorted octahedral coordination sphere at Pt(IV) derived from three facial Me groups, an iodo ligand and a chelating diselenoether, d(Pt–C) = 2.080(3) – 2.114(4) Å, d(Pt–Se) = 2.5530(4), 2.5629(4) Å, d(Pt1–I) = 2.7663(3) Å. The seven-membered chelate ring gives rise to a Se1–Pt1–Se2 angle of 98.317(12)°, and somewhat longer Pt-Se bonds than seen in the only other reported crystal structure of a trialkyl Pt(IV) complex with bidentate selenoether coordination, [$PtMe_3I$(MeSeCH=CHSeMe)] (Figure 2.5 above, Pt-Se = 2.525(4), 2.532(4) Å),[19] reflecting the considerable steric demands of the wide angle diselenoether. The selenoether adopts a *DL* configuration in which the SeMe substituents lie on opposite sides of the $PtSe_2$ plane, and the aromatic ring is oriented towards the Me ligand opposite the sterically large iodo ligand. This *DL* configuration can be contrasted with the *meso* configuration of the recently published [$Mo(CO)_4(o\text{-}C_6H_4\{CH_2SeMe\}_2)$] (Figure 2.13), in which not only are both methyl groups on the same side of the Se_2Mo plane, but are also on the same side as the xylyl backbone, even though this would seem to be sterically unfavourable.[33] In the analogous stibine complex [$PtMe_3I(o\text{-}C_6H_4\{CH_2SbMe_2\}_2)$] (Figure 2.13), whilst there are now two terminal methyl groups which prevent a similar *meso*/*DL* configuration, the xylyl backbone still adopts a position away from the iodide ligand. This complex also has a similar bond angle at Pt (Sb-Pt-Sb = 95.246 (11)°).[28] The –$SeCH_2(o\text{-}C_6H_4)CH_2Se$– unit can also be observed in two new crystal structures of Pt complexes, [$PtMe_3L^6$]I and [$PtMe_3L^9$]I, discussed in Chapter 5.

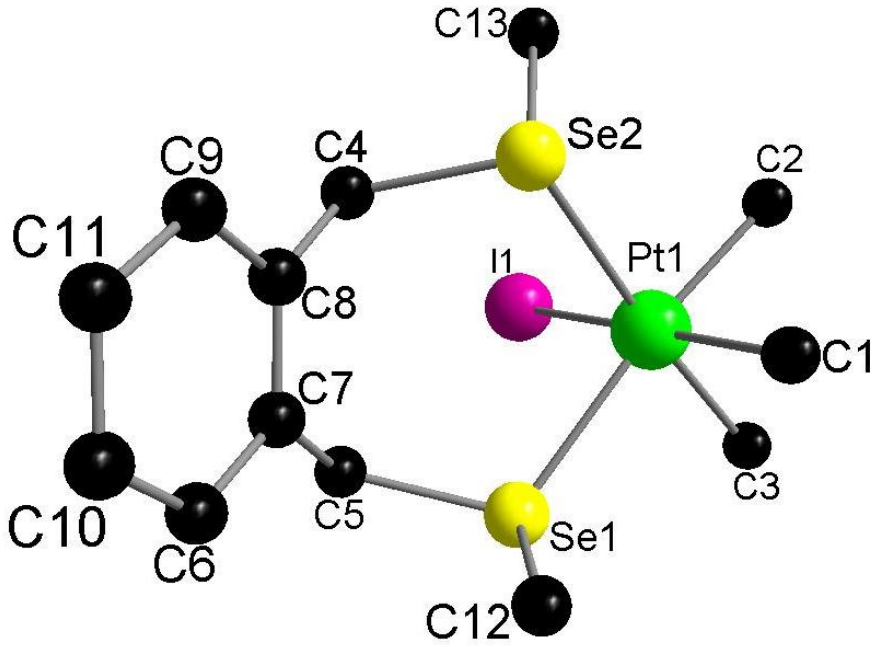

Figure 2.12: Crystal structure of [$PtMe_3I(o\text{-}C_6H_4\{CH_2SeMe\}_2)$]. H atoms omitted for clarity.

Table 2.3: Selected bond lengths and angles for [$PtMe_3I(o\text{-}C_6H_4\{CH_2SeMe\}_2)$].

Bond	**Length / Å**	**Bond**	**Angle / °**	**Bond**	**Angle / °**
C1–Pt1	2.085(4)	C2–Pt1–C1	84.28(15)	C3–Pt1–Se2	175.67(11)
C2–Pt1	2.080(3)	C2–Pt1–C3	87.39(15)	Se1–Pt1–Se2	98.317(12)
C3–Pt1	2.114(4)	C1–Pt1–C3	88.25(16)	C2–Pt1–I1	94.58(11)
Se1–Pt1	2.5530(4)	C2–Pt1–Se1	172.68(11)	C1–Pt1–I1	177.53(11)
Se2–Pt1	2.5629(4)	C1–Pt1–Se1	95.03(11)	C3–Pt1–I1	89.51(12)
I1–Pt1	2.7663(3)	C3–Pt1–Se1	85.30(10)	Se1–Pt1–I1	85.815(11)
		C2–Pt1–Se2	88.97(11)	Se2–Pt1–I1	93.116(10)
		C1–Pt1–Se2	89.06(11)		

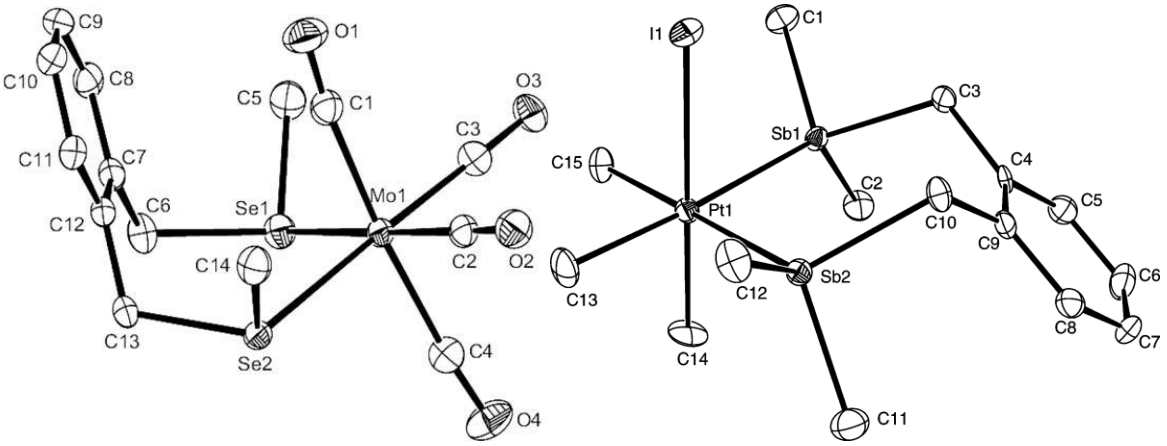

Figure 2.13: Crystal structures of [$Mo(CO)_4(o\text{-}C_6H_4\{CH_2SeMe\}_2)$][33] (left) and [$PtMe_3I(o\text{-}C_6H_4\{CH_2SbMe_2\}_2)$][28] (right). Ellipsoids at 50 % probability, H atoms omitted for clarity.

It was hoped that a cationic complex with tridentate selenoether coordination might be generated with the tripodal ligand $MeC(CH_2SeMe)_3$. $MeC(CH_2SeMe)_3$ has so far only been observed to bond to Pt in a bidentate manner, either with halide co-ligands $[PtCl_2(MeC\{CH_2SeMe\}_3)]$[7] or as a homoleptic complex $[Pt(MeC\{CH_2SeMe\}_3)_2](PF_6)_2$,[8] but tridentate *fac* coordination has previously been observed for $MeC(CH_2SeMe)_3$ with a number of other metals, including $[Mn(CO)_3L]CF_3SO_3$,[34] $[Rh(cod)L]PF_6$ and $[Ir(cod)L]PF_6$,[35] along with a homoleptic complex $[Ru(L)_2](CF_3SO_3)_2$.[36] $MeC(CH_2SeMe)_3$ was reacted in 1:1 molar ratio with $[PtMe_3I]$ in refluxing chloroform. A yellow solid was produced, which was identified as $[PtMe_3I(\kappa^2\text{-}MeC\{CH_2SeMe\}_3)]$ by electrospray MS, microanalysis and VT multinuclear NMR spectroscopy. The data are consistent with bidentate coordination of the tripod selenoether at the distorted octahedral Pt(IV) centre. However, the mixture of invertomers, together with the low symmetry of the molecule, makes it very difficult to assign the spectra in detail. There are three significant invertomers present, identified by the three peaks in the ^{195}Pt NMR spectrum recorded at 223 K. Figure 2.14 shows the possible invertomers for bidentate coordinating selenoethers on $[PtMe_3I]$. For $[PtMe_3I(MeSe\{CH_2\}_3MeSe)]$, where $R = R_1 = H$, the orientations of the R groups do not matter and there are only the three distinguishable invertomers shown below. However, in the case of $[PtMe_3I(MeC\{CH_2SeMe\}_3)]$ the R groups are now inequivalent ($R = Me$, $R_1 = CH_2SeMe$) and the possible orientations of these groups generates even more non-superimposable invertomers. The ^{77}Se NMR spectrum of $[PtMe_3I(MeC\{CH_2SeMe\}_3)]$ shows a total of six selenium environments with Pt coupling and a further four without, making the exact nature of the invertomer populations difficult to calculate. The four environments for the Se atom in the uncoordinated arm of the tripodal ligand indicate that there may be an interaction between this Se and the bulky iodide ligand.

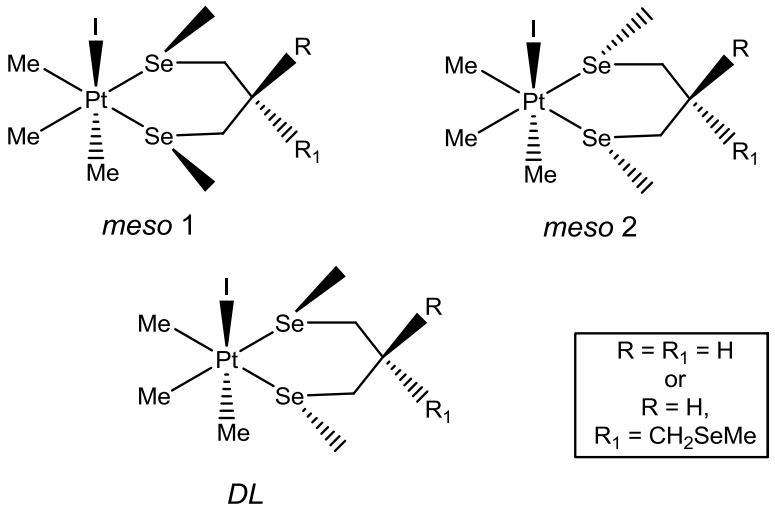

Figure 2.14: Invertomers of $[PtMe_3I(\kappa^2\text{-selenoether})]$.

Attempts to promote κ^3 co-ordination in this complex were undertaken, both by stirring the preformed $[PtMe_3I(\kappa^2\text{-}MeC\{CH_2SeMe\}_3)]$ in acetonitrile with $TlPF_6$, and by reaction of $PtMe_3I$,

$TlPF_6$ and $MeC(CH_2SeMe)_3$ in refluxing chloroform. Both methods resulted in the production of an orange/red oil. IR spectra were recorded on these oils, and were identical to the IR spectrum of $[PtMe_3I(\kappa^2\text{-}MeC\{CH_2SeMe\}_3)]$, showing no evidence for incorporation of PF_6^-. This indicates that under these reaction conditions no dissociation of the iodide ligand occurred, as $TlPF_6$ would rapidly react with uncoordinated I^- to produce TlI as a precipitate, removing the iodide from the reaction. NMR spectroscopic analysis also failed to show any evidence of $[PtMe_3(MeC\{CH_2SeMe\}_3)]^+$, the only significant product being $[PtMe_3I\{\kappa^2\text{-}MeC(CH_2SeMe)_3\}]$. *fac*-$[PtMe_3(Se\{CH_2CH_2SeMe\}_2)]BF_4$ is a stable, soluble white solid, made by reaction of $[(PtMe_3)_2SO_4]\cdot 4H_2O$ and $Se(CH_2CH_2SeMe)_2$ in acetone, followed by addition of $NaBF_4$.[21] However, the facultative triselenoether has greater conformational flexibility than the tripod, which is dependant on maintaining a tetrahedral geometry at the apical carbon. Thus it appears that $MeC(CH_2SeMe)_3$ is not well-suited to *facial* coordination on the small trimethyl Pt(IV) fragment.

Treatment of $[PtMe_3I]$ with one molar equivalent of the cyclic selenoether [8]aneSe_2 in refluxing $CHCl_3$ produced a cream solid after the solvent was reduced *in vacuo* and addition of diethyl ether. This cream solid was analysed by electrospray MS, microanalysis and ^1H, $^{13}C\{^1H\}$, $^{77}Se\{^1H\}$ and ^{195}Pt NMR spectroscopy. The electrospray MS show clusters of peaks with the correct *m*/*z* and isotope patterns for both $[PtMe_3([8]aneSe_2)]^+$ and $[PtMe([8]aneSe_2)]^+$. The coupling constants observed in the NMR spectra of $[PtMe_3I([8]aneSe_2)]$ ($^2J_{PtH}$ and $^1J_{PtC}$ from the Me *trans* Se, and $^1J_{PtSe}$) are consistently smaller than those observed for the planar $[PtMe_2([8]aneSe_2)]$, as expected based upon the different coordination environments. The $^{13}C\{^1H\}$ NMR spectrum has four distinct CH_2 resonances from [8]aneSe_2, which are caused by the lack of axial symmetry within the complex. The $^{77}Se\{^1H\}$ NMR spectrum shows a single peak with δ = 65.3 ppm and $^1J_{PtSe}$ = 244. This is very similar to data reported for $[PtMe_3I(MeSe\{CH_2\}_3SeMe)]$ (Table 2.4).

$[PtMe_3I([16]aneSe_4)]$ was obtained in similar fashion to $[PtMe_3I([8]aneSe_2)]$ by treatment of $[PtMe_3I]$ with one molar equivalent of [16]aneSe_4 in refluxing $CHCl_3$. The cream solid isolated was characterised by multinuclear NMR spectroscopy, electrospray MS and microanalysis. The electrospray MS showed a cluster of peaks with the correct *m*/*z* and isotope patterns for $[PtMe_3([16]aneSe_4)]^+$. The ^{77}Se NMR spectrum shows two peaks, which are substantially to low frequency of the "free" ligand value. This is somewhat surprising, as even the resonance arising from the two uncoordinated Se atoms of the [16]aneSe_4 ring is some 40 ppm to low frequency of [16]aneSe_4 itself. This suggests that the presence of the trimethylPt(IV) fragment bound to the other two Se atoms significantly influences the electronic environment at the remote, "free" Se atoms and may suggest that the uncoordinated Se atoms lie near to the iodo ligand. The ^{195}Pt NMR spectrum shows a singlet at -3616 ppm, which is only slightly different to $[PtMe_3I([8]aneSe_2)]$ (δ =

-3589), suggesting that total ring size is a relatively unimportant influence on the ^{195}Pt chemical shift.

As with [$PtMe_3I$([8]aneSe_2)] there is a lack of axial symmetry, leading to seven CH_2 resonances in the $^{13}C\{^1H\}$ NMR spectrum from the macrocycle, consistent with bidentate coordination giving a six-coordinate Pt(IV) species with a vertical plane of symmetry.

[$PtMe_3I(\kappa^2$-[16]aneSe_4)] was refluxed in $CHCl_3$ with one mol. equiv. of $TlPF_6$ for 2.5 hours, after which time the almost colourless solution was cannulaed from the fine yellow TlI precipitate. The solution was reduced *in vacuo*, and addition of diethyl ether caused a white solid to precipitate, which was collected by filtration. Analysis of this white solid showed clean abstraction of the iodo ligand, giving [$PtMe_3$([16]aneSe_4)]PF_6. This is the first example of a cationic alkyl Pt(IV) complex with macrocyclic selenoether coordination (for further new examples, see Chapter 5). Electrospray MS (Figure 2.15) shows an intense peak cluster corresponding to [$PtMe_3$([16]aneSe_4)]$^+$ (highest peak 725, calculated for [$^{195}PtMe_3$([16]ane$^{80}Se_4$)]$^+$ 728) with a lower intensity cluster of peaks corresponding to [PtMe([16]aneSe_4)]$^+$, i.e. reductive loss of two Me groups. The MS data is not enough to confirm κ^3-coordination, as the iodide is displaced in the MS of the κ^2-complex to give the same parent ion, [$PtMe_3$([16]aneSe_4)]$^+$, but a *fac*-octahedral Me_3Se_3 donor set around Pt is confirmed by NMR spectroscopy. The ^{195}Pt NMR spectrum exhibits only a small change in going from a Me_3Se_2I ligand set to an Me_3Se_3 ligand set, and shows a singlet at δ = –3648 ppm. The $^{77}Se\{^1H\}$ NMR spectrum for [$PtMe_3$([16]aneSe_4)]PF_6 recorded at 223 K reveals two Se environments at 70 (coordinated Se) and 138 ppm ("free" Se), showing a significant shift from those observed for [$PtMe_3I$([16]aneSe_4)] (116.6 and 119.5 ppm, respectively). Again both the coordinated and "free" Se are to low frequency of [16]aneSe_4 itself (δ =158 ppm). The shift in the "free" Se frequency is probably due to "ring-whizzing", resulting in rapid interchange between the "free" and coordinated Se atoms. A similar mechanism has been proposed for the closely related thioether complex [$PtMe_3(\kappa^3$-[12]aneS_4)]$^+$.[37] This would also explain the broad resonances observed in the $^{13}C\{^1H\}$ and $^{77}Se\{^1H\}$ NMR spectra recorded at room temperature.

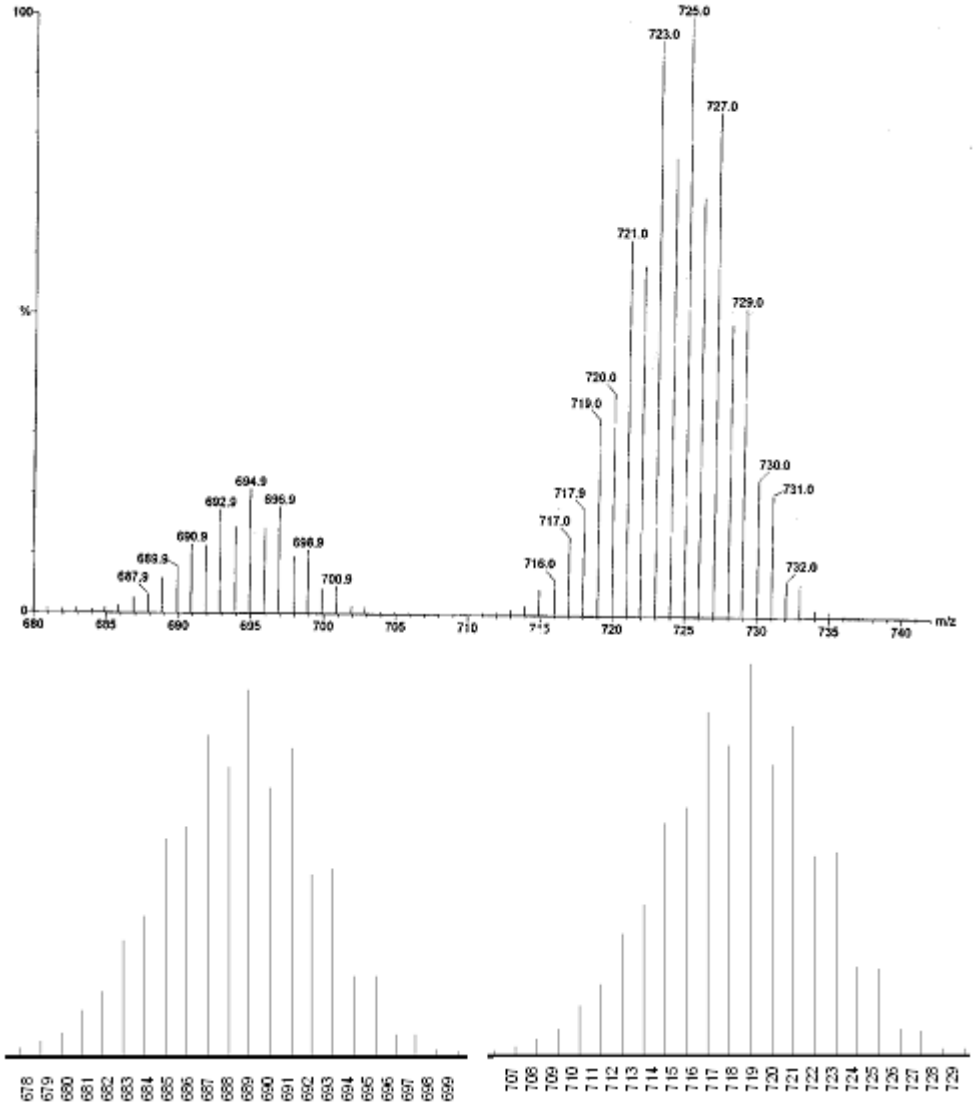

Figure 2.15: Top: ES^+ MS of $[PtMe_3([16]aneSe_4)]PF_6$ in MeCN showing peak clusters corresponding to $[PtMe([16]aneSe_4)]^+$ and $[PtMe_3([16]aneSe_4)]^+$. Bottom: simulated isotope patterns for $[PtMe([16]aneSe_4)]^+$ and $[PtMe_3([16]aneSe_4)]^+$.

Table 2.4 shows the ^{77}Se and ^{195}Pt NMR data for these new $[PtMe_3I(selenoether)]$ complexes and data for similar, previously reported complexes. Comparing the bidentate acyclic ligands, we see that $\Delta(\delta^{77}Se)$ decreases in the order $MeSe(CH_2)_2SeMe > MeSe(CH_2)_3SeMe > o\text{-}C_6H_4(CH_2SeMe)_2$ with $o\text{-}C_6H_4(CH_2SeMe)_2$ showing a coordination shift of -47.8 ppm. This trend is also observed in the dimethylPt(II) complexes in Table 2.2, although $\Delta(\delta^{77}Se)$ does remain positive in these cases. $\delta(^{195}Pt)$ shows the reverse trend for these Pt(IV) complexes, with $[PtMe_3I(MeSe\{CH_2\}_2SeMe)]$ showing the most negative shift (-3598 to -3737 ppm) but whilst $[PtMe_2(MeSe\{CH_2\}_2SeMe)]$ also showed the most negative shift of the dimethylPt(II) complexes (-4395 ppm), $MeSe(CH_2)_3SeMe$ and $o\text{-}C_6H_4(CH_2SeMe)_2$ showed very similar ^{195}Pt shifts. $[PtMe_3I(MeSe\{CH_2\}_3SeMe)]$, $[PtMe_3I(\kappa^2\text{-}MeC\{CH_2SeMe\}_3)]$ and $[PtMe_3I([8]aneSe_2)]$ show very similar ^{77}Se and ^{195}Pt NMR shifts, which is expected as the coordination sphere at Pt and the backbone between the chelating

Se atoms are the same. [$PtMe_3I(\kappa^2$-[16]aneSe_4)] shows significantly different ^{77}Se and ^{195}Pt NMR shifts, which may arise from a stronger macrocyclic effect than exhibited by [8]aneSe_2, or may be caused by the possible "ring whizzing".[37] More discussion of the tridentate cationic [$PtMe_3$([16]aneSe_4)]PF_6 can be found in Chapter 5.

Table 2.4: Selected NMR data for Pt(IV) complexes with selenoethers. a = $^1J_{(Pt\text{-}Se)}$/ Hz in parentheses. b = δ(complex) – δ(free ligand); the unweighted average of the chemical shifts of the different invertomers was used for complex. Coordinated and uncoordinated Se shifts calculated separately. c = Spectra recorded in $CDCl_3$. d = Spectra recorded in $CH_2Cl_2/CDCl_3$ at 223 K. e = Chemical shift of uncoordinated Se atoms present in ligand. f = Spectra recorded in $CDCl_3$ at 243 K.

Complex	**δ^{77}Se /ppm[a]**	**$\Delta(^{77}Se)$[b]**	**δ^{195}Pt /ppm**	**Reference**
[$PtMe_3I$(MeSe{CH_2}$_2$SeMe)][c]	177.8 (321.4) 181.2 (343.9) 181.7 (263.7) 178.1 (255.1)	58.7	-3598.1 -3667.7 -3737.7	18
[$PtMe_3I$(MeSe{CH_2}$_3$SeMe)][c]	55.2 (260.3) 52.0 (252.9) 58.4 (240.2)	-18.8	-3470.1 -3541.0	18
[$PtMe_3I(\kappa^2$-MeC{CH_2SeMe}$_3$)][d]	53.0 (252) 51.6 (160) 49.3 (258) 38.5 (252) 37.4 (162) 37.3 (256) 35.1[e] 33.0[e] 29.0[e] 27.3[e]	21.5 8.1	-3446 -3543 -3550	This work
[$PtMe_3I$(*o*-C_6H_4{CH_2SeMe}$_2$)][d]	114 (289) 98.7 (280) 97.8 (312) 95.5 (286)	-47.8	-3382 -3468	This work
[$PtMe_3I$([8]aneSe_2)][c]	65.3 (244)	-68.7	-3589	This work
[$PtMe_3I(\kappa^2$-[16]aneSe_4)][f]	116.6 (266) 119.5[e]	-41.4 -38.5	-3616	This work
[$PtMe_3(\kappa^3$-[16]aneSe_4)]PF_6[d]	70 (249) 138[e]	-88 -20	-3648	This work

The only previously reported [$PtMe_3I$] complexes with telluroether ligands are [$PtMe_3I$(*o*-$C_6H_4\{TeMe\}_2$)] and [$PtMe_3I(RTe\{CH_2\}_3TeR)$] (R = Me, Ph),[23] providing examples of 5 and 6 membered chelate rings. The success of the reaction of the *o*-xylyl selenoether with [$PtMe_3I$] prompted the reaction of the corresponding telluroether. Reaction of [$PtMe_3I$] with *o*-$C_6H_4(CH_2TeMe)_2$ in refluxing chloroform for 16 hours produced an orange solid identified as [$PtMe_3I$(*o*-$C_6H_4\{CH_2TeMe\}_2$)]. The ^{125}Te NMR spectrum (Figure 2.16) showed the presence of three invertomers in significant proportions. These presumably correspond to *meso* 1 and 2 and *DL* formed when the xylyl backbone lies on the opposite side of the Me_2-Pt-Te_2 plane to the bulky iodide (see Figure 2.11). The pyramidal inversion at 298 K is relatively slow in the telluroether complex compared to the selenoether, as expected (see Chapter 1).

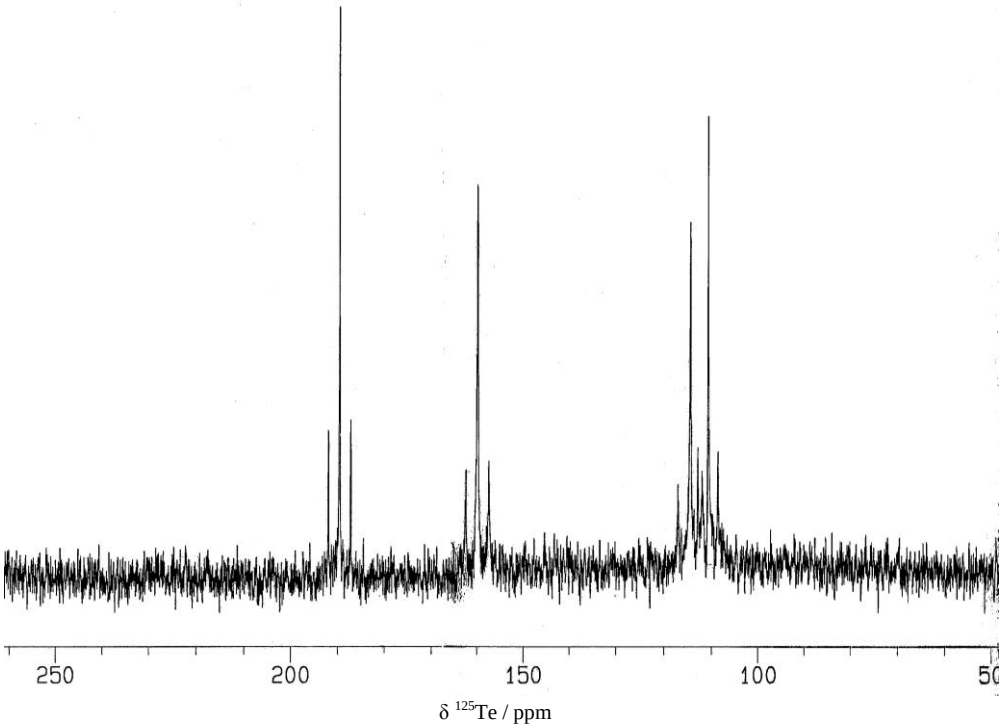

Figure 2.16: ^{125}Te NMR spectrum of [$PtMe_3I$(*o*-$C_6H_4\{CH_2TeMe\}_2$)] recorded in $CH_2Cl_2/CDCl_3$ at 243 K.

Reaction of [$PtMe_3I$] with one equivalent of $MeTeCH_2TeMe$ in chloroform produced a dark brown solid, identified as [$(PtMe_3I)_2(MeTeCH_2TeMe)$]. The NMR data collected are consistent with a di-iodo-bridged species in which the telluroether also bridges between the Pt atoms, i.e. [$Me_3Pt(\mu^2$-$I)_2(\mu^2$-$MeTeCH_2TeMe)PtMe_3$], which leads to two non-superimposable, and therefore NMR distinguishable, invertomers which are shown in Figure 2.17. These can both be seen in the ^{195}Pt and ^{125}Te NMR spectra in a ratio of ~2.5:1, both showing a major peak (δ ^{195}Pt = -3430, ^{125}Te = 173.2 ppm) and a minor peak (δ ^{195}Pt = -3451, ^{125}Te = 171.1 ppm). When recorded at room temperature, the ^{1}H NMR spectrum was broad, but cooling to 248 K allowed identification of six

different resonances from methyl groups on Pt. Four resonances would be expected, from Me *trans* I and Me *trans* Te on each invertomer. The telluroether ligand must cause a separation of the two Me groups *trans* I, possibly by reducing the symmetry in some way. This has been observed in the thioether complex $[(PtMe_3I)_2(MeSCH\{Me\}SMe)]$, as the methyl group on the 1C linkage destroys the symmetry of the molecule, but not in $[(PtMe_3I)_2(MeSCH_2SMe)]$ where the Me groups *trans* I are equivalent.[19] $^{13}C\{^1H\}$ NMR spectroscopy again had to be run at 248 K to obtain a clear spectrum, and revealed five peaks assignable to methyl groups on Pt, whereas six were expected from the ^1H NMR data. Presumably, two resonances occurred at the same chemical shift. ES^+ MS did not show any peaks consistent with this species, but this is not unexpected. In the mononuclear complexes, the iodide ligand is easily displaced to allow detection of $[PtMe_3L]^+$. As the two iodide ligands are bridging between the platinum atoms, they are much harder to displace to generate a cation.

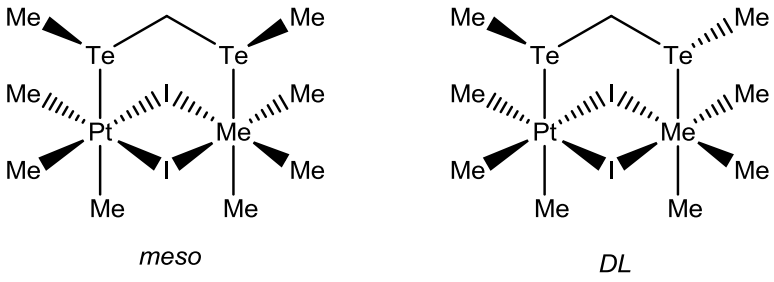

Figure 2.17: Invertomers of $[(PtMe_3I)_2(MeTeCH_2TeMe)]$.

The ease of formation and relatively high stability of the telluroether complexes both as solids and in solution was somewhat unexpected, as hard/soft acid/base theory would suggest that Pt(II) would form more stable complexes than Pt(IV) with soft telluroether ligands. It is probably due to highly σ-donating Me_3 donor set surrounding the platinum and the coordinatively saturated Pt(IV) which makes oxidative addition of the Te-C bond unlikely (as does the oxidation state).

Because of the relative lack of characterised complexes, comparison of the effects of different ligand backbones for telluroethers is restricted compared to selenoethers. It can be observed that the dinuclear bridged complex $[(PtMe_3I)_2(MeTeCH_2TeMe)]$ has a significantly less negative $\delta(^{195}Pt)$ than the mononuclear complexes, and that all the complexes shift $\delta(^{125}Te)$ of the ligands in a low frequency direction. Comparison with the analogous selenoether complexes detailed in Table 2.4 shows that the selenoether complexes have less negative $\delta(^{195}Pt)$ than the telluroethers, and that whilst $[PtMe_3I(MeE\{CH_2\}_3EMe)]$ have comparable sized shifts in the ligand from "free" to coordinated ($\Delta(^{77}Se)$ = -18.8, $\Delta(^{125}Te)$ = -12.8), in the xylyl ligand complexes $[PtMe_3I(o\text{-}C_6H_4\{CH_2EMe\}_2)]$ there is a significant difference ($\Delta(^{77}Se)$ = -47.8, $\Delta(^{125}Te)$ = -120.3).

Table 2.5: Selected NMR data for Pt(IV) complexes with telluroethers. a = $^{1}J_{(Pt\text{-}Te)}$/ Hz in parentheses. b = δ(complex) – δ(free ligand); the unweighted average of the chemical shifts of the different invertomers was used for complex. c = spectra recorded in $CH_2Cl_2/CDCl_3$ at 243 K. d = spectra recorded in $CDCl_3$ at 303 K. e = no ^{77}Te NMR data reported; coupling constant taken from ^{195}Pt NMR spectrum.

Complex	**δ^{125}Te /ppm[a]**	**$\Delta(^{125}Te)$[b]**	**δ^{195}Pt /ppm**	**Reference**
$[(PtMe_3I)_2(MeTeCH_2TeMe)]$[c]	173.2 (713) 171.1 (605)	-39.8	-3430 -3451	This work
$[PtMe_3I(o\text{-}C_6H_4\{TeMe\}_2)]$[d]	e (not given) (699, 467) (521)		-4235 -4289 -4382	23
$[PtMe_3I(MeTe\{CH_2\}_3TeMe)]$[d]	82.5 (571) 92.1 (585) 89.4 (485) 100.6 (514)	-12.8	-4071 -4125 -4211	23
$[PtMe_3I(o\text{-}C_6H_4\{CH_2TeMe\}_2)]$[c]	189.5 (602) 159.9 (618) 114.5 (638) 110.8 (537)	-120.3	-3968 -4022 -4119	This work

2.6 – Reductive Elimination

It has been shown that a number of Pt(IV) complexes of the type $[PtMe_3I(L–L)]$ with bidentate ligands including $Ph_2P(CH_2)_2PPh_2$;[38] $R_2Sb(CH_2)_3SbR_2$, R = Me, Ph;[28] and $o\text{-}C_6H_4(CH_2SbMe_2)_2$[28], undergo clean reductive elimination of ethane upon thermolysis, however no analysis of this kind has been carried out for Pt(IV) complexes with chalcogenoethers. As has already been observed, the positive electrospray MS of $[PtMe_3I(L)]$ (L = $MeC(CH_2SeMe)_3$, [8]aneSe_2) and $[PtMe_3([16]aneSe_4)][PF_6]$ show peak clusters consistent with both $[PtMe_3(L\text{-}L)]^+$ and $[PtMe(L\text{-}L)]^+$. The isotope pattern for the latter of these species provides clear evidence for the species being singly charged, and this Pt(II) species is presumably formed *via* reductive loss of ethane from the parent cation. In order to investigate possible reductive ability in other Pt(IV) seleno- and telluroether complexes, samples of $[PtMe_3I(o\text{-}C_6H_4\{CH_2EMe\}_2)]$ (E = Se, Te) were heated to observe if reductive elimination of ethane would occur. $[PtMe_3I(o\text{-}C_6H_4\{CH_2TeMe\}_2)]$ does not melt on heating, merely decomposing at ~130°C giving a black solid. The corresponding Pt(IV) selenoether complex melts at ~150°C and then darkens slowly as the temperature is increased, indicating the onset of decomposition. A solid sample of this complex was heated for 1h at *ca.* 160°C and the residue investigated by ^{1}H NMR spectroscopy, which revealed loss of the Pt-Me and Se-Me resonances. This shows that these species tend toward decomposition, and do not undergo clean reductive elimination under these conditions.

2.7 – Oxidative Addition

It has been shown that [$PtMe_2$([9]aneS_3)] can be reacted with MeI in CH_2Cl_2 to yield the Pt(IV) complex [$PtMe_3$([9]aneS_3)]I in 68% yield, and [$PtEt_2$([9]aneS_3)] can undergo similar oxidative addition to [$PtMeEt_2$([9]aneS_3)]I.[27] In order to probe the reaction chemistry of the novel dimethylPt(II) selenoether complexes, freshly prepared solutions of [$PtMe_2$(*o*-C_6H_4{CH_2SeMe}$_2$)] and [$PtMe_2$(MeSe{CH_2}$_3$SeMe)] in CH_2Cl_2 were stirred overnight with excess MeI, giving light yellow solids after filtration and recrystallisation from CH_2Cl_2/hexane. The ^{1}H and ^{77}Se{^{1}H} NMR spectra of solutions of these products show that oxidative addition of MeI occurs cleanly, with complete conversion of the Pt(II) complexes to [$PtMe_3I$(*o*-C_6H_4{CH_2SeMe}$_2$)] and [$PtMe_3I$(MeSe{CH_2}$_3$SeMe)] respectively.

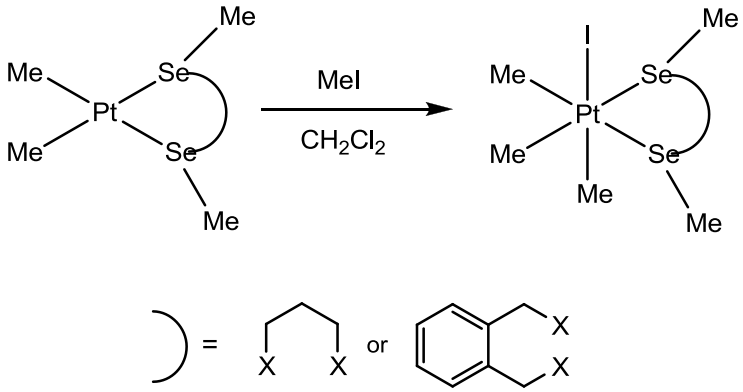

Figure 2.18: Reaction scheme for oxidative addition to Pt(II) dimethyl complexes.

2.8 - Conclusions

The first known examples of alkyl Pt(II) complexes with macrocyclic selenoethers [$PtMe_2$L] (L = [8]aneSe_2 and [16]aneSe_4) have been synthesised and characterised as part of a series of dimethyl Pt(II) complexes with selenoether ligands (L = MeSe(CH_2)$_n$SeMe, n = 2, 3; *o*-C_6H_4(CH_2SeMe)$_2$). These complexes proved to be unstable in solutions of chlorinated solvents, and only poorly soluble in unchlorinated solvents. Similar reactions with telluroether ligands (MeTe(CH_2)$_3$TeMe, *o*-C_6H_4(CH_2TeMe)$_2$) produced no isolatable products. No examples of complexes exhibiting bridging ligand behaviour could be obtained, either using $MeSeCH_2SeMe$, or using 0.5 equivalents of [16]aneSe_4.

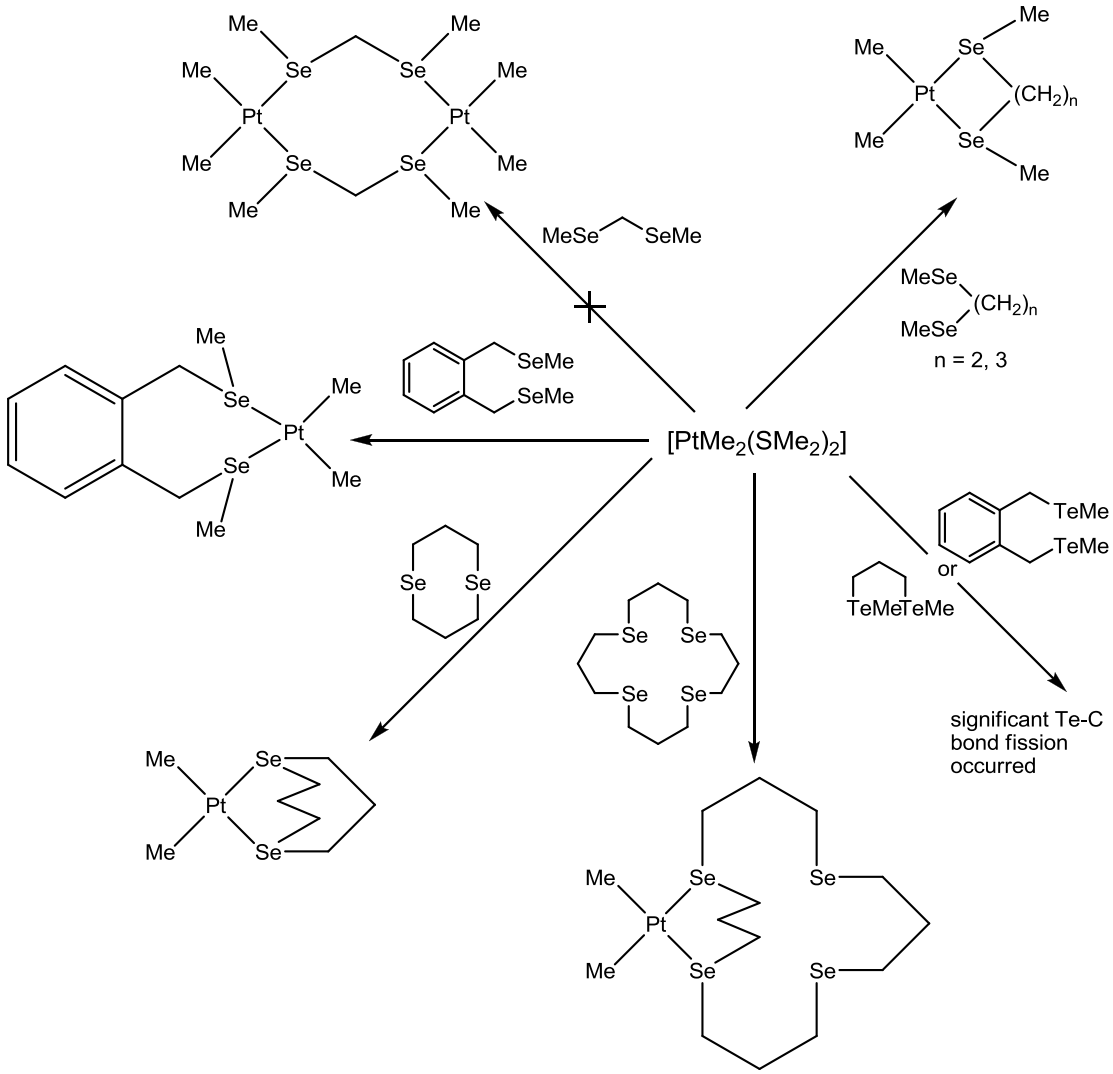

Figure 2.19: Summary of dimethyl Pt(II) complexes investigated in this chapter.

A new series of $[PtMe_3I(\kappa^2\text{-L-L})]$ complexes has been synthesised and characterised, which includes the first examples of this type with macrocyclic selenoethers (L-L = *o*-$C_6H_4(CH_2EMe)_2$, E = Se, Te; $MeC(CH_2SeMe)_3$; [8]aneSe_2 and [16]aneSe_4). The first bridging ditelluroether trimethyliodo Pt(IV) complex, $[(PtMe_3I)_2(MeTeCH_2TeMe)]$ has also been characterised. The two potentially tridentate ligands $MeC(CH_2SeMe)_3$ and [16]aneSe_4) were investigated to promote κ^3 coordination. The tripodal ligand showed no evidence for κ^3 coordination, but $[PtMe_3(\kappa^3\text{-}[16]aneSe_4)]PF_6$ was isolated and characterised, which is the first cationic trialkyl Pt(IV) complex with a macrocyclic selenoether ligand, and an unusual example of κ^3-[16]aneSe_4 coordination.

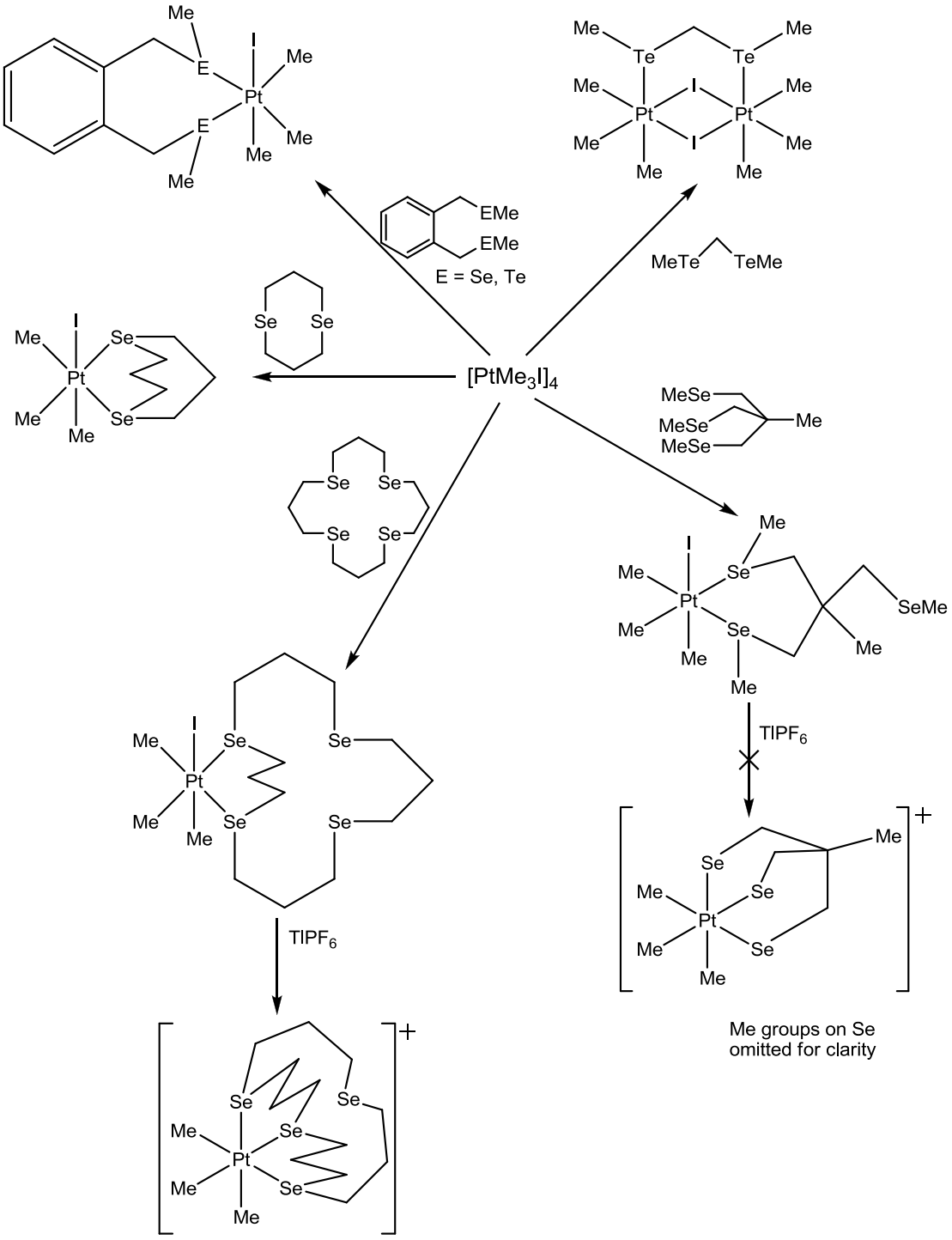

Figure 2.20: Summary of Pt(IV) complexes investigated in this chapter.

The possibility of these new complexes exhibiting redox behaviour was examined, with reductive elimination of ethene being observed from the Pt(IV) complexes $[PtMe_3I([8]aneSe_2)]$ and $[PtMe_3([16]aneSe_4)][PF_6]$, yielding Pt(II) complexes. No such behaviour was observed for $[PtMe_3I(o\text{-}C_6H_4\{CH_2EMe\}_2)]$ (E = Se, Te). Oxidative addition of MeI to the Pt(II) complexes $[PtMe_2L]$ (L = $MeSe(CH_2)_3SeMe$ or $o\text{-}C_6H_4(CH_2SeMe)_2$) was shown to occur cleanly to produce the Pt(IV) complexes $[PtMe_3IL]$.

2.9 – Experimental

The ligands $MeE(CH_2)_nEMe$ (E = Se, n = 1, 2, 3;[24] E = Te, n = 1, 3[25]), *o*-$C_6H_4(CH_2EMe)_2$ (E = Se,[6] Te[11]), $MeC(CH_2SeMe)_3$,[24] [8]aneSe_2[26] and [16]aneSe_4[26] and the complexes $[PtCl_2(SMe_2)_2]$[29] and $[PtMe_2(SMe_2)_2]$[29] were prepared by literature preps.

[$PtMe_2(MeSe\{CH_2\}_2SeMe)$]: A 1.6 M solution of MeLi (0.2 cm^3, 0.32 mmol) in Et_2O was slowly added to an ice-cold suspension of $[PtCl_2(SMe_2)_2]$ (0.050 g, 0.128 mmol) in 20 cm^3 dry Et_2O. After 5 min a further 0.1 cm^3 MeLi (1.6 M in Et_2O, 0.16 mmol) were added and the solution was warmed to room temperature. After ca. 10 min the yellow colour disappeared and a white precipitate formed. At this stage 10 cm^3 of H_2O and 1 equiv. of $MeSe(CH_2)_2SeMe$ (0.028 g, 0.128 mmol) were added. The mixture was stirred for 2.5 h giving a cream precipitate which was filtered off and washed with Et_2O. The yellow solid was then dissolved in CH_2Cl_2 (10 cm^3), filtered and the solvent was removed *in vacuo*. Yield 0.023 g (41%). $C_6H_{16}PtSe_2$ (441.2): calcd. C 16.3, H 3.7; found C 15.9, H 3.3. Electrospray MS (MeCN): found *m/z* = 468, 453, 426, 411; calcd. for $[^{195}PtMe(Me^{80}Se\{CH_2\}_2{}^{80}SeMe)(MeCN)]^+$ *m/z* = 469, $[^{195}Pt(Me^{80}Se\{CH_2\}_2{}^{80}SeMe)(MeCN)]^+$ 454, $[^{195}PtMe(Me^{80}Se\{CH_2\}_2{}^{80}SeMe)]^+$ 428, $[^{195}Pt(Me^{80}Se\{CH_2\}_2{}^{80}SeMe)]^+$ 413. ^1H NMR (400 MHz, $CDCl_3$, 273 K): δ = 0.72 (s, PtMe, $^2J_{PtH}$ = 84 Hz), 0.77 (s, PtMe, $^2J_{PtH}$ = 85 Hz), 2.16 (s, SeMe, $^3J_{PtH}$ = 22 Hz), 2.36 (s, SeMe, $^3J_{PtH}$ = 21 Hz), 2.55 – 3.25 (m, 4 H, $SeCH_2$). $^{13}C\{^1H\}$ NMR ($CDCl_3$, 223 K): δ = -12.8 (PtMe, $^1J_{PtC}$ = 760 Hz), -12.6 (PtMe, 735 Hz), 9.9, 11.1 (SeMe), 29.2, 29.5 ($SeCH_2$). $^{77}Se\{^1H\}$ NMR ($CDCl_3$, 223 K): δ = 247.9 (major form, $^1J_{PtSe}$ = 457 Hz), 250.1 (minor form, 438 Hz). ^{195}Pt NMR ($CDCl_3$, 223 K): δ = -4383 (major), -4395 (minor).

[$PtMe_2(MeSe\{CH_2\}_3SeMe)$]: Method as above using $MeSe(CH_2)_3SeMe$. Beige solid. Yield 64%. $C_7H_{18}PtSe_2$ (455.2): calcd. C 18.5, H 4.0; found C 18.6, H 4.2. Electrospray MS (MeCN): found *m/z* = 482, 466, 425; calcd. for $[^{195}PtMe(Me^{80}Se\{CH_2\}_3{}^{80}SeMe)(MeCN)]^+$ *m/z* = 483, $[^{195}Pt(Me^{80}Se\{CH_2\}_3{}^{80}SeMe)(MeCN)]^+$ 468, $[^{195}PtMe(Me^{80}Se\{CH_2\}_3{}^{80}SeMe)]^+$ 427. ^1H NMR (400 MHz, $CDCl_3$, 248 K): δ = 0.51 (s, PtMe, $^2J_{PtH}$ = 84 Hz), 0.55 (s, PtMe, 84 Hz), 2.20 (br, 2 H, $CH_2CH_2CH_2$), 2.31, 2.33 (s, 6 H, SeMe), 2.83, 2.99 (m, 4 H, $SeCH_2$). $^{13}C\{^1H\}$ NMR ($CDCl_3$, 223 K): δ = -8.9 (PtMe, $^1J_{PtC}$ = 749 Hz), -8.7 (PtMe, 748 Hz), 10.5, 10.9 (SeMe), 26.0, 26.7, 27.6 (CH_2). $^{77}Se\{^1H\}$ NMR ($CDCl_3$, 223 K): δ = 114.0 ($^1J_{PtSe}$ = 427 Hz), 102.1 (429 Hz). ^{195}Pt NMR ($CDCl_3$, 223 K): δ = -4247 (major), -4309 (minor).

[$PtMe_2$(*o*-$C_6H_4\{CH_2SeMe\}_2$)]: Method as above using *o*-$C_6H_4(CH_2SeMe)_2$. Cream solid. Yield 56%. $C_{12}H_{20}PtSe_2$ (517.3): calcd. C 27.9, H 3.9; found C 28.6, H 3.7. Electrospray MS (MeCN): found *m/z* = 506; calcd. for $[^{195}PtMe(o\text{-}C_6H_4\{CH_2{}^{80}SeMe\}_2)]^+$ *m/z* = 504. ^1H NMR (400 MHz, $CDCl_3$, 298 K): δ = 0.34 (s, 6 H, PtMe, $^2J_{PtH}$ = 83 Hz, $^3J_{SeH}$ = 14 Hz), 2.3 (s, 6 H, SeMe, $^3J_{PtH}$ = 23

Hz, $^2J_{SeH}$ = 9 Hz), 4.3 (br, 4 H, $SeCH_2$), 7.0 – 7.2 (br m, 4 H, *o*-C_6H_4); (213 K): δ = 0.23 (s, PtMe, $^2J_{PtH}$ ~ 80 Hz), 0.25 (s, PtMe, ~ 80 Hz), 1.89, 2.21, 2.44 (s, SeMe), 3.8 - 5.0 (m, $SeCH_2$), 6.9 - 7.3 (m, 4 H, *o*-C_6H_4). $^{13}C\{^1H\}$ NMR ($CDCl_3$, 298 K): δ = -8.6 (PtMe, $^1J_{PtC}$ = 779 Hz), 11.0 (SeMe), 29.8 ($SeCH_2$), 126.0 – 134.5 (*o*-C_6H_4); (193 K): δ = -8.8 (PtMe, $^1J_{PtC}$ = 760 Hz), -8.3 (PtMe, 751 Hz), -7.4 (PtMe, 763 Hz), 10.3, 11.1, 13.2 (SeMe), 27.8, 28.6, 31.3 ($SeCH_2$), 127.4 – 134.6 (*o*-C_6H_4). $^{77}Se\{^1H\}$ NMR ($CDCl_3$, 298 K): δ = 171.6 ($^1J_{PtSe}$ = 520 Hz); (193 K): δ = 169.1 (526 Hz), 160.6 (492 Hz), 155.9 (438 Hz). ^{195}Pt NMR ($CDCl_3$, 298 K): δ = -4275; (193 K): δ = -4308, -4316.

[$PtMe_2$([8]aneSe_2)]: Method as above using [8]aneSe_2. Beige solid. Yield 64%. $C_8H_{18}PtSe_2$ (467.2): calcd. C 20.6, H 3.9; found C 21.3, H 4.2. Electrospray MS (MeCN): found 494, 453; calcd. for $[^{195}PtMe([8]ane^{80}Se_2)(MeCN)]^+$ *m*/*z* = 495, $[^{195}PtMe([8]ane^{80}Se_2)]^+$ 454. ^1H NMR (300 MHz, $CDCl_3$, 298 K): δ = 0.5 (s, $^2J_{PtH}$ = 82 Hz, 6 H, PtMe), 2.2 (m, 4 H, $CH_2CH_2CH_2$), 2.8 (m, 8 H, $SeCH_2$) ppm. $^{13}C\{^1H\}$ NMR (dmf/D_6-Me_2CO, 298 K): δ = –7.6 ($^1J_{PtC}$ = 794 Hz, 2 C, PtMe), 24.0 (4 C, $SeCH_2$), 27.3 (2 C, $CH_2CH_2CH_2$) ppm. $^{77}Se\{^1H\}$ NMR (dmf/D_6-Me_2CO, 298 K): δ = 140.8 ($^1J_{PtSe}$ = 323 Hz) ppm. ^{195}Pt NMR (CH_2Cl_2/$CDCl_3$, 298 K): δ = –4318 ppm.

[$PtMe_2$([16]aneSe_4)]: Method as above using [16]aneSe_4. Yellow solid. Yield 61%. $C_{14}H_{30}PtSe_4$ (709.3): calcd. C 23.7, H 4.3; found C 23.1, H 4.2. Electrospray MS (MeCN): found *m*/*z* = 695; calcd. for $[^{195}PtMe([16]ane^{80}Se_4)]^+$ *m*/*z* = 700. ^1H NMR (300 MHz, D_6-dmso, 298 K): δ = 0.48 (s, $^2J_{PtH}$ = 81 Hz, 6 H, PtMe), 1.92 (m, 8H, $CH_2CH_2CH_2$) 2.61 (t, 16 H, $SeCH_2$) ppm.

$K_2[PtCl_6]$: $H_2[PtCl_6].6H_2O$ (5 g, 9.65 mmol) was dissolved in H_2O (15 cm^3). KOH (1.09 g, 20 mmol) was added and the reaction stirred overnight. The yellow solid was filtered off and dried *in vacuo*. Yield: 3.32 g, 70%.

[$PtMe_3I$]:[32] Magnesium turnings (1.10 g, 45.2 mmol) in diethyl ether (20 cm^3) were activated with 1,2-dibromoethane and iodine. Methyl iodide (5.0 cm^3, 80 mmol) was added dropwise over 20 minutes. The resulting black suspension was stirred until all the magnesium was dissolved. The mixture was allowed to settle, filtered under N_2 into a dropping funnel and added slowly to an ice-cooled solution of $K_2[PtCl_6]$ (2.0 g, 4.12 mmol) in diethyl ether (10 cm^3) and benzene (40 cm^3). After addition, the yellow mixture was allowed to warm to room temperature and stirred overnight. The white salts were then allowed to settle, and filtered off under N_2. The nearly colourless filtrate was cooled to 0ºC, and ice cold acetone (5 cm^3) added slowly dropwise. The dark orange mixture with black solids was opened to the air and ice cold water (25 cm^3) was added, followed by 10% HCl (30 cm^3). The dark solids were filtered off, and the filtrate separated. The aqueous layer was extracted with benzene (3 x 30 cm^3), and the extracts combined with the organic layer. The orange

solution was dried with $MgSO_4$, and then taken to dryness on a rotary evaporator. The light brown solid was recrystallised from dichloromethane and acetone. Yield: 0.4106 g (27%). ^{1}H NMR (C_6D_6): 1.85 (s, $^2J_{H\text{-}Pt}$ = 78.2 Hz).

[PtMe$_3$I(*o*-C$_6$H$_4${CH$_2$SeMe}$_2$)]: [PtMe$_3$I] (0.0734 g, 0.2 mmol) was dissolved in hot chloroform (10 cm^3). *o*-$C_6H_4(CH_2SeMe)_2$ (0.0584 g, 0.2 mmol) in chloroform (10 cm^3) was added and the mixture stirred under nitrogen for 20 hours. The solvent was reduced *in vacuo*, and the cream solid was precipitated by addition of diethyl ether. Yield 0.100 g (75%). $C_{13}H_{23}IPtSe_2.0.5Et_2O$ (696.3): calcd. C 25.9, H 4.0, found C 26.3, H 3.8. Electrospray MS (MeCN): found 533; calculated for [^{195}PtMe$_3$(*o*-C$_6$H$_4${CH$_2$^{80}SeMe}$_2$)]$^+$ 534. ^{1}H NMR ($CDCl_3$, 298 K): broad; (223 K): δ = 0.90 (s, PtMe, $^2J_{Pt\text{-}H}$ = 79 Hz), 1.12 (s, PtMe, 70 Hz), 1.20 (s, PtMe, 70 Hz), 1.22 (s, PtMe, 70 Hz), 1.36 (s, PtMe, 68 Hz), 2.3 (sh), 2.55, 2.6 (sh, 6 H, SeMe), 3.9 – 5.2 (m, 4 H, CH_2), 7.05 – 7.45 (m, 4 H, *o*-C_6H_4). ^{13}C{^{1}H} NMR ($CDCl_3$, 298 K): broad; (213 K): δ = 1.8 (PtMe, $^1J_{Pt\text{-}C}$ = 628 Hz), 2.6 (PtMe, 622 Hz), 5.2 (PtMe, 616 Hz), 5.85 (PtMe, 624 Hz), 6.2 (PtMe, 660 Hz), 13.7, 14.5, 14.69, 14.72 (SeMe), 27.7, 28.6, 34.3 (sh), 34.6 ($SeCH_2$), 126.8 - 139.9 (*o*-C_6H_4). ^{77}Se{^{1}H} NMR ($CDCl_3$, 298 K): not observed; (213 K): δ = 114.0 ($^1J_{Pt\text{-}Se}$ = 289 Hz); 98.7 (280 Hz), 97.8 (312 Hz), 95.5 (286 Hz) (minor isomer). ^{195}Pt NMR ($CDCl_3$, 298 K): not observed; (213 K): δ = -3382, -3468 (the minor isomer is not observed)

[PtMe$_3$I(κ^2-MeC{CH$_2$SeMe}$_3$)]: Method as above using $MeC(CH_2SeMe)_3$. Yellow solid. Yield 63%. $C_{11}H_{27}IPtSe_3$ (718.2): calcd. C 18.4, H 3.8, found C 18.7, H 3.5. Electrospray MS (MeCN): found *m/z* = 591, 561; calcd. for [^{195}PtMe$_3$(MeC{CH$_2$^{80}SeMe}$_3$)]$^+$ *m/z* = 594; [^{195}PtMe(MeC{CH$_2$^{80}SeMe}$_3$)]$^+$ 564. ^{1}H NMR (400 MHz, $CDCl_3$, 298 K): very broad; (223 K): δ = 0.9 – 1.6 (overlapping resonances, PtMe, CMe), 2.0 – 3.7 (overlapping resonances, SeMe and $SeCH_2$). ^{13}C{^{1}H} NMR ($CDCl_3$, 223 K): δ = 0.35 – 1.06 (s, PtMe *trans* I), 5.9 – 6.8 (s, PtMe *trans* Se), 7.8 – 12.4 (SeMe), 25.2 – 25.5 (MeC), 31.5 – 42.5 ($SeCH_2$). ^{77}Se{^{1}H} NMR ($CDCl_3$, 298 K): no spectrum; (223 K): δ = 53.0 ($^1J_{PtSe}$ = 252 Hz), 51.6 (160 Hz), 49.3 (258 Hz), 38.5 (252 Hz), 37.4 (162 Hz), 37.3 (256 Hz), 35.1, 33.0, 29.0, 27.3 (uncoordinated Se). ^{195}Pt NMR ($CDCl_3$, 223 K): δ = -3446, -3543, -3550.

[PtMe$_3$I([8]aneSe$_2$)]: Method as above using [8]aneSe_2. Cream solid. Yield 45%. $C_9H_{21}IPtSe_2$ (609.2): calcd. C 17.7, H 3.4; found C 17.8, H 3.3. Electrospray MS (MeCN): found 494, 483, 453; calcd. for [^{195}PtMe$_3$([8]ane^{80}Se$_2$)(MeCN)]$^+$ 495, [^{195}PtMe$_3$([8]ane^{80}Se$_2$)]$^+$ 484, [^{195}PtMe([8]ane^{80}Se$_2$)]$^+$ 454. ^{1}H NMR (300 MHz, $CDCl_3$, 298 K): δ = 1.0 (s, $^2J_{PtH}$ = 71.8 Hz, 3 H, PtMe *trans* I), 1.6 (s, $^2J_{PtH}$ = 65.2 Hz, 6 H, PtMe *trans* Se), 2.1–3.4 (m, 12 H, CH_2) ppm. ^{13}C{^{1}H} NMR ($CDCl_3$): δ = 3.5 ($^1J_{PtC}$ = 612 Hz, 1 C, PtMe *trans* I), 3.9 ($^1J_{PtC}$ = 674 Hz, 2 C, PtMe *trans*

Se), 20.8 (2 C), 21.4 (2 C, $SeCH_2$), 22.5 (1 C), 26.8 (1 C, CH_2CH_2) ppm. $^{77}Se\{^1H\}$ NMR ($CDCl_3$, 298 K): δ = 65.3 ($^1J_{PtSe}$ = 244 Hz) ppm. ^{195}Pt NMR ($CDCl_3$): δ = –3589 ppm.

[$PtMe_3I(\kappa^2$-[16]aneSe_4)]: Method as above, but using [16]aneSe_4. Cream solid. Yield 59%. $C_{15}H_{33}IPtSe_4.CHCl_3$ (970.6): calcd. C 19.8, H 3.5; found C 19.4, H 3.8. Electrospray MS (MeCN): found 724; calcd. for $[^{195}PtMe_3([16]ane^{80}Se_4)]^+$ 728. ^1H NMR (300 MHz, $CDCl_3$, 298 K): δ = 1.15 (s, $^2J_{PtH}$ = 71.6 Hz, 3 H, PtMe *trans* I), 1.55 (s, 6 H, PtMe *trans* Se, $^2J_{PtH}$ = 66.5 Hz), 2.5–3.1 (m, 24 H, CH_2) ppm. $^{13}C\{^1H\}$ NMR ($CDCl_3$, 243 K): δ = 3.7 ($^1J_{PtC}$ = 619 Hz, 2 C, PtMe *trans* Se), 4.35 (1 C, PtMe *trans* I, 654 Hz), 22.1 (1 C), 22.7 (2 C, $SeCH_2$), 23.0 (2 C), 25.7 (2 C), 26.3 (2 C), 29.3 (2 C), 29.9 (1 C, CH_2) ppm. $^{77}Se\{^1H\}$ NMR ($CDCl_3$, 243 K): δ = 116.6 ($^1J_{PtSe}$ = 266 Hz, 2 Se), 119.5 (2 Se) ppm. ^{195}Pt NMR ($CDCl_3$, 243 K): δ = –3616 ppm.

[$PtMe_3(\kappa^3$-[16]aneSe_4)]PF_6: $TlPF_6$ (0.063 g, 0.18 mmol) was added to a solution of [$PtMe_3I$] (0.06 g, 0.163 mmol) and [16]aneSe_4 (0.079 g, 0.163 mmol) in $CHCl_3$ (8 cm^3). The reaction mixture was refluxed under N_2 for 2.5 h to give a fine yellow precipitate (TlI) and an almost colourless solution which was separated *via* cannula. After concentrating the solution in vacuo to ca. 2 cm^3, Et_2O was added to give a white solid which was collected by filtration, washed with Et_2O and dried *in vacuo*. Yield 0.049 g, 35%. $C_{15}H_{33}F_6PPtSe_4$ (869.3): calcd. C 20.7, H 3.8, found C 21.3, H 3.7. Electrospray MS (MeCN): found 725, 695; calcd. for $[^{195}PtMe_3([16]ane^{80}Se_4)]^+$ 728, $[^{195}PtMe([16]ane^{80}Se_4)]^+$ 698. ^1H NMR (300 MHz, $CDCl_3$, 298 K): δ = 1.06 (s, $^2J_{PtH}$ = 61 Hz, 3 H, PtMe), 1.13 (s, $^2J_{PtH}$ = 66Hz, 6 H, PtMe), 1.8–3.3 (br. m, 24 H, CH_2) ppm. $^{13}C\{^1H\}$ NMR (CH_2Cl_2/$CDCl_3$, 298 K): very broad (223 K): δ = 2.4 ($^1J_{PtC}$ = 612 Hz, 1 C, PtMe), 3.0 ($^1J_{PtC}$ = 647 Hz, 2 C, PtMe), 22.3–29.1 (CH_2) ppm. $^{77}Se\{^1H\}$ NMR ($CDCl_3$, 298 K): no spectrum; (223 K): δ = 138 (1 Se), 70 ($^1J_{PtSe}$ = 249 Hz, 3 Se) ppm. ^{195}Pt NMR (CH_2Cl_2/$CDCl_3$, 298 K): δ = –3648 ppm. IR (Nujol): $\tilde{\nu}$ = 840 [$\nu(PF_6^-)$], 557 [$\delta(PF_6^-)$]cm^{-1}.

[$PtMe_3I(o$-$C_6H_4\{CH_2TeMe\}_2$)]: Method as above using o-$C_6H_4(CH_2TeMe)_2$. Orange solid. Yield 60%. $C_{13}H_{23}IPtTe_2\cdot\frac{1}{2}Et_2O$ (793.6): calcd. C 22.7, H 3.6, found C 23.1, H 3.5. Electrospray MS (MeCN): found 629; calculated for $[^{195}PtMe_3(o\text{-}C_6H_4\{CH_2{}^{130}TeMe\}_2)]^+$ 634. ^1H NMR ($CDCl_3$, 298 K): broad; (248 K): δ 0.85 – 1.6 PtMe, 2.1 – 3.1 TeMe, 3.9 – 5.0 (m, 4H) CH_2, 8.1 – 6.9 (*m*, 4H) *o*-C_6H_4. $^{13}C\{^1H\}$ NMR ($CDCl_3$, 298 K): broad; (243 K): δ 7.3, 6.8, 4.6, 4.3, 3.9, 2.9, 1.8 (PtMe), -5.7, -6.7, -12.4, -12.45 (TeMe), 16.9, 16.7, 12.4, 10.4 ($TeCH_2$), 135.3 – 126.5 (*o*-C_6H_4). $^{125}Te\{^1H\}$ NMR ($CDCl_3$, 243 K): δ 189.5, $^1J_{PtTe}$ = 602 Hz; 159.9, $^1J_{PtTe}$ = 618 Hz, 114.5, $^1J_{PtTe}$ = 638 Hz, 110.8, $^1J_{PtTe}$ = 537 Hz. ^{195}Pt NMR ($CDCl_3$, 298 K): not observed; (223 K): δ -3968, -4022, -4119.

[($PtMe_3I)_2$($MeTeCH_2TeMe$)]: [$PtMe_3I$] (0.146 g, 0.4 mmol) was dissolved in hot chloroform (10 cm^3). $MeTeCH_2TeMe$ (0.06 g, 0.2 mmol) in chloroform (10 cm^3) was added and the reaction stirred at RT for 20 hours. Solvent was removed *in vacuo* and the dark brown solid recrystallised from CH_2Cl_2/hexane. Yield 0.143 g (68%). ^{1}H NMR (400 MHz, $CDCl_3$, 298 K): broad; (248 K): δ = 1.06 (s, PtMe, $^2J_{PtH}$ = 76 Hz), 1.14 (s, PtMe, 72 Hz), 1.16 (s, PtMe, 74 Hz), 1.22 (s, PtMe, 76 Hz), 2.06 (s, PtMe, 68 Hz), 2.07 (s, PtMe, 68 Hz), 2.01, 2.18 (s, TeMe), 4.46, 4.55 (m, $TeCH_2$). $^{13}C\{^1H\}$ NMR ($CDCl_3$, 298 K): broad; (243 K): δ = -18.7 (major form, $TeCH_2$) -16.1 (minor form, $TeCH_2$), -8.5 (major form, TeMe), -7.95 (minor form, TeMe), 6.55 (PtMe, $^1J_{PtC}$ = 670 Hz), 7.0 (PtMe, 678 Hz), 7.7 (PtMe, 600 Hz), 7.8 (PtMe, 660 Hz), 9.1 (PtMe, 607 Hz). $^{125}Te\{^1H\}$ NMR ($CDCl_3$, 243 K): δ = 173.2 ($^1J_{PtTe}$ = 713 Hz); 171.1 (605 Hz). ^{195}Pt NMR ($CDCl_3$, 223 K): δ = -3430 (major), -3451 (minor).

2.10 – X-Ray Crystallography

Details of the crystallographic data collection and refinement parameters are given in Table 2.6. Yellow/orange single crystals of [$PtMe_3I(o\text{-}C_6H_4\{CH_2SeMe\}_2)$] were obtained by slow evaporation of a solution of the complex in CH_2Cl_2/hexane. Structure solution and refinement were routine.[39,40] Selected bond lengths and angles for [$PtMe_3I(o\text{-}C_6H_4\{CH_2SeMe\}_2)$] are presented in Table 2.3.

Table 2.6: Crystallographic data collection and refinement parameters. $R1 = \Sigma||F_o| - |F_c||/\Sigma|F_o|$; $wR_2 = [\Sigma w(F_o^2 - F_c^2)^2/\Sigma wF_o^4]^{1/2}$

Complex	**[$PtMe_3I(o\text{-}C_6H_4\{CH_2SeMe\}_2)$]**
Formula	$C_{13}H_{23}IPtSe_2$
M	659.22
Crystal System	Monoclinic
Space Group	*C2/c*
a/Å	13.3002(7)
b/Å	11.6116(7)
c/Å	22.5391(12)
α/°	90
β/°	102.788(2)
γ/°	90
U/Å^3	3394.5(3)
Z	8
μ(Mo-Kα)/ mm^{-1}	14.356
R_{int}	0.0224
Total no. reflns.	10840
Unique reflections	3861
No. of parameters	159
$R1$ [$I_o > 2\sigma(I_o)$]	0.0196
$R1$ [all data]	0.0215
wR_2 [$I_o > 2\sigma(I_o)$]	0.0443
wR_2 [all data]	0.0451

2.11 – References

1. Levason, W.; Manning, J. M.; Pawelzyk, P.; Reid, G. *Eur. J. Inorg. Chem.* **2006**, 4380 – 4390.

2. Chiffey, A. F.; Evans, J.; Levason, W.; Webster, M. *J. Chem. Soc., Dalton Trans.* **1994**, 2835 – 2840.

3. Gulliver, D. J.; Hope, E. G.; Levason, W.; Murray, S. G.; Marshall, G. L. *J. Chem. Soc., Dalton Trans.* **1985**, 1265 – 1269.

4. Champness, N. R.; Levason, W.; Quirk, J. J.; Reid, G.; Frampton, C. *Polyhedron* **1995**, *14*, 2753 – 2758.

5. Champness, N. R.; Kelly, D. F.; Levason, W.; Reid, G.; Slawin, A. M. Z.; Williams, D. J. *Inorg. Chem.* **1995**, *34*, 651 – 657.

6. Levason, W.; Nirwan, M.; Ratnani, R.; Reid, G.; Tsoureas, N.; Webster, M. *Dalton Trans.* **2007**, 439 – 448.

7. Hope, E. G.; Levason, W.; Murray, S. G.; Marshall, G. L *J. Chem. Soc., Dalton Trans.* **1985**, 2185 – 2190.

8. Levason, W.; Orchard, S. D.; Reid, G. *Inorg. Chem.* **2000**, *39*, 3853 – 3859.

9. Kemmitt, T.; Levason, W. *Inorg. Chem.* **1990**, *29*, 731 – 735.

10. Kemmitt, T.; Levason, W.; Webster, M. *Inorg. Chem.* **1989**, *28*, 692 – 696.

11. Levason, W.; Patel, B.; Reid, G.; Ward, A. J. *J. Organomet. Chem.* **2001**, *619*, 218 – 225.

12. Barton, A. J.; Levason, W.; Reid, G.; Ward, A. J. *Organometallics* **2001**, *20*, 3644 – 3649.

13. Levason, W.; Orchard, S. D.; Reid, G.; Tolhurst, V-A. *J. Chem. Soc., Dalton Trans.* **1999**, 2071 – 2076.

14. Abel, E. W.; Bhargava, S. K.; Kite, K.; Orrell, K. G.; Sik, V.; Williams, B. L.; *Polyhedron* **1982**, *1*, 289 – 298.

15. Abel, E. W.; Evans, D. G.; Koe, J. R.; Hursthouse, M. B.; Mazid, M. *J. Chem. Soc., Dalton Trans.* **1992**, 663 – 667.

16. Abel, E. W.; Koe, J. R.; Hursthouse, M. B.; Malik, K. M. A.; Mazid, M. A. *J. Chem. Soc., Dalton Trans.* **1994**, 2645 – 2650.

17. Abel, E. W.; Khan, A. R.; Kite, K.; Orrell, K. G.; Sik, V. *J. Chem. Soc., Dalton Trans.* **1980**, 1175 – 1181.

18. Abel, E. W.; Orrell, K. G.; Platt, A. W. G. *J. Chem. Soc., Dalton Trans.* **1983**, 2345 – 2351.

19. Abel, E. W.; Bhargava, S. K.; Orrell, K.G.; Platt, A. W. G.; Sik, V.; Cameron, T.S. *J. Chem. Soc., Dalton Trans.* **1985**, 345 – 353.

20. Abel, E. W.; Khan, A. R.; Kite, K.; Orrell, K. G.; Sik, V. *J. Chem. Soc., Dalton Trans.* **1980**, 1169 – 1174.

21. Abel, E. W.; Kite, K.; Perkins, P. D. *Polyhedron* **1986,** *5*, 1459 – 1465.

22. Levason, W.; Quirk, J. J.; Reid, G.; Frampton, C.S. *Inorg. Chem.* **1994**, *33*, 6120 – 6122.

23. Abel, E.; Orrell, K. G.; Scanlan, S. P.; Stephenson, D.; Kemmitt, T.; Levason, W. *J. Chem. Soc., Dalton Trans.* **1991**, 591 – 595.

24. Gulliver, D. J.; Hope, E. G.; Levason, W.; Murray, S. G.; Potter, D. M.; Marshall, G. L. *J. Chem. Soc. Perkin Trans. II* **1984**, 429 – 434.

25. Hope, E. G.; Kemmitt, T.; Levason, W. *Organometallics* **1988**, *7*, 78 – 83.

26. Batchelor, R. J.; Einstein, F. W. B.; Gay, I. D.; Gu, J-H.; Johnston, B. D.; Pinto, B. M. *J. Am. Chem. Soc.* **1989**, *111*, 6582 – 6591.

27. Bennett, M. A.; Canty, A. J.; Felixburger, J. K.; Rendina, L. M.; Sunderland, C.; Willis, A. C. *Inorg. Chem.* **1993**, *32*, 1951 – 1958.

28. Brown, M. D.; Levason, W.; Reid, G.; Webster, M. *Dalton Trans.* **2006**, 1667 – 1674.

29. Hill, G. S.; Irwin, M. J.; Levy, C. J.; Rendina, L. M.; Puddephatt, R. J. *Inorg. Synth.* **1998**, *32*, 149 – 153.

30. Levason, W.; Orchard, S. D.; Reid, G. *Coord. Chem. Rev.* **2002**, *225*, 159 – 199.

31. Hope, E.; Levason, W. *Coord. Chem. Rev.* **1993**, *122*, 109 – 170.

32. Baldwin, J. C.; Kaska, W. C. *Inorg. Chem.* **1975**, *14*, 2020.

33. Levason, W.; Ollivere, L. P.; Reid, G.; Tsoureas, N.; Webster, M. *J.Organomet. Chem.* **2009**, *694*, 2299 – 2308.

34. Connolly, J.; Genge, A. R. J.; Levason, W.; Orchard, S. D.; Pope, S. J. A.; Reid, G. *J. Chem. Soc., Dalton Trans.* **1999**, 2343 – 2351.

35. Levason, W.; Orchard, S. D.; Reid, G.; Street, J. M. *J. Chem. Soc., Dalton Trans.* **2000**, 2537 – 2543.

36. Levason, W.; Orchard, S. D.; Reid, G. *Chem. Commun.* **1999**, 1071 – 1072.

37. Abel, E. W.; Beer, P. D.; Moss, I.; Orrell, K. G.; Sik, V.; Bates, P. A.; Hursthouse, M. B. *J. Organomet. Chem.* **1988**, *341*, 559 – 567.

38. Brown, M. P.; Puddephatt, R. J.; Upton, C. E. E. *J. Chem. Soc., Dalton Trans.* **1974**, 2457 – 2465.

39. Sheldrick, G. M. SHELXS-97, program for crystal structure solution, University of Göttingen, Germany, **1997**.

40. Sheldrick, G. M. SHELXS-97, program for crystal structure refinement, University of Göttingen, Germany, **1997**.

Chapter 3: Selenium-Rich Selenium/Oxygen Macrocycles[1]

3.1 – Mixed Chalcogenoether Macrocycles

A small number of mixed donor O/Se macrocycles have been reported in the literature (see Figure 3.1 for some examples). There are relatively fewer known O/Se macrocycles than O/S macrocycles, and these macrocycles generally have greater or equal numbers of O atoms to Se atoms.[2,3] A number of different routes have been published, including $NaBH_4$ reduction of a dibromide and a diselenocyanate.[4] For example, reaction of $Br(\{CH_2\}_2O)_n(CH_2)_2Br$ (n = 1, 2) with $NCSe(\{CH_2\}_2O)_m(CH_2)_2SeCN$ (m = 1, 2) which produces $[12]aneO_2Se_2$, $[15]aneO_3Se_2$ or $[18]aneO_4Se_2$.[5] Another route is to use a selenolate precursors such as *o*-$C_6H_4(SeK)_2$, which can be reacted in refluxing thf with *o*-$C_6H_4(Se\{(CH_2)_2O\}_p\{CH_2\}_2Cl)_2$ (p = 1, 2, 3) to produce the benzyl-alkyl-backbone macrocycles shown in Figure 3.1. Yields of these macrocycles can be improved by generating the selenolate by reaction of *o*-$C_6H_4(SeH)_2$ with Cs_2CO_3 in dmf *in situ* before addition of the dichloroselenoether.[6]

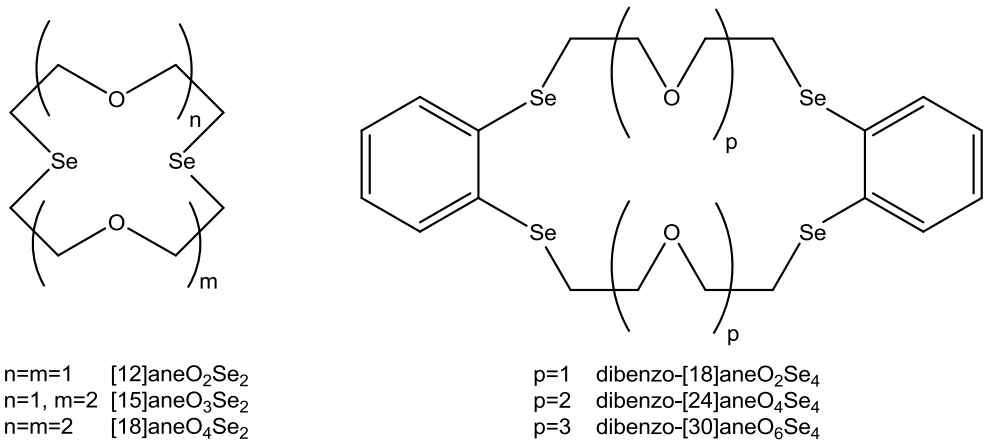

Figure 3.1: Some examples of mixed donor O/Se macrocycles.[5,6]

The choice of precursor has been shown to be crucial, as can be illustrated by the preparations of $[9]aneO_2Se$ and $[12]aneO_2Se_2$ shown in Figure 3.2. When the dibromoether $Br(CH_2)_2O(CH_2)_2O(CH_2)_2Br$ and $NCSe(CH_2)_2SeCN$ are used as the precursors, ring contraction occurs *via* elimination of one Se, most probably by the Na template intermediate shown. However, when the functional groups are reversed, and 1,2-dibromoethane is reacted with $NCSe(CH_2)_2O(CH_2)_2O(CH_2)_2SeCN$, no such elimination occurs, and the four donor macrocycle $[12]aneO_2Se_2$ is formed.[5]

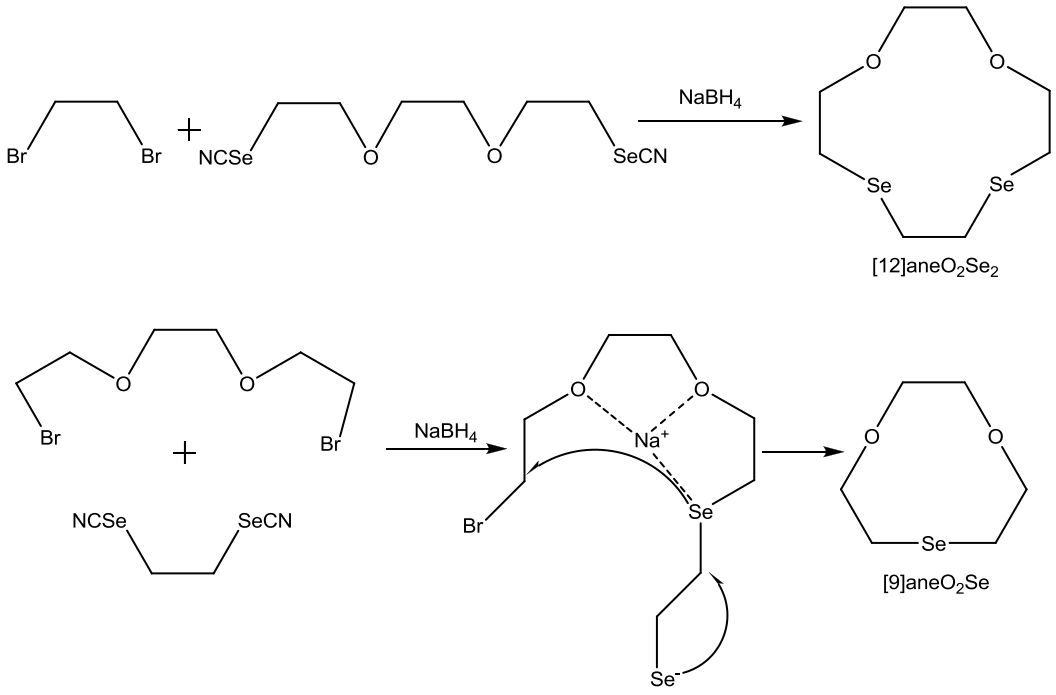

Figure 3.2: Scheme for the production of [9]aneO_2Se and [12]aneO_2Se_2.[5]

The mixed O/Te macrocycle, [18]aneO_4Te_2 (Figure 3.3) is produced by the reaction of Na_2Te and $Cl(CH_2)_2O(CH_2)_2O(CH_2)_2Cl$ in liquid ammonia at -78°C. After the reaction mixture has warmed to room temperature, it is hydrolysed and extracted with CH_2Cl_2, which is then removed *in vacuo* to produce an orange solid. Recrystallisation of this crude material with CH_2Cl_2 and diethyl ether produces [18]aneO_4Te_2 as a yellow, slightly air sensitive solid. If the crude material is not recrystallised, but instead is passed down a silica column, elution with hexane/ethyl acetate separates [9]aneO_2Te as an air-sensitive yellow solid, but [18]aneO_4Te_2 does not elute and is lost on the column.[7] An analogous reaction using Na_2Se gives evidence of the production of a small amount of [9]aneO_2Se and [18]aneO_4Se_2, but the yield is poor and most of the dichloroether precursor is recovered unreacted. Even raising the temperature to -33°C for the addition results in substantial amounts of unreacted $Cl(CH_2)_2O(CH_2)_2O(CH_2)_2Cl$.[7] In an alternate method, a dilute solution of $Cl(CH_2)_2O(CH_2)_2O(CH_2)_2Cl$ in EtOH was added slowly dropwise to a dilute solution of Na_2Se in EtOH, which allowed [18]aneO_4Se_2 to be collected by recrystallisation (~ 8 % yield), and a small amount of [9]aneO_2Se to be distilled from the residue.[7]

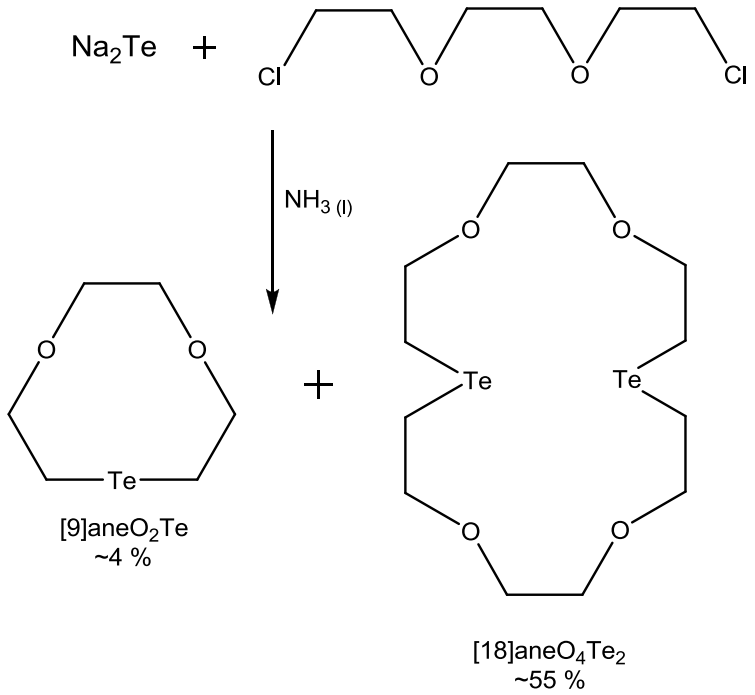

Figure 3.3: Reaction scheme for the production of [9]aneO$_2$Te and [18]aneO$_4$Te$_2$.[7]

There are only two mixed donor S/Se macrocycles in the literature. One is a cyclophane containing two Se donors and two S donors from thiophene, made by $NaBH_4$ reduction of 2,5-bis(selenocyanatomethyl)thiophene and 2,5-bis(bromomethyl)thiophene.[4] The other is [16]aneS$_2$Se$_2$ which is produced by the dropwise addition of separate solutions in dmf of Br(CH$_2$)$_3$Br and HS(CH$_2$)$_3$Se(CH$_2$)$_3$Se(CH$_2$)$_3$SH to a 60°C solution of Cs_2CO_3 in dmf. [16]aneS$_2$Se$_2$ is obtained in 22 % yield, and is purified by column chromatography (eluent: hexane/ethyl acetate, 250:1.5).[8]

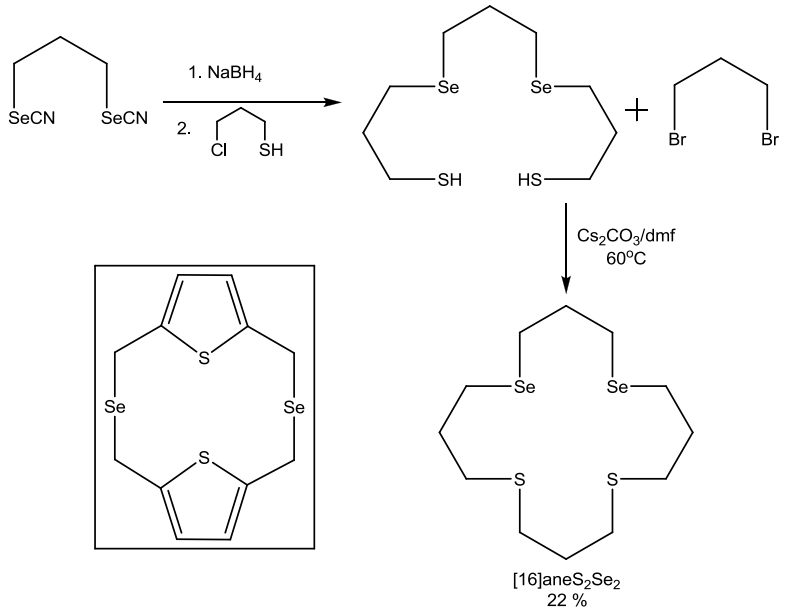

Figure 3.4: Production scheme for [16]aneS$_2$Se$_2$.[8] Inset: thiophene derived Se/S macrocycle.[4]

There are four known S/Te macrocycles, which are shown in Figure 3.5. These are produced by reaction of Na_2Te with $Cl(CH_2)_nS(CH_2)_mS(CH_2)_nCl$ (n=m=2; n=3,m=2; n=m=3) in the case of the tridentate macrocycles, and Na_2Te with $Cl(CH_2)_3S(CH_2)_2S(CH_2)_2S(CH_2)_3Cl$ for the tetradentate.

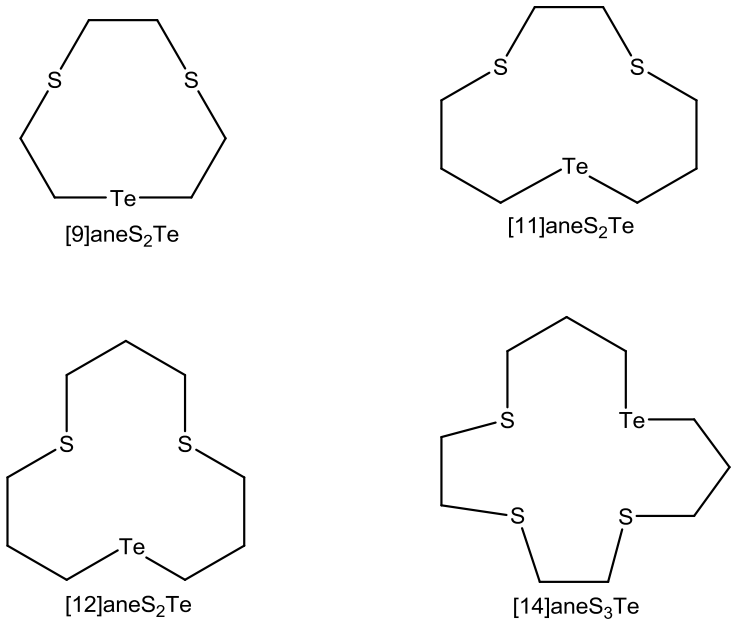

Figure 3.5: Mixed donor S/Te macrocycles.[9,10]

All these reactions took place in liquid ammonia, with production of [11]aneS$_2$Te, [12]aneS$_2$Te and [14]aneS$_3$Te occurring at -78°C and purification by means of column chromatography, while [9]aneS$_2$Te required the addition of the dichlorothioether to be undertaken at -45°C and was isolated by recrystallisation from CH_2Cl_2 and MeOH.[9,10] Crystal structures have been published for [11]aneS$_2$Te and [12]aneS$_2$Te (Figure 3.6).[10]

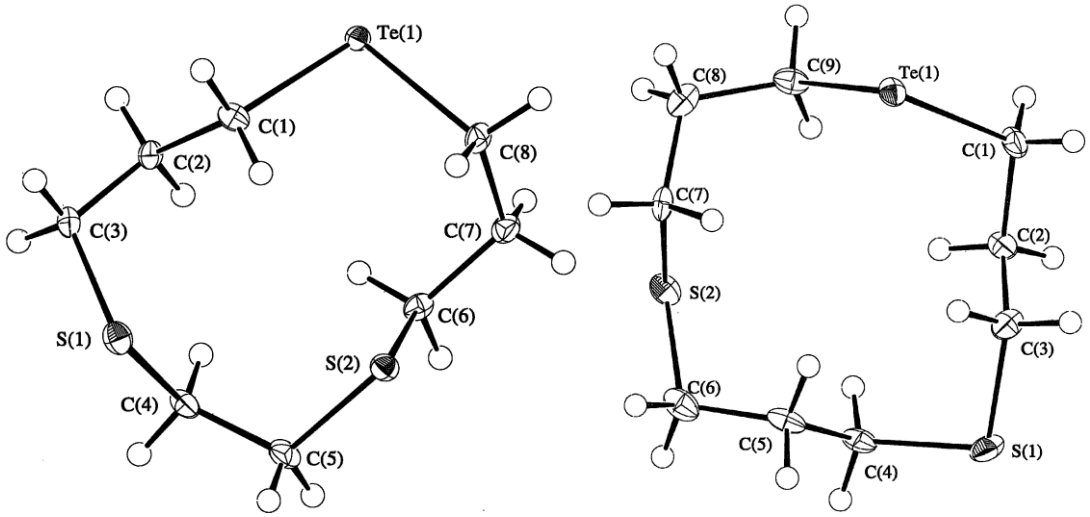

Figure 3.6: Crystal structures of [11]aneS$_2$Te and [12]aneS$_2$Te. Ellipsoids shown at 40 % probability.[10]

Both the O/Te macrocycles and S/Te macrocycles are unusual in terms of telluroether chemistry in that they show examples of stable C_2 backbones between Te and a second donor atom. Where the second donor atom is another Te, it has been shown that the elimination of ethene is facile (see chapters 1 and 4). The stronger O-C and S-C bonds, and the absence of a second Te to form a ditelluride is sufficient to overcome the possibility of elimination.[7]

3.2 – Aims

The aim of this chapter is to investigate routes to mixed donor macrocycles of the type O_xSe_{2x}, and develop multi-gram yielding routes. A variety of backbones will be investigated. Complexation chemistry with some common transition metals will also be investigated.

3.3 – Production of O_xSe_{2x} Macrocycles

The first attempt at making O_xSe_{2x} macrocycles took *α, α'*-diselenocyanato-*o*-xylene and $O(CH_2CH_2Br)_2$ as starting materials. It was decided to use these precursors as $O(CH_2CH_2Br)_2$ is commercially available, and *o*-$C_6H_4(CH_2SeCN)_2$ has been made and used before in our group in Southampton. It was also thought that the xylyl backbone to the diselenocyanate precursor should help promote cyclisation over polymerisation. *o*-$C_6H_4(CH_2SeCN)_2$[4] was reacted with sodium metal in liquid NH_3 at –78°C to generate the diselenolate anion (Figure 3.7). A solution of $O(CH_2CH_2Br)_2$ in thf was added dropwise over several hours whilst the reaction mixture was maintained at –40°C in a cardice/acetone bath. Analysis of the crude material obtained after work-up by NMR spectroscopy showed negligible amounts of cyclised species and significant amounts of unreacted dibromoether.

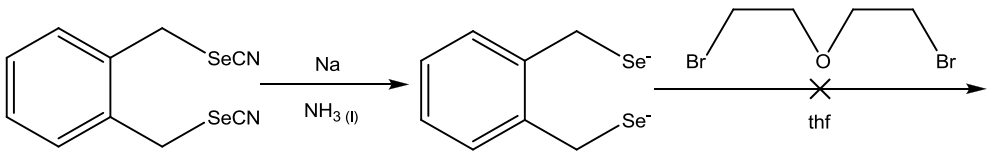

Figure 3.7: Reaction scheme for initial attempt to produce O_xSe_{2x} macrocycles.

This is similar to the production of [9]aneO_2Se and [18]aneO_4Se_2 which saw low reactivity between the selenolate anion and dichloroether,[7] however it was hoped that the use of the dibromoether would make the reaction more favourable. Previous work in this group has led to the understanding that Se^- displaces Br^- more readily than Cl^-, so to observe even worse reaction rates here was disappointing. The ether O atom may have a deactivating effect on the C atoms α to the Br atoms. The xylyl backbone to the diselenocyanate means that elimination reactions similar to those seen in the production of [12]aneO_2Se_2 (Figure 3.2) are very unlikely.[5]

To counteract this possible deactivation it was decided to reverse the precursors, namely to try reacting *o*-$C_6H_4(CH_2Br)_2$ with $O(CH_2CH_2SeCN)_2$. To this end $O(CH_2CH_2Br)_2$ was added dropwise to a solution of KSeCN in acetone and stirred for ~12 hours. KBr was removed by filtration, and the acetone removed *in vacuo*. Dissolution in CH_2Cl_2 was required to allow residual KBr to be filtered off. $O(CH_2CH_2SeCN)_2$ was thus obtained in good yield as a yellow oil. Repeat preparations of this precursor showed that if left for longer periods of time stirring in acetone (e.g. two or three days), decompostition started to occur. It is vital that the solvent removal be effected promptly to maximise the yield. $O(CH_2CH_2SeCN)_2$ was characterised by ^1H, $^{13}C\{^1H\}$, and ^{77}Se NMR, and by EIMS.

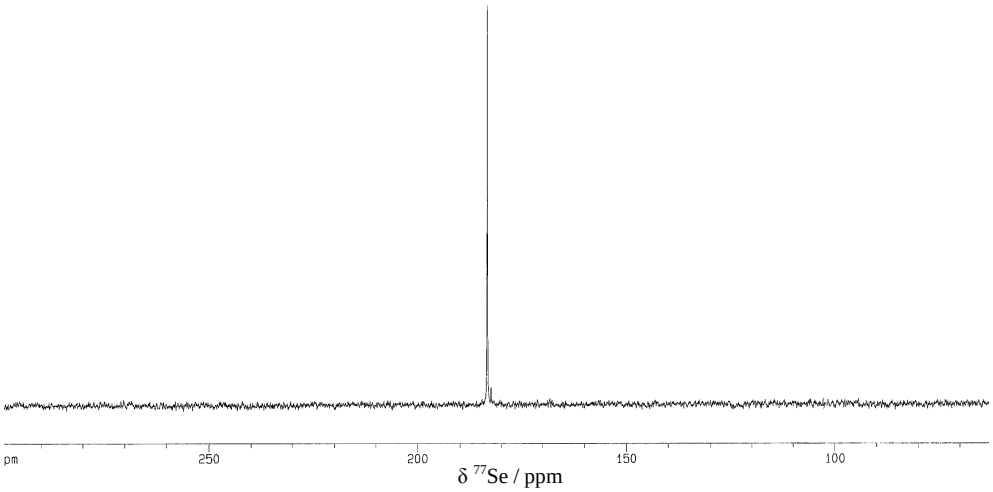

Figure 3.8: $^{77}Se\{^1H\}$ NMR spectrum of $O(CH_2CH_2SeCN)_2$ recorded in $CDCl_3$.

$O(CH_2CH_2SeCN)_2$ was reacted with sodium metal in liquid NH_3 at –78°C to give a light yellow solution. One molar equivalent of *α, α'*dibromo-*o*-xylene was added dropwise as a solution in thf over a period of 3 hours, whilst the reaction was maintained at ~ –50°C. Upon complete addition, the reaction mixture was allowed to warm slowly to RT, and left overnight under flow of N_2 to allow the NH_3 to boil off. Following hydrolysis and extraction with CH_2Cl_2, the combined organics were dried over $MgSO_4$ and the solvent removed *in vacuo*. This yielded a crude mixture of yellow oil and off-white waxy solid. Dissolution in minimum CH_2Cl_2 followed by addition of hexane allowed recrystallisation of the solid which was filtered off and dried *in vacuo*. This white crystalline solid was analysed by ^1H, $^{13}C\{^1H\}$, and ^{77}Se NMR, and by EIMS.

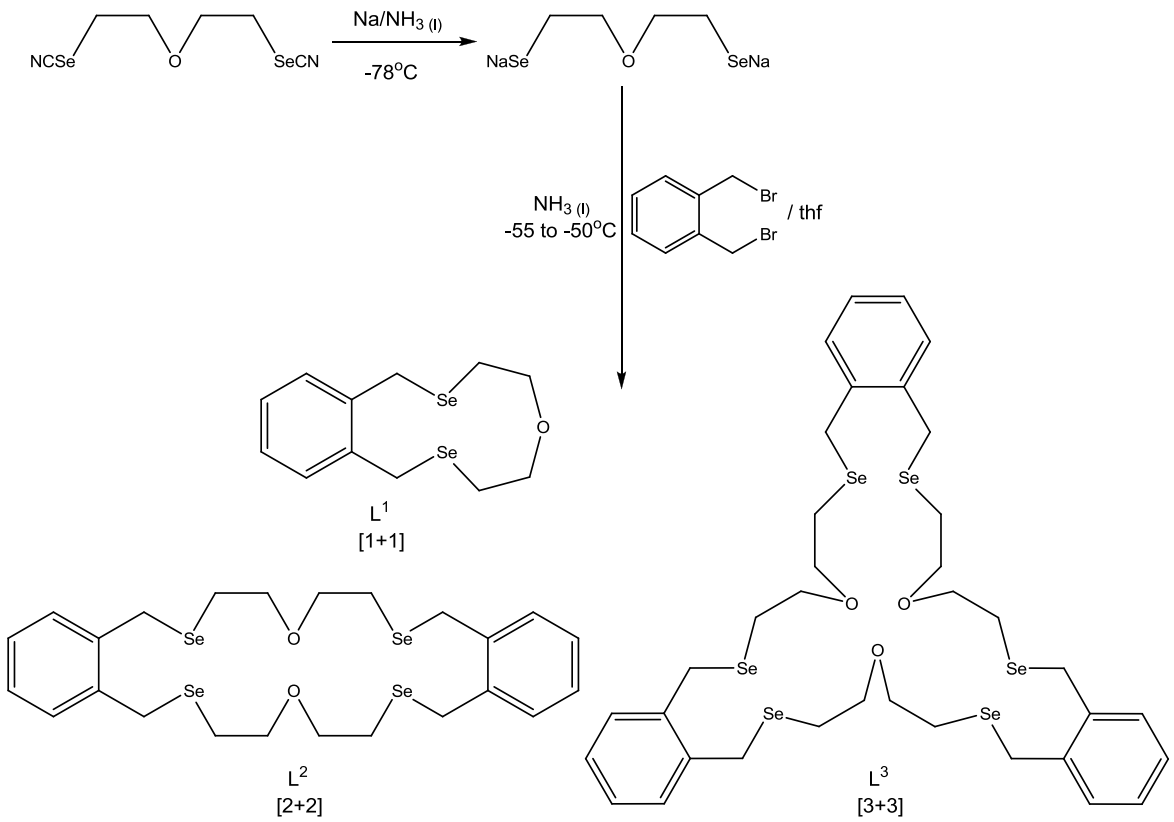

Figure 3.9: Reaction scheme for production of O_xSe_{2x} macrocycles *via* $Na/NH_{3\,(l)}$ route.

^{77}Se NMR spectrum of the white solid in $CDCl_3$ showed a singlet at δ = 215 ppm (Figure 3.10). This clearly indicated a single selenium containing species. ^{1}H and $^{13}C\{^{1}H\}$ NMR data were also consistent with the solid being a single species, with both aromatic and CH_2 linkages present. A singlet was observed in the ^{1}H NMR spectrum at 4.19 ppm which is consistent with a *o*-$C_6H_4CH_2Se$ linkage (*c.f.* 4.05 ppm in *o*-$C_6H_4(CH_2SeMe)_2$).[11] ^{77}Se-H coupling was observed on the singlet and one triplet resonance in the ^{1}H NMR spectrum, and on two on the resonances in the $^{13}C\{^{1}H\}$ NMR spectrum, confirming formation of the xylyl linkage and retention of the $Se(CH_2)_2O$ linkages.

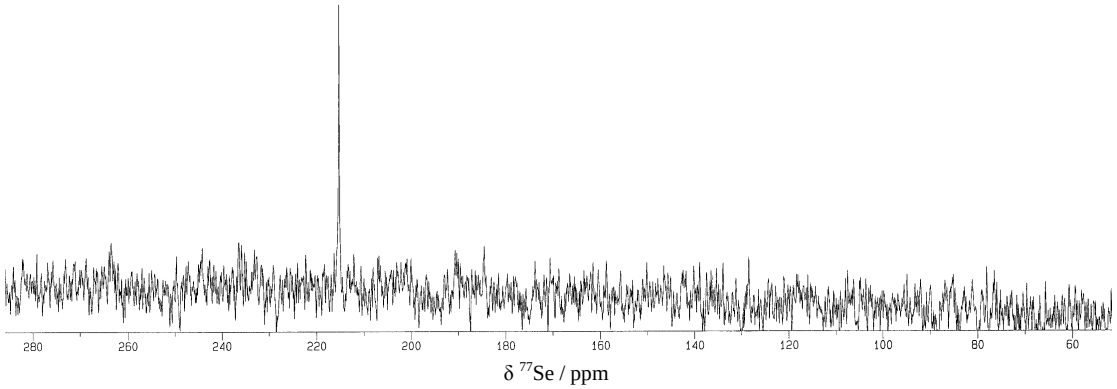

Figure 3.10: $^{77}Se\{^{1}H\}$ NMR spectrum of L^2 recorded in $CDCl_3$.

The NMR spectra were all consistent with the white solid being a single, macrocyclic species, but could not identify the size of this macrocycle. EIMS allowed it to be identified as the [2+2] addition product (see Figure 3.9), showing a peak cluster around *m/z* = 672 with the correct isotope pattern for L^2 (calculated for $C_{24}H_{32}O_2{}^{80}Se_4$ = 672). A peak cluster consistent with fragmentation *via* loss of one xylyl linkage (*m/z* = 565) was also observed.

The remaining yellow oil was dissolved in a minimum of CH_2Cl_2 and adsorbed onto a silica column. A mixture of hexane/ethyl acetate (19:1) was used as eluent as this ratio has been shown to give good separation when used with selenoether macrocycles. A first fraction of yellow solid (after drying *in vacuo*) was obtained, which was analysed by EIMS, ^1H, $^{13}C\{^1H\}$ and $^{77}Se\{^1H\}$ NMR spectroscopy. ^1H and $^{13}C\{^1H\}$ NMR spectroscopy showed it to be a similar, macrocyclic species, while its $^{77}Se\{^1H\}$ NMR spectrum showed a single peak at 205 ppm, showing it to be a different species to the crystallised product, L^2. Again, EIMS allowed the size to be ascertained, showing this fraction to be the [1+1] cyclisation product, L^1 (see Figure 3.9). The small ring size of L^1 explains the why the proton resonances from the Se-C*H*$_2$-C*H*$_2$-O linkage appear as distorted triplets in the ^1H NMR spectrum (Figure 3.11), as there must be ring strain at the O atom preventing these protons from exchanging as freely as they do in a non-constrained system.

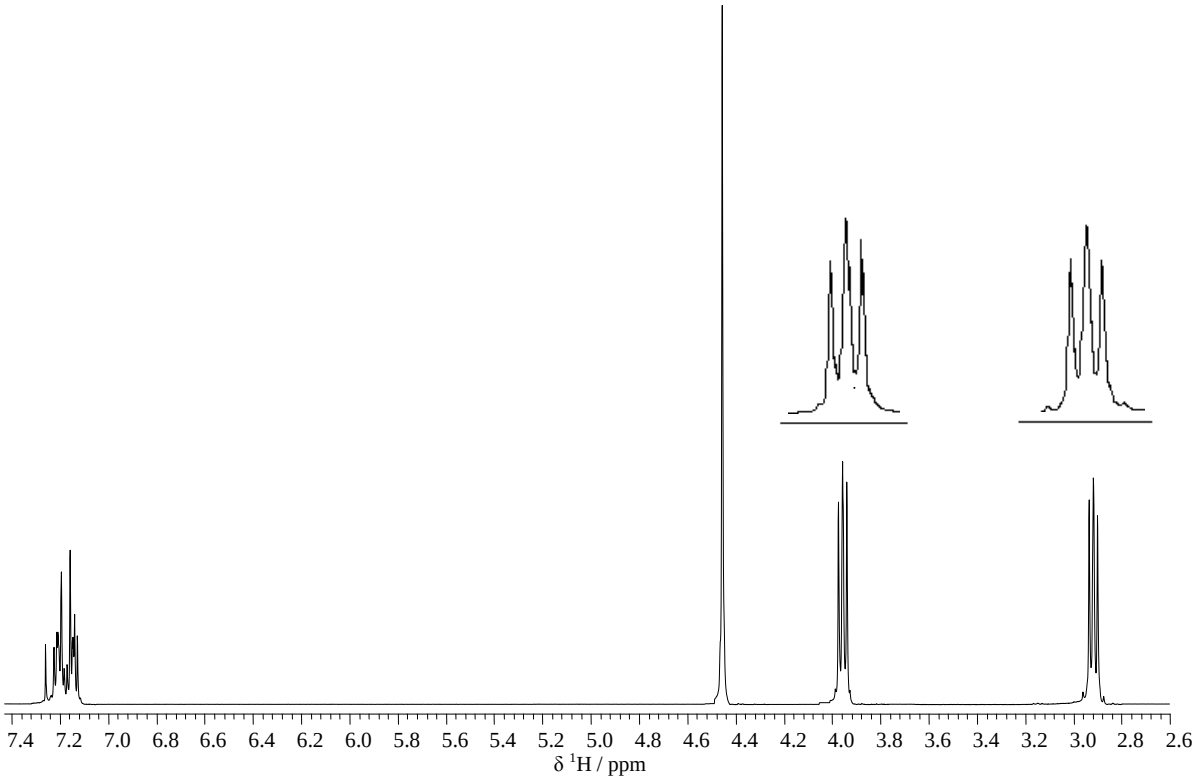

Figure 3.11: ^1H NMR spectrum of L^1 recorded in $CDCl_3$.

Increasing the ethyl acetate content of the eluent (hexane:ethyl acetate 9:1) allowed a second fraction to be obtained, which was also demonstrated by NMR spectroscopy to be a macrocyclic species. Figure 3.12 below shows the ^{1}H NMR spectrum of this fraction run in solution of $CDCl_3$. The peak at 4.0 ppm relates to the xylyl-Se linking CH_2, and clearly shows $^{2}J_{SeH}$ coupling of 5.6 Hz. This is roughly half the size of the coupling observed on *o*-$C_6H_4(CH_2SeMe)_2$ ($^{2}J_{SeH}$ = 13 Hz).[11] The sharply defined triplets for the $SeCH_2CH_2O$ protons indicates a greater freedom of movement, and flexibility compared to L^1, showing it to be from a larger ring. The peaks at 2.7 ppm also show $^{2}J_{SeH}$ coupling (7 Hz), showing these to be the protons on the carbon α to Se. The complex coupling of aromatic protons doesn't allow distinct allocation of the resonances to individual protons, as with most of these ligands, however, there are two distinct sets, for the *ortho* and *meta* pairs.

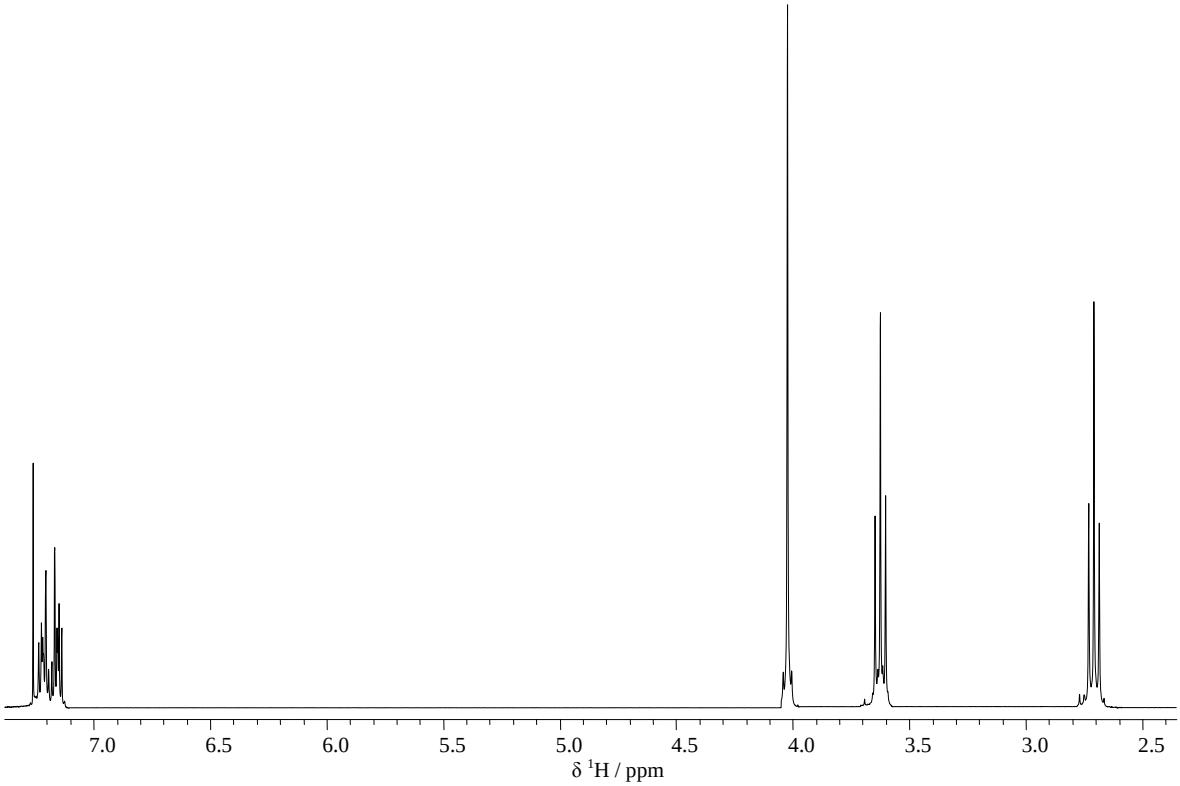

Figure 3.12: ^{1}H NMR spectrum of L^3 recorded in $CDCl_3$.

The ^{77}Se{^{1}H} NMR spectrum shows a single peak at 213 ppm, which is similar to that of L^2, but the APCI MS shows this to be the [3+3] product, L^3 (Figure 3.9). As Figure 3.13 demonstrates, the APCI MS shows a peak cluster around 1027 m/z, which corresponds to $L^3 \cdot Na^+$.

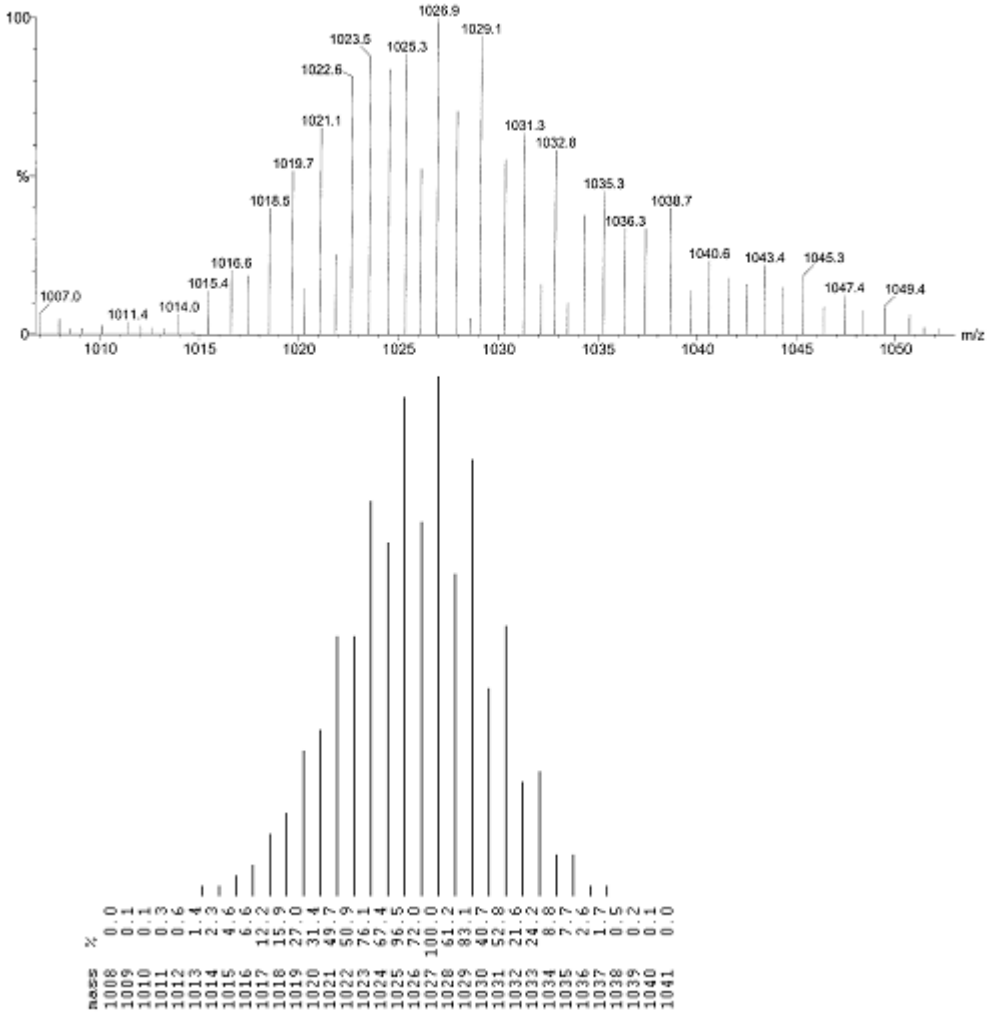

Figure 3.13: Top: APCI MS of L^3. Bottom: calculated isotope pattern for $C_{36}H_{48}O_3Se_6 \cdot Na^+$.

The proton NMR spectra for these three related macrocycles are similar, but not identical, as can be seen from Table 3.1. The small, constrained ring size of L^1 has a distinct effect both on shifts and coupling patterns, but the larger L^2 and L^3 also have slightly different chemical shifts, indicating ring size to have an effect beyond that of steric constraints.

Table 3.1: ^{1}H NMR data of L^1-L^3. Spectra recorded in $CDCl_3$. $^2J_{SeH}$ / Hz values in parentheses.

Macrocycle	**δ C_6H_4 / ppm**	**δ *o*-$C_6H_4CH_2$ / ppm**	**δ $SeCH_2CH_2O$ / ppm**	**δ $SeCH_2CH_2O$ / ppm**
L^1	7.1 – 7.2	4.5	2.9	4.0
L^2	7.2 – 7.4	4.2 (6.5)	2.8 (6.5)	3.7
L^3	7.1 – 7.3	4.0 (5.6)	2.7 (7)	3.6

Crystal structures of L^1 and L^2 were obtained from crystals grown by slow evaporation of a solution of the macrocycles in CH_2Cl_2/hexane. L^1, shown in Figure 3.14, has the O lone pairs somewhat *endo* to the ring, whilst the Se lone pairs are *exo*. The Se atoms are on opposite sides of

the plane of the xylyl ring, and <C-Se-C are more acute than <C-O-C, which is rather obtuse (113.1°), reflecting the constrained nature of the ring. The only other small Se containing ring which has had a crystal structure published is [12]aneSe_3, which has C_3 linkages between the Se atoms, and consequently has greater flexibility. This can be seen in the slightly shorter C-Se bond lengths, which are between 1.923(9) and 1.963(7) Å.[8]

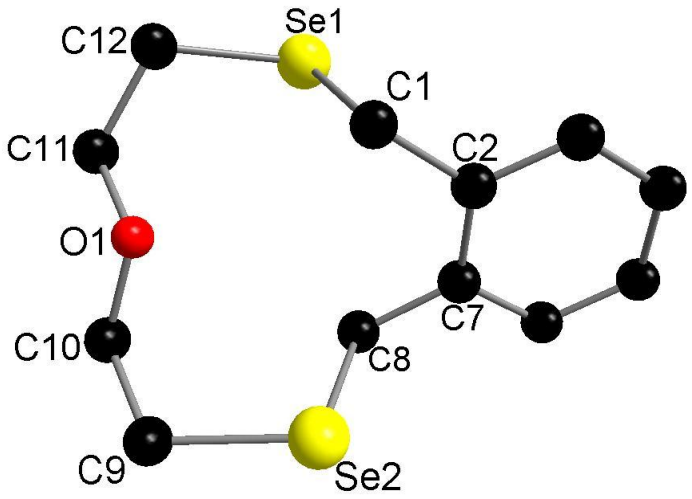

Figure 3.14: Crystal structure of L^1. H atoms omitted for clarity.

Table 3.2: Selected bond lengths and angles for L^1.

Bond	**Length / Å**	**Bond**	**Length / Å**	**Bond**	**Angle / °**
Se1–C1	1.981 (3)	Se2–C9	1.972 (3)	C1–Se1–C12	98.42 (13)
Se1–C12	1.965 (3)	O1–C10	1.427 (4)	C8–Se2–C9	103.47 (13)
Se2–C8	1.981 (3)	O1–C11	1.416 (4)	C10–O1–C11	113.1 (2)

L^2 (Figure 3.15) is a centrosymmetric molecule with the aromatic rings coplanar and the Se based lone pairs pointing *exo* to the ring. Table 3.3 shows selected bond lengths and angles. <C-Se-C are again considerably more acute (*ca.* 100°) compared to <C-O-C (*ca.* 110°) which is consistent with increased p-orbital character in the Se-C bonds. The nearest comparable structure is that of dibenzo-[26]O_2Se_4 (Figure 3.16) which shows Se directly bonded to a benzene ring to have a much shorter bond length (~1.918 Å) than Se bound to an aliphatic carbon. The bond angles at Se are comparable to the new structure of L^2 (97.1, 100.8°).[6]

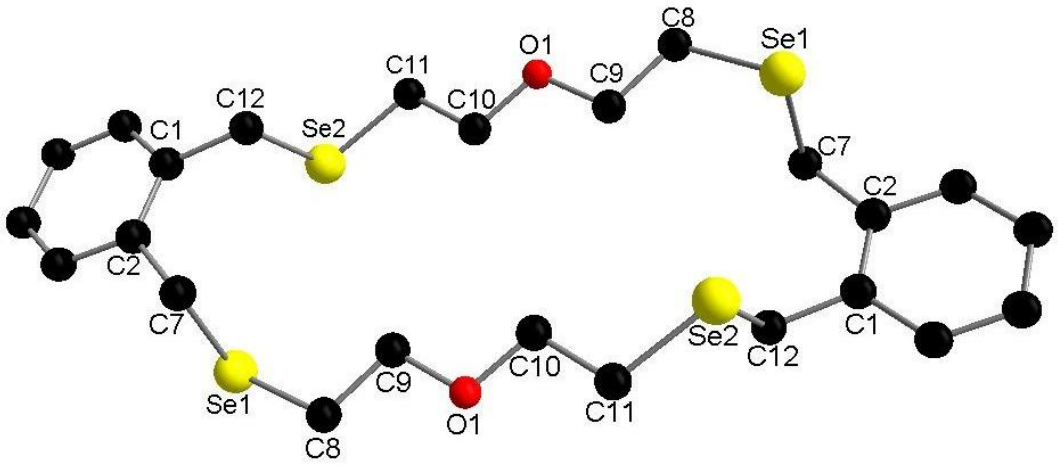

Figure 3.15: Crystal structure of L^2. H atoms omitted for clarity.

Table 3.3: Selected bond lengths and angles for L^2.

Bond	**Length / Å**	**Bond**	**Length / Å**	**Bond**	**Angle / °**
Se1–C7	1.983 (8)	Se2–C12	1.972 (8)	C7–Se1–C8	101.0 (3)
Se1–C8	1.936 (8)	O1–C9	1.448 (9)	C11–Se2–C12	100.3 (4)
Se2–C11	1.957 (8)	O1–C10	1.421 (9)	C9–O1–C10	110.9 (5)

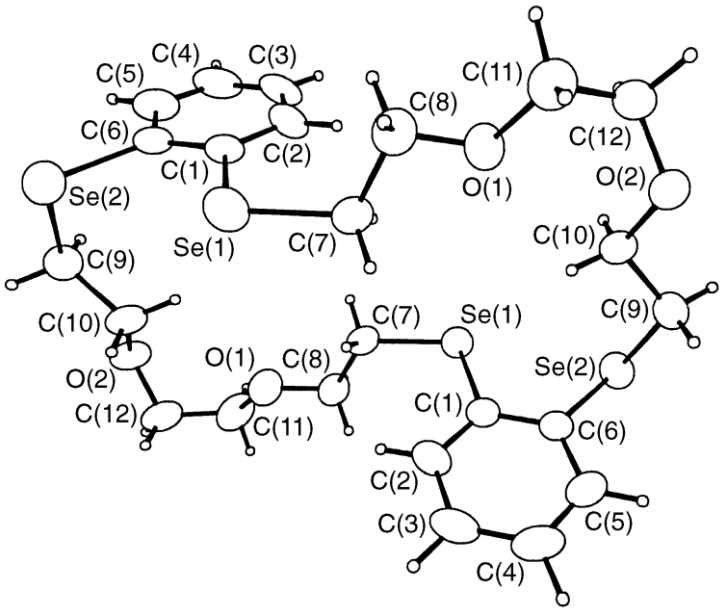

Figure 3.16: Crystal structure of dibenzo-[26]O_2Se_4. Ellipsoids shown at 30 % probability.[6]

The small ring macrocycle [9]aneO_2Se is produced using $NaBH_4$ as a reducing agent,[5] as are the Se_3 and Se_2N macrocycles described in Chapter 4. In order to assess this different reducing agent as a method of producing O_xSe_{2x} macrocycles, *o*-$C_6H_4(CH_2Br)_2$ and $O(CH_2CH_2SeCN)_2$ were dissolved separately in anhydrous thf/EtOH and added simultaneously dropwise to an excess of $NaBH_4$ in anhydrous thf/EtOH over 4 hours. Once addition was complete, the reaction mixture

was left stirring under N_2 at room temperature for 3 days. White inorganic salts were then filtered off, and the solvent removed *in vacuo* to produce a slightly oily cream residue. This was redissolved in toluene and filtered. Again, the solvent was removed *in vacuo* to yield a cream solid. ^{1}H and $^{13}C\{^{1}H\}$ NMR spectroscopy showed clean production of macrocycle, and $^{77}Se\{^{1}H\}$ NMR spectroscopy showed this white solid to be purely L^1. Altering the reaction conditions from the $Na/NH_{3\,(l)}$ method detailed above to this $NaBH_4$ reduction changed the yield of L^1 from 2 % to 96 %.

In view of the success of the production of L^1-L^3, the versatility of these methods were tested for aliphatic macrocycles with $Br(CH_2)_3Br$ substituted for the xylyl precursor, *o*-$C_6H_4(CH_2Br)_2$. Reaction of $O(CH_2CH_2SeCN)_2$ with sodium metal in liquid NH_3 at –78°C was followed by dropwise addition of $Br(CH_2)_3Br$ in thf, whilst maintaining the reaction at *c.a.* –40°C. The reaction was left to warm gradually to room temperature, hydrolysed with degassed water and extracted with CH_2Cl_2. Upon drying, the resulting mixture was analysed by multinuclear NMR spectroscopy. The spectra obtained showed a complicated mixture of products, which included both cyclic and oligomeric species (as is expected from this method of reaction) but also showed compounds with vinyl selenoether functions. There was no sign of similar vinyl functional groups in the crude mixture obtained for L^1-L^3. The vinyl species are consistent with the $SeCH_2CH_2O$ linkages being susceptible to C-O and/or C-Se scission. As was noted in Chapter 1, attempts to form compounds of the type $RTeCH_2CH_2TeR$ results in elimination of $CH_2{=}CH_2$ and formation of R_2Te_2.[12] The tetraselenoether macrocycle [14]aneSe_4 also readily undergoes elimination of dimethylene linkages (see Chapter 4).[13] Recent work in this group on arsine ligands has shown that the dimethylene linked $O(CH_2CH_2AsMe)_2$ readily undergoes C-O and C-As scission but this is not observed for the Ph analogue.[14]

Column chromatography was attempted, in case the oligomeric and vinyl functionalised constituents could be removed cleanly to leave samples of pure macrocycle, but this proved not to be the case. All fractions obtained from the column were still mixtures of products, and it could not be determined if the column itself were causing further decomposition, which has been observed for [14]aneSe_4.[13]

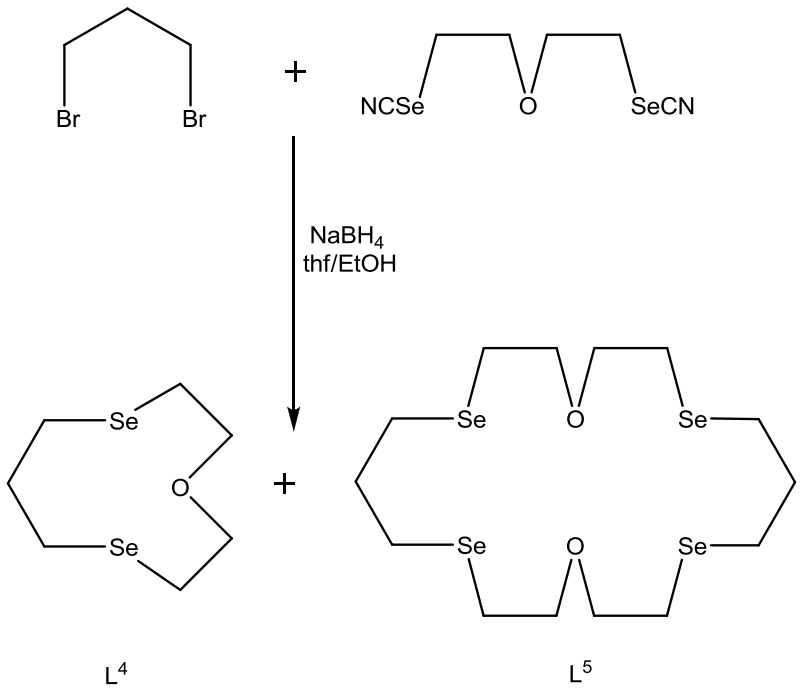

Figure 3.17: Reaction scheme for production of L^4 and L^5 *via* $NaBH_4$ reduction.

An attempt was now made using $NaBH_4$ as the reducing agent. $Br(CH_2)_3Br$ and $O(CH_2CH_2SeCN)_2$ were dissolved separately in anhydrous thf/EtOH. The solutions were added simultaneously dropwise to excess $NaBH_4$ in anhydrous thf/EtOH over a period of *ca.* 2 h. The reaction mixture was then left to stir under N_2 for 72 h at room temperature. The resulting cloudy solution was filtered to produce a clear pale yellow solution which was concentrated *in vacuo* to a cloudy oil, which was redissolved in toluene, filtered, and again dried *in vacuo* to produce yellow-brown oil. The $^{77}Se\{^1H\}$ NMR spectrum of this crude mixture showed two selenium environments (δ = 148.0, 158.3 ppm). The crude oil was dissolved in a minimum volume of CH_2Cl_2, adsorbed onto a silica column and eluted with hexane/ethyl acetate (19:1). The first fraction (Rf = 0.85) from the column was dried *in vacuo* to give a light yellow oil. This oil was analysed by EIMS, and ^1H, $^{13}C\{^1H\}$ and $^{77}Se\{^1H\}$ NMR spectroscopy.

$^{13}C\{^1H\}$ NMR spectroscopy showed four peaks, as expected for the desired macrocyclic product, with three peaks between 20-30 ppm and the fourth much higher at 70.7 ppm as would be expected for C next to ether O. The $^{77}Se\{^1H\}$ NMR spectrum showed a single peak at 158.3, indicating that this oil was a single species of macrocycle. EIMS confirmed this macrocycle to be the [1+1] product, L^4, showing a main peak cluster around 272 ($C_7H_{14}O^{80}Se_2$ = 274) and a fragment corresponding to loss of $O(CH_2CH_2)_2$ around 202 ($C_3H_6{}^{80}Se_2$ = 202). The ^1H NMR spectrum of L^4 (Figure 3.18) clearly shows the expected four proton environments. The quintet at δ = 2.05 ppm and triplet at 2.96 ppm are from the C_3 linkages between Se atoms, and show the expected binomial coupling patterns. However, the two resonances resulting from the C_2 Se-O linkages exhibit

distorted triplet coupling, indicating the ring strain at the O atom is preventing H equivalency. A similar effect was observed on L^1 (Figure 3.11).

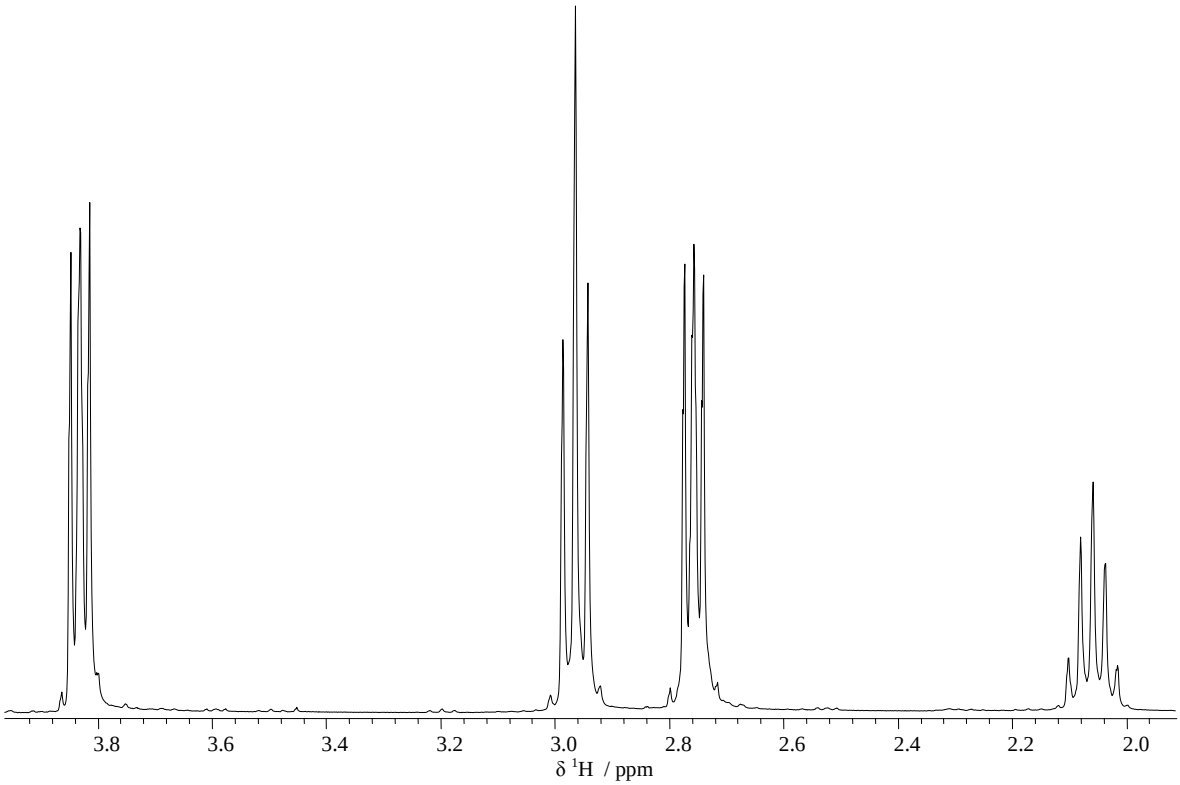

Figure 3.18: ^{1}H NMR spectrum of L^4 recorded in $CDCl_3$.

A second fraction from the column (Rf = 0.48) yielded an off-white solid when dried *in vacuo*, which was analysed by EIMS, and ^{1}H, ^{13}C{^{1}H} and ^{77}Se{^{1}H} NMR spectroscopy. The ^{77}Se{^{1}H} NMR spectrum showed a single peak at 148 ppm, indicating this could be a second macrocyclic species. EIMS confirmed this, with a main peak cluster centred around 546 ($C_{14}H_{28}O_2{}^{80}Se_4$ = 546) and a fragment cluster at 424 corresponding to loss of $Se(CH_2)_3$. In contrast to L^4, the ^{1}H NMR spectrum of L^5 shows the expected binomial distributions in all the proton environments, showing this macrocycle to be large enough for there to be no strain at the O atoms. Curiously, however, the protons on the C atoms either side of Se (on the C_2 linkage or on the C_3 linkage) have coalesced into a single resonance at δ = 2.73 ppm. The resonances have all been shifted upfield from their L^4 positions. The ^{13}C {^{1}H} NMR spectrum again showed four C environments, as expected, with three between 20 and 30 ppm, and one much higher at 70.6 ppm, corresponding to the C atoms next to O.

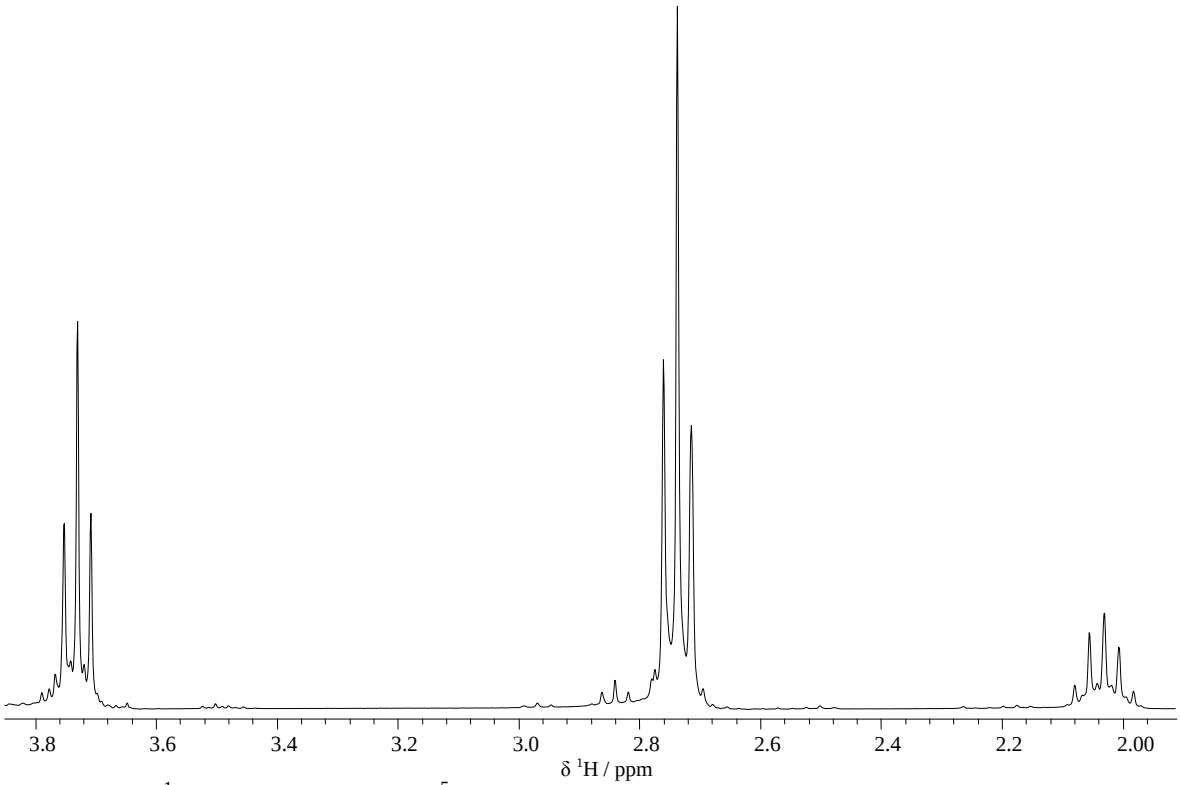

Figure 3.19: ^{1}H NMR spectrum of L^{5} recorded in $CDCl_3$.

Table 3.4 shows the $^{77}Se\{^{1}H\}$ NMR shifts for a range of mixed donor O/Se macrocycles. Whilst size of macrocycle clearly affects the $^{77}Se\{^{1}H\}$ NMR shifts of macrocycles with similar backbones, there is no overall trend apparent. Similarly, number of O donors, Se donors and aromatic rings also cause no quantifiable effect which might allow a method of calculating expected $^{77}Se\{^{1}H\}$ NMR shifts to be established.

Table 3.4: ^{77}Se $\{^{1}H\}$ NMR spectroscopic data for mixed donor O/Se macrocycles.

Macrocycle	**δ ^{77}Se / ppm**	**Reference**
[9]aneO_2Se	204	7
L^4 ([10]aneOSe_2)	158	This work
L^1 (benzo-[11]OSe_2)	205	This work
[18]aneO_4Se_2	144	7
L^5 ([20]aneO_2Se_4)	148	This work
dibenzo-[18]O_2Se_4	278	6
L^2 (dibenzo-[22]O_2Se_4)	216	This work
dibenzo-[24]O_4Se_4	268	6
dibenzo[30]O_6Se_4	265	6
L^3 (tribenzo-[33]O_3Se_6)	213	This work

3.4 – Coordination Chemistry of O_xSe_{2x} Macrocycles

The new oxygen/selenium macrocycles L^1 and L^2 were reacted with three different transition metals (Ag(I), Cu(I) and Pt(II)) in order to probe their ligating properties. $AgBF_4$ was dissolved in ice-cold MeOH in a foil wrapped flask. Initial attempts to add the macrocycles directly to the MeOH solution showed them to be only very sparingly soluble in alcohols. Instead, solutions were

made of the ligands in CH_2Cl_2, which were cooled and added to the MeOH solution of $AgBF_4$. The reaction mixture was stirred for ~2 hours. The L^1 reaction then had the solvent removed *in vacuo* to give a brown solid, which was redissolved in MeCN and filtered to remove the brown solids, which were probably decomposed Ag salts. The filtrate was dried *in vacuo* to yield a cream solid, which decomposed gradually over time (even when kept in a foil wrapped flask) and rapidly in solution. ES^+ MS identified the product as $[Ag(L^1)_2]BF_4$. The L^2 complex $[AgL^2]BF_4$ was isolated by reducing the reaction mixture *in vacuo* and filtering, which generated a cream solid. This was more stable than $[Ag(L^1)_2]BF_4$ both as a solid and in solution, but is still somewhat light-sensitive. Figure 3.20 shows the ES^+ MS and calculated isotope pattern of $[AgL^2]BF_4$.

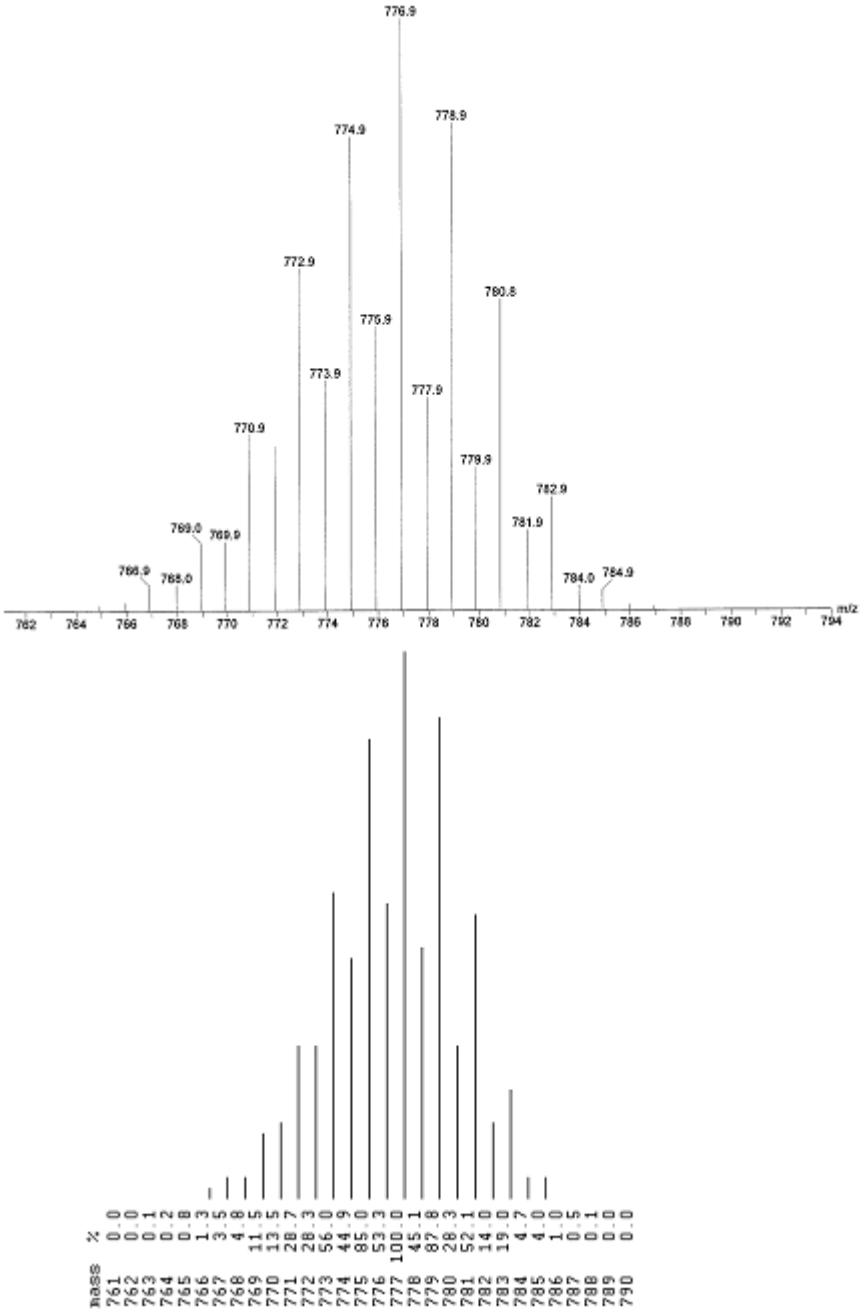

Figure 3.20: Top: ES^+ MS of $[Ag(L^2)]BF_4$. Bottom: Calculated isotope pattern for $[AgC_{24}H_{32}O_2Se_4]^+$.

Complexes with Cu(I) were made by dissolving $[Cu(MeCN)_4]BF_4$ in MeOH and adding a CH_2Cl_2 solution of macrocycle. Two equivalents of L^1 were added and the reaction stirred for 3 hours before removing the solvent *in vacuo*. The resulting solid was added to CH_2Cl_2, filtered and the filtrate dried *in vacuo* to give a pale green solid, characterised by microanalysis, ES^+ MS, IR and ^1H NMR spectroscopy as $[Cu(L^1)_2]BF_4$. The ES^+ MS is shown in Figure 3.21, and shows peak clusters corresponding to both $[Cu(L^1)_2]^+$ and to the complex with loss of one ligand and addition of one MeCN, $[CuL^1(MeCN)]^+$. The complex is poorly soluble in chlorocarbons, and generally somewhat unstable in solution.

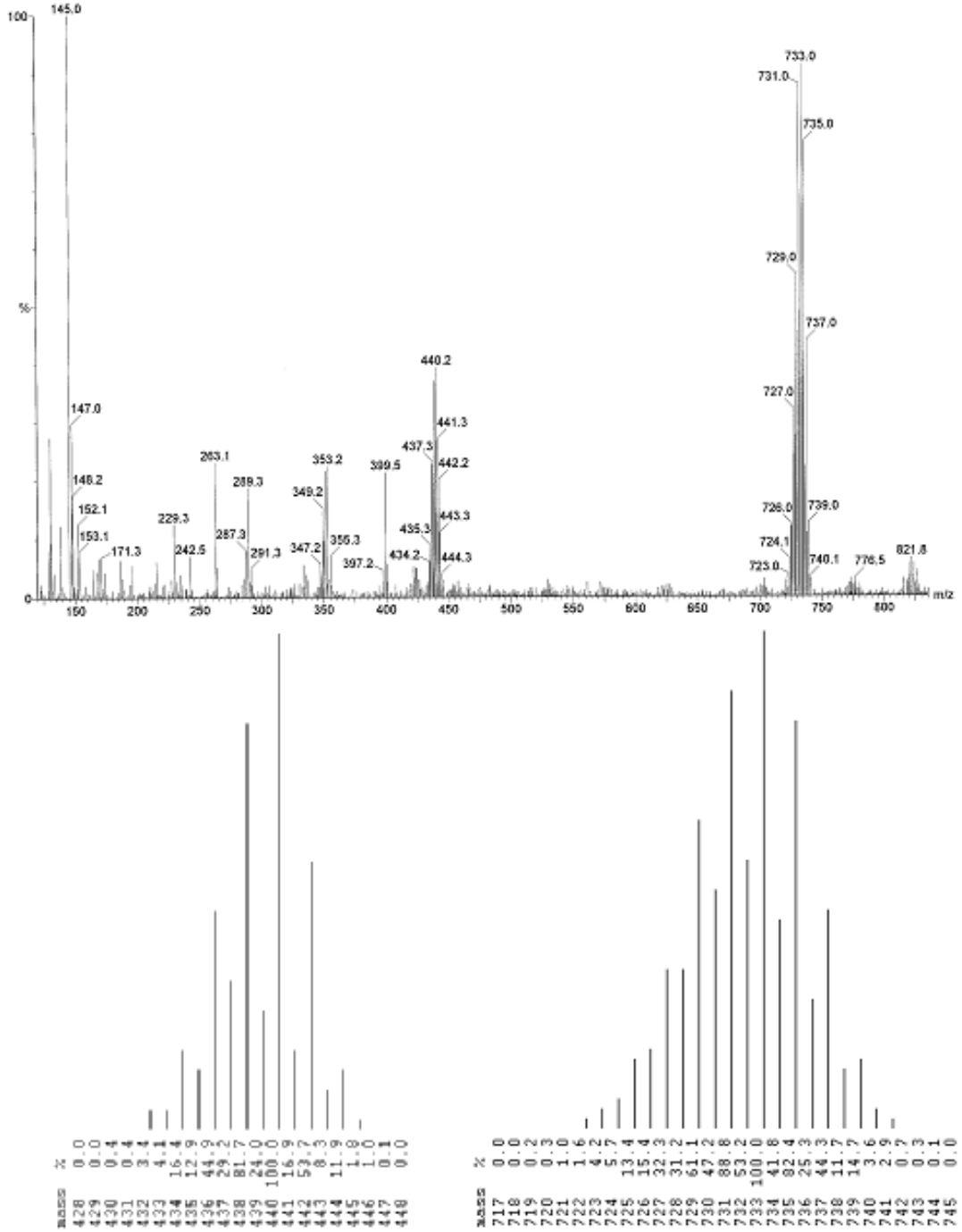

Figure 3.21: Top: ES^+ MS of $[Cu(L^1)_2]BF_4$. Bottom: Calculated isotope patterns for $[Cu(C_{12}H_{16}OSe_2)(MeCN)]^+$ (left) and $[Cu(C_{12}H_{16}OSe_2)_2]^+$ (right).

One equivalent of L^2 in CH_2Cl_2 with $[Cu(MeCN)_4]BF_4$ in MeOH was stirred for a total of four hours. A cream-white solid precipitated from the solution after approximately one hour, and remained unchanged. This solid was a very fine powder, and was collected by decanting the solvent off. The solid was then washed with diethyl ether, and dried *in vacuo*. This white solid was characterised by microanalysis, ES^+ MS, IR and ^1H NMR spectroscopy as $[CuL^2]BF_4$. As with the silver complexes, this Cu complex was more stable than the L^1 complex. The ^1H and $^{13}C\{^1H\}$ NMR spectra collected for these new silver and copper complexes are consistent with rapidly exchanging systems, which is expected for Ag(I) and Cu(I) selenoether complexes.[2]

$PtCl_2$ was refluxed in MeCN until complete dissolution had occurred, generating $[PtCl_2(MeCN)_2]$. One molar equivalent of L^1 was added as a solution in CH_2Cl_2 and the yellow mixture stirred for overnight. The solution was then reduced *in vacuo* and diethyl ether added to precipitate a yellow solid, which was collected by filtration. This was identified as $[PtCl_2L^1]$ by microanalysis, IR, ^1H and $^{77}Se\{^1H\}$ NMR spectroscopy. The NMR data were collected from solutions in CD_3CN, as the solid was insoluble in chlorocarbons.

A similar reaction with 0.5 equivalents of L^2 produced a yellow solid, characterised as $[(PtCl_2)_2L^2]$ by microanalysis, IR, ^1H, $^{77}Se\{^1H\}$ and ^{195}Pt NMR spectroscopy. As with the monomeric L^1 complex, $[(PtCl_2)_2L^2]$ is insoluble in chlorocarbons and poorly soluble in MeCN and acetone. In both Pt(II) complexes *cis* coordination is most likely, due to the steric constraints of the macrocycles, and this was confirmed by the presence of two Pt-Cl stretching vibrations in their IR spectra. It has been observed that $O(CH_2CH_2SeMe)_2$ requires very specific reaction conditions to promote tridentate coordination involving all three donor atoms over bidentate coordination through the two Se atoms.[15] In light of this, it is expected that these macrocycles would preferentially bind through the Se atoms, and this is confirmed by the $^{77}Se\{^1H\}$ and ^{195}Pt NMR spectra. This behaviour has also been observed crystallographically for $[PtCl_2([18]aneO_4Se_2)]$ (Figure 3.22).[7] The poor solubility of all these new complexes prevented the growth of crystals suitable for X-ray analysis.

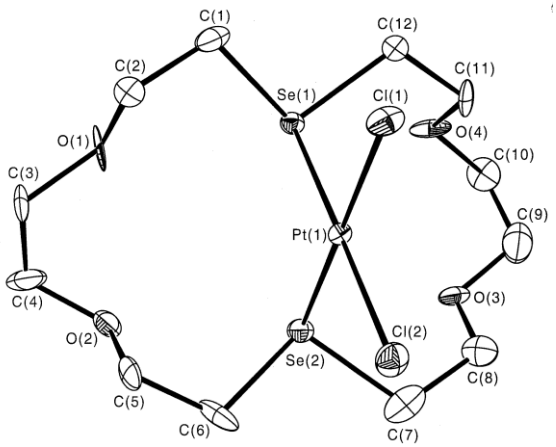

Figure 3.22: Crystal structure of $[PtCl_2([18]aneO_4Se_2)]$. Ellipsoids shown at 40 % probability, H atoms omitted for clarity.[7]

3.5 – Conclusion

Five novel macrocycles containing a mixed O/Se donor set have been synthesised and characterised (Figure 3.23). These new macrocycles are all of the type O_xSe_{2x}, which considerably increases the range of selenium-rich mixed donor O/Se macrocycles known. Two methods of production have been established for L^1 from the same precursors, demonstrating that reaction conditions are very important for determining preferred ring size. A $NaBH_4$ reduction generates only L^1 in 96 % yield, whilst using a low temperature $Na/NH_{3\ (l)}$ reduction generates L^1-L^3 in one pot, with L^2 being the dominant product (35 % yield L^2). L^4 and L^5 are not cleanly produced by $Na/NH_{3\ (l)}$ reduction, but can be produced by $NaBH_4$ reduction, with L^4 being the dominant product (71 % yield L^4, 8 % yield L^5).

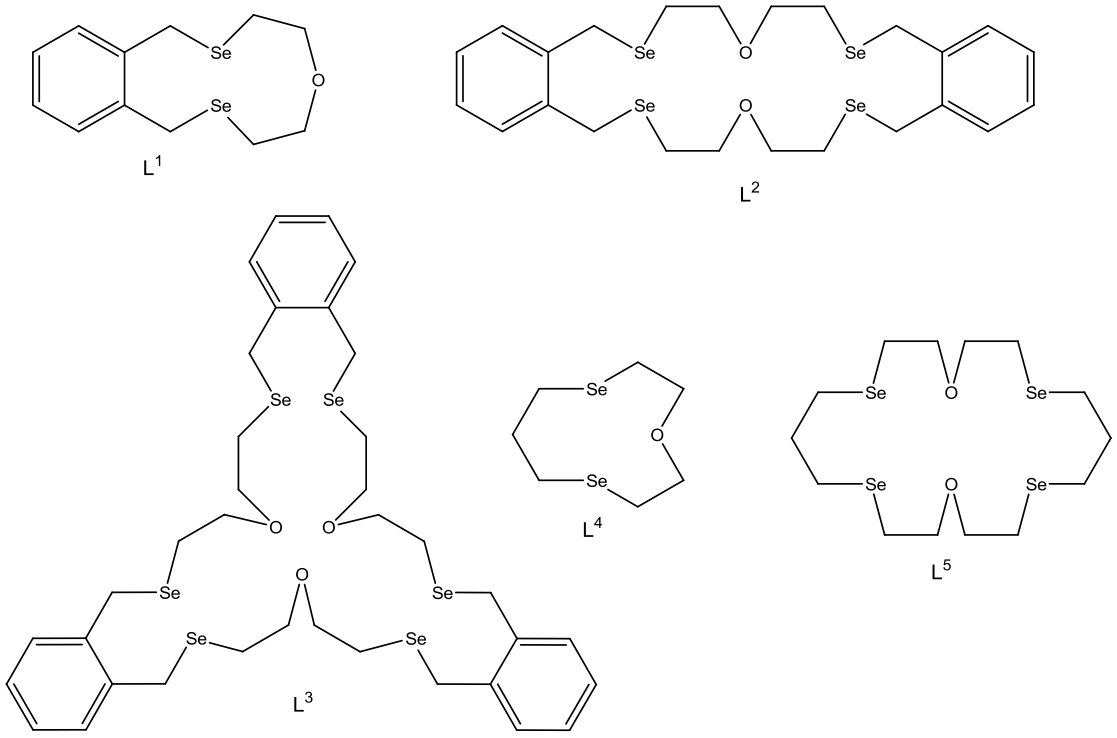

Figure 3.23: Novel O_xSe_{2x} macrocycles produced in this chapter.

A set of complexes involving L^1 and L^2 have been synthesised and characterised to investigate ligating properties of these new macrocycles. The Ag(I) and Cu(I) complexes involving the smaller macrocycle, L^1 are less stable than the analogous complexes with L^2. The Pt(II) complexes are insoluble in chlorocarbons, and show *cis* coordination of the macrocycles through the Se atoms.

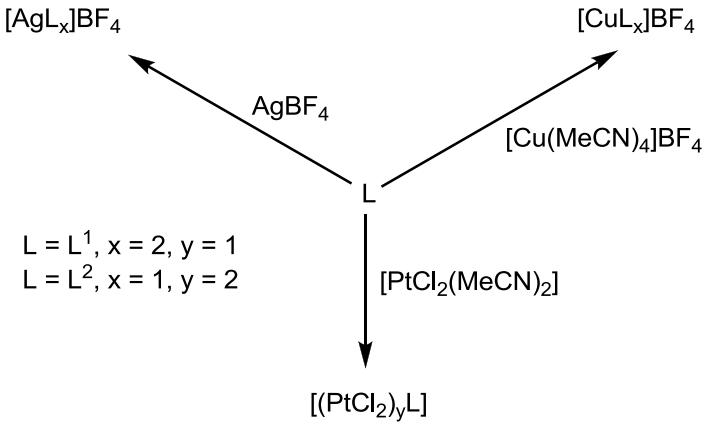

Figure 3.24: Summary of metal complexes produced with novel O_xSe_{2x} macrocycles.

3.6 – Experimental

$O(CH_2CH_2SeCN)_2$: KSeCN (4.17 g, 28.95 mmol) was dissolved in anhydrous acetone (100 cm^3) in a three necked flask. $O(CH_2CH_2Br)_2$ (3.36 g, 14.47 mmol) dissolved in anhydrous acetone (70 cm^3) was then added dropwise over a period of *ca.* 3 h and the reaction mixture was stirred overnight, giving a colourless solution and a white precipitate. The solution was then filtered to remove the KBr and concentrated to give a yellow oil. Yield: 62%. EIMS: *m*/*z* = 284 $[O(CH_2CH_2{}^{80}SeCN)_2]^+$. ^{1}H NMR ($CDCl_3$): δ = 3.87 (*t*, CH_2O, $^3J_{HH}$ = 6 Hz), 3.23 (*t*, $SeCH_2$, $^3J_{HH}$ = 6 Hz, $^2J_{SeH}$ = 27 Hz). $^{13}C\{^1H\}$ NMR ($CDCl_3$): δ = 102.0 (SeCN, $^1J_{SeC}$ = 237 Hz), 70.2 (CH_2O), 29.8 (CH_2Se, $^1J_{SeC}$ = 45 Hz). $^{77}Se\{^1H\}$ NMR ($CDCl_3$): δ = 190.4. This freshly prepared compound was used in subsequent reactions without further purification.

Preparation of L^1–L^3—Method 1: In a 1 litre round bottomed flask containing anhydrous thf (100 cm^3) and maintained at −78 °C (acetone/CO_2 slush), NH_3 (400 cm^3) was condensed. A small piece of sodium was added and the solution turned deep blue. $O(CH_2CH_2SeCN)_2$ (6.0 g, 21.2 mmol) dissolved in thf (100 cm^3) was then added dropwise with constant stirring. This is followed by addition of Na (1.95 g, 84.8 mmol). The reaction mixture was stirred for around 1 h to give a pale yellow mixture. A solution of *o*-$C_6H_4(CH_2Br)_2$ (5.61 g, 21.2 mmol) in thf (100 cm^3) was added dropwise over 3 h with the reaction temperature maintained at between −40 to −50 °C. The reaction mixture was left at room temperature overnight to allow the NH_3 to evaporate. The mixture was hydrolysed with degassed water and extracted with CH_2Cl_2. The CH_2Cl_2 layer was then concentrated to get a yellow oil from which a white solid separates out. Recrystallisation from CH_2Cl_2/hexane yields **L^2** as a white solid.

L^2: Yield: 2.5 g, 35%. EIMS: *m*/*z* = 672 $[L^2]^+$, 565 $[L^2 - o\text{-}C_6H_4(CH_2)_2]^+$. Required for $C_{24}H_{32}O_2Se_4$ (668.35): C, 43.1; H, 4.8; found: C, 43.2; H, 5.2%. ^{1}H NMR ($CDCl_3$): δ = 7.25–7.38 (*m*, *o*-C_6H_4, 4H), 4.19 (*s*, $SeCH_2$, 4H, $^2J_{SeH}$ = 6.5 Hz), 3.75 (*t*, CH_2O, 4H), 2.84 (*t*, CH_2CH_2Se, 4H, $^2J_{SeH}$ = 6.5 Hz) ppm. $^{13}C\{^1H\}$NMR($CDCl^3$): δ = 137.8 (*ipso*-C, *o*-C_6H_4), 131.3, 127.9 (aromatic C), 72.1 (OCH_2), 26.0, 25.2 ($SeCH_2$) ppm. $^{77}Se\{^1H\}$ NMR ($CDCl_3$): δ = 216 ppm.

The filtrate was retained and concentrated to give a yellow/orange oil. The crude oil was dissolved in CH_2Cl_2 and adsorbed onto a silica column and eluted with hexane/ethyl acetate (19:1) to give first **L^1** (Rf (silica plate) = 0.69)

L^1: Yield: 0.13 g, 2%. Crystals of L^1 suitable for X-ray structure analysis were obtained by recrystallisation of this fraction from CH_2Cl_2/hexane. EIMS: *m*/*z* = 336 $[L^1]^+$. Required for $C_{12}H_{16}OSe_2$ (334.17): C, 43.1; H, 4.8; found: C, 42.3; H, 5.5%. ^{1}H NMR ($CDCl_3$): δ = 7.2–7.1 (*m*, 4H, *o*-C_6H_4), 4.5 (*s*, 4H, $SeCH_2$), 4.0 (*m*, 4H,OCH_2), 2.9 (*m*, 4H, CH_2Se). $^{13}C\{^1H\}$ NMR ($CDCl_3$): δ = 138.5 (*ipso C*), 131.3, 128.0 (aromatic *C*), 72.5 (OCH_2), 26.1, 25.2 ($SeCH_2$). $^{77}Se\{^1H\}$ NMR($CDCl_3$, 300 K): δ = 205.

A second fraction, containing **L^3** was eluted using hexane/ethyl acetate (9:1) (Rf (silica plate) = 0.67).

L^3: Yield: 0.15 g, 2%. APCI MS: *m*/*z* = 1027 [L^3 + Na]$^+$. ^{1}H NMR ($CDCl_3$): δ = 7.1–7.3 (*m*, 12H, *o*-C_6H_4), 4.0 (*s*, 12H, SeC*H*$_2$, $^2J_{SeH}$ = 5.6 Hz), 3.6 (*t*, 12H, OC*H*$_2$), 2.7 (t, 12H, C*H*$_2$Se, $^2J_{SeH}$ = 7 Hz). ^{13}C{^{1}H} NMR($CDCl_3$): δ =137.8 (*ipso*-*C*), 131.4, 127.9 (aromatic *C*), 71.9 (O*C*H$_2$), 25.7, 24.4 (Se*C*H$_2$). ^{77}Se{^{1}H} NMR ($CDCl_3$, 300 K): δ = 213.

Preparation of L^1 – Method 2: α,α-Dibromo-*o*-xylene (1.49 g, 5.6 mmol) and O(CH$_2$CH$_2$SeCN)$_2$ (1.59 g, 5.6 mmol) were each dissolved separately in a mixture of anhydrous thf (160 cm^3) and anhydrous ethanol (40 cm^3). They were added simultaneously dropwise into a flask containing $NaBH_4$ (1.5 g, excess) in a solution of anhydrous thf/ethanol (450 cm^3/50 cm^3) over a period of *ca.* 4 h. The reaction mixture was then left to stir under N_2 for 72 h at room temperature. The resulting cloudy solution was filtered to produce a clear pale yellow solution which was reduced under vacuum to give a cloudy oil. Toluene (250 cm^3) was then added to the oil and the resulting solution filtered to remove any undissolved solids before being concentrated under reduced pressure to produce L^1 as a cream solid. Yield: 1.76 g, 96%. EIMS: *m*/*z* = 336 [L^1]$^+$. ^{1}H NMR($CDCl_3$): δ = 7.3–7.1 (*m*, 4H, *o*-C_6H_4), 4.5 (s, 4H, SeC*H*$_2$), 4.0 (*m*, 4H, OC*H*$_2$), 2.9 (*m*, 4H, C*H*$_2$Se). ^{13}C{^{1}H} NMR ($CDCl_3$): δ = 138.5 (*ipso*-*C*), 131.3, 128.0 (aromatic *C*H), 72.5 (O*C*H$_2$), 26.1, 25.2 (Se*C*H$_2$). ^{77}Se{^{1}H} NMR ($CDCl_3$, 300 K): δ = 205.

Preparations of L^4 and L^5: 1,3-Dibromopropane (0.308 g, 1.52 mmol) and O(CH$_2$CH$_2$SeCN)$_2$ (0.430 g, 1.52 mmol) were each dissolved in a mixture of anhydrous thf (50 cm^3) and anhydrous ethanol (14 cm^3). They were added simultaneously dropwise into a flask containing $NaBH_4$ (0.5 g, excess) in a solution of anhydrous thf/ethanol (320 cm^3/20 cm^3) over a period of *ca.* 2 h. The reaction mixture was then left to stir under N_2 for 72 h at room temperature. The resulting cloudy solution was filtered to produce a clear pale yellow solution which was concentrated under vacuum to give a cloudy oil. Toluene (150 cm^3) was then added to the oil and the resulting solution filtered to remove any undissolved solids before being concentrated under reduced pressure to produce yellow-brown oil. ^{77}Se{^{1}H} NMR spectrum (crude mixture): δ = 148.0 (minor), 158.3 (major). The crude oil was dissolved in a minimum volume of CH_2Cl_2 and adsorbed onto a silica column and eluted with hexane/ethyl acetate (19:1) to give first **L^4** (Rf (silica plate) = 0.85) as a light yellow oil.

L^4: Yield: 0.31 g, 71%. EIMS: *m*/*z* = 272 [L^4]$^+$, 202 [L^4 − O(CH$_2$CH$_2$)$_2$]$^+$. ^{1}H NMR ($CDCl_3$): δ = 3.83 (*m*, 4H, CH_2O), 2.96 (*t*, 4H, CH_2Se), 2.75 (*m*, 4H, CH_2 Se), 2.05 (*quintet*, 2H, $CH_2CH_2CH_2$). ^{13}C{^{1}H} NMR ($CDCl_3$): δ = 70.7 (CH_2O), 29.8 ($CH_2CH_2CH_2$), 23.2 (CH_2Se), 22.9 (CH_2Se). ^{77}Se{^{1}H} NMR (CH_2Cl_2, 300 K): δ = 158.3.

A second fraction, containing $\mathbf{L^5}$ was eluted using hexane/ethyl acetate (19:1) (Rf (silica plate) = 0.48) as an off-white solid.

L^5: Yield: 0.08 g, 8%. EIMS: *m*/*z* 546 $[L^5]^+$, 424 $[L^5 - Se(CH_2)_3]^+$. ^{1}H NMR ($CDCl_3$): δ =3.73 (*t*, 4H,CH_2O), 2.73 (*t*, 8H,CH_2Se), 2.03 (*quintet*, 2H, $CH_2CH_2CH_2$). $^{13}C\{^1H\}$ NMR ($CDCl_3$): δ = 70.6 (CH_2O), 30.6 ($CH_2CH_2CH_2$), 22.9 (CH_2Se), 22.1 (CH_2Se). $^{77}Se\{^1H\}$ NMR (CD_2Cl_2, 300 K): δ = 148.0.

Metal complexes

$[Ag(L^1)_2]BF_4$: $AgBF_4$ (0.029 g, 0.15 mmol) was taken up in MeOH (40 cm^3) in a foil wrapped flask in an acetone/dry ice slush bath and stirred. Two mol. equiv. of L^1 (0.100 g, 0.30 mmol) in CH_2Cl_2 (5 cm^3) was added, and the reaction was stirred for 3 h. Solvent was removed *in vacuo* to produce a brown solid which was redissolved in MeCN and filtered to remove an insoluble brown solid. The solvent was removed *in vacuo* to give a cream coloured solid which turns dark brown on standing and more rapidly in solution. Yield: 56%. Electrospray MS (MeCN): *m*/*z* = 777 $[Ag(L^1)_2]^+$. ^{1}H NMR (CD_3CN): δ = 7.1 (*s*, 4H, *o*-C_6H_4), 4.1 (br *s*, 4H, CH_2), 3.7 (br *m*, 4H, CH_2), 2.9 (*t*, 4H, CH_2). IR (Nujol): ν = 1049 $\nu(BF_4)$ cm^{-1}.

$[AgL^2]BF_4$: To $AgBF_4$ (0.044 g, 0.21 mmol) in MeOH (20 cm^3) in a foil-wrapped flask maintained at 0 °C (ice) was added L^2 (0.119 g, 0.18 mmol) in CH_2Cl_2 (5 cm^3). After stirring for 2 h the solution was concentrated *in vacuo* to *ca.* 10 cm^3, giving a white precipitate which was collected by filtration and dried *in vacuo*. Yield: 48%. Electrospray MS (MeCN): *m*/*z* = 777 $[Ag(L^2)]^+$. Required for $C_{24}H_{32}AgBF_4O_2Se_4 \cdot 0.5CH_2Cl_2$ (905.49): C, 32.5; H, 3.7; found: C, 32.4; H, 3.2%. ^{1}H NMR ($CDCl_3$): δ = 7.17 (br *s*, aromatic CH, 8H), 3.95 (*s*, CH_2Se, 8H), 3.65 (*m*, CH_2O, 8H), 3.00 (*m*, CH_2Se, 8H) (together with a resonance due to the associated CH_2Cl_2 solvate). $^{13}C\{^1H\}$ NMR ($CDCl_3$): δ = 136.59 (*ipso*-C), 131.83, 128.90 (C_6H_4), 68.14 (CH_2O), 30.11, 29.12 (CH_2Se). IR (Nujol mull): ν = 1066 (br) $\nu(BF_4)$ cm^{-1}.

$[Cu(L^1)_2]BF_4$: $[Cu(MeCN)_4]BF_4$ (0.047 g, 0.15 mmol) was taken up in MeOH (40 cm^3) and stirred. Two mol. equiv. of L^1 (0.100 g, 0.30 mmol) in CH_2Cl_2 (5 cm^3) was added, and the reaction was stirred for 3 h. The solvent was removed *in vacuo*, and the resulting solid dissolved in CH_2Cl_2 (20 cm^3), filtered and the filtrate dried *in vacuo* to give a pale green solid. Yield: 68%. Required for $C_{24}H_{32}BCuF_4O_2Se_4$ (818.70): C, 35.2; H, 3.9; found: C, 34.6; H, 4.1%. Electrospray MS (MeCN): *m*/*z* = 733 $[Cu(L^1)_2]^+$, 440 $[Cu(L^1)(MeCN)]^+$. ^{1}H NMR ($CDCl_3$): δ = 7.1–7.3 (*m*, *o*-C_6H_4, 4H), 4.2 (br *s*, OCH_2, 4H), 3.9 (br *s*, $SeCH_2$, 4H), 2.9 (br *s*, $SeCH_2$, 4H). IR (Nujol): ν = 1060 br $\nu(BF_4)$ cm^{-1}.

[CuL^2]BF$_4$: [Cu(MeCN)$_4$]BF$_4$ (0.047 g, 0.149 mmol) was taken up in MeOH (40 cm^3) and stirred. One mol. equiv. of L^2 (0.100 g, 0.149 mmol) was added, and the reaction was stirred for 1 h. A cream-white solid was formed and the stirring was continued for another 3 h. The solvent was then decanted and the solid was washed with diethyl ether and dried *in vacuo* to give a white solid. Yield: 71%. Required for $C_{24}H_{32}BCuF_4O_2Se_4$ (818.7): C, 35.2; H, 3.9; found: C, 35.9; H, 4.0%. Electrospray MS (MeCN): *m*/*z* = 733 [Cu(L^2)]$^+$. ^{1}H NMR ($CDCl_3$): δ = 7.15–7.30 (br *m*, *o*-C_6H_4), 3.84 (br *s*, CH_2Se), 3.64 (br,CH_2O), 2.90 (br *s*, CH_2Se). IR (Nujol mull): ν = 1060 br s ν(BF_4) cm^{-1}.

[PtCl$_2$L^1]: $PtCl_2$ (0.127 g, 0.477 mmol) was dissolved in MeCN (50 cm^3). The solution was refluxed and stirred until all of the $PtCl_2$ dissolved giving a light yellow solution. To the solution L^1 (0.160 g, 0.477 mmol) was added. The reaction mixture was stirred overnight at room temperature. The yellow solution was reduced to *ca.*5 cm^3 *in vacuo.* Cold diethyl ether (~15 cm^3) was added dropwise to precipitate a yellow solid, which was filtered off and dried *in vacuo.* Yield: 70%. Required for $C_{12}H_{16}Cl_2OPtSe_2$ (600.16): C, 24.0; H, 2.7; found: C, 24.0; H, 2.4%. ^{1}H NMR (CD_3CN): δ = 7.1–7.3 (br *m*, *o*-C_6H_4, 4H), 4.4 (*m*, CH_2, 4H), 3.9 (*m*, CH_2, 4H), 3.0–3.3 (br *m*, CH_2, 4H). ^{77}Se{^{1}H} NMR (CD_3CN): δ = 292 (^{195}Pt satellites not resolved). IR (Nujol): ν = 314, 305 ν(PtCl) cm^{-1}.

[(PtCl$_2$)$_2$L^2]: Method as for [PtCl$_2$(L^1)] above but using L^2 in a 2:1 metal:ligand ratio. Yellow solid. Yield: 70%. Required for $C_{24}H_{32}Cl_4O_2Pt_2Se_4\cdot 0.5C_4H_{10}O$ (1237.37): C, 25.2; H, 3.0; found: C, 25.0; H, 2.6%. ^{1}H NMR (D_6-acetone): δ = 7.4–7.7 (*m*, 8H, *o*-C_6H_4), 3.0–4.3 (*m*, CH_2, 12H) (together with resonances for the associated Et_2O solvate). ^{77}Se{^{1}H} NMR ($CH_3CN/CDCl_3$): δ = 292.4 ($^1J_{PtSe}$ = 383 Hz). ^{195}Pt NMR(MeCN/$CDCl_3$): δ = −3681. IR (Nujol mull): ν = 317 m, 306 s ν(PtCl) cm^{-1}.

3.7 – X-Ray Crystallography

Details of the crystallographic data collection and refinement parameters are given in Table 3.5. Yellow single crystals of L^1 were obtained by recrystallisation from CH_2Cl_2/hexane. Colourless crystals of L^2 were obtained by recrystallisation from CH_2Cl_2/hexane. Structure solution and refinement were routine.[16,17] Selected bond lengths and angles for L^1 are presented in Table 3.2 and for L^2 are presented in Table 3.3.

Table 3.5: Crystallographic data collection and refinement parameters. $R1 = \Sigma||F_o| - |F_c||/\Sigma|F_o|$; $wR_2 = [\Sigma w(F_o^2 - F_c^2)^2/\Sigma wF_o^4]^{1/2}$

Compound	**L^1**	**L^2**
Formula	$C_{12}H_{16}OSe_2$	$C_{24}H_{32}O_2Se_4$
M	334.17	668.34
Crystal System	Triclinic	Monoclinic
Space Group	*P*-1	$P2_1/c$
a/Å	7.9226(3)	9.085(3)
b/Å	7.9777(3)	4.824(1)
c/Å	10.1093(3)	28.058(7)
α/°	108.105(2)	90
β/°	92.408(2)	95.32(2)
γ/°	91.037(2)	90
U/Å^3	606.45(4)	1223.0(6)
Z	2	2
μ(Mo-Kα)/ mm^{-1}	6.068	6.018
R_{int}	0.045	0.084
Total no. reflns.	13054	11967
Unique reflections	2783	2802
No. of parameters	136	136
$R1$ [$I_o > 2\sigma(I_o)$]	0.031	0.072
$R1$ [all data]	0.039	0.108
wR_2 [$I_o > 2\sigma(I_o)$]	0.070	0.174
wR_2 [all data]	0.073	0.196

3.8 – References

1. Levason, W.; Manning, J. M.; Nirwan, M.; Ratnani, R.; Reid, G.; Smith, H.; Webster, M. *Dalton Trans.* **2008**, 3486 – 3492.

2. Levason, W.; Orchard, S. D.; Reid, G. *Coord. Chem. Rev.* **2002**, *225*, 159 – 199.

3. Levason, W.; Reid, G. In: *Comprehensive Co-ordination Chemistry II*, Vol. 1, Elsevier Ltd., 2003, 399 – 410.

4. Hojjatie, M.; Muralidharan, S.; Freiser, H. *Tetrahedron*, **1989**, *45*, 1611 – 1622.

5. Higughi, H.; Tani, K.; Otsubo, T.; Sakata, Y.; Misumi, S. *Bull. Chem. Soc. Jpn.* **1987**, *60*, 4027 – 4036.

6. Mazouz, A.; Meunier, P.; Kubicki, M. M.; Hanquet, B.; Amardeil, R.; Bournet, C.; Zahidi, A. *J. Chem. Soc., Dalton Trans.* **1997**, 1043 – 1048.

7. Hesford, M. J.; Levason, W.; Matthews, M. L.; Reid, G. *Dalton Trans.* **2003**, 2852 – 2858.

8. Batchelor, R. J.; Einstein, F. W. B.; Gay, I. D.; Gu, J-H.; Mehta, S.; Pinto, B. M.; Zhou, X-M. *Inorg. Chem.* **2000**, *39*, 2558 – 2571.

9. Levason, W.; Orchard, S. D.; Reid, G. *Chem. Commun.* **2001**, 427 – 428.

10. Hesford, M. J.; Levason, W.; Matthews, M. L.; Orchard, S. D.; Reid, G. *Dalton Trans.* **2003**, 2434 – 2442.

11. Levason, W.; Nirwan, M.; Ratnani, R.; Reid, G.; Tsoureas, N,; Webster, M. *Dalton Trans.* **2007**, 439 – 448.

12. Hope, E. G.; Kemmitt, T.; Levason, W. *Organometallics* **1988**, *7*, 78 – 83.

13. Batchelor, R. J.; Einstein, F. W. B.; Gay, I. D.; Gu, J-H.; Johnston, B. D.; Pinto, B. M. *J. Am. Chem. Soc.* **1989**, *111*, 6582 – 6591.

14. Davis, M. F.; Jura, M.; Levason, W.; Reid, G.; Webster, M. *J. Organomet. Chem* **2007**, *692*, 5589 – 5597.

15. Abel, E. W.; Kite, K.; Perkins, P. S. *Polyhedron*, **1986**, *5*, 1459 – 1465.

16. Sheldrick, G. M. SHELXS-97, program for crystal structure solution, University of Göttingen, Germany, **1997**.

17. Sheldrick, G. M. SHELXS-97, program for crystal structure refinement, University of Göttingen, Germany, **1997**.

Chapter 4: Novel Selenium-Rich Macrocycles[1]

4.1 – Introduction

Whilst there are many thioether macrocycles known, and their chemistry is well defined, there are relatively few selenoether macrocycles, and even fewer telluroether macrocycles. This is due to the increased fragility of Se-C/Te-C bonds, which presents problems in finding suitable reaction conditions or precursors. For example, thiols are much easier to prepare and handle than selenols, which readily oxidise to diselenides, and tellurols, which are thermally unstable. Both selenols and tellurols are also extremely malodorous and toxic.[2]

In 1988, Pinto et al. reported the first examples of homoleptic selenoether macrocycles in a communication[3] and in 1989 published full details of the production of a series of macrocycles, shown in Figure 4.1 below.[4] These were all produced using a pseudo-high dilution method. Diselenocyanate precursors (either $NCSe(CH_2)_2SeCN$ or $NCSe(CH_2)_3SeCN$) were reduced by sodium in liquid ammonia to generate the diselenolate anion *in situ*. Addition of the dibromoalkane reagents takes place at low temperature (-40 to -50°C) reducing the reaction rate to promote cyclisation over polymerisation, whilst maintaining sufficient solubility of the reagents in liquid NH_3. Column chromatography allowed isolation of pure samples of the macrocycles in reasonable yield.[4]

Production of C_1/C_3-linked macrocycles [12]aneSe_4 and [18]aneSe_6 occurs in low yield, with polymeric byproducts accounting for ~75 % of the starting materials. The methyl substituted macrocycles had even poorer yields. The C_2/C_3-linked [14]aneSe_4 was produced in higher yield, ~34 %, but significant decomposition occurred during isolation by column chromatography. It is likely that this is associated with Se-C cleavage in the C_2 linkages, similar to the ethene elimination often observed for $RSeCH_2CH_2SeR$ (see Chapter 1). The C_3-linked macrocycles, [8]aneSe_2, [16]aneSe_4 and [24]aneSe_6 are obtained in much better yield, >70 %, with ~40 % yield of [16]aneSe_4 *via* a "one-pot" reaction. In all case, the [2+2] cyclisation product was the highest yielding macrocycle. Attempts to produce C_2-linked [12]aneSe_4 using 1,2-diselenocyanoethane and 1,2-dibromoethane resulted in deposition of elemental selenium and evolution of ethene.[4]

X-ray crystal structures have been obtained for [12]aneSe_4, [18]aneSe_6, [16]aneSe_4, [24]aneSe_6 and [14]aneSe_4. None of the structures display intramolecular contacts, but some intermolecular associations between Se atoms were observed. All the structures display a preference for *gauche* torsion angles about the Se-C bonds, with every Se-C bond in [24]aneSe_6 having a *gauche* torsion

angle. However, [16]aneSe$_4$ adopts a [3535] quadrangular structure, rather than the [4444] structure which would allow all C-Se-C-C sequences to have *gauche* torsion angles.[4]

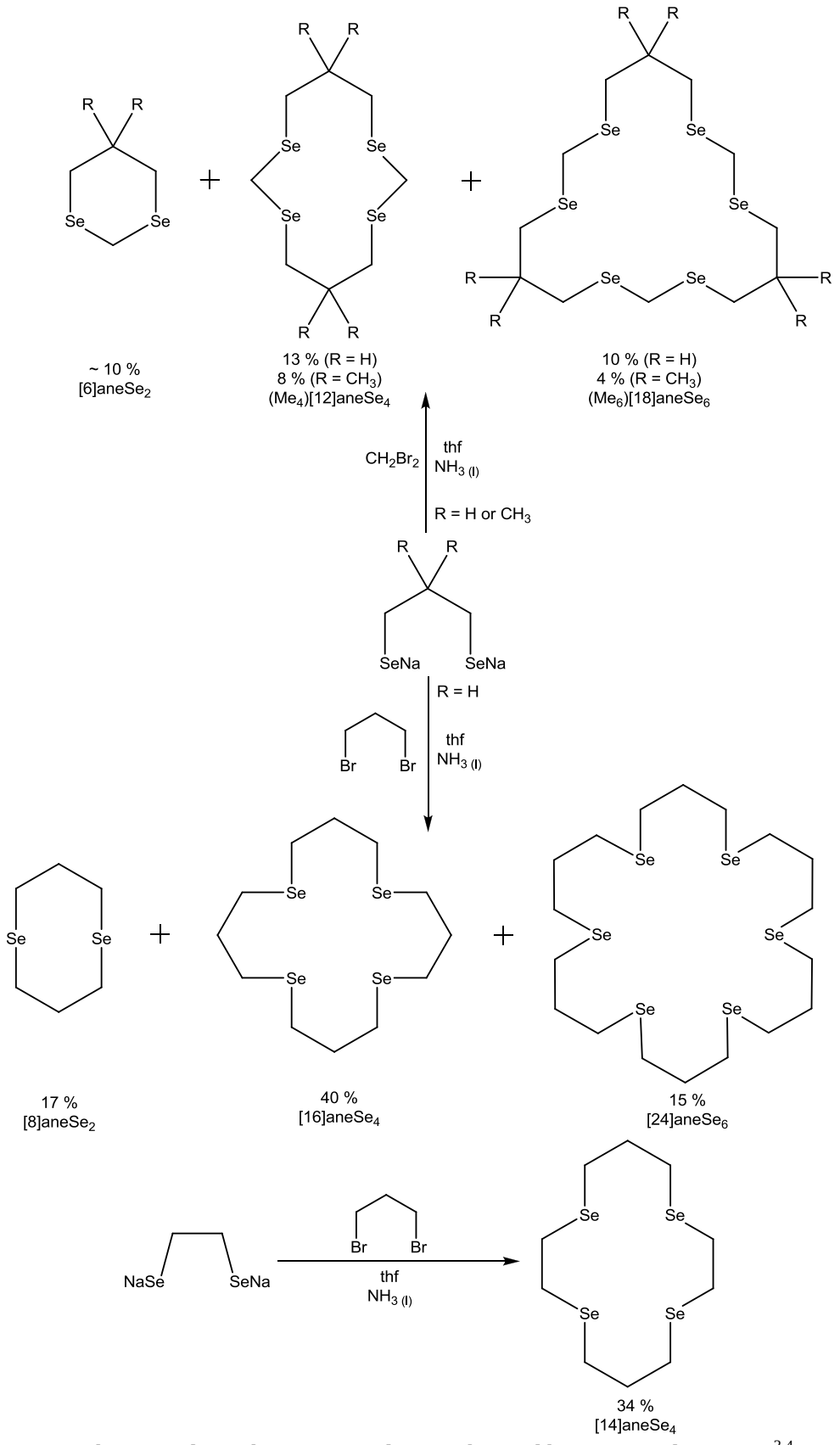

Figure 4.1: First known selenoether macrocycles, synthesised by Pinto et al. in 1988.[3,4]

Unlike amine or phosphine macrocycles, which can be easily functionalized by changing the terminal substituent on the donor atom, chalcogenoether macrocycles require functionalizing groups to be incorporated into the backbone. Hydroxyl functionalized selenoether macrocycles were reported by Pinto et al. in 1996, with [8]aneSe_2(OH) and [16]ane$Se_4$$(OH)_2$ being produced by a modification of the route shown in Figure 4.1, using $NCSeCH_2CH(OH)CH_2SeCN$ with $NaBH_4$ as the reducing agent, and the reaction was carried out at room temperature.[5] The favoured product was the [1+1] cyclisation, with [8]aneSe_2(OH) being produced in 43 % yield, while [16]ane$Se_4$$(OH)_2$ was only produced in 11 % yield. The mono-functionalised [16]aneSe_4(OH) was produced by reacting propane-1,3-bisselenocyanate with 1-chloro-3-propanol to make a diol, which was subsequently tosylated. The ditosyldiselenoether was reacted with a hydroxyl substituted diselenocyanate to generate [16]aneSe_4(OH) in 62 % yield (Figure 4.2).[5] Both mono-functionalised macrocycles were shown to react with acroyl chloride in thf/CH_2Cl_2 to produce an acrylate ester functionalized macrocycle, which could then be polymerized to give the first polymer-bound selenoether macrocycles.[5]

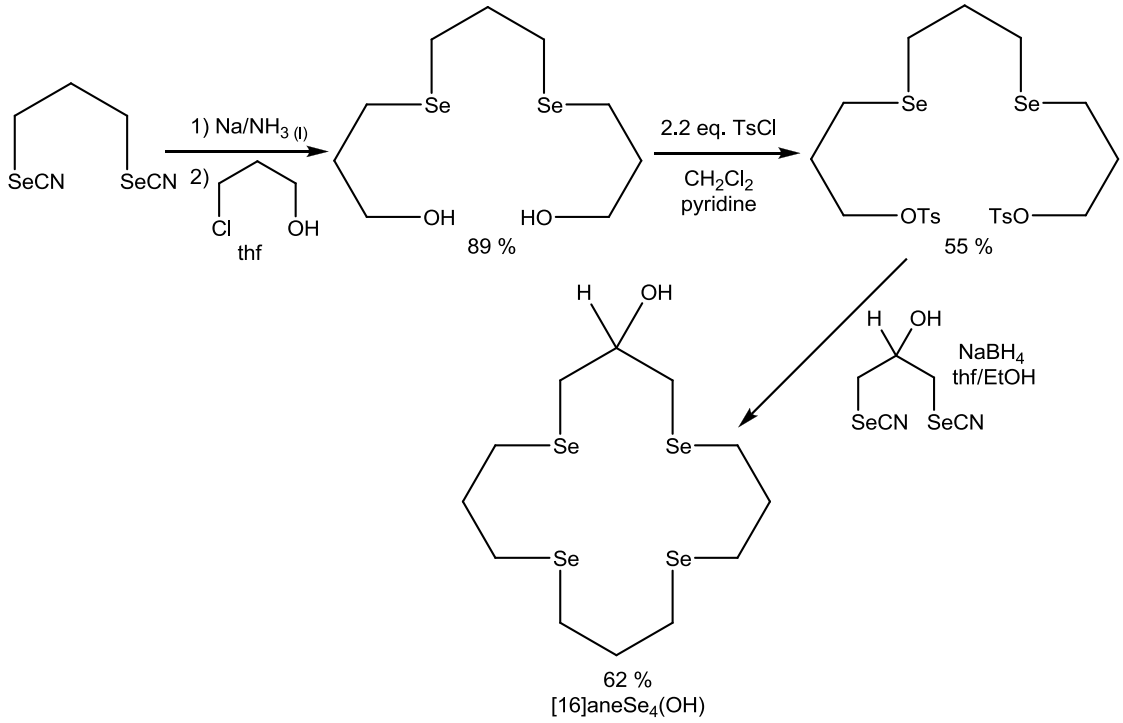

Figure 4.2: Scheme for the production of monofunctionalised [16]aneSe_4(OH).[5]

Reaction of $NCSe(CH_2)_3SeCN$ with $Na/NH_{3\ (l)}$ followed by dropwise addition of α, α′-dibromo-*o*-xylene has been shown to produce the cyclic diselenoether 3*H*-1,4,5,7-tetrahydro-2,6-benzodiselenonine (sebc) in 80 % yield, with only trace amounts of other Se containing products.[6] This would indicate that the more rigid structure of α, α′-dibromo-*o*-xylene predisposes the system to [1+1] cyclisation, a feature this thesis has attempted to exploit. The crystal structure of sebc has the lone pairs *exo* to the ring, and C-Se-C angles in the range 100.8 (4) – 102.6 (4)° (see Figure

4.20). It is worth noting that sebc, like [8]aneSe_2, is not technically a macrocycle, the classical definition of which requires 3 or more heteroatoms. However, given the low number of selenoether macrocycles and lack of reported coordination chemistry, they are generally classed with them in literature reviews.[7] A number of other cyclophanes containing two Se atoms have been reported, but so far no complexation chemistry has been reported for these cyclophanes.[8]

Reduction of the polymeric phenylene diselenide, *o*-$(C_6H_4Se_2)_n$ with sodium borohydride, followed by reaction with 1,2-bis((3-chloro-1-propyl)selenio)benzene has been shown to lead to dibenzo[14]aneSe_4 in 60 % yield as shown below (Figure 4.3). This reaction was carried out on a milligram scale, and produced 0.29 g of macrocycle. Attempts to make 1,2-bis((2-chloro-1-ethyl)selenio)benzene resulted in episelenonium ions forming, which decomposed *via* loss of ethene.[9]

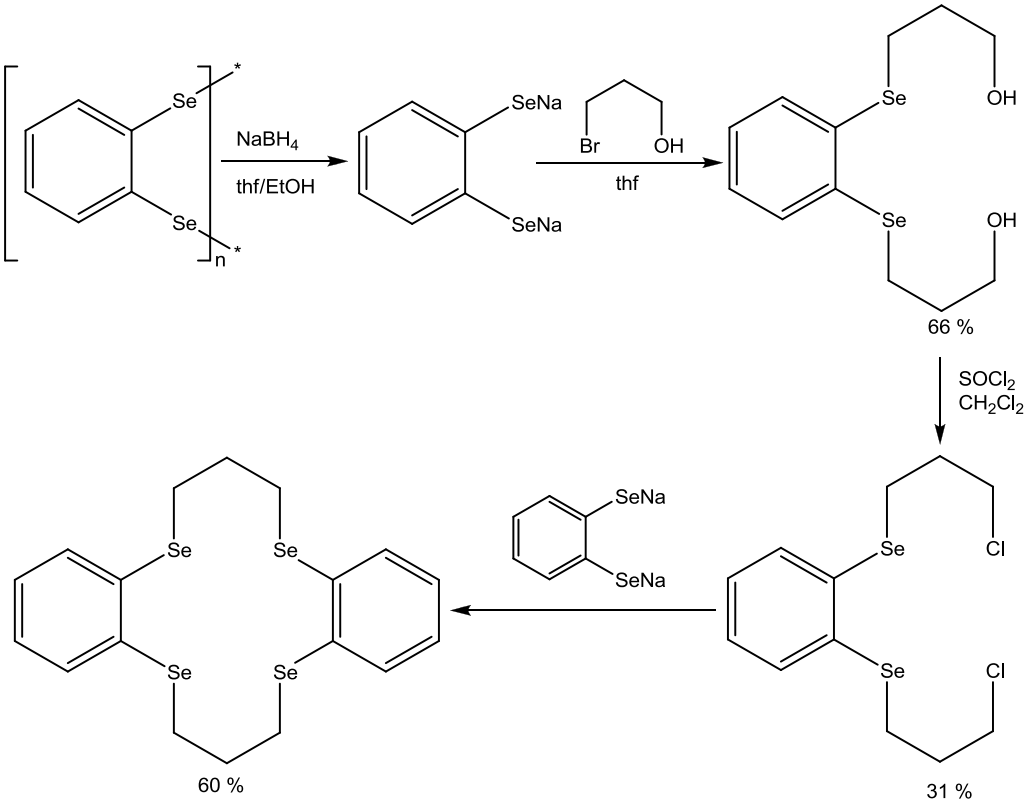

Figure 4.3: Scheme for production of dibenzo[14]aneSe_4.[9]

The crystal structure of dibenzo[14]aneSe_4 is a disordered superposition of two conformers, a (67 %) and b (33 %) as shown in Figure 4.4. The two arene rings are nearly coaxial, with the dihedral angle between the planes being only 6.0 (3)°. However, the distance between the two rings (5.05 Å) is slightly too large to form stable sandwich complexes without some structural rearrangement, although the C_3 linkages may be flexible enough to accommodate this.[9]

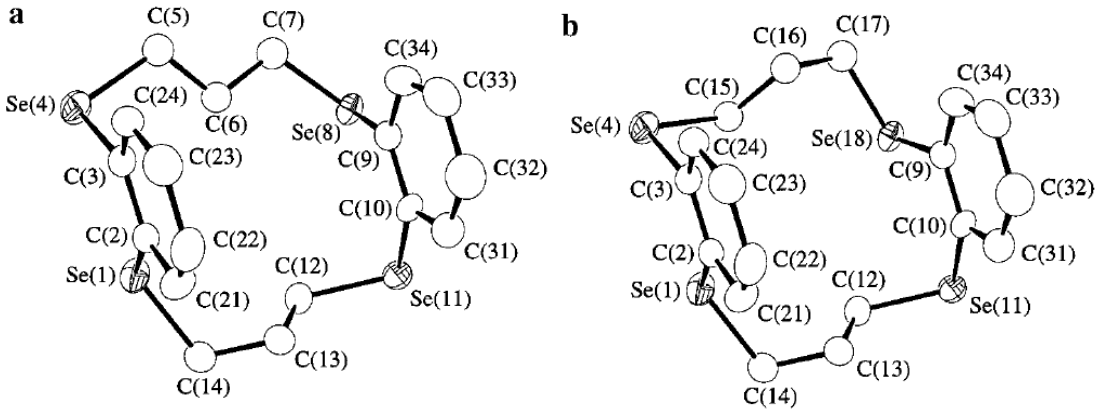

Figure 4.4: Crystal structures of the major (a) and minor (b) conformers of dibenzo[14]aneSe_4. Ellipsoids shown at 50% probability, H atoms omitted for clarity.[9]

A few selenoether macrocycles with naphthalene backbones have been reported. Reaction of naphtha-[1,8-*cd*]-l ,2-diselenole with sodium borohydride generates the sodium salt, which can then be reacted with 1,3-dibromopropane. Use of stoichiometric quantities of 1,3-dibromopropane generates 3,4-dihydro-2*H*-naphtho[1,8-*bc*]-1,5-diselenocine, whilst use of a large excess results in the acyclic disubstitited product (Figure 4.5). This can then be reacted with either another equivalent of to produce 9,10,20,21-tetrahydro-8*H*,l9*H*-dinaphtho[1′ ,8′-*jk;*1,8-*bc*][1,5,9,13]tetraselenacyclohexadecine,[10] or with sodium selenide to produce 3,4,7,8-tetrahydro-2*H*,6*H*-naphtho[1,8-*bc*]-1,5,9-triselenacyclododecine.[11] The crystal structure of 9,10,20,21-tetrahydro-8*H*,l9*H*-dinaphtho[1′,8′-*jk;*1,8-*bc*][1,5,9,13]tetraselenacyclohexadecine shows transannular contacts between the selenium atoms (3.19 and 3.17 Å) which are significantly shorter than the sum of the Van der Waals radii (4.0 Å).[10]

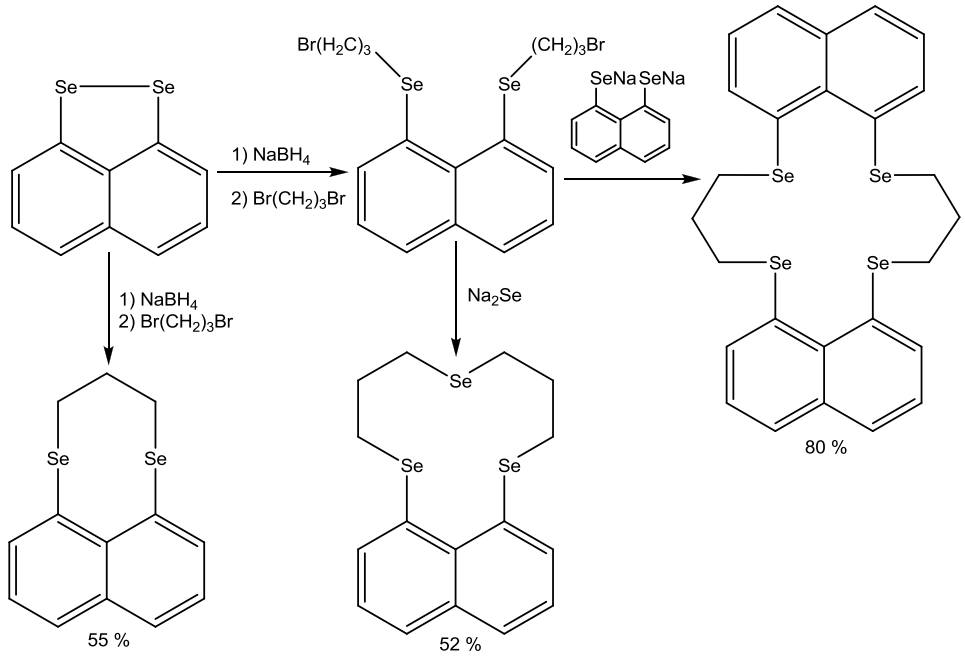

Figure 4.5: Scheme for the production of macrocyclic selenoethers containing naphthalene rings.[11]

The tridentate selenium-naphthalene macrocycle above is one of a very small number of macrocycles with odd numbers of selenium atoms. Pinto et al. described a route to Se_3 and Se_5 donor macrocycles in 1995 (Figure 4.6).[12] These macrocycles are produced *via* classical high dilution, with 20 cm^3 of solution of the two final reactants being added simulataneously dropwise over 20 hours to between 100-300 cm^3 thf/EtOH suspension of $NaBH_4$. These reactions proceeded on the milligram scale, producing 0.175 g [12]aneSe_3 and 0.22 g [20]aneSe_5.

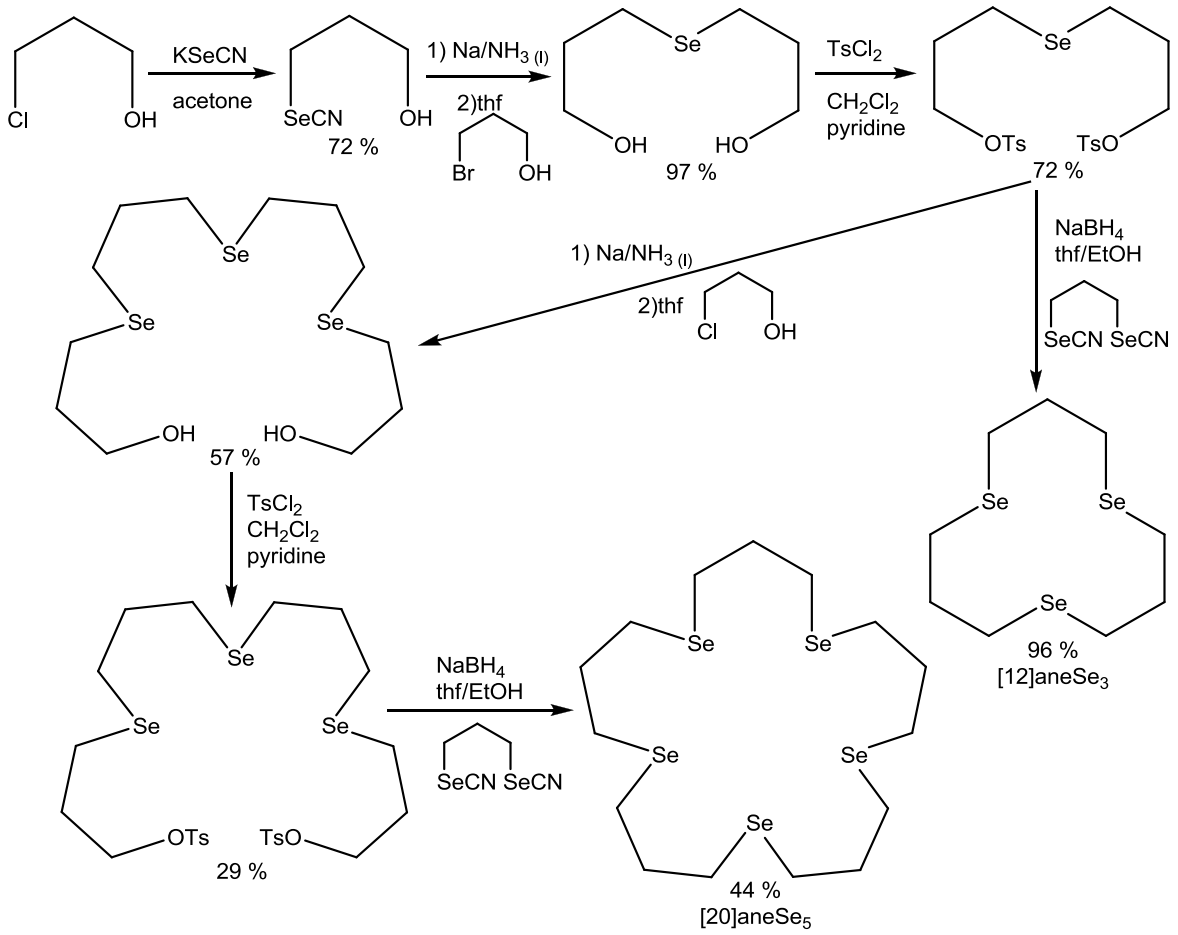

Figure 4.6: Scheme for production of [12]aneSe_3 and [20]aneSe_5.[12]

The crystal structure of [12]aneSe_3 (Figure 4.7) has no crystallographic symmetry, but does have approximate local mirror symmetry across a plane passing through Se(9) and C(3). It shows each C-Se-C-C segment to be in the preferred *gauche* geometry. The analogous [12]aneS_3 has two *anti* C-S-C-C segments.[13]

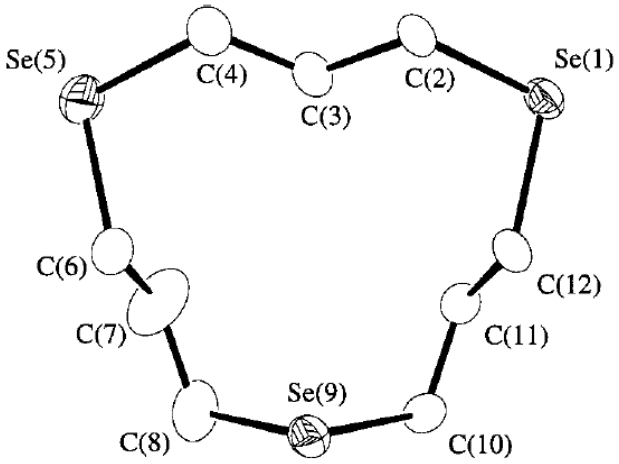

Figure 4.7: Crystal structure of [12]aneSe_3. Ellipsoids shown at 50% probability, H atoms omitted for clarity.[9]

The methyl-substituted selenoether macrocycles Me_4[8]aneSe_2, Me_6[12]aneSe_3 and Me_8[16]aneSe_4 have been produced by the catalytic macrocyclization of 3,3-dimethylselenetane (dmSe) by $Re_2(CO)_9$(dmSe) or $Re_2(CO)_9$(NCMe) (Figure 4.8). While sodium templating may play a role in the macrocyclic preparations discussed above, this is the only published example of selenoether macrocycles being produced by a template method using a transition metal. The crystal structures of these three macrocycles all have the *gem*-methyl groups *exo* to the ring.[14]

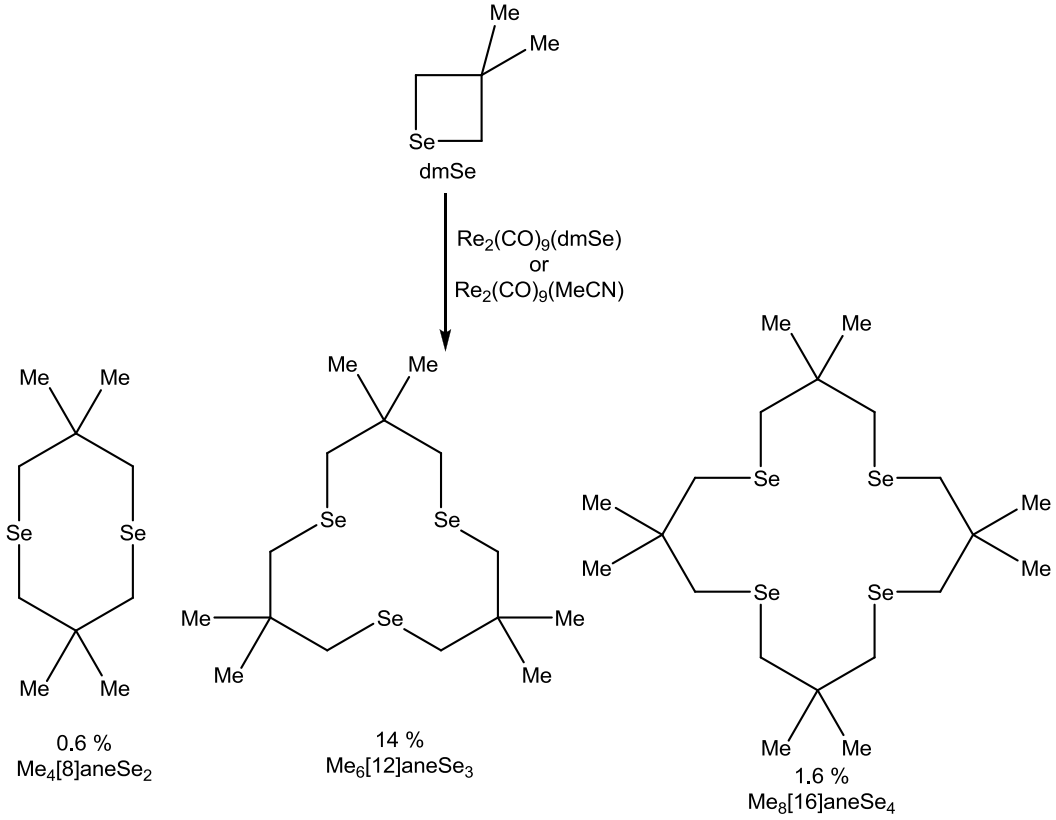

Figure 4.8: Catalytic macrocyclisation of 3,3-dimethylselenetane.[14]

The triselenacyclophanes shown below (Figure 4.9) were isolated as byproducts from the production of the analogous diselenaphane. These diselenaphanes were produced in the hope that they would provide a route to meta-cyclophanes, however it was shown that selenoxide elimination in cyclophanes is much less facile than in alicyclic examples, and no significant advantage was gained over use of thiocyclophanes.[2]

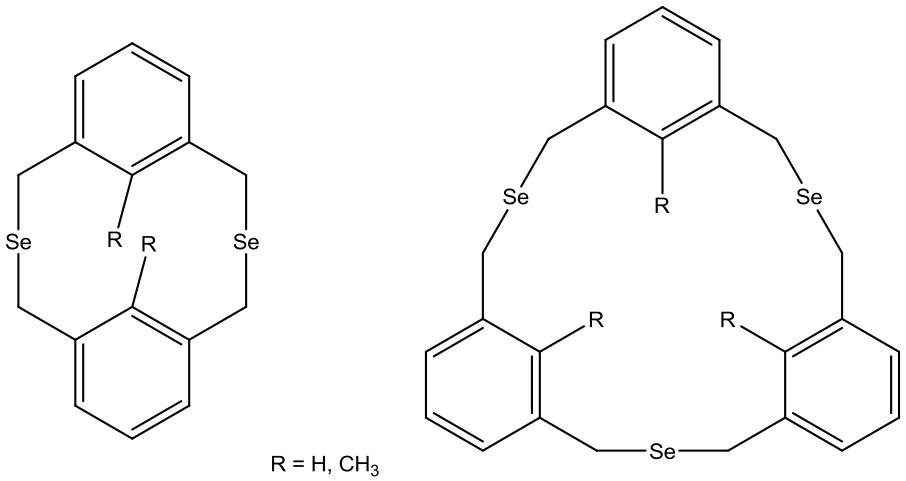

Figure 4.9: Di- and tri-selenacyclophanes.[2]

While a number of mixed donor macrocycles containing tellurium have been characterised (see Chapter 3), there are only two known homoleptic macrocyclic telluroethers – [8]aneTe$_2$[15] and [12]aneTe$_3$ and the hexachloride derivative Cl$_6$[12]aneTe$_3$.[14] Reaction of 1,3-dibromopropane with sodium telluride, followed by addition of another equivalent of the dihalide generates [8]aneTe$_2$ in undisclosed yield.[15] Reduction of this with Cl$_2$ in benzene yields the insoluble ditellurane, which upon refluxing in dmf at 160°C, gives Cl$_6$[12]aneTe$_3$. This has been reduced with thiophenol to produce 0.064 g [12]aneTe$_3$. Whilst the yield is exceptionally good, there is no report of the reaction being scaled up to produce practical quantities of the macrocycle.[16]

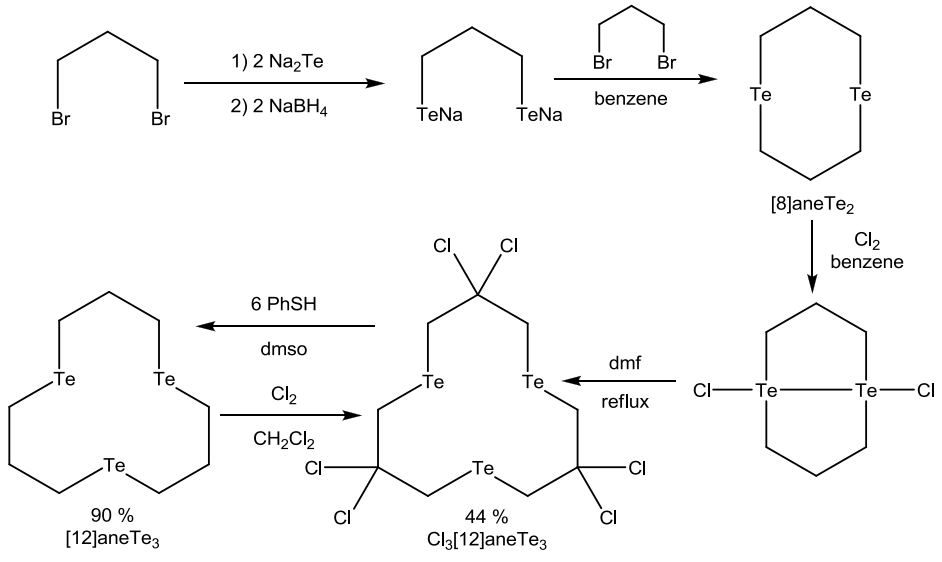

Figure 4.10: Scheme for production of [8]aneTe$_2$ and [12]aneTe$_3$.[15,16]

Chapter 3 discusses the production of mixed donor macrocycles containing more than one type of chalcogen. Here, macrocycles containing mixed donor sets of the type Se/N and Te/N are considered. There have only been a small number of mixed donor Se/N macrocycles reported, and even fewer Te/N macrocycles. Hojjatie et al. have produced three Se/N macrocycles, where the nitrogen donor is part of a pyridyl ring. These are made *via* high dilution reactions in extremely high yield, using $NaBH_4$ to reduce either 2,6-bis(bromomethyl)pyridine with the appropriate diselenocyanate or 2,6-bis(selenocyanatomethyl)pyridine with the appropriate dibromide. These high yields are probably due to the highly pre-organised nature of the precursors used.[8]

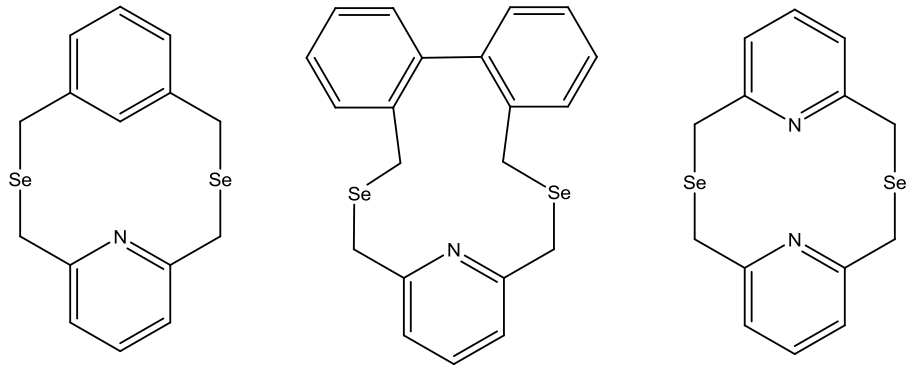

Figure 4.11: Mixed donor Se/N macrocycles produced by high dilution $NaBH_4$ reduction.[8]

There are only two examples of Schiff bases with the heavier chalcogens, one with Se and one with Te (Figure 4.12). The N_6Se_2 Schiff base is made by reaction of bis(2-formylphenyl)selenide and diethylenetriamine in MeCN.[17] The N_4Te_2 Schiff base is made *via* a similar reaction, using the analogous telluride and ethane-1,2-diamine.[18] Both reactions produce the Schiff base in good yield (>80 %).

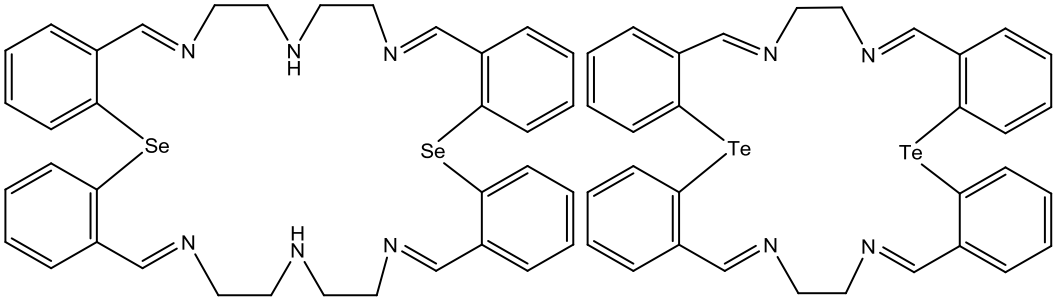

Figure 4.12: Mixed donor Schiff base macrocycles. Left: N_6Se_2.[17] Right: N_4Te_2.[18]

There are two examples of mixed donor N/Se cryptands, with one also having an analogous N/Te cryptand. Figure 4.13 shows the N_3Se_3 cryptand, 1-nitro-8-methyl-6,10,19-triselena-3,13,16-triazabicyclo[6.6.6]icosane, which has been produced as a coordinated ligand on Co(III). A Co(III) complex of the tripodal N_3Se_3 ligand shown in Figure 4.13 was treated with HCHO and $MeNO_2$ in

water. There are no reports indicating that the sarcophagine-like N_3Se_3 cryptand has been demetallated.[19]

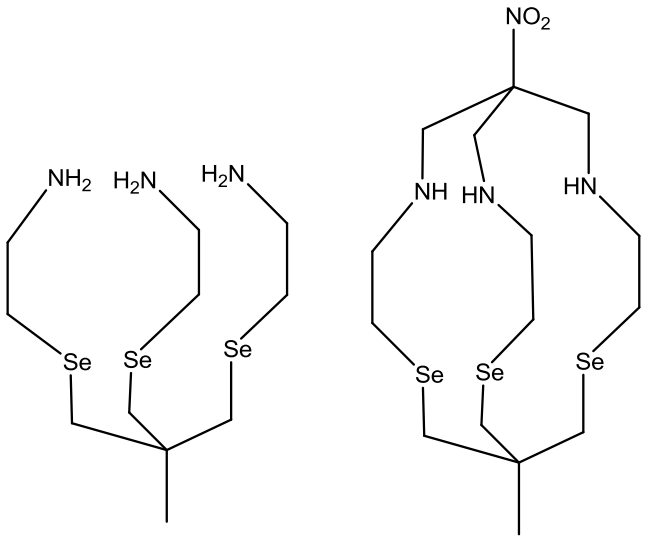

Figure 4.13: Tripodal N_3Se_3 ligand and N_3Se_3 cryptand.[19]

The larger N_8E_3 cryptands (E = Se, Te) are produced by adding three equivalents of bis(2-formylphenyl) selenide/telluride in MeOH to two equivalents of $N(CH_2CH_2NH_2)_3$ and one equivalent of CsCl in MeOH at room temperature. The cryptands precipitate out, and are collected by filtration in good yield (Se 90 %, Te 79 %).[17]

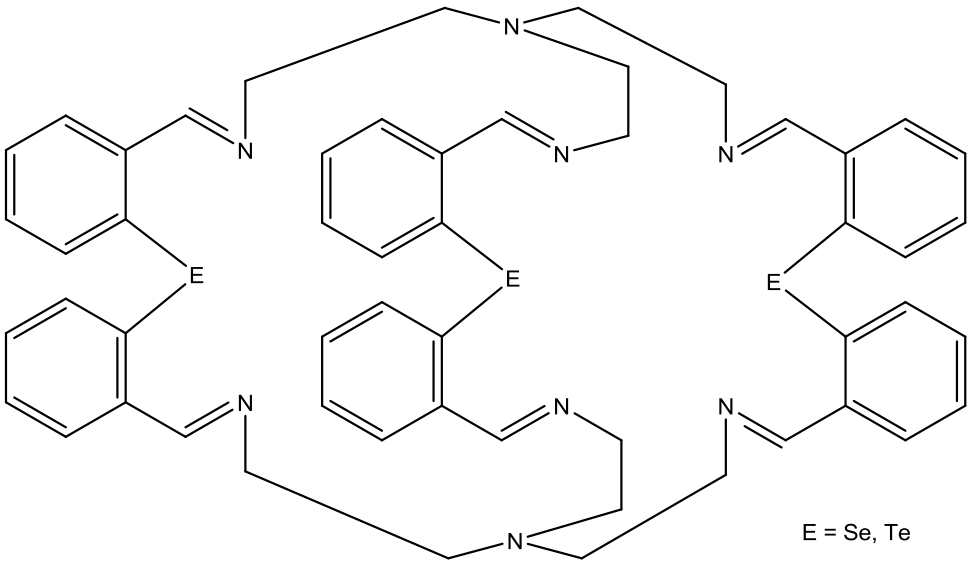

Figure 4.14: Mixed donor N_8Se_3 or N_8Te_3cryptand.[17]

4.2 – Aims

This chapter investigates methods of producing tridentate homoleptic selenoether macrocycles. As mentioned in Chapter 1, the small ring thioether macrocycle [9]aneS_3 has been shown to be a very effective ligand, especially to metals in unusual oxidation states. Given the better σ-donor nature

of selenium, a small ring tridentate selenoether macrocycle could be a very effective ligand, and the only known examples have only been produced on a milligram scale. Reaction methods discussed in Chapter 3 will be investigated, in the hope of producing high yielding, multi-gram routes into new Se_3 ligands. The flexibility of the high dilution $NaBH_4$ method will be further tested on a second donor set, Se_2N macrocycles, combining the soft Se with the harder pyridyl N donor. This will investigate whether it can be used with more flexible precursors, as opposed to the purely rigid, preorganised precursors used by Hojjatie et al.[8]

4.3 – Production of Homoleptic Se_3 Macrocycles

The first stage in the production of Se_3 macrocycles was to produce suitable precursors. The ditosylate precursor $Se(\{CH_2\}_3OTs)_2$ was produced by the route described by Pinto et al. (Figure 4.6, above).[12] KSeCN was reacted with 3-bromo-1-propanol in refluxing acetone for two days. The white solid was filtered off, and the yellow solution was dried *in vacuo* to give a yellow oil, identified by ^1H and $^{13}C\{^1H\}$ NMR spectroscopy as 3-selenocyanato-1-propanol, in 78 % yield. $^{77}Se\{^1H\}$ NMR spectroscopy of the neat oil with an external D_2O lock showed it to have δ = 211.1 ppm. This oil was reacted, without further purification, with sodium metal in liquid ammonia to generate the selenolate anion, to which was added one equivalent of 3-bromo-1-propanol. After hydrolysis and extraction with dichloromethane, the yellow organics were dried *in vacuo* to leave $Se(\{CH_2\}_3OH)_2$ as a yellow oil. ^1H and $^{13}C\{^1H\}$ NMR spectra agreed with the literature values. $^{77}Se\{^1H\}$ NMR spectroscopy of the neat oil showed complete conversion of $NCSe(CH_2)_3OH$, with the diol having δ = 152.1 ppm. $Se(\{CH_2\}_3OH)_2$ was stirred overnight with *p*-toluenesulfonyl chloride in CH_2Cl_2/pyridine. After washing (hydrochloric acid, sodium hydrogencarbonate, water and brine) and drying *in vacuo*, a yellow oil which darkened slowly over time, was isolated. Column chromatography removed minor byproducts to leave a white solid which was identified by ^1H and $^{13}C\{^1H\}$ NMR spectroscopy as $Se(\{CH_2\}_3OTs)_2$. Figure 4.15 shows the $^{77}Se\{^1H\}$ NMR spectrum in $CH_2Cl_2/CDCl_3$, which shows a single peak at 150 ppm.

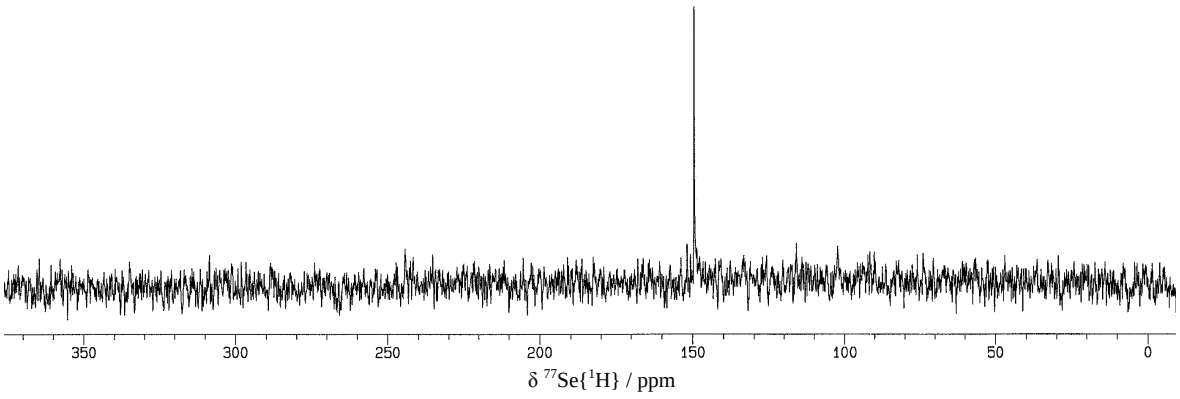

Figure 4.15: ^{77}Se NMR spectrum of $Se(\{CH_2\}_3OTs)_2$ in $CH_2Cl_2/CDCl_3$.

The first reaction performed (Figure 4.16, below) was an attempt to react $NCSe(CH_2)_3SeCN$ with $Na/NH_{3\ (l)}$ to make the selenolate dianion,[4] followed by dropwise addition of $Se(\{CH_2\}_3OTs)_2$ in anhydrous thf in an analogous reaction to that of Pinto et al. for [8]aneSe_2 and larger rings (Figure 4.1).[4] The reaction was carefully maintained at -45°C during the three hour addition of the ditosylate precursor, then allowed to warm slowly to room temperature. After hydrolysis and extraction with dichloromethane it was hoped that the crude red-brown oil isolated would contain a mixture of [12]aneSe_3 and [24]aneSe_6.

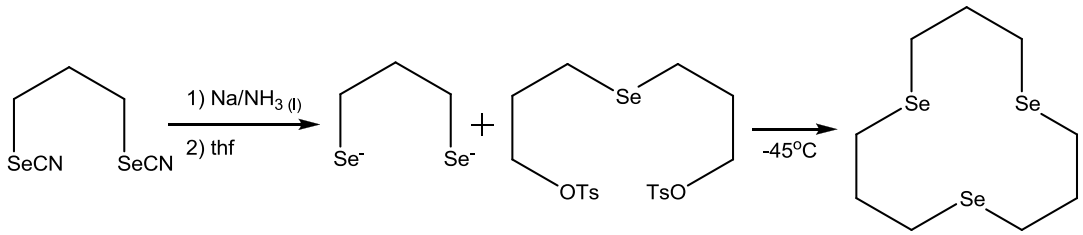

Figure 4.16: Attempted reaction of $NCSe(CH_2)_3SeCN$ and $Se(\{CH_2\}_3OTs)_2$ with $Na/NH_{3\ (l)}$.

$^{77}Se\{^1H\}$ NMR spectroscopy revealed that the oil contained a mixture of selenium containing products, with the dominant feature being a cluster of four peaks at ~152 ppm. [24]aneSe_6 has δ = 153 ppm, and it is not unreasonable that the [2+2] product would dominate (see Chapter 3). However, [24]aneSe_6 would show only a single peak, and previous work in this group has shown that the polymer by-products of the [8]aneSe_2/[16]aneSe_4/[24]aneSe_6 reaction also tend to have $\delta \approx$ 153 ppm. Any unreacted ditosylate would also occur around this point. More peaks were observed at 198 and 264 ppm, with a minor peak at 131 ppm, which could correspond to [12]aneSe_3.[12] Column chromatography (eluent = hexane:ethyl acetate, 19:1) resulted in three fractions with selenium containing compounds. Both the second and third fractions contained the peak group at ~152 ppm, and the peak at 198 ppm. ^1H and $^{13}C\{^1H\}$ NMR spectra showed many overlapping groups of peaks, with some aromatics being observed, indicating the presence of tosyl groups. The first fraction had three peaks in the $^{77}Se\{^1H\}$ NMR spectrum, including the peak at 131 ppm. However, as there was only a few milligrams of this fraction isolated from > 7 g $Se(\{CH_2\}_3OTs)_2$, and this was still not pure macrocycle, it was clear that this method was not going to be practical in producing gram quantities of macrocycle, and it was not pursued further.

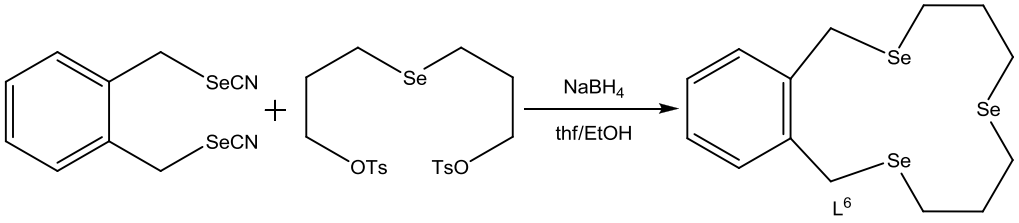

Figure 4.17: Production scheme for L^6 by $NaBH_4$ reduction.

As shown in Chapter 3, a $NaBH_4$ reduction can be used to produce Se_2O macrocycles with a variety of backbones. Hojjatie et al. have also shown this route to be effective for Se/N and Se_2 cyclophanes.[8] It was decided to investigate the possibilities of this route. $Se(\{CH_2\}_3OTs)_2$ and $NCSe(CH_2)_3SeCN$ both have flexible backbones, with no pre-organisation. As all the previous successes of using an $NaBH_4$ reduction have used at least one (if not two) pre-organised precursors, it was decided to test this method for Se_3 macrocycles using *o*-$C_6H_4(CH_2SeCN)_2$, as this is pre-orientated to promote cyclisation over polymerisation. Initially, the reaction was attempted on a small scale. Separate solutions of $Se(\{CH_2\}_3OTs)_2$ (0.101 g, 0.2 mmol) and *o*-$C_6H_4(CH_2SeCN)_2$ (0.063 g, 0.2 mmol) in 18 cm^3/7 cm^3 anhydrous thf/EtOH were added simultaneously dropwise to a solution of 0.5 g $NaBH_4$ in 270 cm^3/30 cm^3 anhydrous thf/EtOH over two hours. The reaction mixture was then left stirring for three days. The reaction mixture was filtered, to remove white solids, and dried *in vacuo.* The solids gained were then redissolved in CH_2Cl_2 and again filtered, with the filtrate being dried *in vacuo* to yield a cream solid. This solid was characterised by ^1H, $^{13}C\{^1H\}$ and ^{77}Se NMR spectroscopy and EI MS. $^{77}Se\{^1H\}$ NMR spectrum (Figure 4.18) shows two Se environments, which have surprisingly similar chemical shifts (δ = 181, 183 ppm). *o*-$C_6H_4(CH_2SeMe)_2$ has a $^{77}Se\{^1H\}$ NMR chemical shift of 149 ppm,[20] while $MeSe(CH_2)_3SeMe$ occurs at 74 ppm,[21] and $Se(\{CH_2\}_3SeMe)_2$ occurs at 73 ppm (terminal Se) and 154 ppm (central Se).[21]

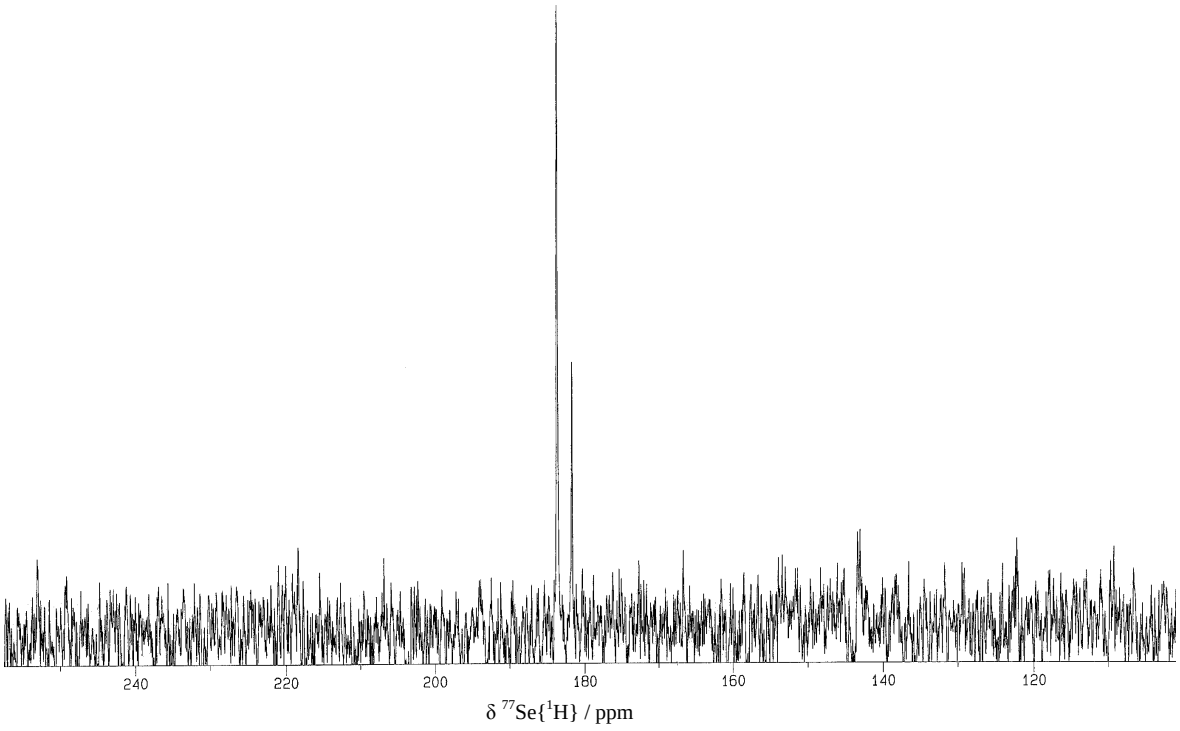

Figure 4.18: $^{77}Se\{^1H\}$ NMR spectrum of L^6 recorded in CH_2Cl_2 with an external D_2O lock.

The other data collected were all consistent with production of L^6, indicating that the cyclic nature of the molecule plays a large role in the chemical shifts here. The ^1H NMR spectrum obtained showed peaks consistent with the desired macrocycle, comprising a singlet at δ = 4.12 ppm corresponding to the *o*-$C_6H_4CH_2$ protons, a quintet at 2.17 ppm and a triplet at 3.71 ppm from the C_3 linkage and a multiplet at 7.21-7.37 ppm from the aryl protons. The $^{13}C\{^1H\}$ NMR spectrum three peaks between 128 and 137 ppm, corresponding to the aromatic carbons, and four peaks between 21 and 31 ppm corresponding to the aliphatic carbons. The EI MS showed a peak cluster at *m/z* = 426, confirming production of the [1+1] macrocycle ($C_{14}H_{20}{}^{80}Se_3$ = 426).

This small scale reaction had a yield of 92 %. In order to investigate producing this macrocycle on a multigram scale the reaction was repeated, with quantities of the precursors scaled up to 2.42 g $Se(\{CH_2\}_3OTs)_2$ and 1.5 g *o*-$C_6H_4(CH_2SeCN)_2$ in 180 cm^3/20 cm^3 anhydrous thf/EtOH being added to 1.5 g $NaBH_4$ in 450 cm^3/50 cm^3 anhydrous thf/EtOH. This is on the same scale as the preparations of Hojattie et al., but the volume of solvent in the $NaBH_4$ solution used here is lower by half, to reduce costs and solvent removal time. Addition time was increased to 4 hours, while the reaction mixture was again left for three days stirring before work up. 1.88 g L^6 was obtained (93 % yield). ^1H, $^{13}C\{^1H\}$ and $^{77}Se\{^1H\}$ NMR spectra were the same as those collected from the product of the small scale reaction. The crystal structure (Figure 4.19) is from a crystal obtained by the slow evaporation of a saturated solution of L^6 in $CHCl_3$.

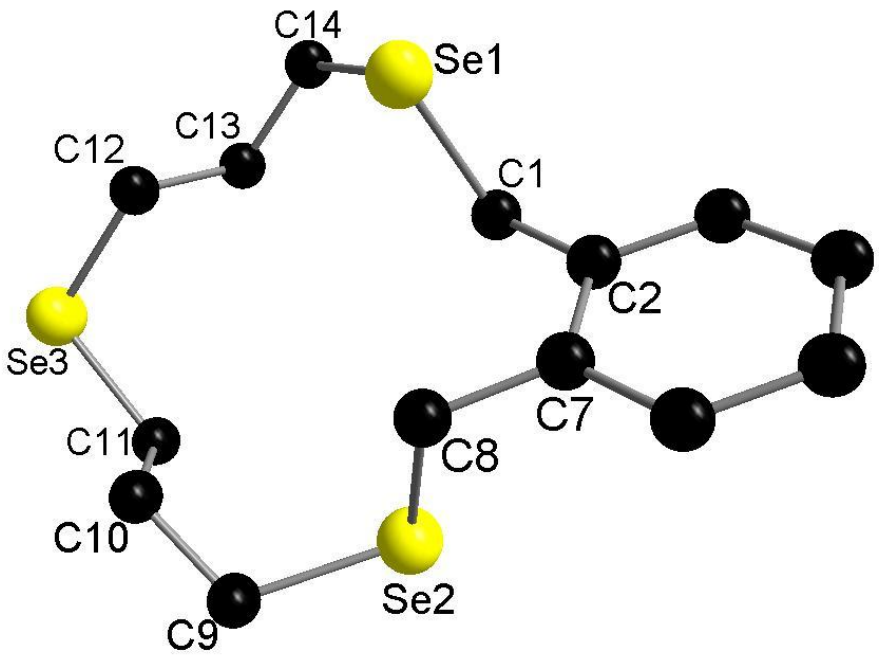

Figure 4.19: Crystal structure of L^6. H atoms omitted for clarity.

Table 4.1: Selected bond lengths and angles for L^6.

Bond	**Length / Å**	**Bond**	**Length / Å**	**Bond**	**Angle / °**
Se1–C1	1.960 (7)	Se2–C9	1.965 (7)	C1–Se1–C14	97.7 (3)
Se1–C14	1.960 (7)	Se3–C11	1.965 (7)	C8–Se2–C8	98.3 (3)
Se2–C8	1.982 (7)	Se3–C12	1.954 (7)	C11–Se3–C12	98.4 (3)

L^6 has approximate non-crystallographic two fold symmetry. Comparing the structure obtained for L^6 with that published for sebc (Figure 4.20) it can be seen that changing from a C_3 linkage between the two Se atoms in sebc to a -$(CH_2)_3Se(CH_2)_3$- linkage allows L^6 to exhibit a structure in which the two Se atoms closest to the xylyl ring adopt *anti* positions, above and below the plane of the aromatic ring, rather than the *syn* positions that sebc is sterically constrained to by its single propyl backbone.[6] This *anti* conformation is also observed in the crystal structure of L^1 (Chapter 3, Figure 3.14). The bond angle at Se3 is considerably more acute (98.4°) than that at the O atom in L^1 (113.1°), reflecting the greater flexibility imparted by the C_3 backbones, as opposed to the C_2 backbones and smaller atom in L^1.

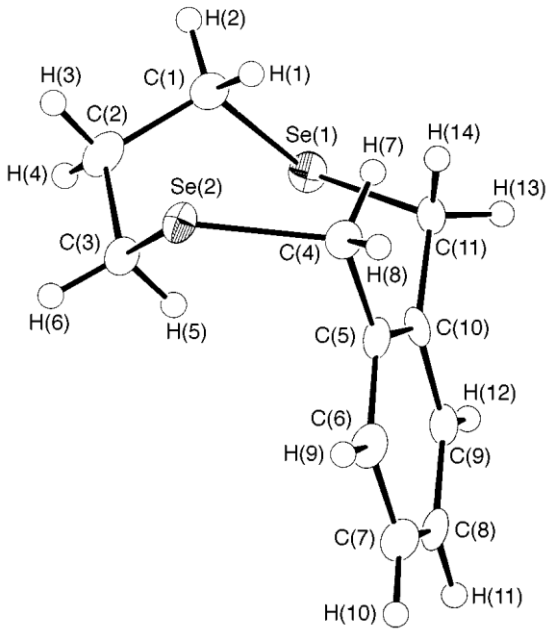

Figure 4.20: Crystal structure of sebc. Ellipsoids shown at 40 % probability.[6]

Following the success of the production of L^6, [12]aneSe_3 (hereafter referred to as L^7) was produced on the larger scale in analogous fashion, from dropwise addition of separate solutions of $Se(CH_2CH_2CH_2OTs)_2$ and $NCSe(CH_2)_3SeCN$ in thf/EtOH to a solution of $NaBH_4$ in thf/EtOH. The solution isolated after filtration of the white solids was dried *in vacuo*, redissolved in CH_2Cl_2, filtered, and again dried *in vacuo* to generate 1.34 g L^7 (77 % yield). The white solid was analysed by ^1H, $^{13}C\{^1H\}$ and ^{77}Se NMR spectroscopy and the data corresponded to the literature values reported by Pinto et al.[12] While this is a very respectable yield for a macrocycle, it is lower than

that obtained by Pinto et al. However, this reaction was on a much larger scale, and used a much faster addition rate. If the addition had proceeded at the rate used by Pinto et al. it would have taken over eight days for complete addition of the precursors. Therefore, a slower addition rate may well result in higher yields.

To introduce a C_2-linkage into a tridentate selenoether, an obvious target precursor was the polymeric diselenide *o*-$(SeC_6H_4Se)_n$ as it has been previously used to form dibenzo[14]aneSe_4.[9] The polymer is preorganised to promote cyclisation, and has the advantage of being unable to form a diselenide *via* the elimination of ethene, as can readily occur with an aliphatic C_2 linkage between Se atoms.[4] *o*-$(SeC_6H_4Se)_n$ is produced by reaction of elemental selenium and sodium to produce NaSeSeNa, followed by addition of 1,2-dibromobenzene in refluxing dmf.[22] The initial attempt produced a red solid which appeared to be consistent with the desired polymer by IR spectroscopy. Addition of sodium borohydride in thf/EtOH caused a colour change, and dissolution, but after addition to the ditosylate precursor $Se(CH_2CH_2CH_2OTs)_2$ under the reaction conditions used for L^6 and L^7, the only selenium containing product obtained was unreacted ditosylate. A second attempt at producing the polymeric diselenide generated only a black, oily solid. The third attempt at producing this polymer used a heating mantle, with a thermometer in the reaction vessel itself, as opposed to an oil bath with temperature probe as before. This increased the certainty of the temperature of the reaction itself, and after workup 3.26 g of *o*-$(SeC_6H_4Se)_n$ was obtained as an orange solid.

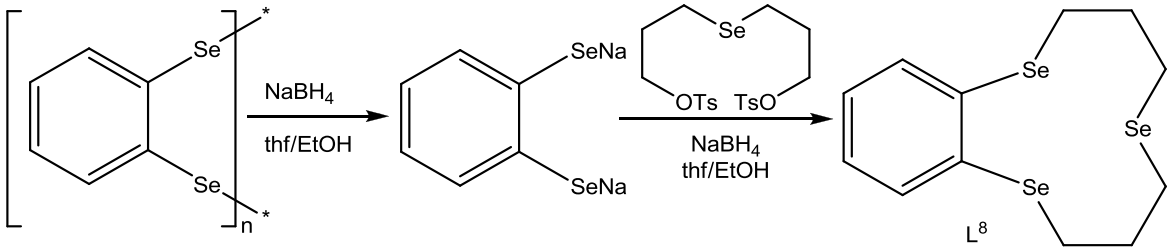

Figure 4.21: Production scheme for L^8 by $NaBH_4$ reduction.

A solution of sodium borohydride in EtOH was added slowly to 1.5 g of this orange solid suspended in thf under N_2. A dark red solution formed immediately, which slowly turned yellow as more $NaBH_4$ was added. Upon complete addition, the solution was stirred for 10 mins, which gave a clear yellow solution. This was transferred by cannula to a dropping funnel containing anhydrous thf/EtOH. This solution was added simultaneously dropwise with a solution of $Se(\{CH_2\}_3OTs)_2$ to a solution of $NaBH_4$ in thf/EtOH in the same manner as for L^6 and L^7 above. Upon workup, a crude mixture was obtained which had several peaks in its $^{77}Se\{^1H\}$ NMR spectrum. The minor peak at 150 ppm corresponded to unreacted ditosylate, which was also observed in the ^1H and $^{13}C\{^1H\}$ NMR spectra. Column chromatography (eluent = hexane:ethyl

acetate, 19:1) removed the ditosylate. The fraction with Rf = 0.87 still showed multiple peaks in the $^{77}Se\{^{1}H\}$ NMR spectrum. The ^{1}H NMR spectrum showed an unexpected singlet at 4 ppm with clear Se-H coupling (14 Hz). This peak would seem to correspond to a C_1 link between Se atoms, and comparison with the literature value for benzo-1,3-diselenol made this the most likely culprit.[23] Unfortunately, there is no $^{77}Se\{^{1}H\}$ NMR data published for it, so no comparison could be made there. It is uncertain how a C_1 linkage would have formed, as it is highly unlikely that the C_3 linkage would have been attacked at C-1 to form an episelenonium ion. There was no CH_2Cl_2 present until the third washing, again making it very unlikely to have contributed to the reaction, especially as the reaction had been opened to air before this, so any unreacted selenolate would most likely have already been quenched.

In order to remove this, and other, byproducts, the oily mixture obtained from the column was distilled in a Kugelrohr apparatus at 120°C/0.01 mm Hg. A yellow oil fractionated, leaving behind a clear light yellow oil. Figure 4.22 below shows the $^{77}Se\{^{1}H\}$ NMR spectrum obtained from the residue, clearly showing two selenium resonances at δ = 292.5 and 208.0 ppm in a roughly 2:1 ratio. The nearest comparable macrocycle would be dibenzo[14]aneSe_4, but no $^{77}Se\{^{1}H\}$ NMR data has been published for this ligand. These shifts are consistent with the high frequency shifts observed for Se adjacent to an aromatic ring (*o*-$C_6H_4(SeMe)_2$ = 202 ppm),[21] and the aliphatic Se has been shifted to a higher frequency than L^6 (181 ppm).

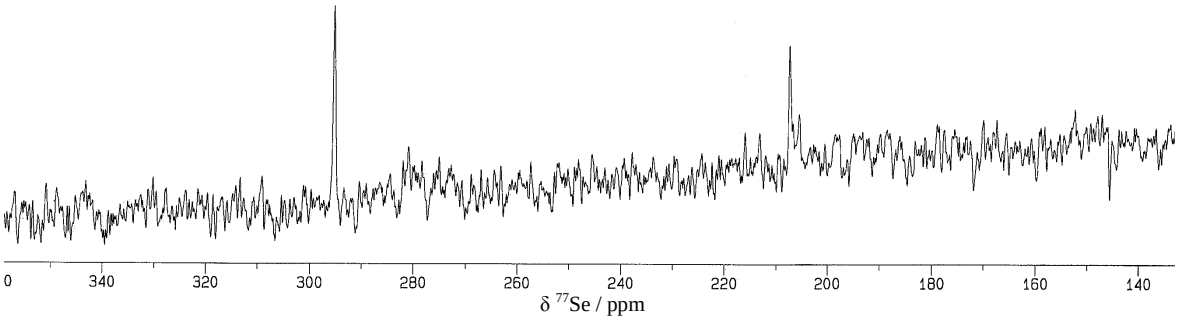

Figure 4.22: $^{77}Se\{^{1}H\}$ NMR spectrum of L^8 recorded in $CH_2Cl_2/CDCl_3$ at 298 K.

4.4 – Production of Mixed Donor Se_2N Macrocycles

As discussed above, Hojjatie et al. have published the preparation of an Se_2N macrocycle, using *m*-$C_6H_4(CH_2SeCN)_2$.[8] In order to experiment with the versatility of this route, it was decided to make the smaller ring macrocycle from *o*-$C_6H_4(CH_2SeCN)_2$. This would be a smaller ring, but both precursors are still preorganised for cyclisation, and the yield should be high. 2,6-Bis(bromomethyl)pyridine was bought from Aldrich and used without further purification. The $NaBH_4$ reduction of *o*-$C_6H_4(CH_2SeCN)_2$ and 2,6-bis(bromomethyl)pyridine was done using the same conditions as for the Se_3 macrocycles above, and was first undertaken on a small scale (0.2

mmol), then increased to a 5 mmol scale reaction which produced 1.94 g L^9. In both cases L^9 was isolated as a cream solid in ~94 % yield.

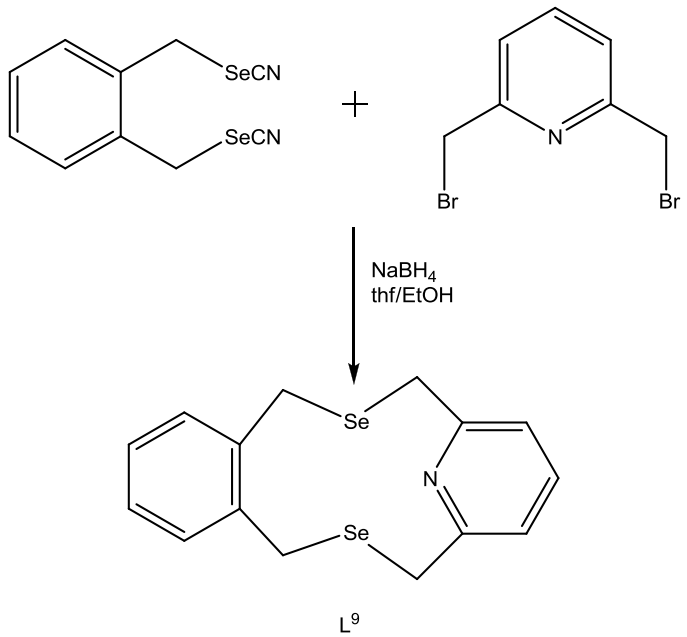

L^9

Figure 4.23: Production scheme for L^9 by $NaBH_4$ reduction.

The concurrent addition of the reactants is an important factor of high dilution reactions, as it hopefully ensures that only one equivalent of each precursor is close enough to react, reducing the possibility of polymerisation. It was thought that combining the two precursor solutions into one dropping funnel might be advantageous, as ensuring the same addition rate from two separate dropping funnels by eye is quite difficult. This combined solution could be added to the $NaBH_4$ solution at a constant, slow rate, and reaction should only occur in the reducing environment of the $NaBH_4$ solution. An attempt was made to produce L^9 by this technique. The solution was worked up in the same way as before. Analysis of the oily mixture obtained after the toluene dissolution and filtration showed no evidence of macrocyclic formation although ^1H NMR spectroscopy also showed no clear evidence of either starting precursor. There was evidence of protonated N, but this species could not be clearly identified. This would seem to indicate that there was some reaction between the precursors in the dropping funnel, and that it was in fact important to keep them separate during the addition process.

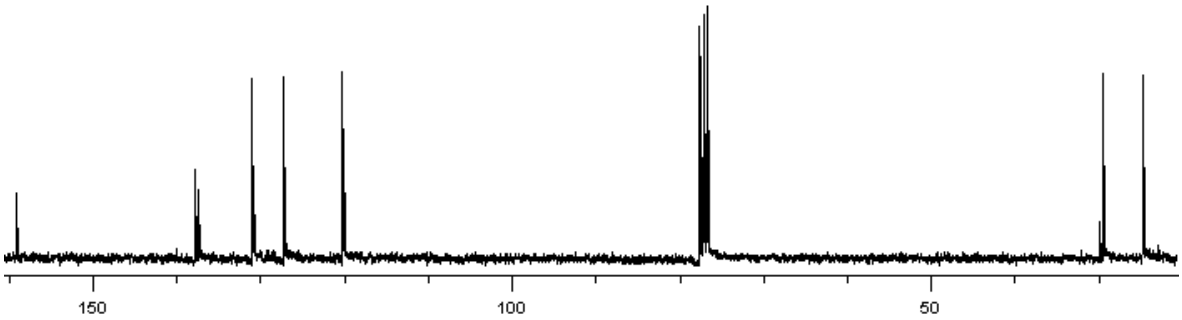

Figure 4.24: $^{13}C\{^{1}H\}$ NMR spectrum of L^9 recorded in $CDCl_3$.

The aromatic protons on the xylyl ring and the pyridyl ring overlap in the ^{1}H NMR spectrum of L^9, but the triplet for the pyridyl proton *para* to the N can be clearly seen at 7.49 ppm. There are two singlets for the two C*H*$_2$ environments at 4.02 and 4.19 ppm, which can be assigned as being attached to the xylyl and pyridyl rings respectively by the clear Se-H coupling observable on the peak at 4.02 (8 Hz). Figure 4.24 shows the $^{13}C\{^{1}H\}$ NMR spectrum, which clearly shows the two aliphatic environments at 24.5 and 29.3 ppm. There are six aromatic peaks, three from the xylyl ring and three from the pyridyl ring, although the C1/2 resonance from the xylyl ring occurs at a very similar shift to the pyridyl C3 resonance (137.7 and 137.2 respectively). The $^{77}Se\{^{1}H\}$ NMR spectrum shows a single peak at 298 ppm. GC-EI MS showed its highest peak cluster around *m/z* = 369 ($C_{15}H_{15}N^{80}Se_2$ = 369). A crystal suitable for X-ray analysis was grown by cooling a CH_2Cl_2/hexane solution of L^9 at -18°C for several days.

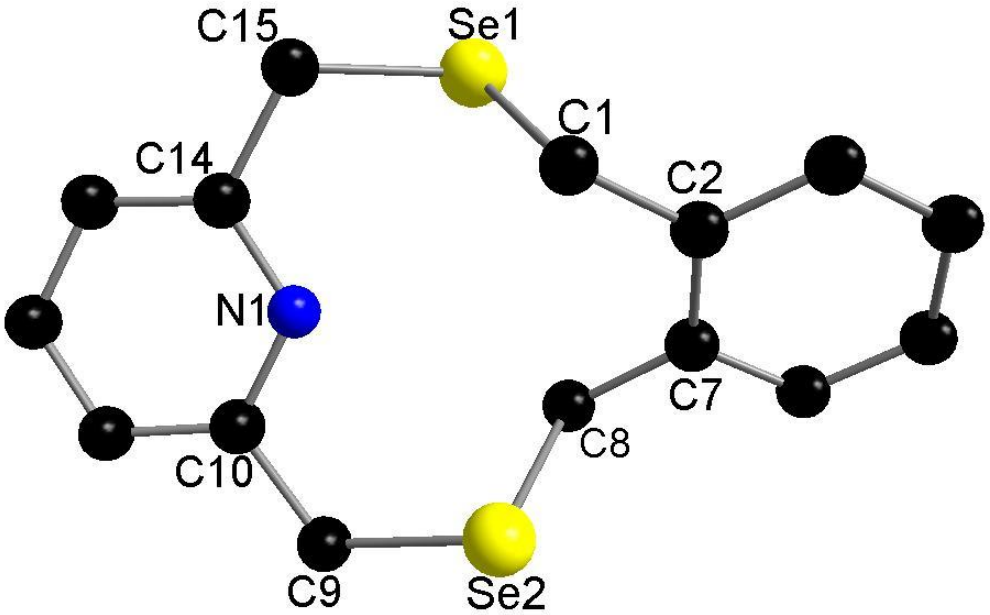

Figure 4.25: Crystal structure of L^9. H atoms omitted for clarity.

Table 4.2: Selected bond lengths and angles for L^9.

Bond	**Length / Å**	**Bond**	**Length / Å**	**Bond**	**Angle / °**
Se1–C1	1.988 (7)	Se2–C9	1.957 (7)	C1–Se1–C15	96.3 (3)
Se1–C15	1.967 (7)	N1–C10	1.340 (9)	C8–Se2–C9	98.0 (3)
Se2–C8	1.992 (7)	N1–C14	1.335 (9)	C10–N1–C14	119.4 (6)

Again, as with L^1 (Chapter 3, Figure 3.14) and L^6 (Figure 4.19) the Se atoms adopt an *anti* configuration, above and below the plane of the xylyl ring. The planes of the two aromatic rings are twisted with respect to each other by 31.4 (3)°. The rigidity of the pyridyl ring prevents any possible ring strain from showing at the N atom, and the angles of N1-C10-C9 and N1-C14-C15 are only slightly more acute than their ideal angle (117.2 (6) and 116.8 (6)° respectively). The bond angles at Se are very similar to those observed in L^6 (Table 4.1). Thus, there appears to be relatively little ring strain in L^9, despite the three bond linkage between Se atoms and N.

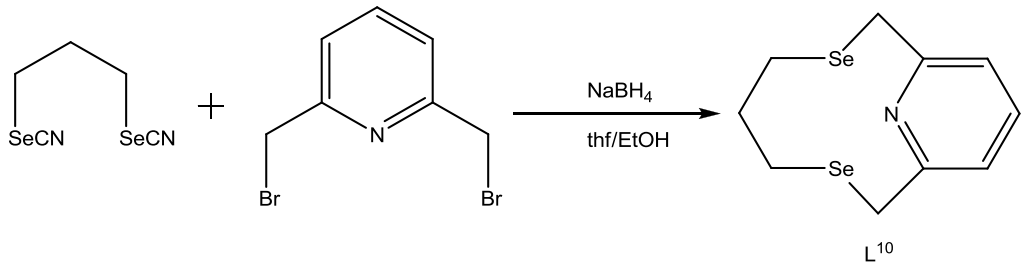

L^{10}

Figure 4.26: Production scheme for L^{10} by $NaBH_4$ reduction.

An attempt was made to introduce a more flexible backbone into a Se_2N macrocycle. This would produce a smaller ring, similar to L^4. However, the analogous reaction in Chapter 3 produced a mixture of [1+1] and [2+2] macrocycles (Figure 3.17). Here, the pyridyl precursor provides some preorganisation to the reaction, which might inhibit production of the [2+2] macrocycle. The same method was used as for L^9 on the larger scale. A cream solid was obtained after work up.

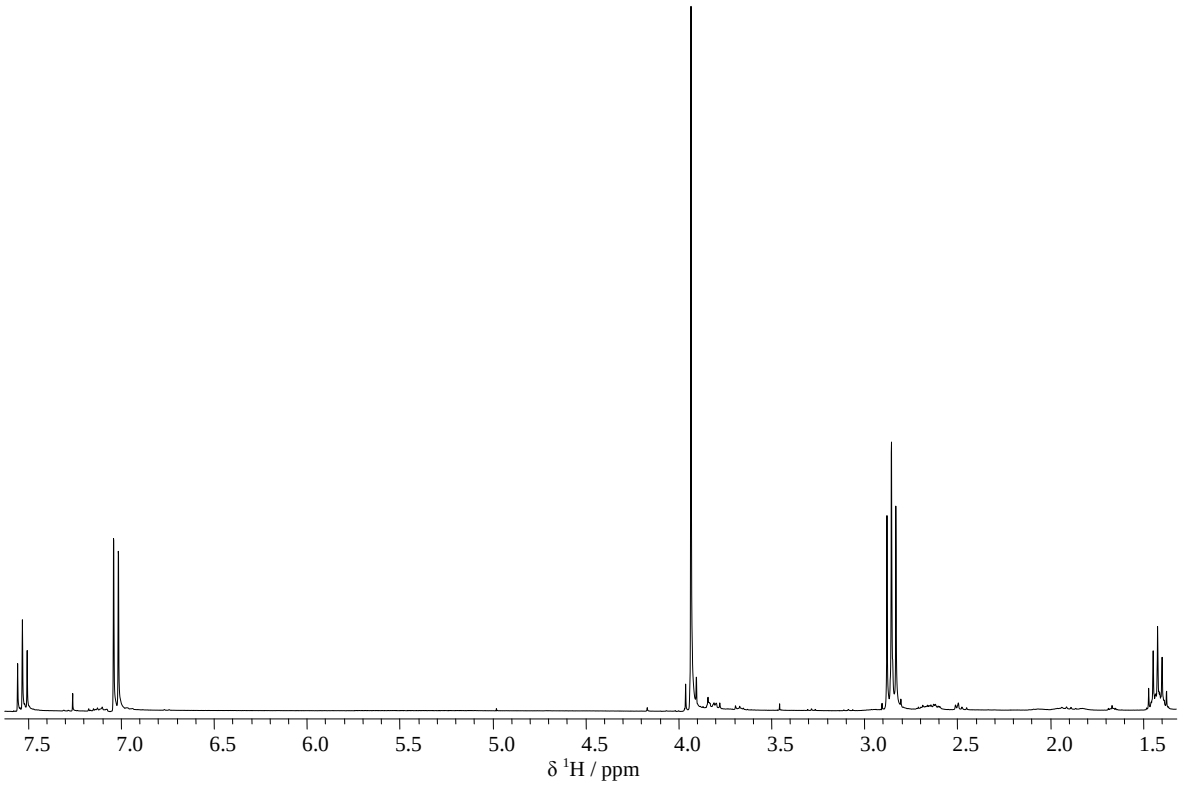

Figure 4.27: ^{1}H NMR spectrum of L^{10} recorded in $CDCl_3$.

The $^{77}Se\{^{1}H\}$ NMR spectrum of this solid showed a single peak, at 298.5 ppm, indicating production of a single macrocyclic species. The shift itself, however, was virtually identical to that of L^9, which was not expected as ^{77}Se NMR shifts are generally very sensitive to the backbones present, and the change from a xylyl to C_3 backbone was expected to cause a significant difference in frequency. A ^{1}H NMR spectrum run on the same sample showed that this was indeed L^{10} (Figure 4.27). The triplet and quintuplet from the C_3 linkage can be clearly seen, and the aromatic region shows a much clearer pattern, with a triplet from the proton *para* to N, and a doublet from the *meta* protons. The $^{13}C\{^{1}H\}$ NMR spectrum was as expected, showing three aromatic C resonances and three aliphatic resonances, two with clear Se-C coupling (24.8 ppm, 33 Hz; 29.4 ppm, 57 Hz). GC-EI MS confirmed that this was the [1+1] product. The yield was 92 %, and there is no evidence of a [2+2] product or any ring strain in any of the spectra collected, unlike the production of L^4/L^5 (Chapter 3).

Table 4.3: $^{77}Se\{^{1}H\}$ NMR shifts of the tridentate macrocycles produced in this thesis.

Ligand	**δ ^{77}Se /ppm**	**Ligand**	**δ ^{77}Se /ppm**	**Ligand**	**δ ^{77}Se /ppm**
L^1	205	L^4	158.3	L^8	292.5, 208.0
L^6	183.9, 181.4	L^7	131.0		
L^9	298.0	L^{10}	298.5		

Table 4.3 shows the $^{77}Se\{^{1}H\}$ NMR shifts of the tridentate macrocycles produced in this thesis, grouped by Se-Se backbone, (xylyl, propyl, benzyl) then by the third donor atom (O, Se, N). It can be seen that changing from a xylyl linkage to a propyl linkage causes a shift to lower frequency, as does having a homoleptic Se_3 donor set.

4.5 – Conclusions

Two novel macrocycles L^6 and L^8 (Figure 4.28) containing three selenium atoms have been synthesised in high yielding $NaBH_4$ reduction reactions. The reaction method suffers no loss in yield upon scaling up from milligram to multi-gram quantities, and could theoretically be scaled up further. The importance of strict temperature control over the production of the polymeric diselenide *o*-$(SeC_6H_4Se)_n$ has been confirmed. The known macrocycle L^7 ([12]aneSe_3) has been shown to be impractical to produce by means of Na/NH_3 reduction, but has been produced on multi-gram scale in high yield by a scaled up $NaBH_4$ reduction.

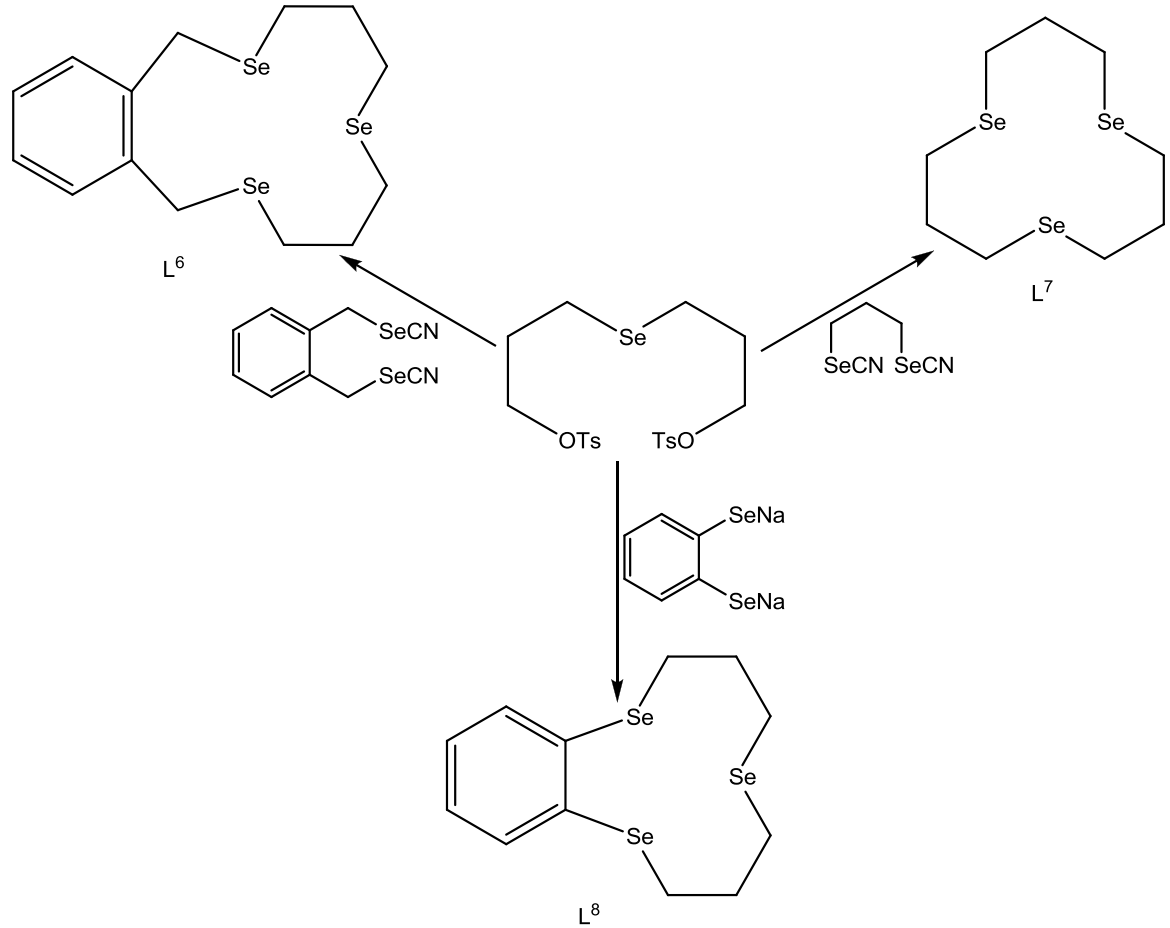

Figure 4.28: Summary of Se_3 macrocycle production in this chapter.

The versatility in addition of different backbones for this reduction reaction has been proved by the production of Se_2O macrocycles (see Chapter 3) and by the production of two novel Se_2N

macrocycles (Figure 4.29) in high yields. The importance of keeping the solutions of precursors separate has been demonstrated. Crystal structures have been obtained of two of the novel macrocycles, L^6 and L^9.

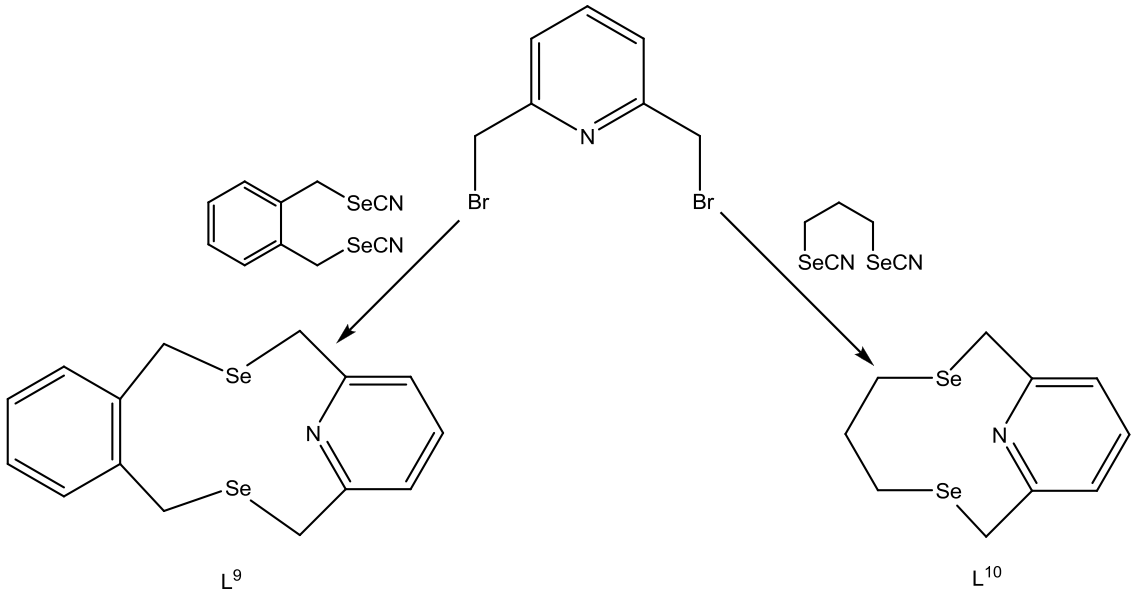

Figure 4.29: Summary of Se_2N macrocycle production in this chapter.

4.6 – Experimental

$NCSe(CH_2)_3OH$: KSeCN (31.315 g, 0.217 mol) and 3-bromo-1-propanol (19.65 cm^3, 0.217 mol) were refluxed in acetone (150 cm^3) for two days. The initial dark purple colour faded to give white solid and yellowish solution. The white solid was filtered off, and the solvent removed from the yellow filtrate by atmospheric distillation. The yellow oil was dried *in vacuo*. Yield: 27.85 g (78%). $^{77}Se\{^1H\}$ NMR (external D_2O): δ 211.1 ppm.

$HO(CH_2)_3Se(CH_2)_3OH$: $HO(CH_2)_3SeCN$ (27.85 g, 0.17 mol) was dissolved in dry THF (150 cm^3) and ammonia (400 cm^3) condensed into the flask. Na (7.8 g, 0.34 mol) was added slowly until a clear solution was produced. 3-bromo-1-propanol (15.4 cm^3, 0.17 mol) was added dropwise. The ammonia was allowed to boil off. The mixture was hydrolysed (250 cm^3) and extracted with CH_2Cl_2 (3 x 200cm^3). The yellow organics were collected, dried over $MgSO_4$ and the solvent removed *in vacuo*. Yield: 22.37g (66 %). $^{77}Se\{^1H\}$ NMR (external D_2O): δ 152.1 ppm.

$TsO(CH_2)_3Se(CH_2)_3OTs$: *p*-Toluenesulfonyl chloride (13.22 g, 0.069 mol) in CH_2Cl_2 (200 cm^3) was added to a solution of $HO(CH_2)_3Se(CH_2)_3OH$ (6.21 g, 0.0315 mol) in CH_2Cl_2 (200 cm^3) and pyridine (17 cm^3). The yellow solution was stirred overnight. The solution was washed with 10% HCl (2 x 100 cm^3), $NaHCO_3$ (2 x 100 cm^3), water (250 cm^3) and brine (200 cm^3) and dried over $MgSO_4$. The solvent was removed *in vacuo*. Yield: 7.631 g (48 %). $^{77}Se\{^1H\}$ NMR (external D_2O): δ 150 ppm

L^6: $Se(CH_2CH_2CH_2OTs)_2$ (2.42 g, 4.78 mmol) and *o*-$C_6H_4(CH_2SeCN)_2$ (1.5 g, 4.78 mmol) were each dissolved separately in a mixture of dry thf (160 cm^3) and dry ethanol (40 cm^3). They were added simultaneously dropwise into a flask containing $NaBH_4$ (1.5 g, excess) in a solution of dry thf/ethanol (450 cm^3/50 cm^3) over a period of *ca*. 4 h. The reaction mixture was then left to stir under N_2 for 72 h at room temperature. The resulting cloudy solution was filtered to produce a clear pale yellow solution which was reduced under vacuum to give a cloudy oil. Toluene (250 cm^3) was then added to the oil and the resulting solution filtered to remove any undissolved solids before being concentrated under reduced pressure to produce L^6 as a cream solid. Yield: 1.88 g, 93%. Required for $C_{14}H_{20}Se_3$ (425.19): C, 39.55; H, 4.74; found: C, 39.33; H, 4.84%. GC-EI MS (CH_2Cl_2): *m/z* = 426 $[C_{14}H_{20}{}^{80}Se_3]^+$. ^1H NMR ($CDCl_3$): δ = 2.17 (quintet, 4H), 3.71 (t, 8H), 4.12 (s, 4H xylyl C*H*$_2$), 7.21-7.37 (multiplet, 4H). $^{13}C\{^1H\}$ NMR ($CDCl_3$): δ =20.6, 20.9, 23.3, 25.7, 30.3, 31.8, 44.4, 127.7, 130.6, 136.2. $^{77}Se\{^1H\}$ NMR (CH_2Cl_2/external D_2O): δ = 181, 183.

L^7: As above, but using $Se(CH_2CH_2CH_2OTs)_2$ (2.42 g, 4.78 mmol) and $NCSe(CH_2)_3SeCN$ (1.204 g, 4.78 mmol). White solid. Yield: 1.34 g, 77%. GC-EI MS (CH_2Cl_2): *m/z* = 364 $[C_9H_{18}{}^{80}Se_3]^+$. ^1H

NMR ($CDCl_3$): δ = 2.01 (q, 2H, $CH_2CH_2CH_2$,), 2.67 (t, 4H $SeCH_2CH_2$). $^{13}C\{^1H\}$ NMR ($CDCl_3$): δ = 21.4 ($SeCH_2$, $^1J_{C\text{-}Se}$ = 62 Hz), 28.4 ($SeCH_2CH_2$), 120.6. $^{77}Se\{^1H\}$ NMR (CH_2Cl_2/external D_2O): δ = 130.

Poly-*o*-phenylenediselenide *o*-$(SeC_6H_4Se)_n$:[22] A round bottomed flask containing freshly powdered selenium (7.9 g, 0.1 mol) and dmf (100 cm^3) was heated to 110°C under N_2. Sodium metal (2.3 g, 0.1 mol) was added slowly in small pieces. Vigourous reaction occurred, leaving a dark reaction mixture. After 1 hour, the temperature was reduced to ~60°C. *o*-Dibromobenzene (11.8 g, 0.05 mol) in dmf (100 cm^3) was added, and the temperature increased to 140°C for 40 hours. On cooling, methanol (200 cm^3) was added, and the mixture poured into brine (500 cm^3). The solids were filtered off and washed with water (200 cm^3), sodium sulphide solution (200 cm^3), water (200 cm^3), and thf (200 cm^3). The orange solid produced was dried *in vacuo*. Yield: 3.26 g, 28 %.

L^8: *o*-$(SeC_6H_4Se)_n$ (1.0 g, 4.0 mmol) was suspended in dry thf (50 cm^3). $NaBH_4$ (0.65 g, excess) in dry EtOH (20 cm^3) was added slowly. The yellow solution formed was transferred by cannula into a dropping funnel containing dry thf (110 cm^3) and dry EtOH (20 cm^3). $Se(CH_2CH_2CH_2OTs)_2$ (1.5 g, 4.78 mmol) was separately dissolved in dry thf (160 cm^3) and dry EtOH (40 cm^3). The two solutions were added simultaneously dropwise (over ca. 4 h) to a suspension of $NaBH_4$ (0.5 g) in dry thf (500 cm^3) and dry ethanol (60 cm^3) under a dinitrogen atmosphere. The reaction mixture was stirred at room temperature (60 h) and then filtered. The solvent was removed in vacuo before the residue was dissolved in toluene, filtered to remove inorganic salts and the solvent removed in vacuo. Column chromatography (eluent: ethyl acetate/hexane 1:19) on the crude oily mixture resulted in a yellow oily substance (Rf = 0.87). Kugelröhr distillation at 120°C/0.01 mm Hg led to distillation of a light yellow oil which solidified on cooling, leaving L^8 as a more viscous yellow oil. EI MS: found m/z = 398 $[L^8]^+$, 356 $[L^8 - C_3H_6]^+$, 236 $[o\text{-}C_6H_4Se_2]^+$, 202 $[Se(CH_2)_3Se]^+$. ^1H NMR ($CDCl_3$, 298 K): δ = 7.67 (m, o-C_6H_4, 2H), 7.19 (m, o-C_6H_4, 2H), 2.99 (m, $SeCH_2$, 4H), 2.62 (m, $SeCH_2$, 4H), 2.07 (m, $CH_2CH_2CH_2$, 4H). $^{13}C\{^1H\}$ NMR ($CDCl_3$, 298 K): δ = 137.1 (C_{ipso}, o-C_6H_4), 135.4, 128.3 (CH, o-C_6H_4), 32.9, 32.5 (both $SeCH_2$), 22.8 ($CH_2CH_2CH_2$). $^{77}Se\{^1H\}$ NMR (CH_2Cl_2/$CDCl_3$, 298 K): δ = 292.5 (2 Se), 208.0 (Se).

L^9: 2,6-Bis(bromomethyl)pyridine (1.5 g, 5.66 mmol) and *o*-$C_6H_4(CH_2SeCN)_2$ (1.77 g, 5.66 mmol) were each dissolved separately in a mixture of dry thf (160 cm^3) and dry ethanol (40 cm^3). They were added simultaneously dropwise into a flask containing $NaBH_4$ (1.5 g, excess) in a solution of dry thf/ethanol (450 cm^3/50 cm^3) over a period of *ca*. 4 h. The reaction mixture was then left to stir under N_2 for 72 h at room temperature. The resulting cloudy solution was filtered to produce a clear pale yellow solution which was reduced under vacuum to give a cloudy oil. Toluene (250 cm^3) was

then added to the oil and the resulting solution filtered to remove any undissolved solids before being concentrated under reduced pressure to produce L^9 as a cream solid. Yield: 1.94 g, 93%. GC-EI MS (CH_2Cl_2): *m/z* = 369 $[C_{15}H_{15}N^{80}Se_2]^+$. ^{1}H NMR ($CDCl_3$): δ = 4.02 (s, xylyl C*H*$_2$, $^2J_{H\text{-}Se}$ = 8 Hz), 4.19 (s, pyridyl C*H*$_2$), 7.04-7.23 (overlapping m, xylyl and pyridyl protons), 7.49 (t, pyridyl H). $^{13}C\{^1H\}$ NMR ($CDCl_3$): δ = 24.5 (xylyl *C*H$_2$), 29.3 (pyridyl *C*H$_2$), 120.0 (pyridyl C2, 4), 127.0 (xylyl C3, 6), 130.8 (xylyl C4, 5), 137.2 (pyridyl C3), 137.7 (xylyl C1, 2), 159.0 (pyridyl C1, 5). $^{77}Se\{^1H\}$ NMR (CH_2Cl_2/external D_2O): δ = 298.

L^{10}: As above, but using 2,6-bis(bromomethyl)pyridine (1.5 g, 5.66 mmol) and $NCSe(CH_2)_3SeCN$ (1.43 g, 5.66 mmol). Yield: 1.59 g, 91.5%. GC-EI MS (CH_2Cl_2): *m/z* = 307 $[C_{10}H_{13}N^{80}Se_2]^+$. ^{1}H NMR ($CDCl_3$): δ = 1.41 (q, 2H, $CH_2CH_2CH_2$,), 2.85 (t, 4H $SeCH_2CH_2$,) 3.93 (s, 4H, pyridyl C*H*$_2$), 7.02 (d, 2H, pyridyl protons), 7.53 (t, 1H, pyridyl proton). $^{13}C\{^1H\}$ NMR ($CDCl_3$): δ = 24.8 (pyridyl *C*H$_2$, $^1J_{C\text{-}Se}$ = 33 Hz), 29.4 (Se*C*H$_2$, $^1J_{C\text{-}Se}$ = 57 Hz), 33.2 ($SeCH_2CH_2$)120.6 (pyridyl C2, 4), 138.1 (pyridyl C3), 159.0 (pyridyl C1, 5). $^{77}Se\{^1H\}$ NMR (CH_2Cl_2/external D_2O): δ = 298.

4.7 – X-Ray Crystallography

Details of the crystallographic data collection and refinement parameters are given in Table 4.4. Yellow single crystals of L^6 and L^9 were obtained by recrystallisation from CH_2Cl_2. Structure solution and refinement were routine.[24,25] Selected bond lengths and angles for L^6 are presented in Table 4.1 and for L^9 are presented in Table 4.2.

Table 4.4: Crystallographic data collection and refinement parameters. $R1 = \Sigma||F_o| - |F_c||/\Sigma|F_o|$; $wR_2 = [\Sigma w(F_o^2 - F_c^2)^2/\Sigma wF_o^4]^{1/2}$.

Complex	**L^6**	**L^9**
Formula	$C_{14}H_{20}Se_3$	$C_{15}H_{15}NSe_2$
M	425.18	367.20
Crystal System	Monoclinic	Triclinic
Space Group	$P2_1/n$	$P\bar{1}$
a/Å	5.2820 (15)	8.368 (2)
b/Å	15.978 (4)	8.925 (2)
c/Å	17.597 (5)	9.562 (3)
α/°	90	100.295 (15)
β/°	90.13 (2)	90.724 (10)
γ/°	90	105.652 (10)
U/Å^3	1485.1 (7)	675.2 (3)
Z	4	2
μ(Mo-Kα)/ mm^{-1}	7.408	5.457
R_{int}	0.065	0.044
Total no. reflns.	14618	11910
Unique reflections	3377	3074
No. of parameters	154	163
$R1$ [$I_o > 2\sigma(I_o)$]	0.060	0.056
$R1$ [all data]	0.099	0.078
wR_2 [$I_o > 2\sigma(I_o)$]	0.099	0.151
wR_2 [all data]	0.114	0.163

4.8 – References

1. Levason, W.; Manning, J. M.; Reid, G.; Tuggey, M.; Webster, M. *Dalton Trans.* **2009**, 4569 – 4577.

2. Mitchell, R. H. *Can. J. Chem.* **1980**, *58*, 1398 – 1406.

3. Pinto, B. M.; Johnston, B. D.; Batchelor, R. J.; Einstein, F. W. B.; Gay, I. D. *Can. J. Chem.* **1988**, *68*, 2956 – 2958.

4. Batchelor, R. J.; Einstein, F. W. B.; Gay, I. D.; Gu, J-H.; Johnston, B. D.; Pinto, B. M. *J. Am. Chem. Soc.* **1989**, *111*, 6582 – 6591.

5. Cordova-Reyes, I.; Hu, H.; Gu, J.-H.; VandenHoven, E.; Mohammed, A.; Holdcroft, S.; Pinto, B. M. *Can. J. Chem.* **1996**, *74*, 533 – 543.

6. Booth, D. G.; Levason, W.; Quirk, J. J.; Reid, G.; Smith, S. M. *J. Chem. Soc., Dalton Trans.* **1997**, 3493 – 3500.

7. Levason, W.; Orchard, S. D.; Reid, G. *Coord. Chem. Rev.* **2002**, *225*, 159 – 199.

8. Hojjatie, M.; Muralidharan, S.; Freiser, H. *Tetrahedron*, **1989**, *45*, 1611 – 1622.

9. Batchelor, R. J.; Einstein, F. W. B.; Gay, I. D.; Gu, J.-H.; Mehta, S.; Pinto, B. M.; Zhou, X.-M. *Inorg. Chem.* **2000**, *39*, 2558 – 2571.

10. Fujihara, H.; Yabe, M.; Ikemori, M.; Furakawa, N. *J. Chem. Soc., Perkin Trans.* **1993**, 2145 – 2146.

11. Fujihara, H.; Yabe, M.; Furakawa, N. *J. Chem. Soc., Perkin Trans.* **1996**, 1783 – 1785.

12. Cordoya-Reyes, I.; VandenHoven, E.; Mohammed, A.; Pinto, B. M. *Can. J. Chem.* **1995**, *73*, 113 – 116.

13. Rawle, S. C.; Admans, G. A.; Cooper, S. R. *J. Chem. Soc., Dalton Trans.* **1988**, 93 – 96.

14. Adams, R. D.; McBride, K. T.; Rogers, R. D. *Organometallics* **1997**, *16*, 3895 – 3901.

15. Fujihara, H.; Ninoi, T.; Akaishi, R.; Erata, T.; Furuwaka, N. *Tetrahedron Lett.* **1991**, *32*, 4537 – 4540.

16. Takaguhi, Y.; Horn, E.; Furukawa, N. *Organometallics* **1996**, *15*, 5112 – 5115.

17. Panda, A.; Menon, S. C.; Singh, H. B.; Butcher, R. J. *J. Organomet. Chem.* **2001**, *623*, 87 – 94.

18. Menon, S. C.; Singh, H. B.; Patel, R. P.; Kulshreshtha, S. K. *J. Chem. Soc., Dalton Trans.* **1996**, 1203 – 1207.

19. Bhula, R.; Arnold, A. P.; Gainsford, G. J.; Jackson, W. G. *Chem. Commun.* **1996**, 143 – 144.

20. Levason, W.; Nirwan, M.; Ratnani, R.; Reid, G.; Tsoureas, N.; Webster, M. *Dalton Trans.* **2007**, 439 – 448.

21. Gulliver, D. J.; Hope, E. G.; Levason, W.; Murray, S. G.; Potter, D. M.; Marshall, G. L. *J. Chem. Soc. Perkin Trans. II* **1984**, 429 – 434.

22. Sandman, D. J.; Allen, G. W.; Acampora, L. A.; Stark, J. C.; Jansen, S.; Jones, M. T.; Ashwell, G. J.; Foxman, B. M. *Inorg. Chem.* **1987**, *26*, 1664 – 1669.

23. Neidlein, R.; Lucchesini, F. *Helv. Chim. Acta*, **1998**, *78*, 1242 – 1248.

24. Sheldrick, G. M. SHELXS-97, program for crystal structure solution, University of Göttingen, Germany, **1997**.

25. Sheldrick, G. M. SHELXS-97, program for crystal structure refinement, University of Göttingen, Germany, **1997**.

Chapter 5: Platinum Complexes with Selenium-Rich Macrocycles[1]

5.1 – Introduction

As discussed in Chapter 4 there are a number (albeit small compared to sulfur) of homoleptic selenoether macrocycles known. The coordination chemistry of some of these ligands has been studied, mainly with the focus on [16]aneSe_4, and has shown a variety of coordination modes, including examples of bridging behaviour, and both *endo* and *exo* coordination.[2,3]

[8]aneSe_2 can displace norbornadiene (nbd) or *N,N,N',N'*-tetramethyl-1,3-diaminopropane (tmpa) to coordinate in a bidentate manner to Group 6 metal carbonyl complexes, $[M(CO)_4([8]aneSe_2)]$ (M = Cr, Mo, W).[4] Seven-coordinate Mo(II) species can be formed by reaction of $[(MoBr_2\{CO\}_4)_2]$ or $[MoI_2(CO)_3(MeCN)_2]$ in CH_2Cl_2 with either [16]aneSe_4 or sebc (see Chapter 4) to form $[(MoX_2\{CO\}_3)_2([16]aneSe_4)]$ or $[MoX_2(CO)_3(sebc)]$ in high yield. Similar reaction with $[WI_2(CO)_3(MeCN)_2]$ yields $[WI_2(CO)_3L]$ (L = [16]aneSe_4 or sebc).[4] These complexes are moderately air-sensitive, poorly soluble in both chlorocarbons and hydrocarbons, and the selenoether ligands are easily displaced in coordinating solvents. Whilst the tetradentate selenoether macrocycle [16]aneSe_4 bridges two Mo(II) centres, with bidentate coordination to each metal (Figure 5.1), no observation of a similar bridging complex with two W(II) centres was made, even though there are two "free" Se donors available.[4] Conformational calculations, and the low solubility of the complexes suggest that the bidentate sebc may be functioning as a bridging ligand between metal centres in polymeric structures (Figure 5.1).[4]

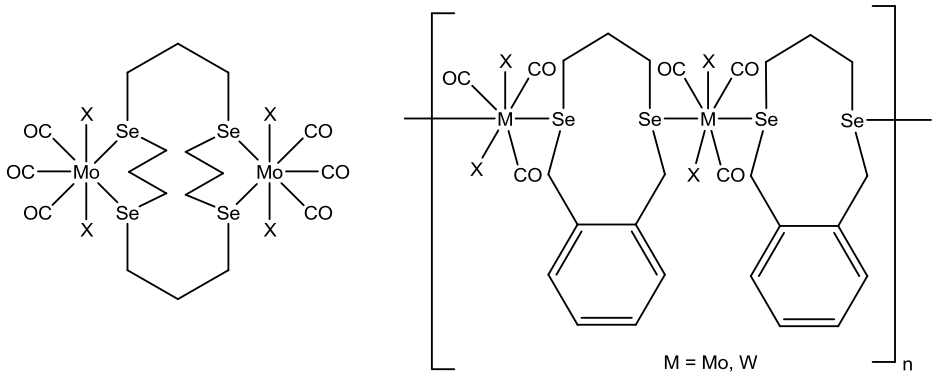

Figure 5.1: Scheme demonstrating the coordination modes observed in $[(MoX_2\{CO\}_3)_2([16]aneSe_4)]$ (left) and $[MX_2(CO)_3(sebc)]$ (right).

The reaction of [16]aneSe_4 with $[CrX_3(thf)_3]$ (X = Cl, Br) and one equivalent of $TlPF_6$ gives the octahedral complexes $[CrX_2([16]aneSe_4)]PF_6$ as blue solids which are slightly soluble in organic solvents but hydrolytically unstable. Similar reactions with two equivalents of [8]aneSe_2 failed.[5]

The neutral *fac*-tricarbonyl species $[MX(CO)_3([8]aneSe_2)]$ (M = Mn, Re; X = Cl, Br, I) are readily formed by reaction of $[MX(CO)_5]$ with $[8]aneSe_2$ in refluxing $CHCl_3$. Similar reaction of 0.5 molar equivalents of $[16]aneSe_4$ with $[MCl(CO)_5]$ affords the dinuclear species $[(MnCl\{CO\}_3)_2([16]aneSe_4)]$ or the mononuclear $[ReCl(CO)_3([16]aneSe_4)]$.[4] A rare example of a cationic complex with a selenoether macrocycle is the Mn(I) species *fac*-$[Mn(CO)_3(\kappa^3$-$[16]aneSe_4)]CF_3SO_3$ which is generated by treatment of $[MnCl(CO)_5]$ with $AgCF_3SO_3$, followed by addition of one equivalent of $[16]aneSe_4$.[4] The reaction of $[Re_2(CO)_9(MeCN)]$ with $Me_6[12]aneSe_3$ yielded the complex $[Re_2(CO)_9(Me_6[12]aneSe_3)]$ in 58% yield. The crystal structure of this complex has κ^1-$Me_6[12]aneSe_3$ in an equatorial coordination site with staggered rotational conformations of the CO ligands on the Ru atoms.[6]

Reaction of $[Ru(dmf)_6]Cl_3$ with 1 molar equivalent of $[16]aneSe_4$ or two molar equivalents of $[8]aneSe_2$ in refluxing EtOH yield *cis*-$[RuCl_2([16]aneSe_4)]$ and *cis*-$[RuCl_2([8]aneSe_2)_2]$ respectively. *cis*-$[RuCl_2([16]aneSe_4)]$ can be converted to the *trans* isomer by refluxing in nitromethane, while *cis*-$[RuCl_2([8]aneSe_2)_2]$ shows no conversion to the *trans* isomer under the same conditions. The dibromo and diiodo complexes $[RuX_2([16]aneSe_4)]$ can be prepared by refluxing $[Ru(dmf)_6](CF_3SO_3)_3$ with $[16]aneSe_4$ and two equivalents of LiBr or NaI respectively in EtOH. $[RuI_2([16]aneSe_4)]$ was too poorly soluble to obtain ^{77}Se NMR data, and allow isomeric characterisation, but *cis*-$[RuBr_2([16]aneSe_4)]$ was characterised, and could be converted to *trans*-$[RuBr_2([16]aneSe_4)]$ in refluxing nitromethane. $[MCl(PPh_3)([16]aneSe_4)]$ have been prepared for M = Ru, Os, and the redox potentials for M(II)-M(III) measured by cyclic voltammetry for all these Ru/Os complexes. With the exception of *cis*-$[RuCl_2([8]aneSe_2)_2]$ (which shows an irreversible oxidation) all the dichloro, dibromo and chlorophosphine complexes exhibit a reversible redox couple.[7]

$[CoX_2([16]aneSe_4)]PF_6$ (X = Cl, Br, I) are stable solids exhibiting tetradentate selenoether coordination. Although they are insoluble in chlorinated solvents, the chloro and bromo species are stable in $MeNO_2$ and MeCN, while the iodo species slowly decomposes in these solvents. They can be produced by reaction of anhydrous $[CoX_2]$ with $[16]aneSe_4$ in $MeNO_2$ solution in air, followed by addition of NH_4PF_6. UV-Vis and $^{77}Se\{^1H\}$ NMR spectroscopic analysis show the chloro and bromo species to have solely *trans* geometry, whilst the iodo species exhibits both *cis* and *trans* species. The analogous reaction with $[8]aneSe_2$ fails to produce any evidence for similar Co(III) species.[8]

$[RhCl_2([8]aneSe_2)_2]BF_4$ has been prepared from $[(Rh\{CO\}_2Cl)_2]$, $[8]aneSe_2$ and HBF_4 in aqueous acetone solution, while $MX_3 \cdot 3H_2O$ (M = Rh, X = Cl; M = Ir, X = Cl or Br) and $[16]aneSe_4$ in refluxing ethanol produces $[MX_2([16]aneSe_4)]^+$. These can be isolated as microcrystalline solids

upon addition of a counter ion such as PF_6^- or BF_4^-. $[RhBr_2([16]aneSe_4)]^+$ can be produced from reaction of $[Rh(H_2O)_6][NO_3]_3$, [16]aneSe$_4$ and 2 equivalents of LiBr. ^{77}Se NMR spectroscopic studies in dmf show that these Rh(III) and Ir(III) species are a mix of *cis* and *trans* isomers in solution, while a crystal structure has been reported of *trans*$[IrBr_2([16]aneSe_4)]BPh_4$.[8]

Reaction of NiX_2 (X = Cl, Br, I) with [16]aneSe$_4$ in anhydrous *n*-butanol generates the paramagnetic complexes $[NiX_2([16]aneSe_4)]$, which are insoluble in chlorocarbons on $MeNO_2$, poorly soluble in MeCN and decompose in solution in dmso. They are also sensitive to moisture.[9]

[8]aneSe$_2$ or sebc can be reacted with MCl_2 (M = Pd, Pt) in MeCN to afford the poorly soluble complexes $[MCl_2(L)]$.[10,11] Adding two equivalents of $TlPF_6$ and an extra equivalent of [8]aneSe$_2$ to the reaction produces $[M([8]aneSe_2)_2](PF_6)_2$.[10] Reaction of MCl_2 (M = Pd, Pt) with one equivalent of [16]aneSe$_4$ and two equivalents of $TlPF_6$ in refluxing MeCN affords the homoleptic, square planar complexes $[M([16]aneSe_4)](PF_6)_2$ (Figure 5.2). Cyclic voltammetry studies on these complexes show an irreversible reduction, but not sign of oxidative activity.[12] However, treatment of $[Pt([16]aneSe_4)](PF_6)_2$ in MeCN with either Cl_2 or Br_2 as a solution in CCl_4 causes oxidative addition to form the Pt(IV) complexes $[PtX_2([16]aneSe_4)](PF_6)_2$. Similar reactions with the Pd(II) complex were unsuccessful in preparing similar Pd(IV) complexes.[13] Pd(II) complexes with [16]aneSe$_4$ can also be prepared with two BF_4^- units to balance the charge, or with one BF_4^- and one non-coordinating Cl^-.[14]

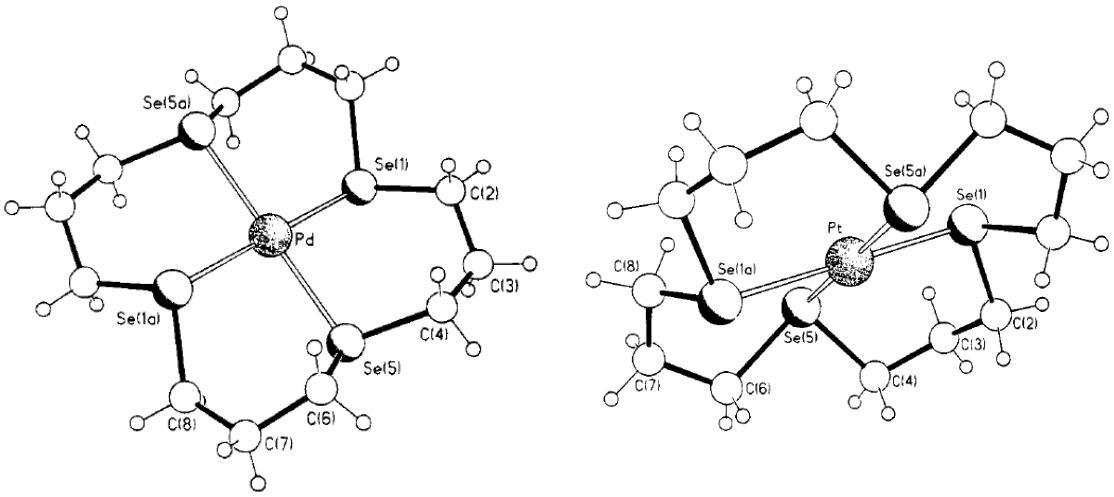

Figure 5.2: Crystal structures of $[Pd([16]aneSe_4)]^{2+}$ (left) and $[Pt([16]aneSe_4)]^{2+}$ (right).[12]

Reaction of $[Cu(MeCN)_4]Y$ (Y = BF_4, PF_6) with two equivalents of [8]aneSe$_2$ or sebc in acetone affords the tetrahedral homoleptic complexes $[Cu(L)_2]Y$ as cream or white solids.[11] The corresponding tetrahedral Ag(I) complexes $[Ag(L)_2]BF_4$ are produced similarly by reaction of $AgBF_4$ with two equivalents of [8]aneSe$_2$ or sebc in acetone. These silver complexes are somewhat

light sensitive and must be kept in the dark.[11] Treatment of [AuCl(tht)] with 0.5 equivalents of [8]aneSe$_2$ or sebc in acetone affords [(AuCl)$_2$L] as white solids. Analytical data suggest linear coordination of an AuCl fragment to each Se donor.[11]

[Cu([16]aneSe$_4${OH}$_2$)](SO$_3$CF$_3$)$_2$ was synthesised by addition of [16]aneSe$_4$(OH)$_2$ in CH$_2$Cl$_2$ to a solution of [Cu(SO$_3$CF$_3$)$_2$] in CH$_3$NO$_2$, producing dark brown crystals. [Cu([8]aneSe$_2${OH})$_2$](SO$_3$CF$_3$)$_2$ and [Cu([16]aneSe$_4${OH})](SO$_3$CF$_3$)$_2$ were produced in a similar way, but [Cu([16]aneSe$_4${OH})](SO$_3$CF$_3$)$_2$ was found to be unstable in CH$_3$NO$_2$ and a mixture of the Cu(II) complex and Cu(I) [Cu([16]aneSe$_4${OH})](SO$_3$CF$_3$) was obtained. Reaction of [Cu(SO$_3$CF$_3$)$_2$] with dibenzo-[14]aneSe$_4$ was unsuccessful.[15] The crystal structure of [Cu([16]aneSe$_4${OH}$_2$)](SO$_3$CF$_3$)$_2$ shows the Cu(II) centre in an approximately octahedral coordination environment, with the four Se donors from the ligand coordinated equatorially and one O donor from an OH group on the ligand and one O donor from a SO$_3$CF$_3$ ion occupying axial positions. The crystal structure of [Cu([8]aneSe$_2${OH})$_2$](SO$_3$CF$_3$)$_2$ is similar, but with both axial positions occupied by O donors from OH groups on the ligands, one O from each ligand. The Cu(I) complex [Cu([16]aneSe$_4${OH})](SO$_3$CF$_3$) has Cu in a tetrahedral environment, with only the four Se donors from the ligand coordinated.[15]

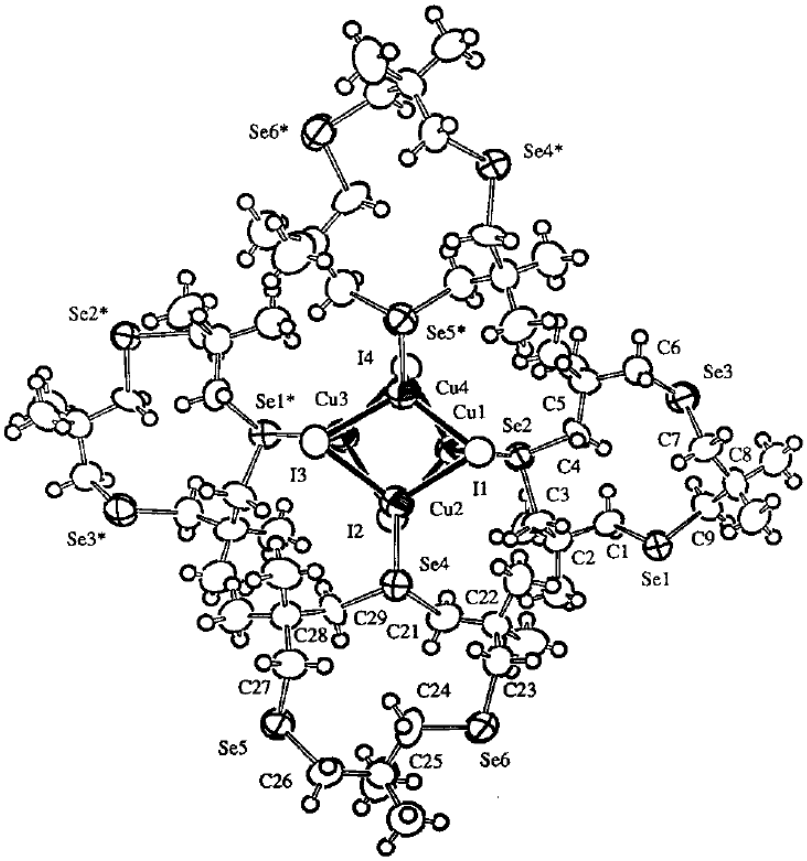

Figure 5.3: Crystal structure of Cu$_4$I$_4$(μ-κ^2-Me$_6$[12]aneSe$_3$)$_2$. Each Cu$_4$I$_4$ cluster is bound to four ligands, two donated from neighbouring clusters.[6]

The structure of $Cu_4I_4(\mu\text{-}\kappa^2\text{-}Me_6[12]aneSe_3)_2$ consists of a three-dimensional network of "cubane-like" Cu_4I_4 clusters linked by four bridging $Me_6[12]aneSe_3$ ligands (Figure 5.3). Each copper atom bonds to one $Me_6[12]aneSe_3$ and three iodide ligands, and the $Me_6[12]aneSe_3$ serves as a bridge to a second Cu_4I_4 cluster. In this way each $Me_6[12]aneSe_3$ ligand utilizes two of its three possible Se donors for coordination. The third selenium atom remains uncoordinated.[6]

Antimony halide complexes of the type $[SbX_3([8]aneSe_2)]$ (X = Cl, Br, I) and $[(SbX_3)_2([16]aneSe_4)]$ (X = Cl, Br, I) have been reported, but little spectroscopic data has been reported owing to poor solubility in non coordinating solvents.[16] A crystal structure of $[(SbBr_3)_2([16]aneSe_4)]$ has been published, showing a two dimensional extended structure in which the selenoether macrocycle coordinates to four separate $SbBr_3$ units, while each $SbBr_3$ unit bridges two macrocycles (Figure 5.4).[17]

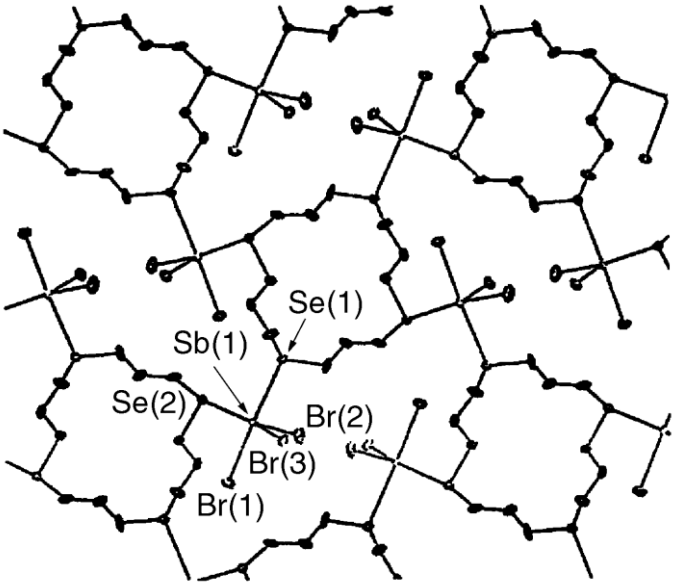

Figure 5.4: View of a portion of the two-dimensional sheet adopted by $[(SbBr_3)_2([16]aneSe_4)]$.[17]

Reaction of BiX_3 (X = Cl, Br) with one molar equivalent of ligand L (L = $[8]aneSe_2$, $[16]aneSe_4$, $[24]aneSe_6$) yields intensely coloured solids of the form $[BiX_3L]$. As with the antimony species above, the bismuth complexes are all poorly soluble in non-coordinating solvents, and the selenoether macrocycles were readily displaced by coordinating solvents. Crystallographic analysis of $[BiCl_3([8]aneSe_2)]$ and $[BiBr_3([16]aneSe_4)]$ shows that these selenoethers form infinite one-dimensional ladder structures, in which Bi_2X_6 "rungs" are linked by the selenoether macrocycles (Figure 5.5). This contrasts with the behaviour of thioether macrocycles, which without exception form discrete molecular species with BiX_3.[18]

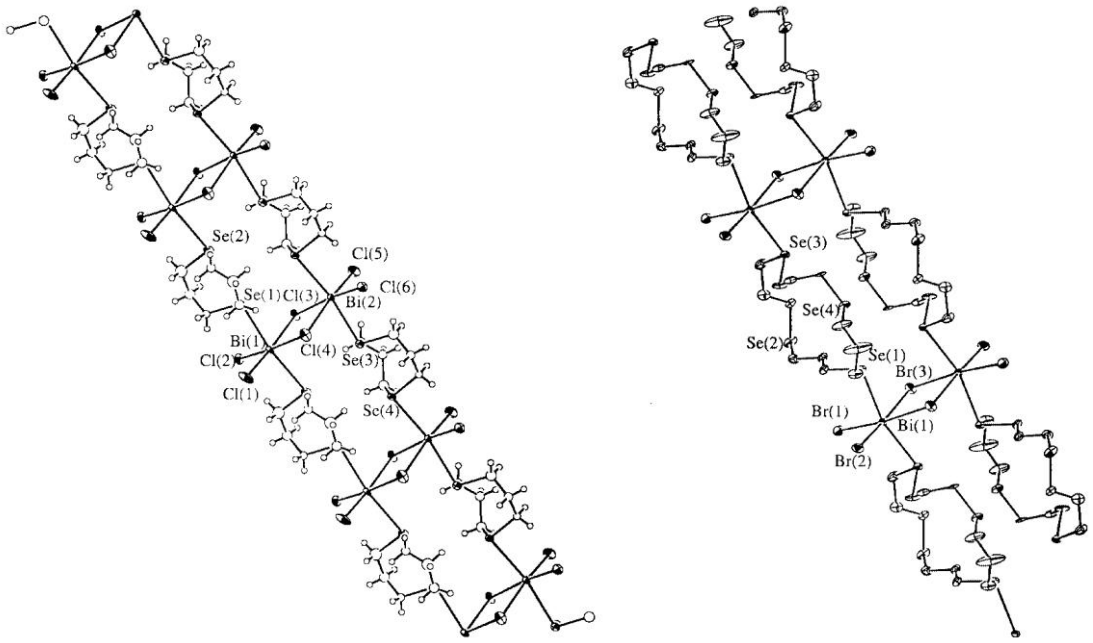

Figure 5.5: Crystal structures of the infinite 1-dimensional ladders adopted by $[BiCl_3([8]aneSe_2)]$ (left) and $[BiBr_3([16]aneSe_4)]$ (right).[18]

A rare example of $[24]aneSe_6$ coordination chemistry is the complex $[(AsCl_3)_4([24]aneSe_6)]$. This is also a rare example of *exo* and *endo* coordination within a single species, as crystallographic analysis (Figure 5.6) showed it to be a discrete unit, rather than a polymeric structure, like $[(AsBr_3)_2([16]aneSe_4)]$. The As_2Cl_6 fragment within the ring is unprecedented for thio- or selenoether macrocycles.[19]

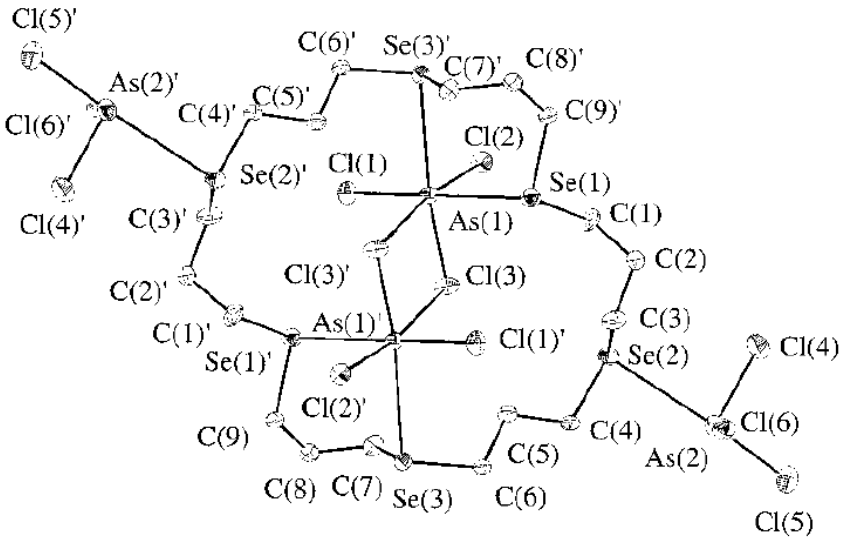

Figure 5.6: X-Ray crystal structure of $[(AsCl_3)_4([24]aneSe_6)]$ showing both *exo* and *endo* coordination.[19]

5.2 – Aims

As discussed in Chapter 2, while there are few platinum complexes with macrocyclic selenoethers there are a number of acyclic selenoether complexes. The small ring thioether macrocycle [9]aneS_3 has been shown to produce stable complexes of Pt(II) with both halide[20,21] and alkyl co-ligands,[22] and even a homoleptic complex $[Pt([9]aneS_3)_2]^{2+}$ which has a quasi-square pyramidal structure, and can be electrochemically oxidised to a highly unusual Pt(III) complex.[23] Pt(II) complexes of the type $[PtR_2([9]aneS_3)]$ (R = Me, Et) can also undergo oxidative addition of MeI or EtI to form the corresponding Pt(IV) complexes.[22] An investigation into the properties of the new Se macrocycles made in Chapter 4 with Pt would allow the coordinating abilities of these macrocycles to be compared to existing data. It was hoped that they would be capable of tridentate coordination such as has been previously observed in $[PtMe_3(\kappa^3\text{-}[16]aneSe_4)]PF_6$, even though this *fac* coordination could not be observed with the tripodal ligand $MeC(CH_2SeMe)_3$ (see Chapter 2).

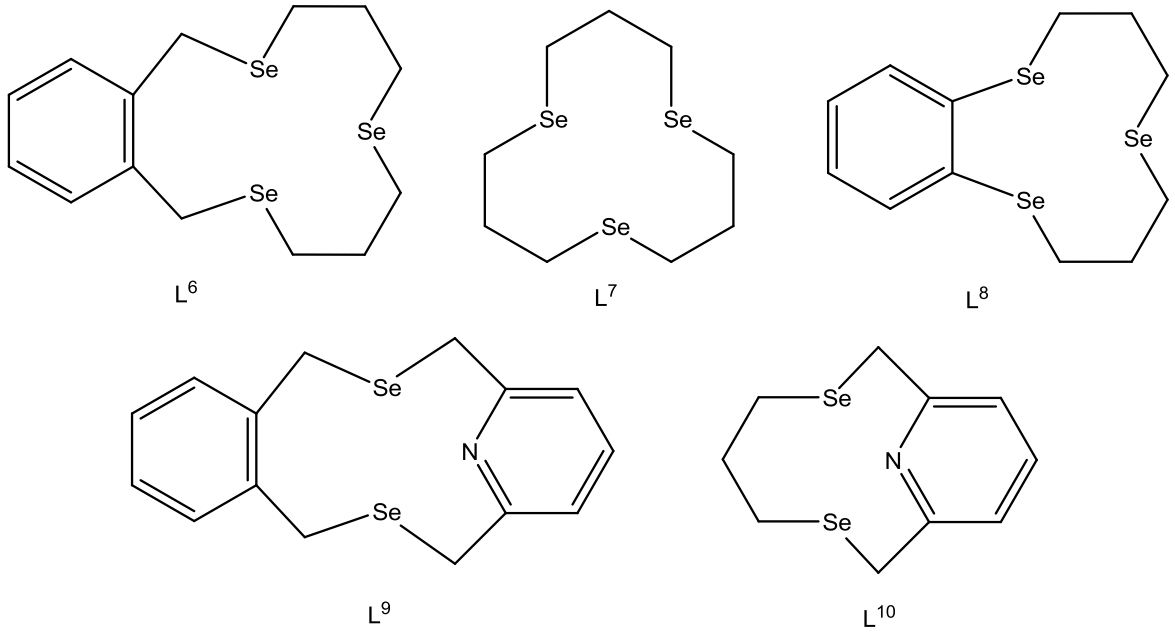

Figure 5.7: Macrocyclic ligands used in this chapter. See Chapter 4 for preparations.

5.3 – Platinum Complexes with Tridentate Selenium-Rich Macrocycles

To start exploring the coordination chemistry of these new macrocycles, $[PtCl_2(MeCN)_2]$ was prepared by refluxing $PtCl_2$ in MeCN to produce a yellow solution, which was filtered to remove any unreacted $PtCl_2$. A solution of L in CH_2Cl_2 was added to the filtrate, where L = L^6–L^8. In each case a yellow precipitate formed rapidly, which was collected by filtration, washed with CH_2Cl_2 to remove unreacted ligand and dried *in vacuo*. The solids were identified as planar *cis*$[PtCl_2L]$ (L^6 – L^8) by microanalysis and IR spectroscopy, but they were all very poorly soluble, which hindered attempts to obtain NMR spectroscopic data. $[PtCl_2([8]aneSe_2)]$ has been produced by the same method, and is also poorly soluble, requiring dmf solutions to obtain NMR spectroscopic data.[10]

$[PtCl_2L^6]$ was just soluble enough in dmf to allow a weak ^{195}Pt NMR spectrum to be obtained, showing a peak at –3644 ppm. $[PtCl_2([8]aneSe_2)]$ has a ^{195}Pt NMR spectrum with δ = –3825 ppm,[10] while dichloro Pt(II) complexes with acyclic selenoethers show ^{195}Pt NMR shifts in the range –3204 to –3479 ppm.[24] L^9 was also reacted with $PtCl_2$ in MeCN in the same way to investigate whether the Se_2N ligands would confer any more solubility on the system, but the resulting precipitate was just as insoluble as the Se_3 ligands. The related complex $[PtCl_2(2\text{-}\{MeSeCH\}C_5H_3N)]$ also has very poor solubility in most solvents, but is soluble and stable in dmso solution.[25] An attempt was made to get NMR data from a dmso solution of $[PtCl_2L^9]$, but the ^1H NMR spectrum obtained only showed peaks corresponding to $[PtCl_2(dmso)_2]$ and uncoordinated L^9.

Chapter 2 detailed the production of dimethylPt(II) complexes with selenoether macrocycles of the form $[PtMe_2L]$ where L = $[8]aneSe_2$ or $[16]aneSe_4$, although these were very poorly soluble, with NMR spectroscopy only possible in dmf solution for $[PtMe_2[8]aneSe_2]$, and $[PtMe_2[16]aneSe_4]$ being even less soluble. $[PtMe_2(SMe_2)_2]$ was generated *in situ* from $[PtCl_2(SMe_2)_2]$ and MeLi in the same manner as in Chapter 2, and one equivalent of L^7 was added as a solution in CH_2Cl_2. The mixture was left stirring for two hours, then the aqueous layer separated and washed with CH_2Cl_2. The organics were reduced *in vacuo* and diethyl ether added to produce a very pale yellow solid precipitate. Analysis of the solid produced showed only $[PtMe_2(SMe_2)_2]$ and uncoordinated L^7. Given lack of solubility in the halide Pt(II) complexes, the ready displacement of L^9 from Pt(II) by coordinating solvents, and the lack of reaction between alkyl Pt(II) and L^7 this line of investigation was not pursued further.

As was discussed in Chapter 2, reaction of $[PtMe_3I]$ with the selenoether macrocycles $[8]aneSe_2$ or $[16]aneSe_4$ in $CHCl_3$ produces 1:1 octahedral complexes of the type $[PtMe_3I(L\text{-}L)]$. In the case of $[16]aneSe_4$, no evidence of a binuclear complex was observed, but with addition of a halide abstracter in the form of $TlPF_6$, tridentate *fac* coordination could be promoted. In the case of the acyclic tridentate selenoether ligand, $MeC(CH_2SeMe)_3$, bidentate coordination was observed, but there was no evidence of tridentate coordination, even upon addition of a halide abstracter.

In order to find out whether the new macrocycles could show tridentate coordination, similar reactions with $[PtMe_3I]$ were undertaken. It was thought that if bidentate coordination was observed, a further reaction in the presence of a halide abstracter would then be undertaken to more strongly promote tridentate coordination. $[PtMe_3I]$ was prepared as described in Chapter 2.

$[PtMe_3I]$ and L^6 were refluxed together in $CHCl_3$ overnight. The yellow solution was reduced *in vacuo* and diethyl ether added. An off-white solid was collected by filtration and dried *in vacuo*.

Thie solid was poorly soluble in chlorocarbons, and slightly more soluble in acetonitrile. Microanalysis confirmed the formulation of this solid as the 1:1 complex $[PtMe_3L^6]I$, as did the ES^+ MS (Figure 5.8). However, neither of these techniques indicate whether the macrocycle is coordinated in a tridentate fashion with associated ionic iodide to balance the charge, or whether the macrocycle is exhibiting bidentate coordination with coordinated iodide completing an octahedral ligand set at the Pt.

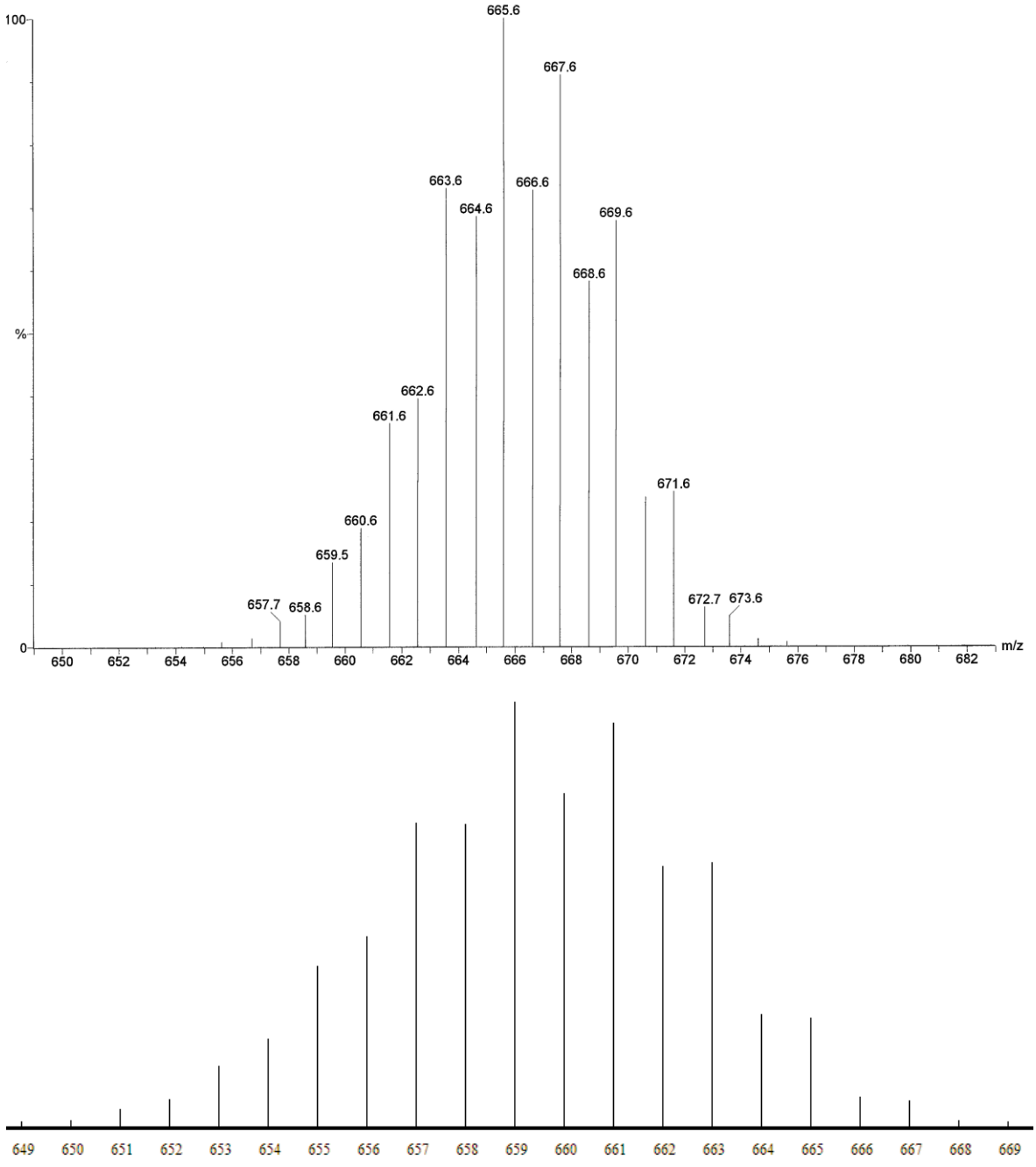

Figure 5.8: Top: ES MS^+ of $[PtMe_3L^6]I$. Bottom: calculated isotope pattern for $[PtMe_3L^6]^+$.

Owing to the limited solubility of the complex, ^1H, $^{77}Se\{^1H\}$ and ^{195}Pt NMR spectra were collected from a solution of $[PtMe_3L^6]I$ in $MeCN/CD_3CN$. A $^{13}C\{^1H\}$ NMR spectrum was not collected, as

the MeCN solvent resonances would have masked key areas of the spectrum, including the region of the Pt-Me resonances. The $^{77}Se\{^{1}H\}$ NMR spectrum recorded at 298 K shows resonances at 154.6 and 88.8 ppm (2 and 1 Se respectively), both of which are shifted to low frequency of the "free" ligand (183 and 181 ppm). This shift in NMR frequency would suggest that all three Se donors are coordinated to Pt, however in $[PtMe_3I([16]aneSe_4)]$ a shift in the frequency of the uncoordinated Se donors was observed (see Chapter 2). Pt-Se coupling could not be clearly identified on either of these resonances due to dynamic processes. Cooling the sample to 233 K led to a slight difference in the shift of the resonances (151.6, 77.9 ppm) and allowed observation of $^{1}J_{PtSe}$ coupling of 328 Hz on the resonance at 151.6 ppm. No clear Pt-Se coupling could be observed on the resonance at 77.9 ppm. The ^{195}Pt spectrum showed a single resonance both at 298 K (–3768 ppm) and at 233 K (–3791 ppm). The $^{77}Se\{^{1}H\}$ and ^{195}Pt NMR spectra indicate that $[PtMe_3L^6]I$ has a single geometric configuration in solution.

The ^{1}H NMR spectrum showed two peaks with PtH coupling, from the three methyl groups on Pt. The peak at 0.82 ppm has $^{2}J_{PtH}$ coupling of 65 Hz and integration of the peaks showed this to be equivalent to 6H. This is from the two Me groups *trans* to the two Se donors closest to the xylyl backbone in L^6. The second peak, at 0.23 ppm is from the third Me group, and has two possibilities. In two possible complexes, this may be *trans* to the third Se donor of L^6, or *trans* to an iodide donor. Previous work on similar Pt(IV) complexes with acyclic bidentate selenoether ligands by Abel et al., and the work detailed in Chapter 2, show that $^{2}J_{PtH}$ (Me *trans* I) coupling is generally $\geq$ 70 Hz, while $^{2}J_{PtH}$ (Me *trans* Se) coupling is usually lower.[26] The $^{2}J_{PtH}$ coupling (65 Hz) shows it to be much more likely that this Me group is *trans* Se rather than I. The other resonances in the ^{1}H NMR spectrum from L^6 all show complex coupling patterns, which is also consistent with the macrocycle being held rigidly *fac* to Pt, with one proton from each CH_2 now held in closer proximity to Pt than the other, causing an inequivalency in environment.

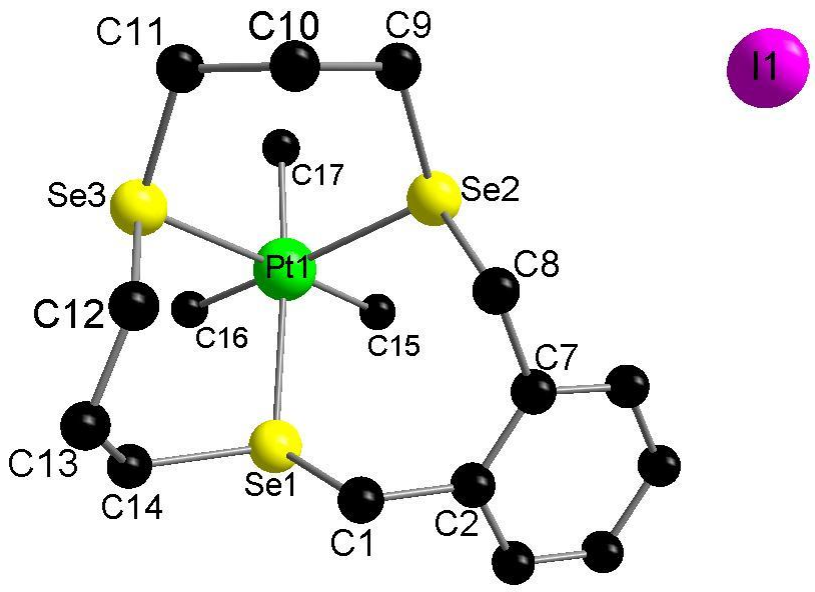

Figure 5.9: Crystal structure of $[PtMe_3L^6]I{\cdot}0.13CH_2Cl_2$. H atoms omitted for clarity.

Table 5.1: Selected bond lengths and angles for $[PtMe_3L^6]I{\cdot}0.13CH_2Cl_2$.

Bond	**Length / Å**	**Bond**	**Angle / °**	**Bond**	**Angle / °**
Pt1–C15	2.093 (7)	C15–Pt1–C16	87.3 (3)	C16–Pt1–Se3	89.0 (2)
Pt1–C16	2.079 (6)	C15–Pt1–C17	88.3 (3)	C17–Pt1–Se1	170.1 (2)
Pt1–C17	2.079 (7)	C15–Pt1–Se1	88.4 (2)	C17–Pt1–Se2	87.0 (2)
Pt1–Se1	2.5430 (7)	C15–Pt1–Se2	85.7 (2)	C17–Pt1–Se3	90.63 (19)
Pt1–Se2	2.5218 (7)	C15–Pt1–Se3	176.2 (2)	Se1–Pt1–Se2	101.99 (2)
Pt1–Se3	2.5236 (7)	C16–Pt1–C17	85.5 (3)	Se1–Pt1–Se3	92.13 (2)
		C16–Pt1–Se1	85.07 (19)	Se2–Pt1–Se3	97.79 (2)
		C16–Pt1–Se2	169.9 (2)		

A crystal suitable for X-ray analysis was grown from a saturated solution of $[PtMe_3L^6]I$ in CH_2Cl_2, and confirms the ionic nature of the complex, and the tridentate coordination of L^6. The Se-Pt-Se bond angles are in the range 92.13 – 101.99°, indicating that the 13-membered ring is rather large for the Pt(IV) ion. A crystal structure of the similar acyclic complex $[PtMe_3I(o\text{-}C_6H_4\{CH_2SeMe\}_2)]$ is discussed in Chapter 2 (Figure 2.12) and has slightly longer Pt-Se distances (2.5530 (4), 2.5629 (4) Å) than $[PtMe_3L^6]^+$. This is probably due to the cationic charge on the macrocyclic complex. $[PtMe_3I(o\text{-}C_6H_4\{CH_2SeMe\}_2)]$ also has a slightly more acute Se-Pt-Se angle (98.317 (12) °) than the corresponding Se1-Pt-Se2 angle here (101.99°). The macrocycle itself exhibits a significant conformational change upon complexation, with Se1 and Se2 now in a mutally *syn* arrangement rather than the *anti* arrangement observed in L^6, and the lone pairs associated with Se3 now occupying an *endo* configuration as opposed to *exo* (see Chapter 4, Figure 4.19).

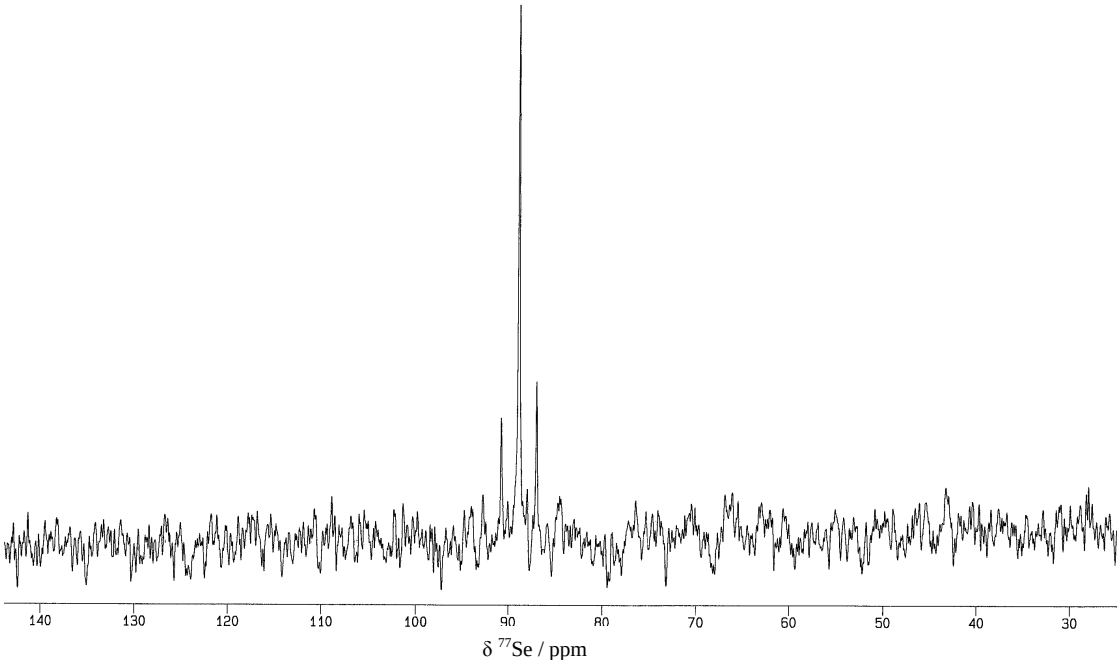

Figure 5.10: $^{77}Se\{^{1}H\}$ NMR spectrum of $[PtMe_3L^7]I$ recorded in $CDCl_3$.

The same reaction was undertaken with L^7 being added as a solution in $CHCl_3$ to $[PtMe_3I]$ in $CHCl_3$. The mixture was refluxed overnight, then filtered, and the filtrate dried *in vacuo* to produce a yellow solid. This was identified as $[PtMe_3L^7]I$ by microanalysis, ES^+ MS, ^{1}H, $^{13}C\{^{1}H\}$, $^{77}Se\{^{1}H\}$ and ^{195}Pt NMR spectroscopy. In contrast to $[PtMe_3L^6]I$, $[PtMe_3L^7]I$ is soluble in chlorocarbons. The *fac* tridentate coordination was much easier to identify on this ligand owing to the rotational symmetry of L^7. The $^{77}Se\{^{1}H\}$ NMR spectrum (Figure 5.10) showed a single peak shifted upfield from "free" ligand, with clear Pt-Se coupling (286 Hz). Similarly, the Pt-Me groups exhibit a single resonance in both the ^{1}H and $^{13}C\{^{1}H\}$ NMR spectra. The ^{1}H NMR spectrum shows both $^{2}J_{PtH}$ and $^{3}J_{SeH}$ coupling on the Me resonance (65 and 11 Hz respectively), while $^{13}C\{^{1}H\}$ NMR spectrum show $^{1}J_{PtC}$ coupling of 308 Hz.

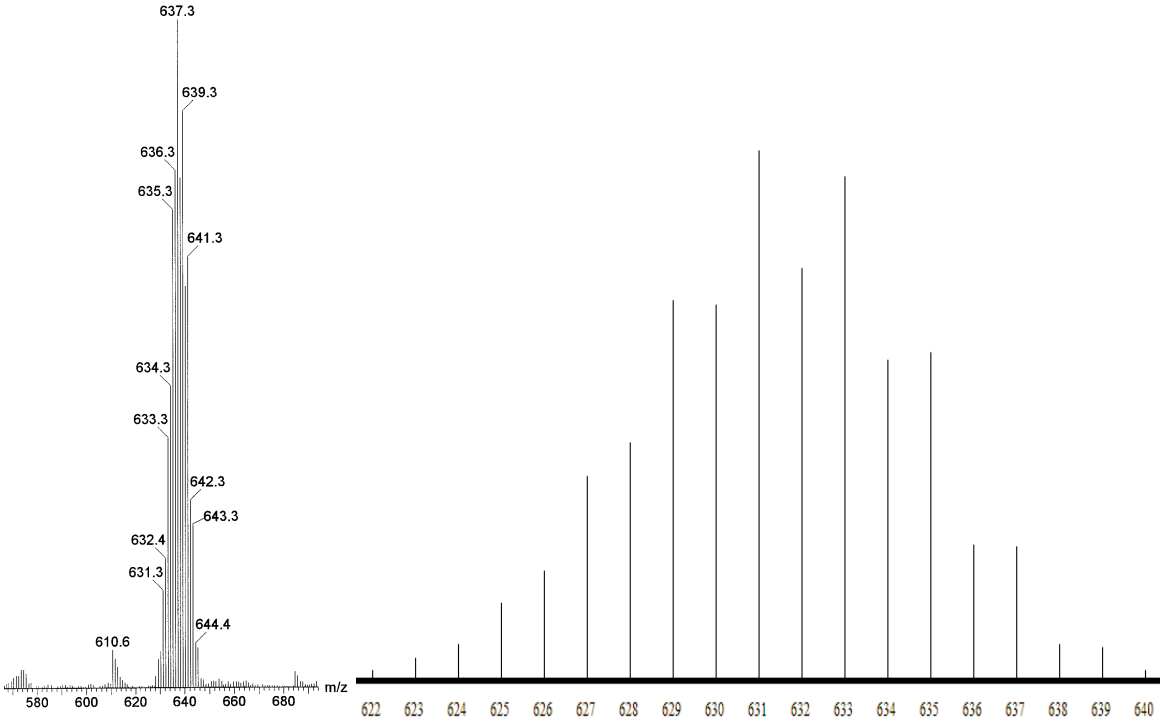

Figure 5.11: Left: ES MS$^+$ of [$PtMe_3L^8$]I. Right: calculated isotope pattern for [$PtMe_3L^8$]$^+$.

One equivalent of L^8 was dissolved in $CHCl_3$ and added to [$PtMe_3I$] in $CHCl_3$. After refluxing overnight, the reaction mixture was filtered, and the filtrate taken to dryness to yield a fawn-coloured solid, which was soluble in chlorocarbons, and analysed by microanalysis, ES$^+$ MS, ^{1}H, ^{13}C{^{1}H}, ^{77}Se{^{1}H} and ^{195}Pt NMR spectroscopy. The only significant peak cluster observed in the ES$^+$ MS spectrum (Figure 5.11) was consistent with [$PtMe_3L^8$]$^+$. Unlike [$PtMe_3I$([8]aneSe_2)] no evidence was seen in the ES$^+$ MS of the tridentate selenoether complexes for a Pt(II) species formed *via* reductive elimination (see Chapter 2). This may be due to the geometric constraints of the tridentate ligands, preventing them from binding in a tridentate fashion to a square planar metal centre. Analysis of the Pt-H coupling on the Me resonances in the ^{1}H NMR spectrum indicated that they were all *trans* Se. ^{77}Se {^{1}H} NMR spectroscopy revealed the expected two selenium environments, both of which showed clear Pt-Se coupling, confirming tridentate coordination. While both Se environments in [$PtMe_3L^6$]I moved to low frequency from the "free" ligand, [$PtMe_3L^8$]I showed the single Se atom between the C_3 backbones to move to low frequency, while the two Se atoms on the aromatic ring shifted to a higher frequency. [$PtMe_3I$(MeSe{CH_2}$_2$SeMe)] also shows this high frequency shift,[27] indicating that the five-membered chelate ring is more dominant than the six-membered chelate ring in determining NMR shift.

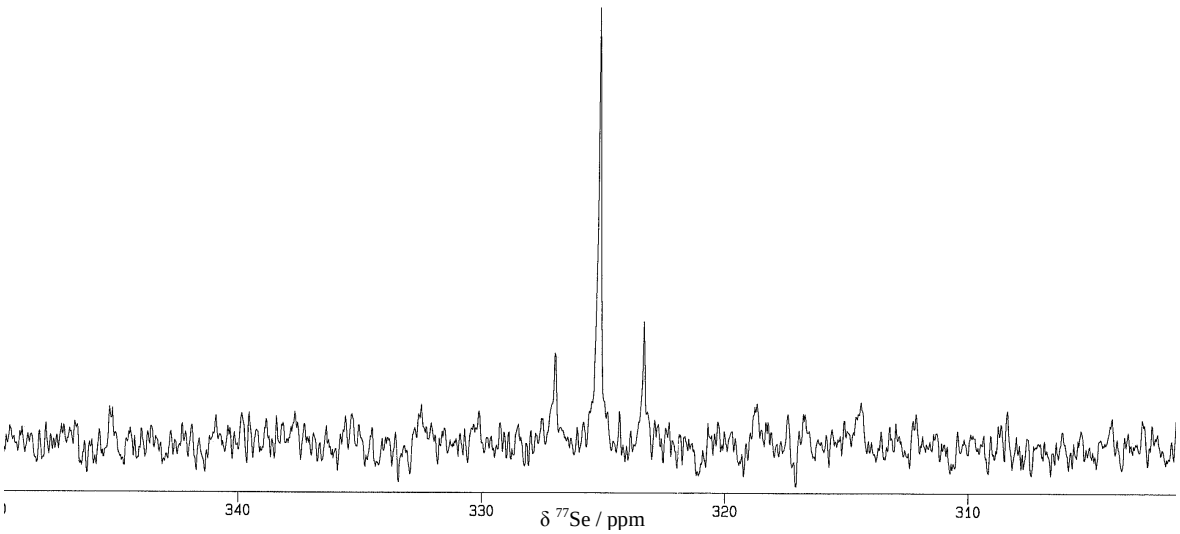

Figure 5.12: $^{77}Se\{^{1}H\}$ NMR spectrum of $[PtMe_3L^9]I$ recorded in $CDCl_3$.

After the success of the reactions with the tridentate homoleptic selenoethers, the analogous reactions were undertaken with the Se_2N macrocycles to assess what difference the harder pyridyl N donor made to reaction chemistry. $[PtMe_3I]$ was dissolved in $CHCl_3$ and one equivalent of L^9 was added in $CHCl_3$. The reaction mixture was refluxed overnight, and then reduced to ~ 5 cm^3 *in vacuo.* Addition of diethyl ether caused a yellow solid to precipitate which was collected by filtration and dried *in vacuo*. This solid was soluble in chlorocarbons, and was analysed by ES^+ MS, ^{1}H, $^{13}C\{^{1}H\}$, $^{77}Se\{^{1}H\}$ and ^{195}Pt NMR spectroscopy. $^{77}Se\{^{1}H\}$ NMR spectroscopy (Figure 5.12) showed a single peak at 325.2 ppm with $^{1}J_{PtSe}$ coupling of 279 Hz, indicating both Se donors to be coordinated to the Pt centre. The ^{195}Pt NMR spectrum (Figure 5.13) showed a single peak at –3082 ppm, consistent with Me_3Se_2N coordination at Pt(IV), rather than Me_3Se_2I coordination, which has been shown to be –3446 to –3667 ppm for acyclic and macrocyclic selenoethers.[27] The Se-N-Se linkage is almost a classic pincer ligand linkage, which in the case of the more studied acyclic P-N-P or S-N-S ligands usually prefers *mer* coordination on metal centres. However, the linkage between the Se atoms closing the macrocycle, prevents the ligand from adopting a *mer* geometry. This confirmed by the ^{1}H NMR spectrum, which shows two resonances for Pt-Me groups (δ = 0.71, 0.94 ppm), with Pt-H coupling consistent with Me *trans* Se (66 Hz) and Me *trans* N (72 Hz).

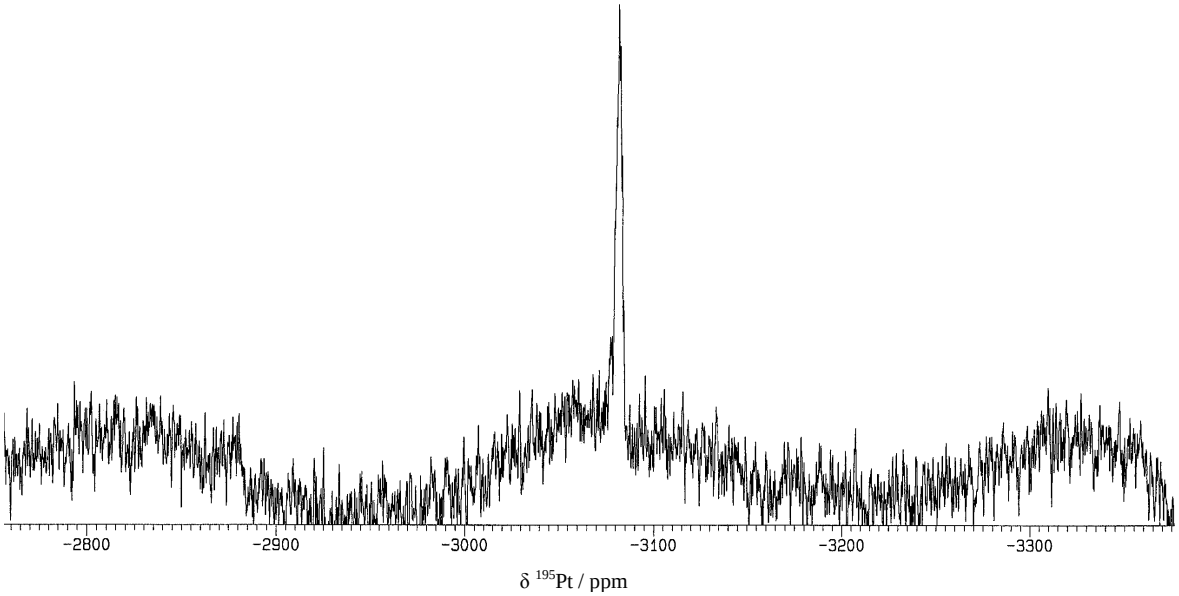

Figure 5.13: ^{195}Pt NMR spectrum of [$PtMe_3L^9$]I recorded in $CDCl_3$.

Small single crystals of [$PtMe_3L^9$]I were grown by slow evaporation of a solution in $CHCl_3$. The structure obtained (Figure 5.14) confirms the *fac* tridentate coordination. The xylyl Se-Se linkage changes in conformation from *anti* to *syn* upon coordination (see Figure 4.25), and C10 and C15 are displaced slightly further away from the pyridyl ring (~0.3 Å). The N···Se distances are scarcely affected by complexation, but the Se···Se distance decreases from 4.812 (1) to 4.087 (3) Å upon complexation. The Se-Pt-Se angle is more obtuse than the equivalent angle in [$PtMe_3L^6$]I (101.99°), while the N-Pt-Se angles are very acute (~79°) indicating the greater strain in accommodating the smaller, more rigid pyridyl linkage as opposed -$(CH_2)_3Se(CH_2)_3$- which is more flexible. The bulky nature of both the pyridyl and xylyl linkages present in L^9 may indicate that tridentate coordination is the only possible mode on an octahedral metal, and that displacement of the I^- is vital to prevent steric clash.

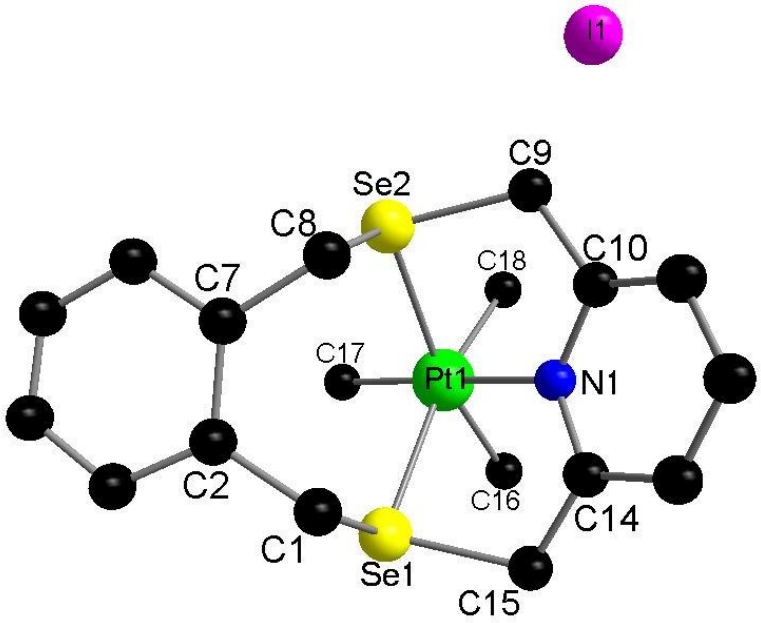

Figure 5.14: Crystal structure of $[PtMe_3L^9]I{\cdot}CHCl_3$. H atoms omitted for clarity.

Table 5.2: Selected bond lengths and angles for $[PtMe_3L^9]I{\cdot}CHCl_3$.

Bond	**Length / Å**	**Bond**	**Angle / °**	**Bond**	**Angle / °**
Pt1–C16	2.08 (2)	C16–Pt1–C17	86.7 (10)	C17–Pt1–Se2	96.9 (7)
Pt1–C17	2.05 (2)	C16–Pt1–C18	83.6 (10)	C18–Pt1–N1	99.4 (9)
Pt1–C18	2.09 (2)	C16–Pt1–N1	98.5 (8)	C18–Pt1–Se1	167.2 (7)
Pt1–N1	2.180 (18)	C16–Pt1–Se1	83.8 (8)	C18–Pt1–Se2	84.2 (7)
Pt1–Se1	2.533 (2)	C16–Pt1–Se2	167.1 (8)	N1–Pt1–Se1	79.6 (5)
Pt1–Se2	2.517 (3)	C17–Pt1–C18	87.2 (11)	N1–Pt1–Se2	79.3 (5)
		C17–Pt1–N1	171.9 (9)	Se1–Pt1–Se2	108.05 (8)
		C17–Pt1–Se1	95.0 (8)		

Reaction of one equivalent of L^{10} with $[PtMe_3I]$ in refluxing $CHCl_3$ caused a yellow solid to precipitate from the reaction mixture. This solid was collected by filtration, washed with $CHCl_3$ and dried *in vacuo*. As with $[PtMe_3L^6]I$, this solid was extremely poorly soluble in chlorocarbons, and only slightly more soluble in MeCN, so again a $^{13}C\{^1H\}$ NMR spectrum was not obtained, and the solid was identified as $[PtMe_3L^{10}]I$ by microanalysis, ES^+ MS, ^1H, $^{77}Se\{^1H\}$ and ^{195}Pt NMR spectroscopy. Figure 5.15 shows the ^1H NMR spectrum, in which the resonances from the methyl groups on Pt can clearly be seen, with $^2J_{PtH}$ coupling evident. This coupling is as expected for Me *trans* Se (67 Hz), and *trans* N (72 Hz). The propyl backbone protons show broad resonances at 1.82 and 3.00 ppm, and the CH_2 linkage on the pyridyl ring has split into a complex pattern of peaks between 4.54 and 4.85 ppm. Again, this is probably due to spatial proximity of protons to Pt.

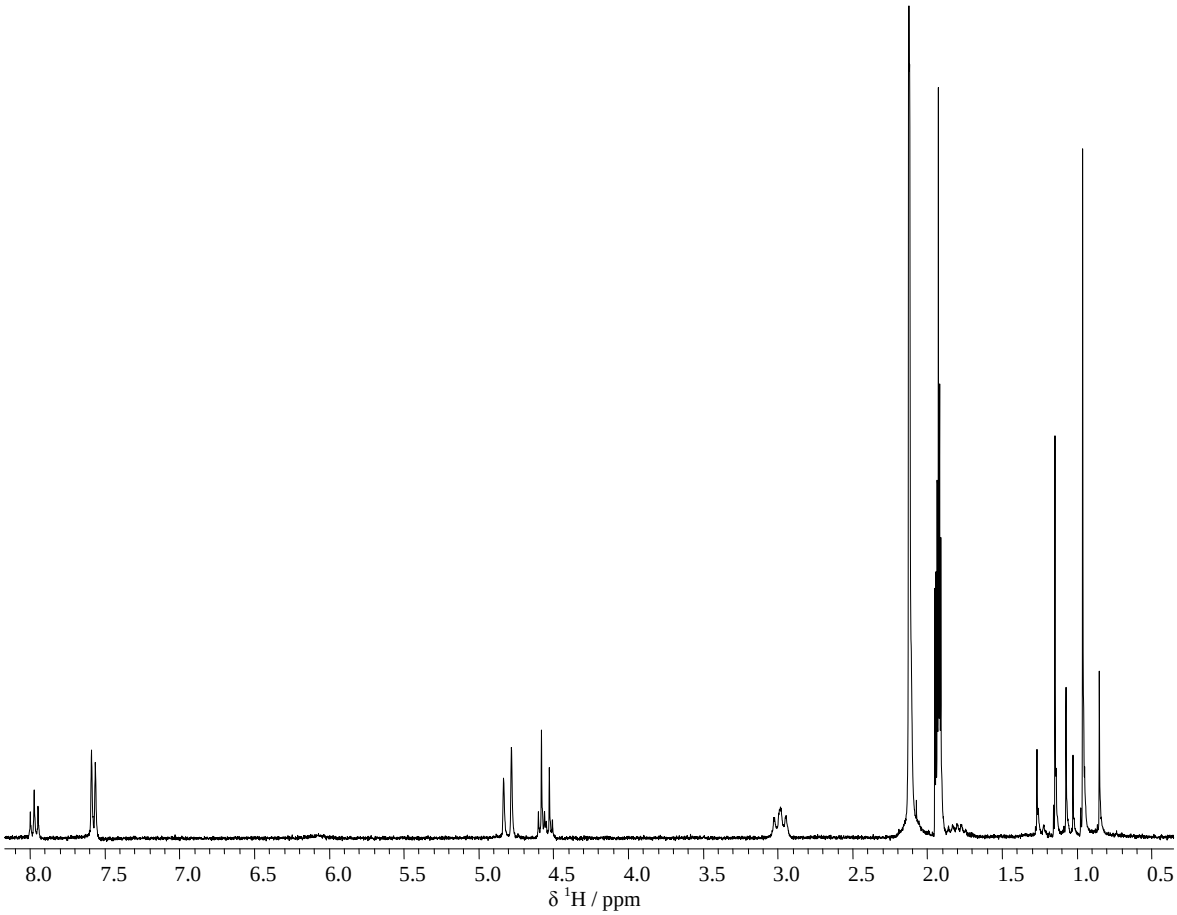

Figure 5.15: ^{1}H NMR spectrum of [$PtMe_3L^{10}$]I recorded in CD_3CN.

5.4 – Conclusions

The first examples of complexes with tridentate homoleptic selenoether macrocycles and tridentate Se_2N macrocycles have been prepared and characterised. Dichloro Pt(II) complexes were prepared for L^6-L^9, but proved to be extremely poorly soluble. This continues a trend towards insolubility observed in Chapter 2. No evidence of dimethyl Pt(II) complexation was observed.

Reaction of [$PtMe_3I$] with L^6-L^{10} resulted in the production of *fac*-coordinated, cationic Pt complexes of the type [$PtMe_3L$]I. This geometry is confirmed by two crystal structures, of [$PtMe_3L^6$]I and [$PtMe_3L^9$]I. The ability to displace coordinated iodide without the aid of an iodide abstractor is independent both of macrocycle ring size and donor set, and demonstrates strong coordinating properties. The nature of the linking groups also plays an important role in determining the solubility of these complexes.

5.5 – Experimental

[$PtCl_2(L^6)$]: [$PtCl_2$] (0.063 g, 0.23 mmol) was dissolved in MeCN (20 cm^3). The solution was refluxed and stirred until all of the [$PtCl_2$] dissolved giving a light yellow solution. To this solution, L^6 (0.105 g, 0.23 mmol) was added in CH_2Cl_2 (10 cm^3). The reaction mixture was refluxed overnight and the yellow solid product was filtered, washed with CH_2Cl_2 and dried *in vacuo*. Yield: 0.113 g, 72 %. Required for $C_{14}H_{20}Cl_2PtSe_3$ (691.17): C, 24.3; H, 2.9; found: C, 24.1; H, 3.1%. ^{195}Pt NMR (D_6-dmf, 298 K): δ = -3644 (weak, due to poor solubility). IR (Nujol): 310 br (Pt–Cl) cm^{-1}.

[$PtCl_2(L^7)$]: [$PtCl_2$] (0.082 g, 0.30 mmol) was refluxed in MeCN (20 cm^3) for one hour. The solution was filtered to remove any unreacted $PtCl_2$. To the yellow filtrate, L^7 (0.112 g, 0.30 mmol) in CH_2Cl_2 (10 cm^3) was added. The reaction mixture was refluxed for 4 hours, then stirred overnight at room temperature. The yellow precipitate was filtered, washed with $CHCl_3$ and dried *in vacuo*. Yield: 0.09 g, 46 %. Required for $C_9H_{18}Cl_2PtSe_3 \cdot 2CHCl_3$ (629.12): C, 15.2; H, 2.3; found: C, 15.2; H, 2.6 %. IR (Nujol): 314 br (Pt–Cl) cm^{-1}.

[$PtCl_2(L^8)$]: As above, using [$PtCl_2$] (0.042 g, 0.158 mmol) and L^8 (0.0629 g, 0.158 mmol). Yield: 78 %. Required for $C_{12}H_{16}Cl_2PtSe_3 \cdot H_2O$ (665.15): C, 21.2; H, 2.7; found: C, 21.5; H, 3.4%. IR (Nujol): 325, 315 (Pt–Cl) cm^{-1}.

[$PtMe_3(L^6)I$]: L^6 (0.122 g, 0.28 mmol) in CH_3Cl (10 cm^3) was added slowly to a solution of [$PtMe_3I$] (0.1 g, 0.27 mmol) in CH_3Cl (10 cm^3). The reaction mixture was refluxed overnight, yielding some pale yellow solid. The chloroform solution was concentrated *in vacuo* and diethyl ether added. The product was filtered off and then washed with methanol (50 cm^3) and dried *in vacuo* giving an off-white solid. Yield: 0.19 g, 88 %. Required for $C_{17}H_{29}IPtSe_3$ (792.27): C, 25.7; H, 3.69; found: C, 25.7; H, 3.80 %. ES^+ MS (CH_3CN): *m/z* = 665 $[C_{17}H_{29}{}^{195}Pt^{80}Se_3]^+$. ^{1}H NMR ($CD_3CN$): δ = 0.32 (s, 3H PtCH_3, $^2J_{Pt\text{-}H}$ = 65 Hz), 0.82 (s, 6H PtCH_3, $^2J_{Pt\text{-}H}$ = 66 Hz, $^3J_{Se\text{-}H}$ = 11 Hz), 2.5, 2.7, 3.1, 3.2, 4.3, 4.9 (multiplets) 7.3 – 7.5 (multiplet, 4H xylyl protons). ^{77}Se{^{1}H} NMR (CD_3CN, 298 K): δ = 88.8, 154.6 (^{195}Pt satellites not resolved); (CD_3CN, 233 K): δ = 151.6 ($^1J_{PtSe}$ = 328 Hz, 2Se), 77.9 (Se). ^{195}Pt NMR (CD_3CN): δ = –3768; (CD_3CN, 233 K): δ = –3791.

[$PtMe_3(L^7)$]I: To a solution of [$PtMe_3I$] (0.1 g, 0.27 mmol) in CH_3Cl (10 cm^3) was added a solution of L^7 (0.098 g, 0.27 mmol) in CH_3Cl (10 cm^3). The reaction was refluxed overnight. On cooling, the reaction mixture was filtered and the light yellow product obtained by removal of solvent from the filtrate. Yield: 0.14 g, 72 %. Required for $C_{12}H_{27}IPtSe_3$ (730.21): C, 19.7; H, 3.7. Found: C, 19.9; H 3.5%. ES^+ MS (CH_3CN): *m/z* = 603 $[C_{12}H_{27}{}^{195}Pt^{80}Se_3]^+$. ^{1}H NMR ($CDCl_3$): δ =

0.97 (s, 9H PtCH_3, $^2J_{Pt\text{-}H}$ = 65 Hz, $^3J_{Se\text{-}H}$ = 10 Hz), 2.213 (overlapping multiplets), 2.87 (overlapping multiplets), 3.59 (overlapping multiplets).. $^{13}C\{^1H\}$ ($CDCl_3$): δ = 5.1 (PtMe, $^2J_{Pt\text{-}C}$ = 729 Hz), 24.9 (Se*C*H_2), 25.3 (SeCH$_2$*C*H_2). $^{77}Se\{^1H\}$ NMR ($CDCl_3$): δ = 88.8 ($^1J_{Pt\text{-}Se}$ = 286.4 Hz). ^{195}Pt ($CDCl_3$): δ = –3866.

[PtMe$_3$(L^8)I]: As above, using [PtMe$_3$I] (0.074 g, 0.20 mmol) and L^8 (0.80 g, 0.20 mmol). Fawn coloured solid. Yield: 70 %. Required for $C_{15}H_{25}IPtSe_3 \cdot CHCl_3$ (764.22): C, 21.7; H, 3.0. Found: C, 21.4; H 3.1. ES^+ MS (CH_3CN): *m/z* = 637 $[C_{15}H_{25}{}^{195}Pt^{80}Se_3]^+$. ^{1}H NMR ($CDCl_3$, 298 K): δ = 7.35–7.95 (m, *o*-C_6H_4), 2.0–3.7 (br m, CH_2, 12H), 1.38 (s, $^2J_{PtH}$ = 69 Hz, 2 x PtMe, 6H), 1.23 (s, $^2J_{PtH}$ = 66 Hz, PtMe, 3H). $^{13}C\{^1H\}$ NMR ($CDCl_3$, 298 K): δ = 135.9, 132.5 (aromatic C), 32.4, 25.9, 25.8 (CH_2), 5.4 ($^1J_{PtC}$ = 603 Hz, 2 x PtMe), 1.0 ($^1J_{PtC}$ = 597 Hz, PtMe). $^{77}Se\{^1H\}$ NMR (CD_3Cl, 223 K): δ = 341.5 ($^1J_{PtSe}$ = 293 Hz, 2Se), 71.8 ($^1J_{PtSe}$ = 318 Hz, Se). ^{195}Pt NMR (CD_3Cl, 223 K): δ = –3674.

[PtMe$_3$(L^9)I]: [PtMe$_3$I] (0.048 g, 0.13 mmol) was dissolved in CH_3Cl (10 cm^3). L^9 (0.048 g, 0.13 mmol) in CH_3Cl (10 cm^3) was added. The reaction mixture was refluxed overnight. The yellow solution was reduced to *ca.* 5 cm^3 *in vacuo*. Cold diethyl ether (~15 cm^3) was added dropwise to precipitate a yellow solid, which was filtered off and dried *in vacuo*. Yield: 0.07 g, 75 %. ES^+ MS (CH_3CN): *m/z* = 608 $[C_{18}H_{24}N^{195}Pt^{80}Se_2]^+$. ^{1}H NMR ($CDCl_3$, 298 K): δ = 7.99 (m, aromatic CH), 7.23–7.37 (m, aromatic CH), 5.25 (m, CH_2, 2H), 4.68 (m, CH_2, 2H), 4.62 (m, CH_2, 2H), 3.38 (m, CH_2, 2H), 0.94 (s, $^2J_{PtH}$ = 66 Hz, 6H, 2 x PtMe), 0.71 (s, $^2J_{PtH}$ = 72 Hz, 3H, PtMe). $^{13}C\{^1H\}$ NMR ($CDCl_3$, 298 K): δ = 160.5, 140.6, 132.6, 131.5, 130.0, 126.7 (aromatic C atoms), 40.3 (pyridyl-*C*H_2), 28.0 (Ar-*C*H_2), 7.3 ($^1J_{PtC}$ = 605 Hz, 2 x PtMe), 1.8 (coupling ill-defined, PtMe). $^{77}Se\{^1H\}$ NMR ($CDCl_3$): δ = 325.2 ($^1J_{Pt\text{-}Se}$ = 279 Hz). ^{195}Pt ($CDCl_3$): δ = –3082.

[PtMe$_3$(L^{10})I]: As above, using [PtMe$_3$I] (0.1 g, 0.27 mmol) and L^{10} (0.08 g, 0.27 mmol). The yellow precipitate formed during reaction was filtered off and washed with $CHCl_3$. Yield: 0.12 g, 68%. Required for $C_{13}H_{22}INPtSe_2$ (672.2): C, 23.2; H, 3.30; N, 2.08; found: C, 22.7; H, 3.25; N, 2.01%. ES^+ MS (CH_3CN): *m/z* = 546 $[C_{13}H_{22}N^{195}Pt^{80}Se_2]^+$. ^{1}H NMR ($CD_3CN$, 298 K): δ = 7.98 (t, pyridyl, 1H), 7.59 (d, pyridyl, 2H), 4.54–4.85 (m, pyridyl-C*H*$_2$Se, 4H), 3.00 (br t, SeC*H*$_2$CH$_2$C*H*$_2$Se, 4H), 1.82 (br m, CH$_2$C*H*$_2$CH$_2$, 2H), 1.16 (s, $^1J_{PtC}$ = 72 Hz, 3H, PtMe), 0.98 (s, $^1J_{PtC}$ = 67 Hz, 6H, 2 x PtMe). $^{77}Se\{^1H\}$ NMR (CD_3CN, 233 K): δ = 288 (broad). ^{195}Pt NMR (CD_3CN, 298 K): δ = –3227 (broad); (CD_3CN, 233 K): –3250 (broad).

5.6 – X-Ray Crystallography

Details of the crystallographic data collection and refinement parameters are given in Table 5.3. Colourless single crystals of $[PtMe_3(L^6)]I{\cdot}0.13CH_2Cl_2$ and $[PtMe_3(L^9)]I{\cdot}CHCl_3$ were obtained by recrystallisation from CH_2Cl_2 and $CHCl_3$ respectively. Structure solution and refinement were routine.[28,29] Selected bond lengths and angles for $[PtMe_3(L^6)]I{\cdot}0.13CH_2Cl_2$ are presented in Table 5.1 and for $[PtMe_3(L^9)]I{\cdot}CHCl_3$ are presented in Table 5.2.

Table 5.3: Crystallographic data collection and refinement parameters. $R1 = \Sigma||F_o| - |F_c||/\Sigma|F_o|$; $wR_2 = [\Sigma w(F_o^2 - F_c^2)^2/\Sigma wF_o^4]^{1/2}$

Complex	**$[PtMe_3(L^6)]I{\cdot}0.13CH_2Cl_2$**	**$[PtMe_3(L^9)]I{\cdot}CHCl_3$**
Formula	$C_{17.13}H_{29.26}Cl_{0.26}IPtSe_3$	$C_{19}H_{25}Cl_3INPtSe_2$
M	803.15	853.66
Crystal System	Orthorhombic	Orthorhombic
Space Group	*P*bca	*P*bca
a/Å	10.7267 (10)	12.534 (3)
b/Å	25.698 (2)	22.046 (6)
c/Å	17.4365 (15)	17.858 (5)
α/°	90	90
β/°	90	90
γ/°	90	90
U/Å^3	4806.4 (7)	4935 (2)
Z	8	8
μ(Mo-Kα)/ mm^{-1}	11.692	10.220
R_{int}	0.044	0.128
Total no. reflns.	24343	37833
Unique reflections	5475	4832
No. of parameters	209	247
$R1$ [$I_o > 2\sigma(I_o)$]	0.036	0.098
$R1$ [all data]	0.081	0.173
wR_2 [$I_o > 2\sigma(I_o)$]	0.044	0.168
wR_2 [all data]	0.085	0.205

5.7 – References

1. Levason, W.; Manning, J. M.; Reid, G.; Tuggey, M.; Webster, M. *Dalton Trans.* **2009**, 4569 – 4577.

2. Levason, W.; Orchard, S. D.; Reid, G. *Coord. Chem. Rev.* **2002**, *225*, 159 – 199.

3. Levason, W.; Reid, G. In: *Comprehensive Co-ordination Chemistry II*, Vol. 1, Elsevier Ltd., 2003, 399 – 410.

4. Davies, M. K.; Durrant, M. C.; Levason, W.; Reid, G.; Richards, R. L. *J. Chem. Soc., Dalton Trans.* **1999**, 1077 – 1083.

5. Levason, W.; Reid, G.; Smith, S. M. *Polyhedron*, **1997**, *16*, 4253 – 4256.

6. Adams, R. D.; McBride, K. T.; Rogers, R. D. *Organometallics* **1997**, *16*, 3895 – 3901.

7. Levason, W.; Quirk, J. J.; Reid, G.; Smith, S. M. *J. Chem. Soc., Dalton Trans.* **1997**, 3719 – 3724.

8. Levason, W.; Quirk, J. J.; Reid, G. *J. Chem. Soc., Dalton Trans.* **1996**, 3713 – 3719.

9. Davies, M. K.; Levason, W.; Reid, G. *J. Chem. Soc., Dalton Trans.* **1998**, 2185 – 2189.

10. Champness, N. R.; Levason, W.; Quirk, J. J.; Reid, G.; Frampton, C. *Polyhedron* **1995**, *14*, 2753 – 2758.

11. Booth, D. G.; Levason, W.; Quirk, J. J.; Reid, G.; Smith, S. M. *J. Chem. Soc., Dalton Trans.* **1997**, 3494 – 3500.

12. Champness, N. R.; Kelly, P. F.; Levason, W.; Reid, G.; Slawin, A. M. Z.; Williams. D. J. *Inorg. Chem.* **1995**, *34*, 651 – 657.

13. Levason, W.; Quirk, J. J.; Reid, G.; Frampton, C. S. *Inorg. Chem.* **1994**, *33*, 6120 – 6122.

14. Batchelor, R. J.; Einstein, F. W. B.; Gay, I. D.; Gu, J.; Pinto, B. M.; Zhou, X. *Inorg. Chem.* **1996**, *35*, 3667 – 3674.

15. Batchelor, R. J.; Einstein, F. W. B.; Gay, I. D.; Gu, J.-H.; Mehta, S.; Pinto, B. M.; Zhou, X.-M. *Inorg. Chem.* **2000**, *39*, 2558 – 2571.

16. Barton, A. J.; Hill, N. J.; Levason, W.; Reid, G. *J. Chem. Soc., Dalton Trans.* **2001**, 1621 – 1627.

17. Barton, A. J.; Hill, N. J.; Levason, W.; Patel, B.; Reid, G. *Chem. Commun.* **2001**, 95 – 96.

18. Barton, A. J.; Genge, A. R. J.; Levason, W.; Reid, G. *J. Chem. Soc., Dalton Trans.* **2000**, 2163 – 2166.

19. Barton, A. J.; Hill, N. J.; Levason, W.; Reid, G. *J. Am. Chem. Soc.* **2001**, *123*, 11801 – 11802.

20. Blake, A. J.; Holder, A. J.; Hyde, T. I.; Roberts, Y. V.; Lavery, A. J.; Schröder, M. *J. Organomet. Chem.* **1987**, *323*, 261 – 270.

21. Grant, G. J.; Brandow, C. G.; Galas, D. F.; Davis, J. P.; Pennington, W. T.; Valente, E. J.; Zubkowski, J. D. *Polyhedron* **2001**, *20*, 3333 – 3342.

22. Bennett, M. A.; Canty, A. J.; Felixberger, J. K.; Rendina, L. M.; Sunderland, C.; Willis, A. C. *Inorg. Chem.* **1993**, *32*, 1951 – 1958.

23. Blake, A. J.; Gould, R. O.; Holder, A. J.; Hyde, T. I.; Lavery, A. J.; Odulate, M. O.; Schröder, M. *J. Chem. Soc., Chem. Commun.* **1987**, 118 – 120.

24. Gulliver, D. J.; Hope, E. G.; Levason, W.; Murray, S. G.; Marshall, G. L. *J. Chem. Soc., Dalton Trans.* **1985**, 1265 – 1269.

25. Jones, R. C.; Madden, R. L.; Skelton, B. W.; Tolhurst, V.-A.; White, A. H.; Williams, A. M.; Wilson, A. J.; Yates, B. F. *Eur. J. Inorg. Chem.* **2005**, 1048 – 1055.

26. Abel, E. W.; Khan, A. R.; Kite, K.; Orrell, K. G.; Sik, V. *J. Chem. Soc., Dalton Trans.* **1980**, 1169 – 1174.

27. Abel, E. W.; Orrell, K. G.; Platt, A. W. G. *J. Chem. Soc., Dalton Trans.* **1983**, 2345 – 2351.

28. Sheldrick, G. M. SHELXS-97, program for crystal structure solution, University of Göttingen, Germany, **1997**.

29. Sheldrick, G. M. SHELXS-97, program for crystal structure refinement, University of Göttingen, Germany, **1997**.

Chapter 6: 3d Metals with Selenium Containing Ligands[1,2]

6.1 – Cobalt, Chromium and Vanadium Complexes with Thio- and Selenoether Ligands

There are only a few complexes involving cobalt halides and thio- or selenoethers, and these predominantly involve Co(III), which is unexpected as Co(III) is regarded as a hard metal.[3,4,5] A study of Co(III) halide complexes with tetrathioethers has produced a range of complexes of the type $[CoX_2L]Y$ (X = Cl, Br, I; Y = BPh_4, BF_4; L = $MeSRS(CH_2)_2SRSMe$ (R = $(CH_2)_2$, $(CH_2)_3$, *o*-C_6H_4), [14]aneS_4).[6] This showed that in the case of the open chain tetrathioethers, the most stable complexes were formed where all the chelate rings were five membered. The macrocyclic complex is much more stable towards solvents than the acyclic complexes. Reaction of CoX_2 (X = Cl, Br, I) with $MeSe(CH_2)_2SeMe$ and $NaBPh_4$ generates the dry-air stable complexes $[CoX_2(MeSe\{CH_2\}_2SeMe)_2]BPh_4$, whilst similar reactions with $MeSe(CH_2)_3SeMe$ and $PhSe(CH_2)_2SePh$ produce no isolatable products.[7] A set of Co(III) complexes with a selenoether macrocycle, $[CoX_2([16]aneSe_4)]PF_6$ (where X = Cl, Br, I), have been produced by air oxidation of CoX_2 and [16]aneSe_4 in $MeNO_2$ followed by addition of NH_4PF_6 (see chapter 5).[8]

Co(II) complexes are only known for a small number of thioether ligands, and none are known for selenium or tellurium ligands. Reaction of anhydrous $[CoX_2]$ (X = Cl, Br, I) with dithioethers in dry ethanol has produced a series of Co(II) complexes of the type $[Co(L\text{-}L)_2X_2]$, where L-L = $MeS(CH_2)_2SMe$,[9,10] $EtS(CH_2)_2SEt$[9] or $^{i}PrS(CH_2)_2S^{i}Pr$.[10] The spectroscopic data obtained on these complexes confirmed an octahedral Co environment. A decrease in stability is observed as the terminal substituent becomes more bulky, which may be due to increased solubility leading to greater susceptibility to hydrolysis. Attempted reactions using $^{t}BuS(CH_2)_2S^{t}Bu$ exhibited colour changes indicative of complex formation, but no pure samples could be obtained, whilst using $PhS(CH_2)_2SPh$ produced no evidence of complex formation.[10] Interestingly, reaction of $CoCl_2$ and $MeS(CH_2)_2SMe$ in benzene produces a green compound which analyses as $[Co(MeS\{CH_2\}_2SMe)Cl_2]$ and has bands in its electronic spectra consistent with $[CoCl_4]^{2-}$. $[Co(MeS\{CH_2\}_2SMe)Cl_2]$ is considered to have a polymeric structure, with tetrahedral $[CoCl_4]^{2-}$ and $[Co(MeS\{CH_2\}_2SMe)_2]^{2+}$ units wherein the Co has a distorted octahedral geometry.[10]

A number of Co(II) complexes with homoleptic thioether coordination have been reported. $[Co(MeS\{CH_2\}_2S\{CH_2\}_2SMe)_2](BF_4)_2$,[11] $[Co([9]aneS_3)_2](BF_4)_2$[12] and $[Co([18]aneS_6)](picrate)_2$[11,13] all have crystal structures confirming distorted octahedral geometry about cobalt. The distortion is not uniform, however, as $[Co([9]aneS_3)_2](BF_4)_2$ shows the axial bonds to be slightly shorter than the equatorial bonds, while $[Co(MeS\{CH_2\}_2S\{CH_2\}_2SMe)_2](BF_4)_2$ and $[Co([18]aneS_6)](picrate)_2$

show the reverse. $[Co([9]aneS_3)_2]^{2+}$ and $[Co([18]aneS_6)]^{2+}$ also exhibit reversible oxidations to Co(III) species, with unusually high redox potentials compared to similar amine complexes.[13]

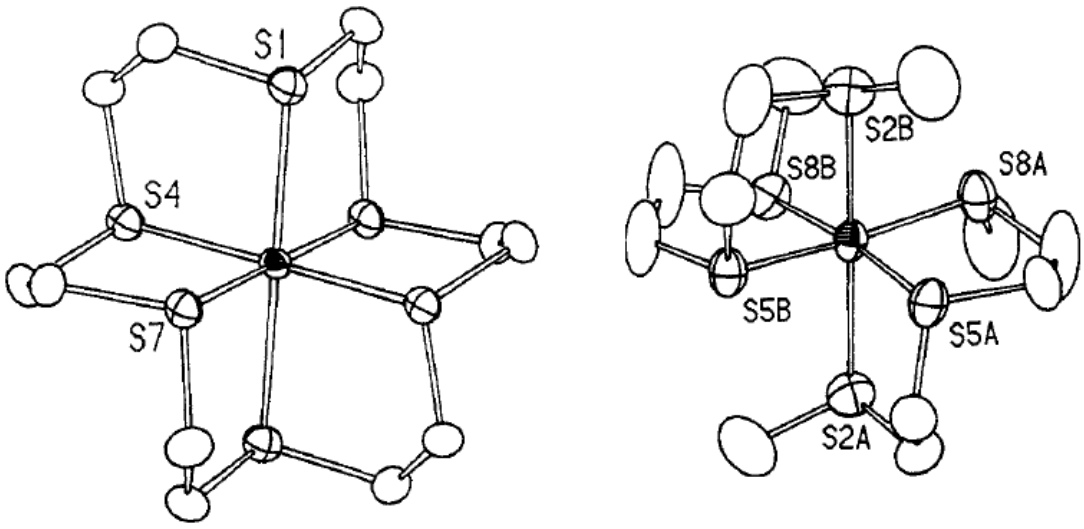

Figure 6.1: Crystal structures of $[Co([18]aneS_6)]^{2+}$ (left) and $[Co(MeS\{CH_2\}_2S\{CH_2\}_2SMe)_2]^{2+}$ (right). Thermal ellipsoids at 50 % probability. H atoms omitted for clarity.[11]

Table 6.1: Average Co-S bond lengths for distorted octahedral homoleptic Co(II) complexes with thioether ligands.

Complex	**Co-S equatorial bond length /Å**	**Co-S axial bond length /Å**	**Reference**
$[Co(MeS\{CH_2\}_2S\{CH_2\}_2SMe)_2](BF_4)_2$	2.254	2.607	11
$[Co([9]aneS_3)_2](BF_4)_2$	2.361	2.240	12
$[Co([18]aneS_6)](picrate)_2$	2.271	2.479	11

A number of Cr(0) complexes with chalcogenoether ligands are known,[5] but the known complexes with Cr(III) are primarily with oxygen and sulfur ligands, with very few examples containing selenoethers.[3,5] Vanadium complexes with selenoethers are even less well known.[5] Given the hard-soft mismatch between chromium/vanadium and selenoethers, this lack of characterised complexes is not surprising.

Reaction of $[CrCl_3(thf)_3]$ with various macrocyclic ligands in dry CH_2Cl_2 produces $[CrCl_3L]$ as pink solids in the case of crown ethers (L = 12-crown-4, 15-crown-5, 18-crown-6),[14] and blue or purple solids in the case of thio- and mixed thio-oxo-macrocycles (L = $[9]aneS_3$,[15] $[10]aneS_3$,[15] $[12]aneS_4$,[14] $[15]aneS_5$,[14] $[9]aneS_2O$,[14] $[15]aneS_2O_3$,[14] $[18]aneS_3O_3$[14]). $[CrCl_3(thf)_3]$ can also be reacted in 2:1 ratio with hexadentate macrocycles to yield $[(CrCl_3)_2(18\text{-crown-6})]$[14] or $[(CrCl_3)_2([18]aneS_6)]$.[15] Similarly, reaction of $[VCl_3(thf)_3]$ produces $[VCl_3L]$ as pink solids (L = 12-crown-4, 15-crown-5, 18-crown-6, $[12]aneS_4$, $[9]aneS_2O$, $[15]aneS_2O_3$, $[18]aneS_3O_3$), or the 2:1 complex $[(VCl_3)_2(18\text{-crown-6})]$.[14] The crown ether complexes must be prepared in rigorously

anhydrous conditions, as they will coordinate water readily, for example crystal structures of $[MCl_3(H_2O)(15\text{-crown-}5)]$ (M = Cr, V) have been reported. This tendency is reduced in the case of the mixed donor macrocycles.[14] $[MCl_3(H_2O)(15\text{-crown-}5)]$ (M = Cr, V) can also be deliberately prepared by stirring $[MCl_3(15\text{-crown-}5)]$ in CH_2Cl_2 with a small amount of water under N_2, but care must be taken as a large amount of water will completely displace the crown.[14] EXAFS experiments on macrocyclic thioether complexes have shown that these complexes have longer Cr-S bonds than Cr-Cl bonds, which is consistent with a weak thioether-Cr interaction.[15]

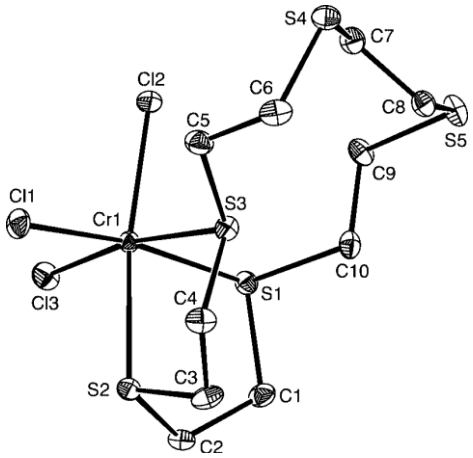

Figure 6.2: Crystal structure of $[CrCl_3([15]aneS_5)]$. Ellipsoids at 50 % probability, H atoms omitted for clarity.[14]

Chromium(III) complexes with an X_3Se_3 donor set have been produced by reaction of $[CrX_3(thf)_3]$ (X = Cl, Br) with the triselenoethers $MeC(CH_2SeMe)_3$ and $Se(\{CH_2\}_3SeMe)_2$ in anhydrous CH_2Cl_2, yielding green powders of the type $[CrX_3L]$.[16] IR spectroscopy appears to assign *fac* geometry to the $MeC(CH_2SeMe)_3$ complexes, and *mer* geometry to the $Se(\{CH_2\}_3SeMe)_2$ complexes. These complexes are moisture sensitive, very poorly soluble in chlorocarbons and decomposed by oxygen or nitrogen donor solvents. The reaction of $[CrX_3(thf)_3]$ in anhydrous $MeNO_2$ with $[16]aneSe_4$ and one equivalent of $TlPF_6$ gave blue $[CrX_2([16]aneSe_4)]PF_6$, but $[CrX_2([8]aneSe_2)_2]PF_6$ could not be produced under similar conditions.[16] $[CrX_2([16]aneSe_4)]PF_6$ have been assigned as the *cis* isomers, and are more soluble in organic solvents than the triselenoether complexes, but are still hydrolytically unstable. The analogous $[CrCl_2([16]aneS_4)]PF_6$ and related $[CrCl_2([14]aneS_4)]PF_6$, which are produced by the same route, have also been identified as existing as the *cis* isomers from their UV-vis spectra.[15] This geometry has been corroborated for $[CrX_2([14]aneS_4)]PF_6$ (X = Cl, Br) by crystal structures.[15,17]

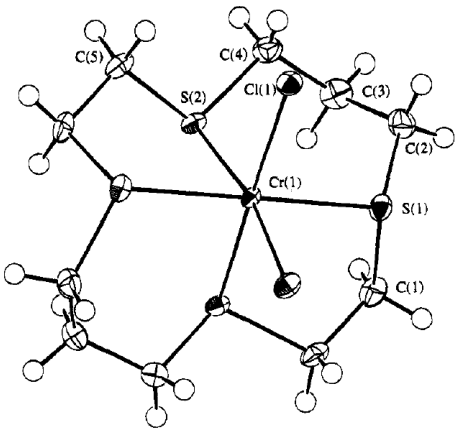

Figure 6.3: Crystal structure of the cation in $[CrCl_2([14]aneS_4)]PF_6$.[17]

The only known V(III) selenoether complexes are $[VCl_3(L\text{-}L)]$ (L-L = $MeSe(CH_2)_nSeMe$, n = 2, 3; $^nBuSe(CH_2)_2Se^nBu$; *o*-$C_6H_4(CH_2SeMe)_2$) and $[VCl_3(SeMe_2)_2]$ which are produced by reacting VCl_4 with excess selenoether in gently refluxing CH_2Cl_2. Use of a 1:1 ratio of vanadium:diselenoether results in the V(IV) species $[VCl_4(L\text{-}L)]$. The V(III) complexes are insoluble in chlorocarbons and MeCN, decomposed by alcohols and moisture sensitive, although they are less readily hydrolysed than the V(IV) complexes.[18]

Vanadium(III) complexes with an X_3S_3 donor set have been produced by reaction of $[VX_3(thf)_3]$ (X = Cl, Br) with $MeC(CH_2SMe)_3$, [9]$aneS_3$ or [10]$aneS_3$ in 1:1 ratio, giving $[VX_3L]$ complexes, or in 2:1 ratio with [18]$aneS_6$ to give $[(VX_3)_2([18]aneS_6)]$.[18] $[VI_3(thf)_3]$ can also be reacted with [9]$aneS_3$ to produce $[VI_3([9]aneS_3)]$.[19] The tridentate ligands are sterically constrained to produce complexes with *fac* geometry, while the hexadentate macrocycle complexes also have UV-vis spectra consistent with *fac* geometry. $[VCl_3([9]aneS_3)]$ can also be produced by reaction of [9]$aneS_3$ with $[VCl_3(MeCN)_3]$ or $[VCl_3(OPMe_2Ph)(PMe_2Ph)_2]$.[19]

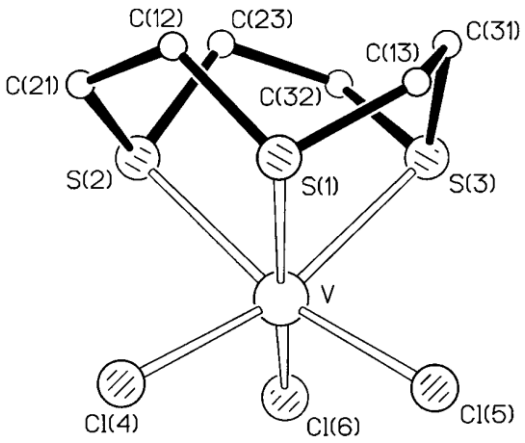

Figure 6.4: Crystal structure of $[VCl_3([9]aneS_3)]$.[19,20]

6.2 – Aims

The aims of this chapter are to investigate the coordination chemistry of selenoether ligands towards 3d metals. To this end, an investigation into Co(II) chemistry with thioether and selenoether acyclic ligands with xylyl backbones, and an investigation into the coordination of the new selenium-rich tridentate macrocycles produced in chapters 3 and 4 with Cr(III) and V(III) has been undertaken. It is hoped that the macrocyclic effect will improve stability of the soft selenoethers towards the hard metals. The presence of the hard O and pyridyl N donors may also increase stability.

6.3 – Cobalt(II) with Acyclic Thio- and Selenoether Ligands

Recently within this research group a crystal structure was obtained of $[CoI_2(C\{CH_2SMe\}_4)]$ (Figure 6.6)[1] and an exploratory reaction of CoI_2 with *o*-$C_6H_4(CH_2SeMe)_2$ had crystalline deposits. $[CoI_2(o\text{-}C_6H_4\{CH_2SMe\}_2)]$ was remade, by adding *o*-$C_6H_4(CH_2SMe)_2$ in anhydrous CH_2Cl_2 was added to CoI_2 in dry *n*-butanol. The reaction was undertaken in a dinitrogen atmosphere using rigorously dry solvents, reactants and glassware. A green solid was obtained after the solvent was removed *in vacuo* and the solid washed with dry hexane. Microanalysis confirmed the 1:1 ratio of ligand:cobalt. Crystals were grown by addition of petroleum ether to the reaction mixture before the solvent was removed, and crystal structure obtained (Figure 6.5). This clearly shows the tetrahedral structure of the complex, with the Co experiencing I_2S_2 coordination. This was somewhat unexpected, as previously reported Co(II) thioether complexes have been of the form $[Co(L\text{-}L)_2X_2]$ (X = Cl, Br, I; L-L = $MeS(CH_2)_2SMe$, $EtS(CH_2)_2SEt$, $^{i}PrS(CH_2)_2S^{i}Pr$) with octahedral structures.[9,10]

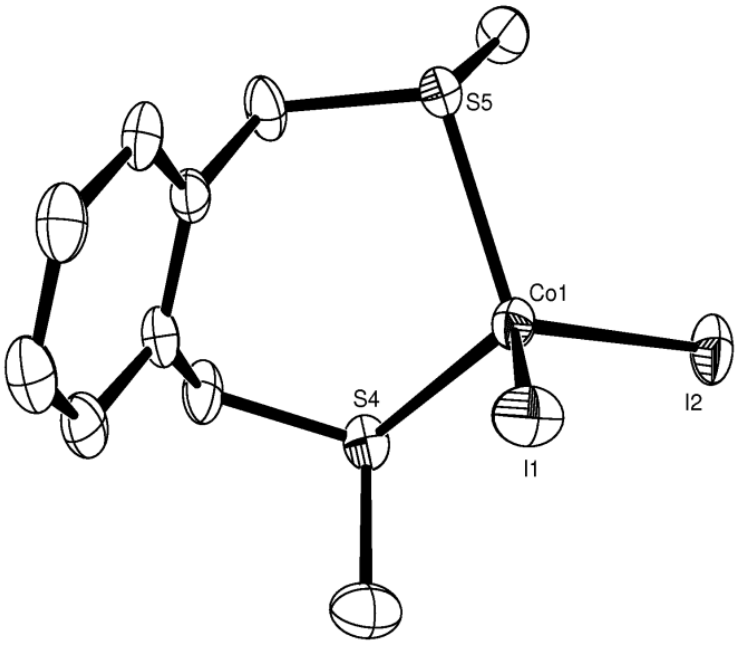

Figure 6.5: Crystal structure of $[CoI_2(o\text{-}C_6H_4\{CH_2SMe\}_2)]$. H atoms omitted for clarity. Ellipsoids at 50 % probability level.

Table 6.2: Selected bond lengths and angles for [CoI_2(*o*-C_6H_4{CH_2SMe}$_2$)].

Bond	**Length / Å**	**Bond**	**Angle / °**
Co1 – I1	2.5395 (5)	I1 – Co1 – I2	117.727 (18)
Co1 – I2	2.5548 (5)	I1 – Co1 – S4	113.29 (3)
Co1 – S4	2.3726 (9)	I1 – Co1 – S5	111.65 (2)
Co1 – S5	2.3457 (9)	I2 – Co1 – S4	99.88 (2)
		I2 – Co1 – S5	111.65 (2)
		S4 – Co1 – S5	107.51 (3)

UV-vis data was obtained on the isolated solid both as diffuse reflectance using $BaSO_4$ and in solution in anhydrous CH_2Cl_2. The solution UV-vis spectrum show extinction coefficients in the range 450 – 1200 cm^{-1} dm^3 mol^{-1}, which would be expected for Laporte-forbidden *d-d* transitions in a non-centrosymmetric environment, confirming the tetrahedral I_2S_2 coordination of [CoI_2(*o*-C_6H_4{CH_2SMe}$_2$)]. Three transitions are observed, corresponding to $^3A_2 \rightarrow {}^3T_2$, $^3A_2 \rightarrow {}^3T_1$ (F) and $^3A_2 \rightarrow {}^3T_1$ (P).

o-$C_6H_4(CH_2SMe)_2$ was then reacted with one equivalent of $CoBr_2$ under the same conditions as for CoI_2. A turquoise solid was obtained, which was identified as [$CoBr_2$(*o*-C_6H_4{CH_2SMe}$_2$)] by microanalysis and UV-vis spectroscopy, which again clearly showed tetrahedral co-ordination. Production of [$CoCl_2$(*o*-C_6H_4{CH_2SMe}$_2$)] was attempted by an analogous route, using $CoCl_2$, but the blue solid observed in the reaction mixture proved to be much less stable and could not be isolated. Reaction of CoI_2 in anhydrous *n*-BuOH with a solution of *o*-$C_6H_4(CH_2SeMe)_2$ in anhydrous CH_2Cl_2 produced a light green solid, which was isolated by removing the solvent *in vacuo* and washing with anhydrous hexane. UV-vis spectroscopy again clearly showed tetrahedral co-ordination with ε_{mol} values of 1082, 823 and 489 cm^1 dm^3 mol^{-1}, although the spectrum is very similar to that of $[CoI_4]^{2-}$.[21] The peaks are all ~ 400 cm^{-1} lower than those in [CoI_2(*o*-C_6H_4{CH_2SMe}$_2$)], which is consistent with the desired product, as the selenoether is expected to exert a weaker ligand field than the analogous thioether.[22] Attempts to produce [$CoBr_2$(*o*-C_6H_4{CH_2SeMe}$_2$)] yielded no isolatable products. This increasing instability as the halogen ligand is altered is the reverse of that observed in Co(III) complexes with $MeSe(CH_2)_2SeMe$, as the diiodide complex [CoI_2($MeSe${CH_2}$_2SeMe)_2$]BPh_4 is less stable and less soluble than its corresponding dibromo or dichloro complexes.[7]

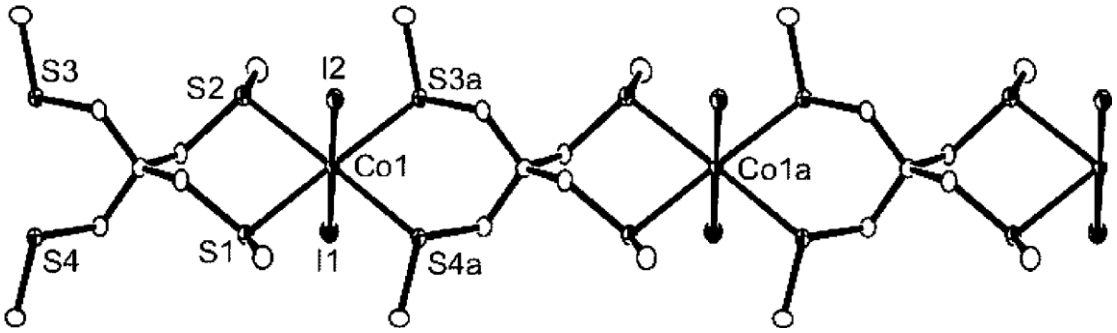

Figure 6.6: View of a portion of the infinite chain structure of $[CoI_2(C\{CH_2SMe\}_4)]$. Ellipsoids shown at 50 % probability.[1]

As work in this group has recently demonstrated that reaction of the spirocyclic thioether $C(CH_2SMe)_4$ with $[CoI_2]$ leads to the formation of $[CoI_2(C\{CH_2SMe\}_4)]$, which shows a rare reversible isomerisation between a polymeric structure in the solid state (shown in Figure 6.6) and discrete units in solution,[1] a reaction between $MeS(CH_2)_3SMe$ in anhydrous CH_2Cl_2 and $[CoI_2]$ in anhydrous *n*-BuOH was attempted. It was hoped that another example of a Co(II)-thioether complex with a 6 membered chelate ring could be produced, however all attempts at this reaction produced only intractable black materials.

6.4 – Chromium(III) and Vanadium(III) Complexes with Selenium-rich Tridentate Macrocycles

$[CrCl_3(thf)_3]$ was made by Soxhlet extraction of anhydrous $CrCl_3$ and zinc dust with thf. The extraction was run for ~15 hours, upon which time the purple solution was reduced *in vacuo* to yield $[CrCl_3(thf)_3]$.[23] The purple solid was handled only in a dinitrogen environment, and was stored in the glove box, as was $[VCl_3(thf)_3]$, which was purchased from Aldrich and used without further purification. All the ligands were dried thoroughly before use, as were all solvents and glassware.

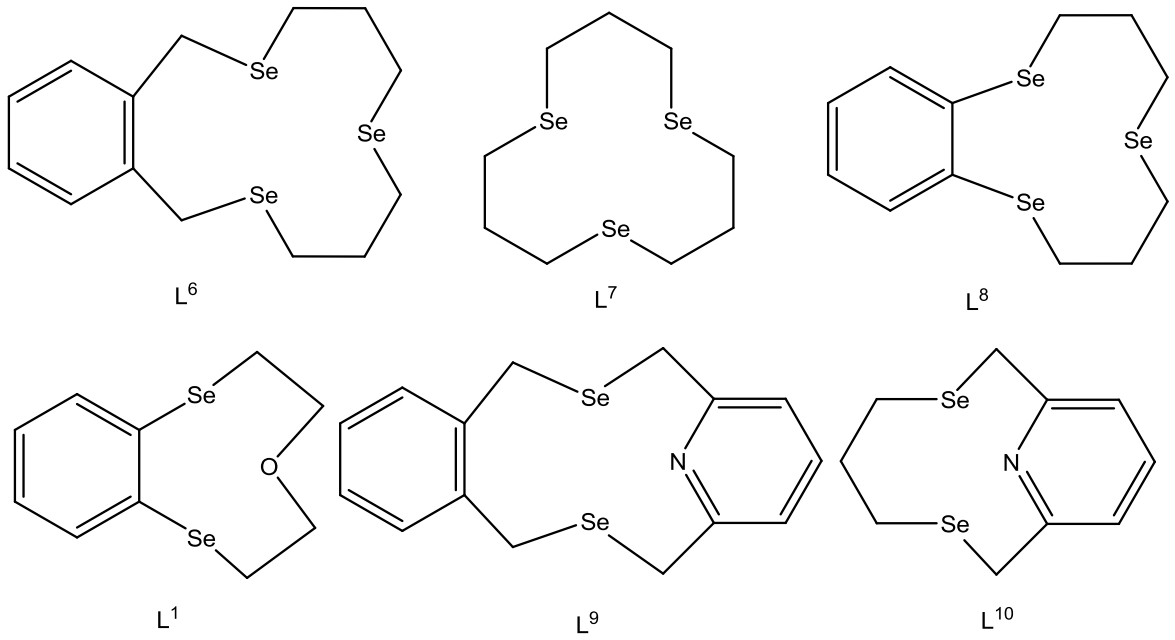

Figure 6.7: Selenium-rich macrocycles used in this chapter. See Chapters 3 (L^1) and 4 (L^6-L^{10}) for preparation.

$[CrCl_3(thf)_3]$ was dissolved in anhydrous CH_2Cl_2, and one equivalent of L^6 was added in anhydrous CH_2Cl_2 in a dinitrogen atmosphere. A fine precipitate formed immediately, which was collected by filtration, washed with anhydrous CH_2Cl_2 and dried *in vacuo.* The purple solid was insoluble in chlorocarbons and hydrocarbons, and relatively sensitive to moisture. It was analysed by microanalysis, IR and UV-vis spectroscopy and by magnetic measurements. Microanalysis and a Nujol mull IR spectrum confirmed the presence of the macrocycle and the complete displacement of the thf, indicating the purple solid to be $[CrCl_3(L^6)]$. The IR spectrum also showed two Cr-Cl stretching bands, at 337 and 319 cm^{-1}, which is consistent with a C_{3v} local symmetry at Cr (a_1 + e). An approximation of the magnetic moment of a complex can be calculated using the spin-only magnetic moment formula:

$$\mu = 2(S\{S+1\})^{1/2}\,\mu_B$$

where *S* is the total spin quantum number.[22] For three unpaired electrons *S* is 1.5, and the expected magnetic moment is 3.87 μ_B. The magnetic susceptibility of $[CrCl_3(L^6)]$ was measured using a Johnson-Matthey magnetic balance and μ_{eff} calculated to be 3.71 μ_B which is consistent with a Cr(III) ion in an octahedral complex.

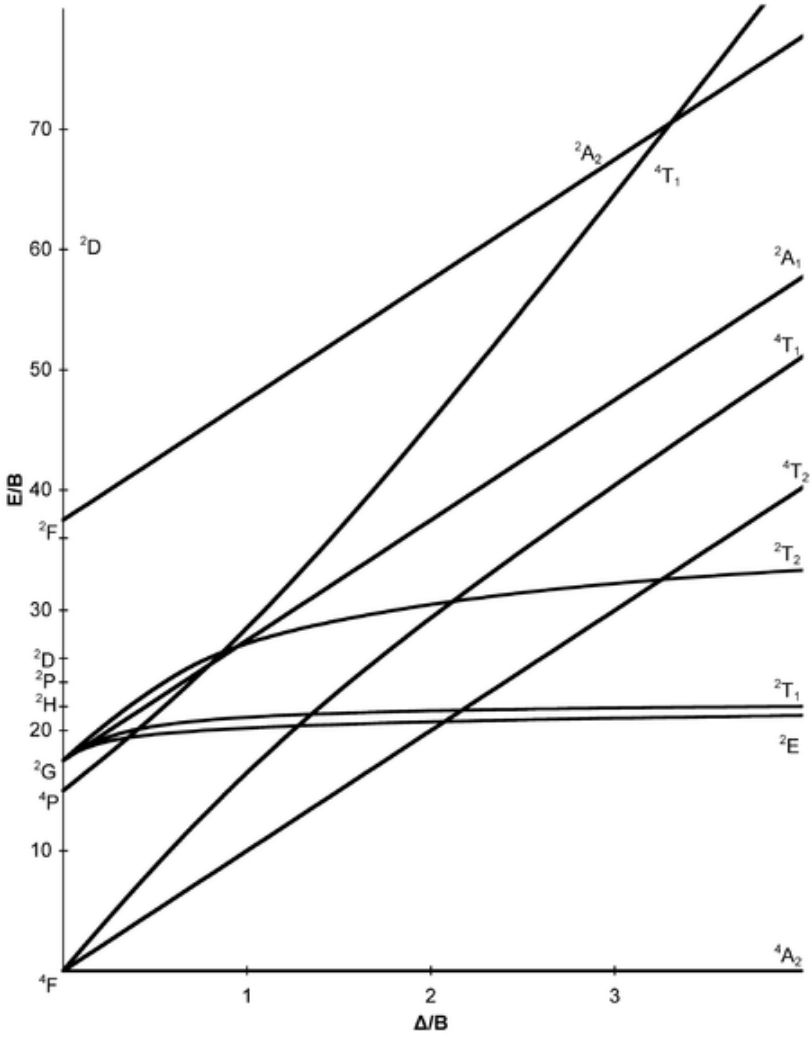

Figure 6.8: Tanabe-Sugano diagram for d^3 metal centres.

A diffuse reflectance UV-vis spectrum was recorded, using $BaSO_4$ as a dilutant, showing three bands. The Russell-Saunders ground state term for Cr^{3+} is ^4F. In an O_h environment, there is only one arrangement of the three electrons in the lower energy d-orbitals, so the ground state is a singlet $^4A_{2g}$ state.[24] Thus, three spin-allowed d-d bands are predicted for Cr(III) species, $^4A_{2g} \rightarrow {}^4T_{2g}$ (ν_1), $^4A_{2g} \rightarrow {}^4T_{1g}$ (F) (ν_2) and $^4A_{2g} \rightarrow {}^4T_{1g}$ (P) (ν_3), of which the latter is rarely observed as it is often obscured by intense charge-transfer bands.[25] Reducing the symmetry from O_h to C_{3v} should theoretically result in splitting of the bands, although in practice only broadening of the bands is observed usually.[15] Owing to the geometric constraints of the ligand used, only the *fac* isomer is expected in $[CrCl_3(L^6)]$. *Dq* can be obtained directly from ν_1 by dividing by 10 (Δ_O = 10 Dq), while the Racah parameter (B) can be extracted from the Tanabe-Sugano diagram for d^3 metal centres (shown in Figure 6.8) by using the ratio of ν_2/ν_1 to obtain the ratio of Δ_O/B. Table 6.3 shows the UV-vis data collected for the new complexes made in this Chapter, along with literature values for similar complexes, and are discussed below. L^8 in anhydrous CH_2Cl_2 was reacted

similarly with a solution of $[CrCl_3(thf)_3]$ in anhydrous CH_2Cl_2 and a deep purple solid precipitated almost immediately. The solid was collected by filtration and dried *in vacuo*. IR and UV-Vis spectra collected on the purple solid were consistent with $[CrCl_3(L^8)]$.

$[CrCl_3(thf)_3]$ was reacted with one equivalent of L^7 under the same conditions. A colour change was observed immediately, and after reducing the solvent volume *in vacuo* a green waxy solid was obtained. Washing with anhydrous hexane and heating in anhydrous CCl_4 were tried, in the hope of generating a non-waxy solid, but without success. A magnetic measurement could not be obtained on this waxy solid, nor could a microanalysis. A Nujol mull IR spectrum and a diffuse reflectance UV-vis spectrum were obtained, and these were consistent with the data obtained from $[CrCl_3(L^6)]$ and $[CrCl_3(L^8)]$, allowing tentative identification of this green solid as $[CrCl_3(L^7)]$.

Table 6.3: Electronic spectroscopy data for $[CrCl_3(L)]$. Spectra recorded in diffuse reflectance mode using $BaSO_4$ as a dilutant. a – B for the Cr(III) free ion = 918 cm^{-1}. b – Spectra recorded in $MeNO_2$. c – Solvent obscured band. d – no data reported.

Complex	**$^4A_{2g}\rightarrow{}^4T_{2g}$ /cm^{-1}**	**$^4A_{1g}\rightarrow{}^4T_{1g}$ /cm^{-1}**	**CT /cm^{-1}**	**Dq /cm^{-1}**	**B /cm^{-1} a**	**β**	**Ref.**
$[CrCl_3(L^6)]$	14530	19230	30300	1453	450	0.49	
$[CrCl_3(L^7)]$	14080	19490	29000	1410	530	0.58	
$[CrCl_3(L^8)]$	14180	19460	~30700	1418	516	0.56	
$[CrCl_3(L^1)]$	14190	19920	29400	1420	575	0.62	
$[CrCl_3(L^9)]$	14080	19300	29400	1408	502	0.55	
$[CrCl_3(L^{10})]$	14165	20020	30700	1417	550	0.60	
$[CrCl_3(MeC\{CH_2SeMe\}_3)]$	14490	20500	27700	1449	617	0.67	16
$[CrCl_3(Se\{(CH_2)_3SeMe\}_2)]$	14620	20300	28900	1462	567	0.61	16
$[CrCl_2([16]aneSe_4)]^{+}$ b	15580	20920	c	1558	511	0.56	16
$[CrCl_3([9]aneS_3)]$	14450	20080	d	1445	556	0.61	15
$[CrCl_3([10]aneS_3)]$	14750	20240	d	1473	590	0.64	15
$[(CrCl_3)_2([18]aneS_6)]$	14450	19530	d	1445	516	0.56	15
$[CrCl_2([14]aneS_4)]^{+}$ b	16500	22400	d	1650	536	0.58	15
$[CrCl_2([16]aneS_4)]^{+}$ b	15820	21790	d	1582	546	0.59	15

$[CrCl_3(thf)_3]$ was reacted similarly on anhydrous CH_2Cl_2 with one equivalent of L^9, which caused a grey precipitate to form. This solid was collected by filtration, dried *in vacuo* and analysed by microanalysis, IR and UV-Vis spectroscopy and magnetic measurements. The IR spectrum showed three bands corresponding to Cr-Cl stretches, consistent with $[CrCl_3(L^9)]$, showing C_s local

symmetry at the Cr atom (2a′ + a″). The microanalysis was consistent with this formulation, and the magnetic measurement also corresponded to 3 unpaired electrons.

$[CrCl_3(thf)_3]$ was reacted similarly on anhydrous CH_2Cl_2 with one equivalent of L^{10}, which caused a purple precipitate to form. This solid was collected by filtration, dried *in vacuo* and analysed by microanalysis, IR and UV-vis spectroscopy and magnetic measurements. The magnetic measurement was the highest observed for these new complexes, being 4.01 μ_B, but this is still consistent with three unpaired electrons (3.87 μ_B). The IR and UV-vis spectra were also consistent with octahedral Cr(III), and the microanalysis confirmed the 1:1 ligand:metal ratio of $[CrCl_3(L^{10})]$.

It was decided to also investigate the reaction of the tridentate saturated backbone Se_2O macrocycle made in Chapter 3 with Cr(III) to observe the changes in moving from the third donor being N to O. L^1 was reacted with $[CrCl_3(thf)_3]$ in anhydrous CH_2Cl_2 in similar fashion, and a purple solid was produced, which was collected by filtration and dried *in vacuo*. It was analysed by microanalysis, IR and UV-vis spectroscopy and magnetic measurements. Microanalysis confirmed the empirical formula to be $[CrCl_3(L^1)]$, while the IR spectrum showed three Cr-Cl stretches at 347, 340 and 331 cm^{-1}, consistent with C_s local symmetry. The magnetic moment was consistent with three unpaired electrons.

Comparing the UV-vis spectroscopic data obtained from the new Cr(III) complexes with those for previously published complexes, it can be seen that the Racah parameter, B, and nephelauxetic ratio, β, for the homoleptic Se_3 ligand complexes ($[CrCl_3(L^6)]$: B = 450 cm^{-1}, β = 0.49, $[CrCl_3(L^7)]$: B = 530 cm^{-1}, β = 0.58, $[CrCl_3(L^8)]$: B = 516 cm^{-1}, β = 0.56) are slightly lower than those for the similar complexes with acyclic triselenoethers $[CrCl_3(MeC\{CH_2SeMe\}_3)]$ (B = 617 cm^{-1}, β = 0.67) and $[CrCl_3(Se\{(CH_2)_3SeMe\}_2)]$ (B = 567 cm^{-1}, β = 0.61) whilst being similar to the macrocyclic $[CrCl_2([16]aneSe_4)]^+$ cation (B = 511 cm^{-1}, β = 0.56).[16] The relatively low values of β are consistent with covalent interactions between the soft selenium ligands and the hard metal centre. They are also slightly lower than those in complexes with similar macrocyclic thioethers, such as $[CrCl_3([9]aneS_3]$ (B = 556 cm^{-1}, β = 0.61) and $[CrCl_3([10]aneS_3)]$ (B = 590 cm^{-1}, β = 0.64).[15] The ligands containing N- and O-donor groups (L^1, L^9 and L^{10}) lead to slightly higher values than those of the analogous homoleptic Se ligands, consistent with the presence of the harder donors. There is little change in the ligand field strength upon addition of the harder N- or O- donors, with *Dq* remaining similar for all the new complexes except $[CrCl_3(L^6)]$. In general, where the donor atoms are the same, the larger ring macrocycle has a higher *Dq*. This can also be observed with the tridentate thioether macrocycles, $[CrCl_3([10]aneS_3)]$ having *Dq* of 1473 cm^{-1} compared to the analogous $[9]aneS_3$ complex where *Dq* is 1445 cm^{-1}. The exception is $[CrCl_3(L^8)]$, which has a

higher *Dq* than [$CrCl_3(L^7)$], which may be a result of ring strain in the ligand imposed by the benzyl backbone.

Time constraints prevented a similar detailed investigation with V(III), but a few preliminary reactions were attempted using [$VCl_3(thf)_3$] in anhydrous CH_2Cl_2. Addition of one equivalent of L^7 in anhydrous CH_2Cl_2 caused no discernable colour change after three hours, and analysis of the solids obtained after reducing the solvent *in vacuo* showed no reaction had occurred. A second attempt, which was left stirring overnight, also showed no reaction. A similar reaction with L^8 quickly yielded a red wax which was insoluble in chlorocarbons or hydrocarbons, and decomposed rapidly in air. All attempts to obtain IR and UV-vis spectra on this red wax failed. An IR spectrum obtained by smearing the CsI plates directly with the wax (attempts to slake it with Nujol failed) showed a large water peak, and the sticky consistency prevented mixing with $BaSO_4$ or even making a thin film for UV-vis spectroscopy.

Addition of one equivalent of either L^1 or L^9 to [$VCl_3(thf)_3$] in CH_2Cl_2 caused an instant colour change to a pink or red solution respectively. Small amounts of powdery solid were isolated from both reactions. Both powders were insoluble in chlorocarbons or hydrocarbons, and again decomposed rapidly in air, which affected attempts to get microanalytical data. One attempt to get microanalytical data on [$VCl_3(L^9)$] gave the composition as 30.8 % C, 3.7 % H and 2.4 % N, which is more consistent with [$VCl_3(L^9)$]·$(H_2O)_3$ (calculated: 31.1 % C, 3.6 % H, 2.4 % N) than [$VCl_3(L^9)$] (calculated: 34.3 % C, 2.8 % H, 2.7 % N). However, this does not indicate whether the red solid obtained had water present, or whether it absorbed water during the analytical process. Analysis by IR spectroscopy indicated possible formation of [$VCl_3(L)$] in both cases, as the spectra for both solids showed three bands which could correspond to V-Cl stretches, at 390, 353 and 324 cm^{-1} for [$VCl_3(L^1)$] and 352, 341 and 317 cm^{-1} for [$VCl_3(L^9)$]. These would be consistent with octahedral [$VCl_3(L)$] showing C_s local symmetry at the V atom ($2a' + a''$).

Table 6.4 shows the electronic spectroscopic data reported for similar thioether macrocycle complexes. Diffuse reflectance UV-vis spectra were obtained for the pink and red solids obtained from the reactions of [$VCl_3(thf)_3$] and L^1 and L^9, and qualitatively appeared to show the expected pattern of peaks for an octahedral complex. However, closer analysis of the data using the appropriate Tanabe-Sugano diagram gave values which do not appear to fit with the earlier data. It is probable that these solids were not pure samples of the desired [$VCl_3(L)$] complexes. There was insufficient time to explore the exact nature of these solids, and further study is required to fully identify them.

Table 6.4: Electronic spectroscopy data for $[VCl_3(L)]$. Spectra recorded in diffuse reflectance mode using $BaSO_4$ as a dilutant. a – B for the V(III) free ion = 861 cm^{-1}.

Complex	**$^3T_{1g} \rightarrow {}^3T_{2g}$ /cm^{-1}**	**$^3T_{1g} \rightarrow {}^3T_{1g}$ /cm^{-1}**	**Dq /cm^{-1}**	**B /cm^{-1} a**	**β**	**Ref**
$[VCl_3(thf)_3]$	13300	19900	1400	553	0.64	19
$[VCl_3(thf_3)] + L^1$	13620	19000	1454	420	0.48	
$[VCl_3(thf)_3] + L^9$	13540	18270	1437	370	0.43	
$[VCl_3([9]aneS_3)]$	18590	27620	1932	690	0.80	19
$[VCl_3([10]aneS_3)]$	19050	27700	2048	640	0.74	19
$[VCl_3([12]aneS_4)]$	12690	18250	1361	432	0.50	14
$[(VCl_3)_2([18]aneS_6)]$	19380	28010	2064	635	0.73	19
$[VCl_3([9]aneS_2O)]$	13440	18880	1436	420	0.48	14

6.5 – Conclusions

A set of new tetrahedral Co(II) complexes with a thio- or selenoether ligand with a xylyl backbone have been produced, wherein the chalcogenoether ligands all coordinated *via* 7 membered chelate rings. The thioether complexes are more stable than the selenoether complexes, but all the complexes are hydrolytically sensitive. Attempts to prepare tetrahedral Co(II) complexes with $MeS(CH_2)_3SMe$, to provide a six-membered chelate ring yielded black intractable materials.

A new series of Cr(III) complexes with small ring Se-rich macrocycles have been characterised. The complexes are hydrolytically sensitive and insoluble to chlorocarbon and hydrocarbon solvents, but have been analysed by UV-vis and IR spectroscopy, and by their magnetic moments. They have been shown to be softer donors than similar thioether macrocycles, as expected. An exploratory number of reactions were attempted with V(III), and showed these complexes to be less stable than the Cr(III) analogues. No examples of homoleptic Se_3 coordination on V(III) could be verified, but some Se_2O and Se_2N coordination was observed.

6.6 – Experimental

[CoI_2{*o*-$C_6H_4(CH_2SMe)_2$}]: [CoI_2] (0.156 g, 0.5 mmol) was dissolved in anhydrous *n*-BuOH (5 cm^3). *o*-$C_6H_4(CH_2SMe)_2$ (0.099 g, 0.5 mmol) in anhydrous CH_2Cl_2 (5 cm^3) was added, and the reaction stirred for 5 hours at room temperature. Solvent was removed from the green solid *in vacuo*, and the solid was washed with anhydrous hexane. Yield: 0.143 g (54 %). Required for $C_{10}H_{14}CoI_2S_2$: C, 23.5; H, 2.76. Found: C, 23.6; H, 2.77 %. UV-vis (solid, $BaSO_4$): 12900, 14080, 15150, 25970 cm^{-1}; (solution, CH_2Cl_2): (ε_{mol}/ cm^{-1} dm^3 mol^{-1}) 13060 (1160), 14240 (818), 15200 (415) cm^{-1}.

[$CoBr_2${*o*-$C_6H_4(CH_2SMe)_2$}]: Method as above using [$CoBr_2$]. Turquoise solid. Yield 75 %. Required for $C_{10}H_{14}CoBr_2S_2 \cdot 1/3BuOH$: C, 30.8; H, 4.0. Found: C, 30.6; H, 3.4 %. UV-vis (solid, $BaSO_4$): 13800, 14930, 15920 cm^{-1}; (solution, CH_2Cl_2): (ε_{mol}/ cm^{-1} dm^3 mol^{-1}) 13790 (327), 15310 (368), 16420 (204) cm^{-1}.

[CoI_2{*o*-$C_6H_4(CH_2SeMe)_2$}]: Method as above using [CoI_2] and *o*-$C_6H_4(CH_2SeMe)_2$. Green solid. Yield 61 %. UV-vis (solid, $BaSO_4$): 12440, 13740, 14740 cm^{-1}; (solution, CH_2Cl_2): (ε_{mol}/ cm^{-1} dm^3 mol^{-1}) 12660 (1068), 13890 (823), 14880 (489) cm^{-1}.

[$CrCl_3(L^6)$]: [$CrCl_3(thf)_3$] (0.1 g, 0.27 mmol) was dissolved in 5 cm^3 anhydrous CH_2Cl_2. A solution of L^6 (0.115 g, 0.27 mmol) in anhydrous CH_2Cl_2 (5 cm^3) was added, and the solution stirred for 30 mins. A purple precipitate formed almost immediately. The solvent was reduced *in vacuo* and the precipitate collected by filtration. Yield: 0.078 g, 68%. Required for $C_{14}H_{20}Cl_3CrSe_3$: C, 28.8; H, 3.5. Found: C, 28.3; H, 4.5%. IR (Nujol, cm^{-1}): 337, 319 (Cr–Cl).UV-vis (solid, $BaSO_4$): 14530, 19230, 30300 cm^{-1}. μ_{eff} = 3.71 μ_B.

[$CrCl_3(L^7)$]: As above using L^9. Green wax. Yield: 43 %. UV-vis (solid, $BaSO_4$): 14080, 19490, 29000 cm^{-1}. IR (Nujol, cm^{-1}): 326 (Cr-Cl).

[$CrCl_3(L^8)$]: As above using L^8. Purple solid. Yield: 49 %. UV-vis (solid, $BaSO_4$): 14180, 19460, ~30700 cm^{-1}. IR (Nujol, cm^{-1}): 346, 320 (Cr-Cl).

[$CrCl_3(L^1)$]: As above using L^1. Purple solid. Yield: 52%. Required for $C_{12}H_{16}Cl_3CrOSe_2$: C, 29.3; H, 3.3. Found: C, 29.3; H, 3.6%. UV-vis (solid, $BaSO_4$): 14200, 19880, 29400 cm^{-1}. IR (Nujol, cm^{-1}): 347, 340, 331 (Cr–Cl). μ_{eff} = 3.56 μ_B.

[$CrCl_3(L^9)$]: As above using L^9. Grey solid. Yield: 70%. Required for $C_{15}H_{15}Cl_3CrNSe_2 \cdot 1/3CH_2Cl_2$: C, 33.2; H, 2.9; N, 2.5. Found: C, 33.1; H, 3.7; N, 3.1%. UV-vis (solid, $BaSO_4$): 14705, 21050, 29070 cm^{-1}. IR (Nujol, cm^{-1}): 355, 344, 326(sh) (Cr–Cl). μ_{eff} = 3.66 μ_B.

[$CrCl_3(L^{10})$]: As above using L^{10}. Yield: 48%. Required for $C_{10}H_{13}Cl_3CrNSe_2$: C, 25.9; H, 2.8; N, 3.0. Found: C, 25.8; H, 3.0; N, 3.0%. UV-vis (solid, $BaSO_4$): 14165, 20020, 30700 cm^{-1}. IR (Nujol, cm^{-1}): 357, 333(br) (Cr–Cl). μ_{eff} = 4.01 μ_B.

6.7 – X-Ray Crystallography

Details of the crystallographic data collection and refinement parameters are given in Table 6.5. Green single crystals of [CoI_2{*o*-$C_6H_4(CH_2SMe)_2$}] were obtained by addition of petroleum ether to the reaction mixture. Structure solution and refinement were routine.[26,27] Selected bond lengths and angles for [CoI_2{*o*-$C_6H_4(CH_2SMe)_2$}] are presented in Table 6.2.

Table 6.5: Crystallographic data collection and refinement parameters. $R1 = \Sigma||F_o| - |F_c||/\Sigma|F_o|$; $wR_2 = [\Sigma w(F_o^2 - F_c^2)^2/\Sigma wF_o^4]^{1/2}$

Complex	**[CoI_2{*o*-$C_6H_4(CH_2SMe)_2$}]**
Formula	$C_{10}H_{14}CoI_2S_2$
M	511.06
Crystal System	Monoclinic
Space Group	*P* $2_1/n$
a/Å	8.3478(3)
b/Å	15.4660(6)
c/Å	11.6952(4)
α/°	90
β/°	91.913(2)
γ/°	90
U/Å^3	1509.09(10)
Z	4
μ(Mo-Kα)/ mm^{-1}	5.476
R_{int}	0.0506
Total no. reflns.	24660
Unique reflections	3490
No. of parameters	138
$R1$ [$I_o > 2\sigma(I_o)$]	0.0278
$R1$ [all data]	0.0432
wR_2 [$I_o > 2\sigma(I_o)$]	0.0673
wR_2 [all data]	0.0755

6.8 – References

1. Evans, J.; Levason, W.; Manning, J. M.; Reid, G.; Tsoureas, N.; Webster, M. *Dalton Trans.* **2007**, 1986 – 1988.

2. Levason, W.; Manning, J. M.; Reid, G.; Tuggey, M.; Webster, M. *Dalton Trans.* **2009**, 4569 – 4577.

3. Murray, S. G.; Hartley, F. R. *Chem. Rev.* **1981**, *81*, 365 – 414.

4. Hope, E.; Levason, W. *Coord. Chem. Rev.* **1993**, *122*, 109 – 170.

5. Levason, W.; Orchard, S. D.; Reid, G. *Coord. Chem. Rev.* **2002**, *225*, 159 – 199.

6. Jenkinson, J. J.; Levason, W.; Perry, R. J.; Spicer, M. D. *J. Chem. Soc., Dalton Trans.* **1989**, 453 – 455.

7. Brown, J. L.; Kemmitt, T.; Levason, W. *J. Chem. Soc., Dalton Trans.* **1990**, 1513 – 1515.

8. Levason, W.; Quirk, J. J.; Reid, G. *J. Chem. Soc., Dalton Trans.* **1996**, 3713 – 3719.

9. Carlin, R. L.; Weissburger, E. *Inorg. Chem.* **1964**, *3*, 611 – 612.

10. Flint, C. D.; Goodgame, M. *J. Chem. Soc. (A)*, **1968**, 2178 – 2182.

11. Hartman, J. R.; Hintsa, E. J.; Cooper, S. R. *J. Am. Chem. Soc.* **1986**, *108*, 1208 – 1214.

12. Setzer, W. N.; Ogle, C. A.; Wilson, G. S.; Glass, R. S. *Inorg. Chem.* **1983**, *22*, 266 – 271.

13. Hartman, J. R.; Hintsa, E. J.; Cooper, S. R. *J. Chem. Soc., Chem. Comm.* **1984**, 386 – 387.

14. Beard, C. D.; Carr, L.; Davis, M. F.; Evans, J.; Levason, W.; Norman, L. D.; Reid, G.; Webster, M. *Eur. J. Inorg. Chem.* **2006**, 4399 – 4406.

15. Pope, S. J. A.; Champness, N. R.; Reid, G. *J. Chem. Soc., Dalton Trans.* **1997**, 1639 – 1644.

16. Levason, W.; Reid, G.; Smith, S. M. *Polyhedron* **1997**, *24*, 4253 – 4256.

17. Champness, N.; Jacob, S. R.; Reid, G.; Frampton, C. S. *Inorg. Chem.* **1995**, *34*, 396 – 398.

18. Hector, A. L.; Jura, M.; Levason, W.; Reid, S. D.; Reid, G. *New J. Chem.* **2009**, *33*, 641 – 645.

19. Davies, S. C.; Durrant, M. C.; Hughes, D. L.; Le Flo'ch, C.; Pope, S. J. A.; Reid, G.; Richards, R. L.; Sanders, J. R. *J. Chem. Soc., Dalton Trans.* **1998**, 2191 – 2198.

20. Durrant, M. C.; Davies, S. C.; Hughes, D. L.; Le Flo'ch, C.; Richards, R. L.; Sanders, J. R.; Champness, N. R.; Pope, S. J. A.; Reid, G. *Inorg. Chim. Acta* **1996**, *251*, 13 – 14.

21. Fine, D. A. *J. Am. Chem. Soc.* **1962**, *84*, 1139 – 1144.

22. Shriver, D. F.; Atkins, P. W. *Inorganic Chemistry*, 3rd ed., Oxford University Press, 1999.

23. Herwig, W.; Zeiss, H. H. *J. Org. Chem.* **1958**, *23*, 1404.

24. Brisdon, A. K. *Inorganic Spectroscopic Methods*, Oxford University Press, 1998.

25. Lever, A. B. P. *Inorganic Electronic Spectroscopy*, 2nd ed., Elsevier, 1984.

26. Sheldrick, G. M. SHELXS-97, program for crystal structure solution, University of Göttingen, Germany, **1997**.

27. Sheldrick, G. M. SHELXS-97, program for crystal structure refinement, University of Göttingen, Germany, **1997**.

Appendix – Spectroscopic Equipment

Infrared spectra were recorded as Nujol mulls between CsI discs using a Perkin-Elmer 983G spectrometer over the range 4000–200 cm^{-1}. ^{1}H and $^{13}C\{^{1}H\}$ NMR spectra were recorded using a Bruker AV300 spectrometer at 298 K unless otherwise stated and are referenced to tetramethylsilane. $^{77}Se\{^{1}H\}$, $^{125}Te\{^{1}H\}$ and ^{195}Pt NMR spectra were recorded using a Bruker DPX400 spectrometer operating at 76.3, 126.3 or 85.7 MHz respectively and are referenced to external neat Me_2Se, external neat Me_2Te and 1 mol dm^{-3} $Na_2[PtCl_6]$ respectively. Mass spectra were run by electron impact on a VG-70-SE Normal geometry double focusing spectrometer, GCEI using a ThermoQuest TraceMS, positive ion electrospray (MeCN solution) or APCI using a VG Biotech platform. UV-visible spectra were recorded either in diffuse reflectance mode with $BaSO_4$ as a dilutant or in absorption mode as solutions in CH_2Cl_2 using a Perkin Elmer Lambda 19 spectrometer. Magnetic measurements used a Johnson-Matthey magnetic balance, with samples loaded in the glove box. Microanalyses were undertaken by the University of Strathclyde microanalytical service or Medac Ltd. X-Ray data collection used a Nonius Kappa CCD diffractometer (T = 120 K) and with graphite-monochromated Mo-K_α X-radiation (λ = 0.71073 Å).

Chemicals and solvents were used as purchased from Aldrich unless otherwise stated. Anhydrous solvents were dried and distilled before use according to normal practices.